

JAMES COOK UNIVERSITY
SCHOOL OF ENGINEERING

EG4011/2

**MODELLING EMBANKMENT
DEFORMATION ON THE TULLY
PROJECT**

Sallyanne Brooke-Taylor

Thesis submitted to the School of Engineering in partial fulfilment
of the requirements for the degree of

**Bachelor of Engineering with Honours (Civil) -
Bachelor of Science (Physics)**

October, 5th 2007

Statement of Access

I, the undersigned, the author of this thesis, understand that James Cook University will make it available for use within the University Library and, by microfilm or other means, allow access to users in other approved libraries. All users consulting with this thesis will have to sign the following statement:

In consulting this thesis I agree not to copy or closely paraphrase it in whole or in part without written consent of the author; and to make proper public written acknowledgement for any assistance which I have obtained from it.

Beyond this, I do not wish to place any restriction on access to this thesis.

Sallyanne Brooke-Taylor

Date

Sources Declaration

I declare that this thesis is my own work and has not been submitted in any form for another degree or diploma at any university or other institution of tertiary education. Information derived from the published or unpublished work of others has been acknowledged in the text and a list of references is given.

Sallyanne Brooke-Taylor

Date

Abstract

The formation of cracks in road pavements constructed on high embankments is a common problem. Surprisingly, there appears to be little published research on the topic, making it difficult for engineers to consider it in their designs. This thesis makes use of numerical models to study the deformations and stresses, both within and beneath embankments, in order to determine whether pavement cracking can be caused directly by the post construction deformations associated with the consolidation of foundation material. In particular, the study deals with the potential for pavement cracking to occur on a new section of the Bruce Highway. The 15km section, just South of Tully in North Queensland, is currently being delivered by The Tully Alliance, comprising of the Department of Main Roads, Maunsell and BMD. In this thesis a number of preliminary models are created to determine the sensitivity of the models to various input parameters. A numerical model of an instrumented trial embankment, which forms part of the new highway, is then created and the results are compared with data collected on site. Finally, a parametric investigation into pavement cracking is conducted. The overall conclusion drawn from the modelling is that, post construction consolidation settlements are unlikely to cause pavement cracking on the Tully project or on road embankments in general.

Acknowledgements

I would like to thank my supervisors Associate Professor Nagaratnam Sivakugan and Mr Michael Matheson for all the assistance they have provided me with throughout the year. They have both been great supervisors and I would especially like to thank Mr Michael Matheson for the motivation he gave me and the numerous hours spent in meetings with me particularly when FLAC was being problematic.

I would also like to acknowledge the Tully Alliance team for providing me with information about the Tully project and the data from the trial embankments.

Many thanks go out to those who took the time to provide me with ideas to fix my problem with FLAC, to Dr Briony Rankine, Dr Bruce Hobbs (CSIRO), Dr Christine Detournay (Itasca), Dr David Sainsbury (Itasca), Dr John McLellan (JCU Geology Department) and Dr Mike Rubenach (JCU Geology Department).

On a more personal note I would like to thank my Mum and Dad. Thank you for everything you have done for me over the last 22 years and for helping me through this last year. Without your constant support, understanding and love I could not have achieved what I have. Thanks also to my brothers, to Andrew thank you for your constant interest in what I am doing and for giving me motivation from afar and to Michael just thanks.

My friends I also thank. Michelle, thank you for putting up with me for three months, for proofreading and also for just being a great friend. To all of my great group of friends thank you for forcing me to maintain some semblance of a social life. Finally, thank you to Daniel who as well as being a great support and maintainer of my social life has helped to keep me motivated and spent a lot of time letting me bounce ideas off him.

Table of Contents

Chapter 1: Introduction	1
1.1 Background.....	1
1.2 Project Objectives	2
1.3 Report Structure	3
 Chapter 2: Literature Review	 5
2.1 Change in Foundation Effective Stress Due Embankment Loads.....	5
2.1.1. Introduction.....	5
2.1.2. 2:1 Distribution Method	5
2.1.3. Boussinesq Method	6
2.1.4. Westergaard's Method.....	8
2.2 Settlements.....	10
2.2.1. Introduction.....	10
2.2.2. Immediate Settlement	11
2.2.3. Consolidation	12
2.2.4. Secondary Compression Settlement	26
2.3 Deformations Beneath Embankments on Soft Soils.....	28
2.3.1. Introduction.....	28
2.3.2. Settlement Patterns.....	28
2.3.3. Lateral Displacements	32
2.3.4. Pore Water Pressure	36
2.4 Geotechnical Site Investigations	37
2.4.1. Introduction.....	37
2.4.2. Boreholes	37
2.4.3. Piezocone Tests.....	40
2.5 Geotechnical Monitoring Equipment	44
2.5.1. Settlement Plates	44
2.5.2. Piezometers.....	45
2.5.3. Inclinometers	45
2.6 Summary of the Literature Review	47
 Chapter 3: Numerical Modelling and FLAC	 48
3.1 Introduction.....	48
3.2 Numerical Modelling Software.....	48
3.3 Finite Element versus Finite Difference	49

3.4	Explicit and Implicit Solution Techniques	49
3.5	FLAC Features.....	50
3.6	Constitutive Models	51
3.6.1.	Elastic Models.....	52
3.6.2.	Elastic-Plastic Models	53
3.6.3.	Critical State Models	58
3.7	Consolidation – Modelling A Coupled Problem in FLAC	58
3.8	Validation of FLAC Solution to a Simple 1-D Consolidation Problem	61
3.8.1.	Problem Definition.....	62
3.8.2.	FLAC Model.....	62
3.8.3.	Theoretical Calculation.....	69
3.8.4.	Comparison of FLAC Results with Theory	69
3.8.5.	Conclusions from the 1-D Consolidation Problem	70
3.9	Summary.....	71
Chapter 4: The Tully Project		72
4.1	Introduction.....	72
4.2	The Trial Embankments	74
4.3	Geotechnical Investigations	78
4.4	Summary.....	79
Chapter 5: Preliminary Consolidation Models.....		80
5.1	Introduction.....	80
5.2	Sensitivity Analysis	80
5.2.1.	Model Geometry and Soil Properties in the Basis Model.....	80
5.2.2.	Boundary Conditions.....	82
5.2.3.	The Solution Process	83
5.2.4.	Required Output.....	85
5.2.5.	Results	85
5.2.6.	Conclusions Drawn from the Sensitivity Analysis.....	94
5.3	Investigation into the Problem of High Immediate Settlements	95
5.3.1.	Modifying the One-Dimensional Model	96
5.3.2.	Investigations Conducted on a Basic Two Dimensional Consolidation Model	98
5.3.3.	Conclusions from the Investigations into the Problem of High Immediate Settlements.....	102
5.4	Summary of the Preliminary Modelling	102

Chapter 6: Numerical Modelling of the Trial Embankments near Tully	103
6.1 Introduction.....	103
6.2 Selection of the Location to Model	103
6.3 Assignment of Foundation and Embankment Properties.....	104
6.3.1. Layer Classification.....	105
6.3.2. Bulk and Shear Moduli.....	105
6.3.3. Dry Density.....	105
6.3.4. Effective Friction Angle, Effective Cohesion and Tensile Strength	106
6.3.5. Permeability, Porosity and Saturation	106
6.4 Model Geometry and Boundary Conditions	107
6.5 Modelling Procedure	109
6.6 Trial Embankment Data from Site	110
6.7 Model Results and Comparisons with Field Results	113
6.7.1. Settlements.....	113
6.7.2. Pore Water Pressure	115
6.8 Summary and Conclusions from the Trial Embankment Modelling.....	117
Chapter 7: Investigation into Pavement Cracking	119
7.1 Introduction.....	119
7.2 Determination of a Failure Criterion for Pavement Cracking.....	119
7.2.1. Approach 1: Yielding of Pavement Zones.....	119
7.2.2. Approach 2: Measurement of Stresses and Displacements	121
7.3 Modelling Strategies Devised and Attempted.....	122
7.3.1. Option 1: Fully Coupled Model with Embankment Placed Incrementally.....	122
7.3.2. Option 2: Model without Flow with the embankment placed incrementally.....	122
7.3.3. Option 3: Model without Flow with the embankment placed instantaneously	123
7.3.4. Option 4: The Two Stage Model.....	124
7.4 Parameters Investigated and Models Created	125
7.5 Results	127
7.6 Discussion and Interpretation	130
7.7 Implications of Results for the Tully Project	134
7.8 Summary and Conclusions of the Investigation into Pavement Cracking	135
Chapter 8: Summary, Conclusions and Recommendations for Further Research	136
8.1 Introduction.....	136
8.2 Preliminary Modelling.....	136

8.3	Trial Embankment Modelling.....	137
8.4	Parametric Investigation into Pavement Cracking and Implications for the Tully Project.....	137
8.5	Recommendations for Further Research	138
References		141
Appendix A: Tully Data.....		144
A-1:	Settlement Predictions and Preloading and Surcharge Requirements	144
A-2:	Geotechnical Site Investigation Data	152
A-2.1:	Map Showing the Location of the Boreholes and Piezocone Tests	152
A-2.2:	Borehole Logs	153
A-2.3:	Consolidation Test Results	161
A-2.4:	Piezocone Results.....	164
Appendix B: Preliminary Modelling Data		168
B-1:	Model FLAC Code.....	168
B-1.1:	Original Two Layer Model	168
B-1.2:	Original Single Layer Model	173
B-1.3:	Code for the Two Dimensional Consolidation Model Created by modifying the One Dimensional Consolidation Model	177
Appendix C: Trial Embankment Code		180
Appendix D: Data and Code from Pavement Cracking Investigation.....		201
D-1:	Code for Pavement Cracking models	201
D-1.1:	Code for first model which determines the settlement profile	201
D-1.2:	Second Model Where the Deformations from the First Model are Applied to the Embankment	215
D-2:	Data from Pavement Cracking Models	230

List of Figures

Figure 2.1: The Vertical Stress Increase with Depth Using the 2:1 Distribution.....	6
Figure 2.2: Vertical Stress Increase beneath a Point Load	6
Figure 2.3: Influence Factor for a Rectangular Loaded Area Based on Boussinesq's Equation (U.S.Navy 1971)	7
Figure 2.4: Influence Factors for the Vertical Stress Increase	8
Figure 2.5: Influence Factor for a Rectangular Loaded Area Based on Westergaard's Equation (Fadum 1948)	9
Figure 2.6: Values of (a) μ_0 and (b) μ_1 for Immediate Settlement Computation (Sivakugan 2008b).....	11
Figure 2.7: The Three Phases in Soils	13
Figure 2.8: Volume - Void Ratio Relationship in a Saturated Soil.....	13
Figure 2.9: Schematic of (a) a Floating Ring Oedometer and (b) a Fixed Ring Oedometer (U.S. Army Corps of Engineers, 1970 vide. Holtz and Kovacs 1981)	14
Figure 2.10: General Features of an e-log σ'_v Curve (Mesri and Choi 1985).....	15
Figure 2.11: Effect of Disturbance on e-log σ'_v Curve (Leonards 1962)	16
Figure 2.12: Effect of Aging on σ'_p (Bjerrum 1973).....	18
Figure 2.13: Consolidation Ratio as a Function of Depth and Time Factors, for Uniform Initial pore pressure in a Doubly Drained Layer (Cernica 1995).....	21
Figure 2.14: Average Degree of Consolidation (U_{avg}) - Time Factor (T).....	22
Figure 2.15: The Influence of Strain Profile on the Rate of Consolidation (After Terzaghi and Frolich (1936) and Janbu (1965) vide. Duncan 1993).....	23
Figure 2.16: Casagrande's Logarithm of Time Method (Holtz and Kovacs 1981)	24
Figure 2.17: Taylor's Square Root of Time Method (Holtz and Kovacs 1981)	24
Figure 2.18: Void Ratio - Log Time Graph Showing the Definition of Secondary	

Compression used in Calculations	26
Figure 2.19: Settlement Patterns beneath Embankments on Soft Ground (Zhang 1999).....	29
Figure 2.20: Measured Settlements beneath the Embankment Constructed to Failure on Maur Clay, Showing Position of Maximum Settlement Predicted by Zhang (Zhang 1999) ...	30
Figure 2.21: Settlement Pattern beneath Trial Embankment on Pacific Highway NSW at Four Different Times (Hsi and MacGregor 1999)	31
Figure 2.22: Settlement Pattern beneath the Brisbane Motorway Embankment (Oh 2006)...	32
Figure 2.23: Definition of the geometry and Deformation Parameters (Tavenas et al. 1979)	34
Figure 2.24: Theoretical Lateral Displacement Profile beneath an Embankment Toe (Tavenas et al. 1979)	34
Figure 2.25: Idealised relation between embankment settlement and maximum lateral displacement beneath the toe (Stewart et al. 1994)	36
Figure 2.26: Triaxial Test Apparatus (Sivakugan 2008a)	39
Figure 2.27: Mohr-Coulomb Failure Envelope	40
Figure 2.28: Soil Classification based on Cone Penetration Test (Sivakugan 2008a)	41
Figure 2.29: Correlation Between Cone Tip Resistance and Effective Friction Angle (Robertson and Campanella 1983)	43
Figure 2.30: Determination of Hydraulic Conductivity or Permeability from a Piezocone Dissipation Test (Mayne 2002 Accessed: 31.05.07)	43
Figure 2.31: Diagram of a Settlement Plate.....	44
Figure 2.32: Diagram of a Vibrating Wire Piezometer (Canterbury_City_Council 2007)	45
Figure 2.33: Inclinometer Probe (Durham_Geo-Enterprises 2006).....	46
Figure 2.34:Simplified Example of Calculations Required to Determine Inclinometer Casing Profile (Durham_Geo-Enterprises 2006).....	47
Figure 3.1: Linear Elastic Stress-Strain Relation.....	52

Figure 3.2: Hyperbolic Stress-Strain Curve (Lewis and Schrefler 1987).....	53
Figure 3.3: Ideal stress strain relations for (a) an elastic-perfectly plastic material and (b) an elastic-plastic material	54
Figure 3.4: Mohr-Coulomb Failure Surface (Høeg 1977).....	55
Figure 3.5: Drucker-Prager Failure Surface (Høeg 1977)	55
Figure 3.6: Plastic Potential Surface and the Normality Condition	56
Figure 3.7: Plastic Strain Hardening and Softening.....	57
Figure 3.8: One-Dimensional Consolidation Problem	62
Figure 3.9: Plot in FLAC of the Distribution of Effective stress and Pore Pressure after 188 120 seconds (2days, 4hrs and 15mins)	67
Figure 3.10: Variation of Pore Pressure, Effective Stress and Total Stress with Time	68
Figure 3.11: Variation of Pore Pressure, Effective Stress and Total Stress with Time, when the Model is Solved Using the STEP Command	68
Figure 3.12: Settlement with Time Comparison	69
Figure 3.13: Comparison of FLAC Results and Theory for Pore Pressure with Time at Four Depths.....	70
Figure 4.1: Alignment of the New Highway Showing the Location of the Trial Embankments	73
Figure 4.2: Location of the Three Trial Embankments (Modified from a drawing provided by the Tully Alliance)	74
Figure 4.3: Location of Instrumentation and Geometry of Trial Embankment 1	75
Figure 4.4: Location of Instrumentation and Geometry of Trial Embankment 2	76
Figure 4.5: Embankment 2, Looking Towards Lagoon Creek	77
Figure 4.6: Top of Inclinometer Casing and Piezometer Monitoring Box next to the Culvert Section of Trial Emankment 2	77

Figure 5.1: Mesh for the Single Layer Models	81
Figure 5.2: Mesh for the two Layer Model.....	81
Figure 5.3: Vertical Displacement beneath the Centre of the Embankment against Time.....	86
Figure 5.4: Pore Water Pressure Distribution in Two Layer Model after Undrained Analysis	87
Figure 5.5: Vertical Effective Stress Distribution in Two Layer Model after Undrained Analysis	87
Figure 5.6: Vertical Displacement Distribution in Two Layer Model after Undrained Analysis	88
Figure 5.7: Pore Water Pressure Distribution in Two Layer Model after Drained Analysis ..	88
Figure 5.8: Vertical Displacement Distribution in Two Layer Model after Drained Analysis	89
Figure 5.9: Pore Pressure Distribution after Undrained Analysis for Single Layer Model where Actual c' and ϕ' values were used for all three stages.....	90
Figure 5.10: Pore Pressure Distribution After Undrained Analysis for Single Layer Model where High c' and ϕ' values were used for the Initialisation Stage.....	91
Figure 5.11: Comparison of Settlement Versus Time for 1-Dimensional Model and 2-Dimensional Variation of the Same Model.....	97
Figure 5.12: Effect of Bulk Modulus of Water on the Settlement versus Time Relationship for the Two Dimensional Models.....	99
Figure 5.13: Grid Showing Applied Stress and Boundary Conditions For Two Dimensional Model without Symmetry	99
Figure 5.14: Settlement Results of the Two Dimensional Model which did not use Symmetry Compared with Previous Models	100
Figure 5.15: Variation of Settlement – Time Curves with Grid Density.....	101
Figure 5.16: Variation of Settlement - Time Graphs with Grid Density Early in the First Hour of the Consolidation Process	101

Figure 6.1: Finite Difference Grid for Trial Embankment Model Showing Different Soil Layers	108
Figure 6.2: Embankment Construction Sequence	109
Figure 6.3: Settlement Plate Results for CH83500	111
Figure 6.4: Piezometer Data at CH83500.....	112
Figure 6.5: Diagrammatic Explanation of Reason for the Lack of an Increase in Pore Pressure in the Top Piezometer.....	112
Figure 6.6: Comparison of Model and Field Settlement Versus Time Curves	113
Figure 6.7: Vertical Displacement Contours after each Stage of Construction	114
Figure 6.8: Comparison of Model and Field Pore Water Pressure Versus Time Results.....	116
Figure 7.1: Element States During the Solution Process of a Preliminary Pavement Model	120
Figure 7.2: Vertical Displacement Contours for a Model with the Embankment Placed Instantaneously.....	123
Figure 7.3: Settlement Pattern beneath a 6m High Embankment during Construction.....	124
Figure 7.4: Dimensions and Grids for (a) the three metre high embankment, (b) the 4.5 metre high embankment and (c) the 6 metre high embankment	126
Figure 7.5: Effect of Embankment Height and Young's Modulus on the Pavement Stresses	127
Figure 7.6: Horizontal Stress Profile at Base of the Pavement for Models with $E_{foundation} = 8$ MPa	127
Figure 7.7: Effect of Settlement beneath the Embankment on Pavement Stresses	128
Figure 7.8: Vertical Displacements at Top and Bottom of Pavement Compared with Settlement beneath the Embankment for 6m High Embankment with $E_{foundation} = 8$ MPa, $E_{Embankment} = 20$ MPa, $E_{pavement} = 200$ MPa.....	129
Figure 7.9: Variation of Maximum Horizontal Tensile Stress in a Pavement with Settlement for a Wide Embankment	133

Figure 7.10: Possible Foundation Profiles 134

Figure 8.1: Variation of Pavement Stress with Lateral Displacement beneath toe of the Embankment 231

List of Tables

Table 3-1: Comparison of Explicit and Implicit Solution Methods (Itasca 2005b)	50
Table 3-2: Different Solution Methods for Modelling Coupled Fluid-Mechanical Problems (Itasca 2005c).....	60
Table 5-1: Results from Single Layer Models with Different Initialisation Procedures	90
Table 5-2: Results From Two Layer Models Where Young's Modulus was Varied	93
Table 6-1: Soil Properties Used in Model of Trial Embankment 2.....	104
Table 7-1: Properties Held Constant Whilst Height and Foundation Stiffness were Varied	125
Table A-1: Settlement Predictions and Preloading Designations (Produced by the Alliance)	144
Table D-1: Data Recorded from Pavement Cracking Investigation Models	230

List of Symbols

B	Breadth of footing
c	Cohesion
c'	Effective cohesion
c_u	Undrained cohesion
c_v	Coefficient of consolidation
C_α	Secondary compression index
C_c	Compression index
C_N	N count overburden correction
C_r	Recompression index
CPT	Cone Penetration Test
$d\varepsilon^p$	Incremental strain vector
D	Constrained (odemeter) modulus
e	Void ratio
e_0	Initial void ratio
e_p	Void ratio at the end of primary consolidation
Δe	Change in void ratio
E_h	SPT hammer efficiency
E_u	Undrained modulus of elasticity
f_s	Sleeve friction
g	Plastic potential function
G	Shear modulus

G_s	Specific gravity of soil grains
H	Height
H_{dr}	Drainage distance
i	Hydraulic gradient
I	Influence factor
k	Coefficient of permeability
k_{FLAC}	Coefficient of permeability as defined by FLAC
$k_{Geotec\ h}$	Coefficient of permeability
K	Bulk modulus
K_w	Bulk modulus of water
K_u	Apparent bulk modulus of soil under undrained conditions
K_o	Coefficient of earth pressure at rest
L	Length of footing
L	Average flow path length
LL	Liquid Limit
m_v	Coefficient of volume compressibility
n	Porosity
N	Number of blows in SPT test
N_k	Cone factor
$(N_1)_{60}$	Number of blows in SPT test corrected for efficiency and overburden
NC	Normally consolidated
P_a	Atmospheric pressure

PI	Plastisity Index
q	Uniform applied surcharge
q_c	Cone resistance
Q	Applied Load
$Q(\sigma)$	Plastic potential surface
R	Settlement reading in an odemeter test
R_k	Ratio of fluid stiffness to soil skeleton stiffness
s_c	Consolidation settlement
s_i	Immediate settlement
s_s	Secondary settlement
s_t	Total settlement
SPT	Standard Penetration Test
t	Time
t_{50}	Time corresponding to 50% consolidation
t_c	Characteristic time scale of the consolidation process
t_p	Primary consolidation time
t_s	Actual time scale of interest
T	Dimensionless time factor
u	Pore water pressure
U_z	Percentage consolidated
v	Pore water velocity
V	Volume

ΔV	Change in volume
V_v	Volume of voids
V_s	Volume of solids
x	Horizontal distance
y_m	Maximum lateral deformation
z	Depth (vertical)
Z	Dimensionless depth factor
ε	Strain
ε_1	Major principle strain
$\Delta\varepsilon_i^p$	Plastic strain in the i direction
γ_w	Unit weight of water
μ_0	Correction factor in immediate settlement calculation
μ_1	Correction factor in ultimate settlement calculation
ν	Poisson's Ratio
ρ_d	Dry density
ρ_w	Density of water
σ	Stress
σ_1	Major principle stress
σ_3	Minor principle stress
σ_p'	Preconsolidation pressure
σ^t	Tension limit
σ_v	Stress in the vertical direction

σ_v'	Effective stress in the vertical direction
σ_{v0}'	Current overburden pressure
$\Delta\sigma_v$	Change in stress in the vertical direction
$\Delta\sigma_{v,average}$	Average change in stress in the vertical direction
ϕ	Friction angle
ϕ'	Effective friction angle
ϕ_u	Undrained friction angle
ψ	Dilation angle

Chapter 1: Introduction

1.1 **Background**

A common problem found in road pavements constructed on high embankments is the formation of significant longitudinal cracks. The formation of such cracks is generally attributed to the pavements being subjected to large displacements which force different parts of the pavement to move in different directions. Pavements, being generally very brittle, are unable to withstand these large displacements, and as a result crack. As well as being aesthetically displeasing, these cracks can be dangerous to road users and are difficult and expensive to repair. However, despite the common occurrence of this problem and the expense of repairs, there appears to be little published research on the causes of it and how to predict when it will occur.

This lack of information makes it difficult for engineers to consider the problem when roads and embankments are designed and can be a cause for concern. One project where there have been concerns regarding the potential for pavement cracking is the Tully project. This project involves the upgrade of a 15 kilometre stretch of the Bruce Highway located just South of Tully in North Queensland. The project, which is being delivered under an “alliance” contractual arrangement between the Department of Main Roads, Maunsell (designer) and BMD (contractor), was prompted by the regular, long closures of the highway due to flooding in the wet season. To reduce the number and length of closures on the new section of highway, high embankments with numerous culverts are being designed. However, the foundation upon which many of the embankments will be constructed is far from ideal. The natural ground in the area, which varies extensively over the length of the upgrade, is highly stratified and in many areas contains very soft clay layers. Such clay layers can often cause problems because they can be highly compressible and, when built on, will deform. Clay layers in general also have very low permeability, and as a result the deformations occur slowly in saturated clays, in a process known as consolidation. The main reason for concern on the Tully project is these clay layers, because they mean that the high embankments are expected to undergo large settlements much of which will occur after the embankment and pavement have been fully constructed. Studies in the literature have shown that often large settlements are accompanied by large lateral displacements, and it is hypothesised that these large post construction deformations within the foundation could lead to significant differential displacements within the embankment which in turn might lead to pavement cracking.

To determine whether pavement cracking is likely to occur as a result of large post

construction foundation deformations, numerical modelling of embankments in FLAC (Fast Lagrangian Analysis of Continua) is used. Numerical modelling has been used quite extensively in geotechnical literature for the prediction of settlements, pore pressures and lateral displacements in the foundations beneath embankments. In general, the literature indicates that settlements and pore pressures are predicted quite well by numerical models. This project is an extension of such modelling, in that the stresses and deformations within the embankment itself are studied as well as those occurring in the foundation.

Conducting this research in conjunction with the Tully project is beneficial, as three trial embankments are being built as part of the project. These trial embankments are embankments which will form part of the final highway and have been equipped with monitoring equipment. The instrumentation is in the form of settlement plates to measure the settlement at the centre of the base of the embankments, piezometers to measure pore pressure within the foundation and inclinometers to measure the lateral displacements beneath the toe of the embankments. By modelling sections of the trial embankments and comparing the model results with the data collected on site, input parameters required for the numerical models can be calibrated. If this calibration is successful then models of other sections of the highway can be created with more confidence that the results will be valid.

1.2 Project Objectives

This thesis has two main objectives which are listed below.

1. To determine whether there is potential for large deformations to cause pavement cracking in the upgrade of the Bruce Highway just South of Tully, and
2. To determine, in general, what parameters govern whether pavement cracking due to delayed consolidation deformations, is likely, and what values these parameters must have to cause it.

These objectives are achieved by the creation of a series of numerical embankment models in the computer program FLAC (Fast Lagrangian Analysis of Continua). A review of current practices and theory, for the determination of settlements, focussing on consolidation settlements, is undertaken to provide a basis for the more simple models to be validated against. Case studies, where the foundation deformations resulting from embankments have been analysed, are also studied. These provide important information about the parameters of interest in such studies, the form of some of the results that can be expected and the amount of success with which numerical models have been implemented in the past to model trial

embankments. Simplified models are then created to perform a sensitivity analysis, before a fully coupled model of a section of a trial embankment is created. The trial embankment model was to be used to calibrate the correlations between the geotechnical information available for the foundation and the FLAC input parameters, for use in models of critical sections of the new length of highway. However, the quality of both the available data and the modelling results has led to a revised approach to fulfilling the objectives. Instead of modelling other sections of the highway, a parametric investigation is conducted and the results are analysed for the implications to the Tully project as well as the implications regarding pavement cracking in general.

1.3 Report Structure

Chapter 2 of this report is a detailed literature review which contains:

1. Some of the common ways of determining the increase in vertical stress at depth in a foundation due to the application of a load, such as an embankment, at the ground surface.
2. A review of the methods used in current practice to determine both immediate and the time dependant settlement, with the main focus being on the process of consolidation. The assumptions behind some of the theoretical work in this area and the difficulties in applying these theories to give accurate predictions are also discussed.
3. A review of studies in the literature which deal specifically with the deformation of foundations beneath embankments. The settlement patterns and lateral displacement patterns are discussed along with relationships for determination of lateral displacements based on settlements. The success and otherwise of numerical models created to predict the settlement, lateral displacement and the dissipation of pore water pressure beneath various trial embankments is also presented.
4. Details of the site investigation methods used to determine the soil profile beneath the highway in the Tully project. Empirical correlations required to obtain the parameters required for modelling the foundations from the different tests are presented here as well.
5. A description of the geotechnical monitoring equipment used in the trial embankments.

Chapter 3 describes some of the basic features of the program FLAC, how it differs from other numerical modelling programs available and why it is chosen. Some of the most

commonly used material models in the numerical modelling of soils, are discussed with a focus on the models which are used in this thesis. A one dimensional consolidation model created in FLAC is also presented, with its results compared to theory.

Chapter 4 outlines the aspects of the Tully Project which are relevant to this thesis, in particular the trial embankments.

Chapter 5 contains the methodology and the results of the preliminary modelling. This includes a sensitivity analysis as well as details of an investigation into a problem involving the coupled consolidation, encountered during the sensitivity analysis.

Chapter 6 contains the methodology and the results of the trial embankment modelling. It details the geometry, modelling process and how values for soil properties are assigned. In addition, the data collected from site is discussed and comparisons between the model results and the field data are made.

Chapter 7 contains the parametric investigation into pavement cracking. This includes details of the failure criteria chosen to classify pavement cracking and the reasons behind the choice of these criteria. A discussion of the modelling techniques developed for this investigation is also included along with the results of the investigation and the implications it has for the Tully Project.

Chapter 8 summarises the models and investigations carried out as part of this thesis and the conclusions drawn from them. It finishes with a list of recommendations for future work which could be conducted to expand on the research in this thesis.

Chapter 2: Literature Review

2.1 Change in Foundation Effective Stress Due Embankment Loads

2.1.1. Introduction

In determining the settlement of a foundation due to an applied load, it is necessary to compute the stress increase ($\Delta\sigma_v$) that the applied load creates at given depths. This is necessary no matter what the purpose of the foundation, be it to support an embankment or a structure.

In the idealised situation where the applied load is acting over an infinite area the problem is one dimensional and the increase in stress at any depth in the soil is equal to the applied pressure at the surface. Whilst applying a load over an infinite area is not practical, this approach can provide a good approximation of the stress increase beneath the centre of a load which covers a large area, for example where several metres of fill are placed over an entire site.

When the applied stress acts over a smaller area, or when one is interested in the stress beneath the edge of a larger area, the assumption of a one dimensional loading situation cannot be made. This is because the applied load will be distributed over a larger area as the depth of interest increases. The result of this is attenuation of the load with increasing depth and also attenuation of the load near the edges of the applied stress. For such cases, where one dimensional loading cannot be assumed, a number of different methods have been derived to calculate stress increase.

2.1.2. 2:1 Distribution Method

The simplest method is the 2:1 method, which gives a nominal average of the additional stress at a given depth. In this method it is assumed that the area over which the load is distributed increases with depth, so that the ‘walls’ of the stress field have a slope of 2:1 vertical: horizontal (see Figure 2.1). The resulting additional average stress at depth z is:

$$\Delta\sigma_{v,average} = \frac{Q}{(B+z)(L+z)} = \frac{qBL}{(B+z)(L+z)} \quad (2.1)$$

where $\Delta\sigma_{v,average}$ is the average increase in vertical stress at depth z , Q is the load applied, q is the uniform pressure applied on the footing, B is the width of the loaded area and L is the length of the loaded area (Holtz and Kovacs 1981).

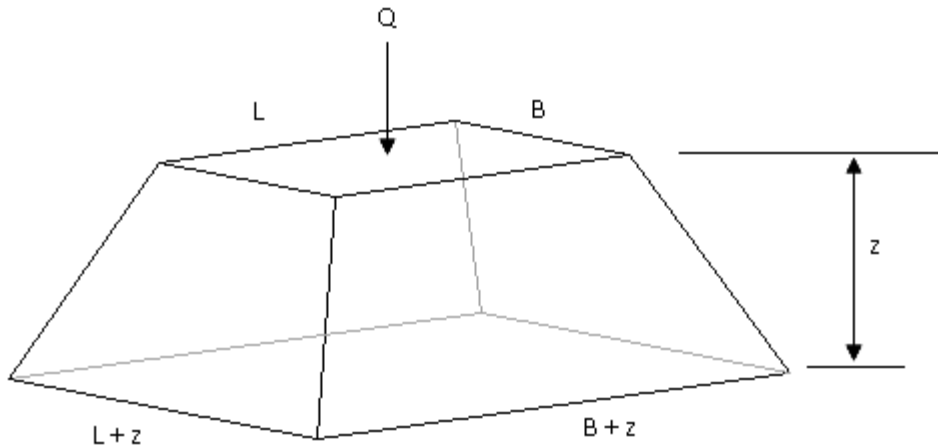


Figure 2.1: The Vertical Stress Increase with Depth Using the 2:1 Distribution

2.1.3. Boussinesq Method

In 1885 Boussinesq developed an equation (2.2) to determine the increase in vertical stress $\Delta\sigma_v$ at a horizontal distance x and depth z beneath a point load Q , refer to Figure 2.2.

$$\Delta\sigma_v = \frac{3Q}{2\pi z^2} \left(\frac{1}{1 + (x/z)^2} \right)^{5/2} \quad (2.2)$$

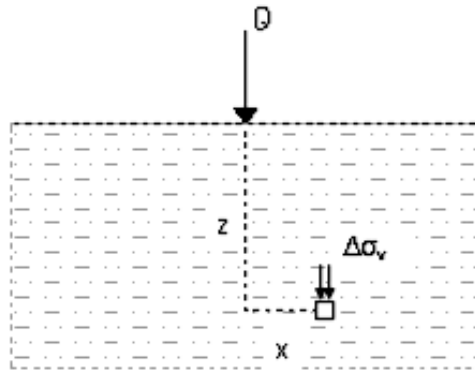


Figure 2.2: Vertical Stress Increase beneath a Point Load

The equation is based on the assumptions that the point load is acting perpendicular to the surface of a homogeneous, isotropic, linearly elastic half-space (Sivakugan 2008b). While none of these assumptions regarding the material are in general true of soils, they are simplifying assumptions often made in soil mechanics.

Integration of Equation (2.2) along a line gives the increase in vertical stress at depth z , due

to a uniformly distributed line load see equation (2.3).

$$\Delta\sigma_v = \frac{2Q}{\pi z} \left(\frac{1}{1 + (x/z)^2} \right)^2 \quad (2.3)$$

Similarly the increase in vertical stress at depth due to a uniform rectangular load can be determined by integration of equation (2.2) over the rectangular area. In 1935 Newmark performed this integration (vide. Holtz and Kovacs 1981). The resulting $\Delta\sigma_v$ beneath a corner of the loaded area can be expressed as:

$$\Delta\sigma_v = qI \quad (2.4)$$

where q is the applied vertical stress and I is an influence factor which is a function of $m = x/z$ and $n = y/z$ and can be determined using Figure 2.3.

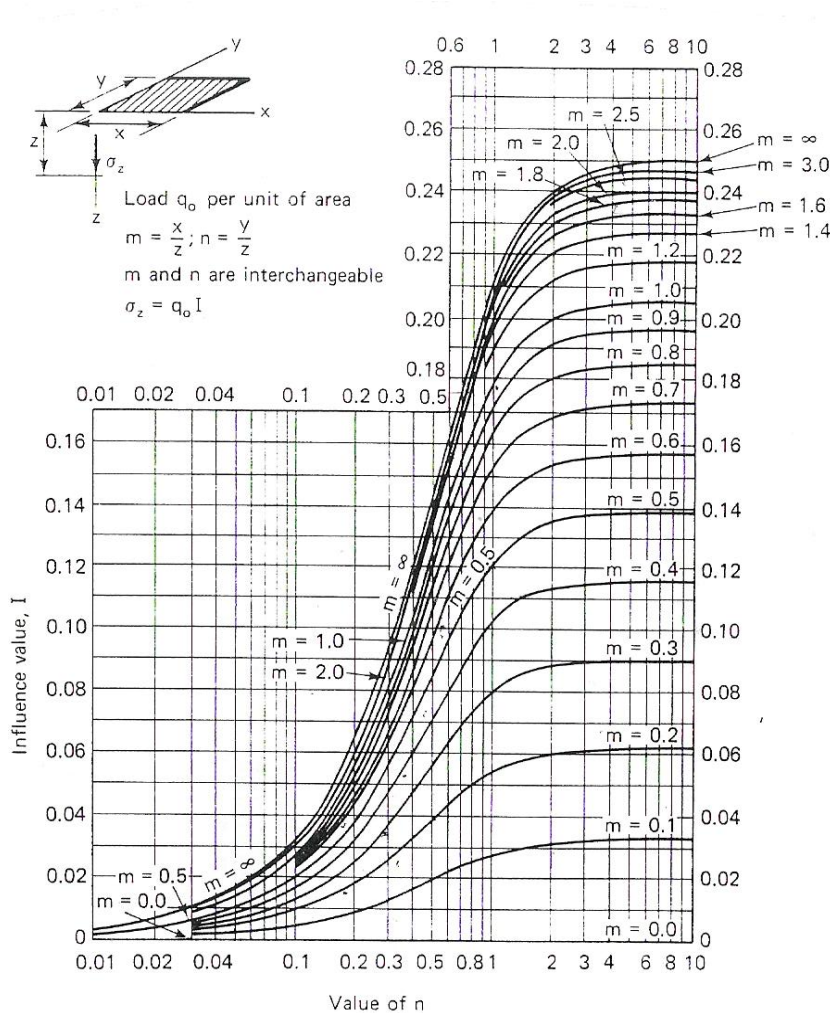


Figure 2.3: Influence Factor for a Rectangular Loaded Area Based on Boussinesq's Equation (U.S.Navy 1971)

Another integration of the Boussinesq equation, which is of more importance to this thesis, is for a trapezoidal loading. Again the increase in vertical stress at depth $\Delta\sigma_v$ can be related to an influence factor and the applied load through equation (2.4). The influence factor in this case is taken from Figure 2.4. This can be used to determine the increase of vertical stress beneath a long embankment.

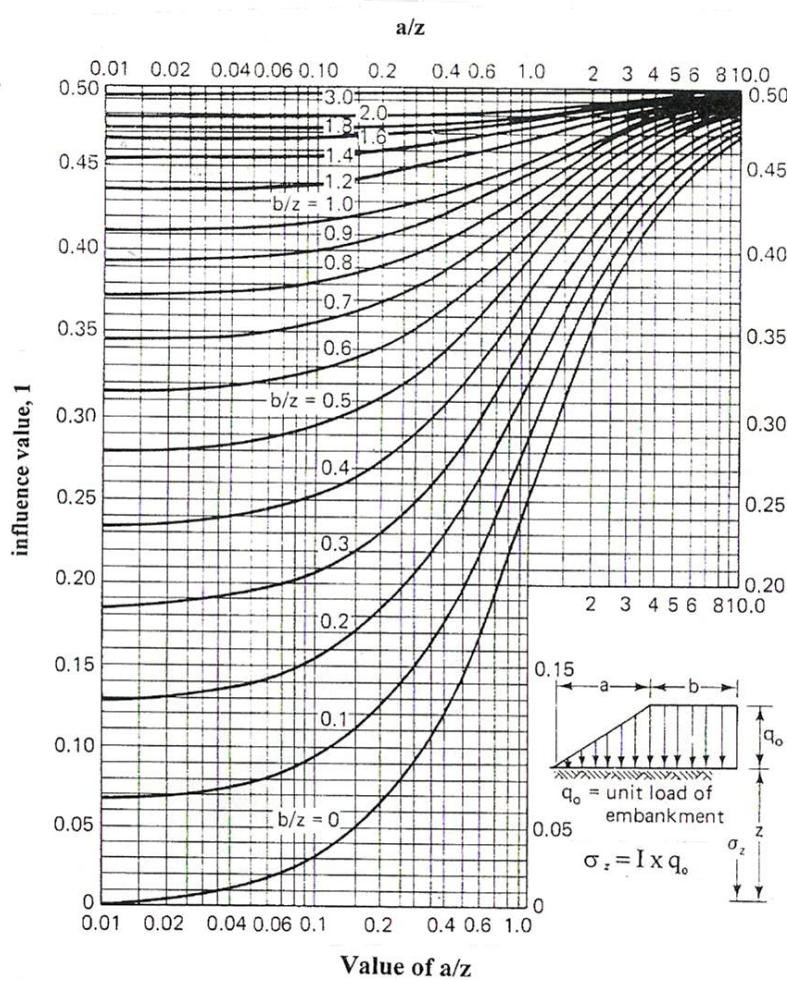


Figure 2.4: Influence Factors for the Vertical Stress Increase

beneath a Long Embankment (Osterberg 1957)

2.1.4. Westergaard's Method

Many natural sedimentary soil deposits are characterised by alternating horizontal layers of granular soils and clays. Such deposits, known as varved clays, have properties that are significantly different from those assumed by Boussinesq. However, their properties do conform to the assumptions made by Westergaard (1938) when he developed a relation to determine the stress increase at a given depth below a point load (refer to Figure 2.2).

Westergaard's equation (2.5) assumes an elastic medium, divided into layers by infinitely thin and rigid sheets, which allow vertical movement but not horizontal movement (Holtz and Kovacs 1981; Sivakugan 2008b).

$$\Delta\sigma_v = \frac{Q}{z^2\pi} \left(\frac{1}{1 + 2(x/z)^2} \right)^{3/2} \quad (2.5)$$

Like Bousinesq's equation, this equation can be integrated to give the increase in stress beneath a uniform line load and a uniform rectangular stress distribution. A chart, similar to Figure 2.3 has been developed from Westergaard's equation, refer to Figure 2.5.

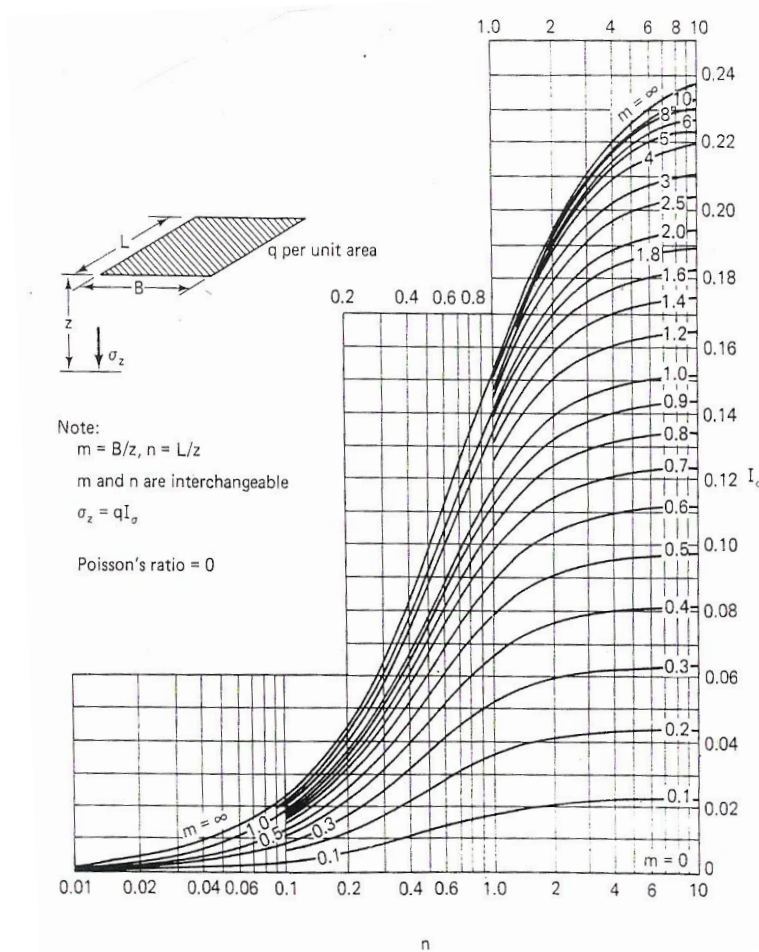


Figure 2.5: Influence Factor for a Rectangular Loaded Area Based on Westergaard's Equation (Fadum 1948)

A comparison between Boussinesq's and Westergaard's equations reveals that for values of $x/z < 1.5$ Bousinesq's equation gives higher stresses, and for values of $x/z > 1.5$ the two theories give approximately equal results (Holtz and Kovacs 1981).

2.2 Settlements

2.2.1. Introduction

Settlement is the total vertical deformation at the surface of a soil caused by a net change in the applied vertical stress. The deformation may be downwards if the applied stress is increased, or upwards if the stress is decreased, in which case the soil is said to undergo swelling. In soils the settlement is broken into three types: initial settlement; primary consolidation settlement; and secondary compression or creep. The total settlement is then the sum of the three components, refer to equation (2.6),

$$s_t = s_i + s_c + s_s \quad (2.6)$$

where s_t is the total settlement, s_i is the immediate settlement, s_c is the consolidation settlement and s_s is the secondary compression (Holtz and Kovacs 1981).

The relative contribution of each of the above three components to the total settlement is highly dependent on the type of soil, its permeability characteristics and its loading history. In granular soils, which are generally considered to be well drained, the majority of settlement is immediate (Sivakugan 2008b), and is the result of grains moving into voids, or moving to create smaller voids. At present the mathematics of this process is still not well understood, and settlements are calculated using one of the many semi-empirical methods developed (Leonards 1962). In some very fine grained or silty sands, the settlement is time dependant (Murthy 2003), but in general consolidation is not a part of the settlement of granular soils.

Cohesive soils on the other hand, have much lower permeability, and can have much higher compressibility. These soils are generally assumed to be saturated, and the rate of settlement is controlled by the rate at which water can drain from the soil. This time-dependant settlement process is known as consolidation. Clay can also experience immediate or distortion settlement, which is often estimated using elastic theory, though, the magnitude of this is generally much smaller than the consolidation settlement. Both granular and cohesive soils also undergo a process called creep, which is a time dependant settlement that occurs at a constant vertical stress. This is the secondary compression settlement in equation (2.6).

The strata beneath the embankments which will be constructed as part of the new section of the Bruce Highway consist of both granular and cohesive soils layers. However, due to the high compressibility of clays in comparison to granular soils, the rest of this section will focus on the settlements of clays, and methods used to calculate them.

2.2.2. Immediate Settlement

Immediate settlement, also called elastic settlement, is as the name suggests, settlement which occurs immediately after the increase in stress is applied. Due to the rapid nature of this settlement, and the low permeability of clays, it is assumed that the soil is undrained for this settlement and acts as an elastic material. Janbu et al. (1956, vide. Sivakugan 2008b) proposed that the magnitude of the initial settlement could be calculated using the following equation,

$$s_i = \frac{qB}{E_u} \mu_0 \mu_1 \quad (2.7)$$

where q is the applied stress, B is the width over which the stress is applied, E_u is the undrained modulus of elasticity and μ_0 and μ_1 are correction factors. The correction factors have since been modified by Christian and Carrier III (1978, vide. Sivakugan 2008b), and can be determined using Figure 2.6.

Alternatively, these settlements could also be computed using a Finite Element, or Finite Difference computer program, such as FLAC, which will be used in this thesis.

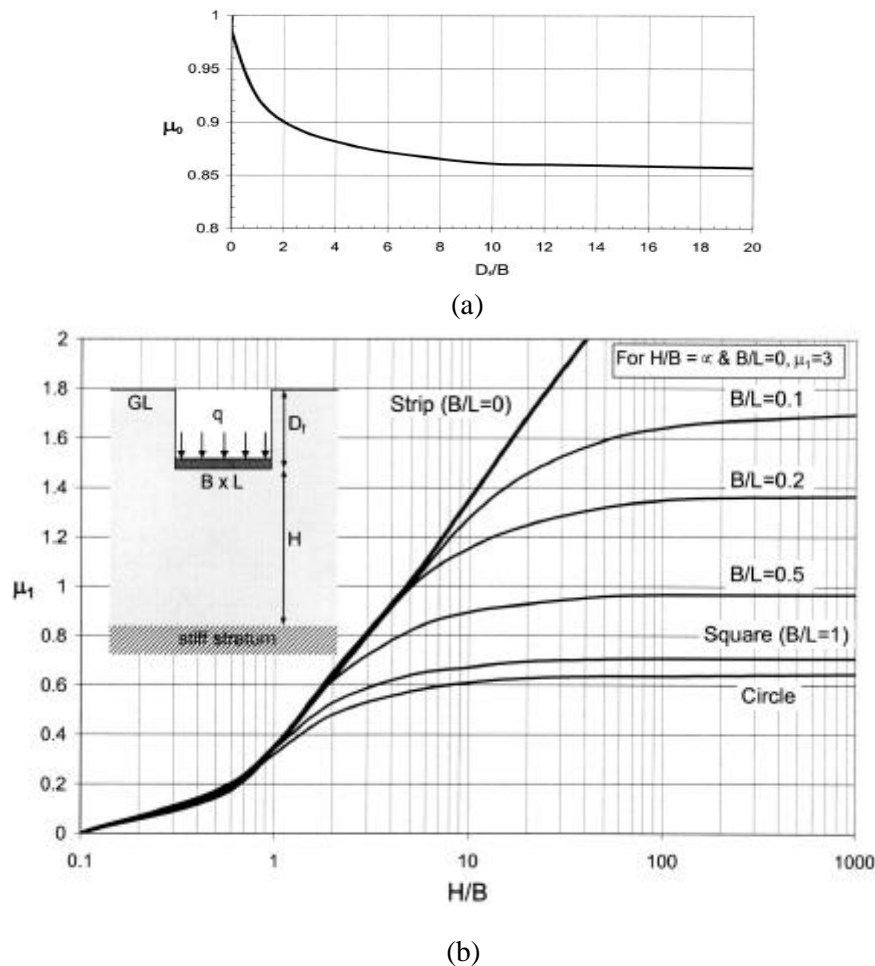


Figure 2.6: Values of (a) μ_0 and (b) μ_1 for Immediate Settlement Computation (Sivakugan 2008b)

2.2.3. Consolidation

When a stress is applied to the surface of a layer of saturated cohesive soil, the stress is initially transferred to the pore water. This effect is a result of the high stiffness of the water compared with the soil skeleton, and the inability of the water to drain from the soil (Leonards 1962). With time the hydraulic gradients induced by the increase in stress cause the pore water to drain from the clay, allowing the clay to compress. As the clay compresses the excess stress from the applied load is transferred to the soil skeleton, and eventually all of the applied stress will be in the soil skeleton. This is the process known as consolidation. In consolidation the difference between total stress and effective stress is particularly important. Effective stress σ'_v is defined by:

$$\sigma'_v = \sigma_v - u \quad (2.8)$$

Where σ_v is the total stress and u is the pore water pressure.

One Dimensional Consolidation

One dimensional consolidation theory is based on the assumptions that all drainage occurs through either the top surface, the bottom surface or both surfaces, and similarly that all deformation only occurs in the vertical direction. With these restrictions it is clear that the settlement per unit of original height is equal to the change in volume per unit of original volume.

$$\frac{s_c}{H} = \frac{\Delta V}{V} \quad (2.9)$$

In geotechnical engineering, however, it is more common to express the volume ratio in terms of a void ratio (e). Void ratio is defined as the ratio of the void volume (V_v) to the volume of solids (V_s), see equation (2.10) and Figure 2.7.

$$e = \frac{V_v}{V_s} \quad (2.10)$$

For the case where the soil is saturated, which is the only case considered in conventional consolidation theory, the volume of air is zero. Therefore, any change in volume of the soil is due to a change in the volume of water in the soil; that is the change in volume is equal to the water squeezed out of the soil. By inspection of Figure 2.8 the following relationship can be deduced:

$$\frac{\Delta V}{V} = \frac{\Delta e \times V_s}{V_s(1 + e_0)} = \frac{\Delta e}{(1 + e_0)} \quad (2.11)$$

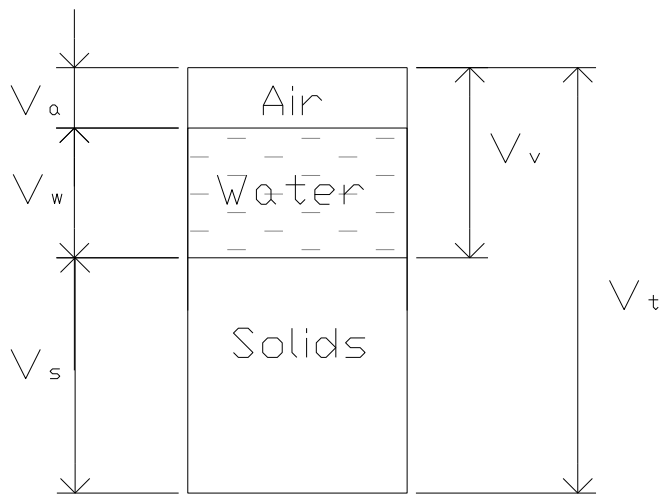


Figure 2.7: The Three Phases in Soils

Hence Equation (2.9) becomes:

$$S_c = \frac{\Delta e}{1 + e_0} H \quad (2.12)$$

To determine the final consolidation settlement using Equation (2.12), it is necessary to determine the change in void ratio induced by a given change in stress. As a result of the complicated, non-linear stress-strain relationship of soils this must be determined by laboratory tests on undisturbed samples of the soil.

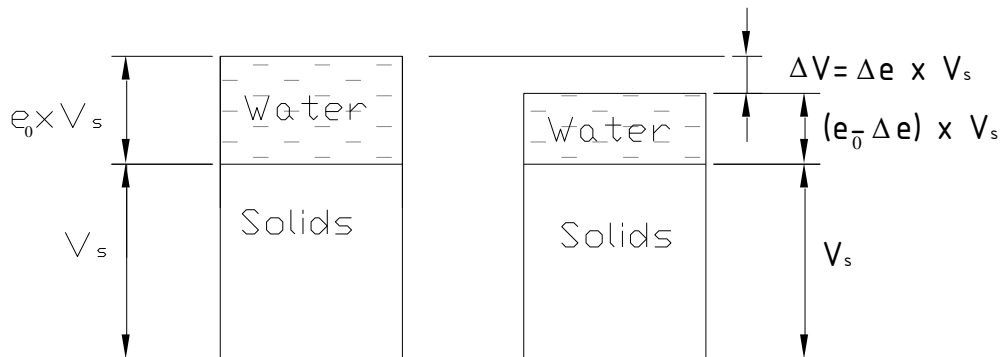


Figure 2.8: Volume - Void Ratio Relationship in a Saturated Soil

Odometer Test and $e - \log \sigma_v'$ Curve

The oedometer test is a laboratory test which simulates one dimensional consolidation. In this test a cylindrical undisturbed sample of the in-situ clay layer, with diameter to height ratio between 2.5 and 5, is placed in an oedometer see Figure 2.9. The sample is then subjected to incremental loading, with the sample being allowed to consolidate and come to equilibrium with negligible further settlement after each load increment. For each load increment the applied stress and the vertical deformation of the sample are measured. The collected data is usually represented by plotting the void ratio (e) of the sample against log of the effective stress ($\log \sigma_v'$). This graph is a representation of the relationship between stress increase and change in void ratio, and, as much research has shown that the end-of-primary-consolidation void ratio-effective stress relationship is independent of the duration of primary consolidation, this graph can be used directly to determine the settlements in the field (Mesri and Choi 1985). The important features of an $e - \log \sigma_v'$ diagram are shown in Figure 2.10.

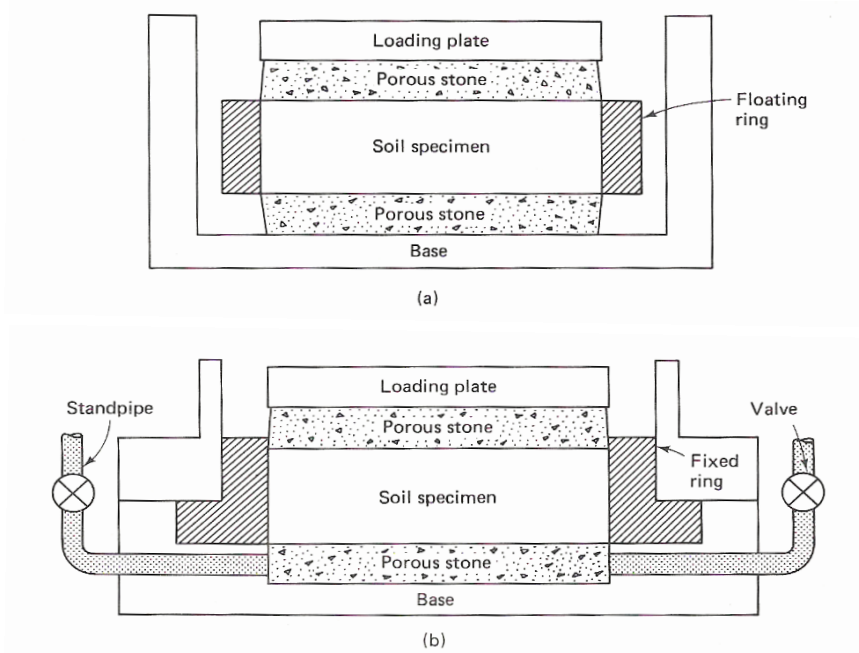


Figure 2.9: Schematic of (a) a Floating Ring Oedometer and (b) a Fixed Ring Oedometer (U.S. Army Corps of Engineers, 1970 vide. Holtz and Kovacs 1981)

The first, comparatively flat section of the $e - \log \sigma_v'$ diagram is the recompression zone. This zone represents the change in void ratio for changes in stress which take the total effective stress of the soil to less than the preconsolidation pressure (σ_p'), which is the maximum effective stress the soil has previously been consolidated at. During recompression, only minor interparticle slip and particle restructuring occurs. For the

purpose of settlement calculations the curve in this region is approximated as a straight line, the slope of which is defined as the recompression index (C_r). Typically C_r is in the range of 0.01 – 0.2, where the lower values correspond to highly structured clays with brittle interparticle bonds, and the higher values correspond to organic silts, highly plastic clays and fissured clays (Mesri and Choi 1985).

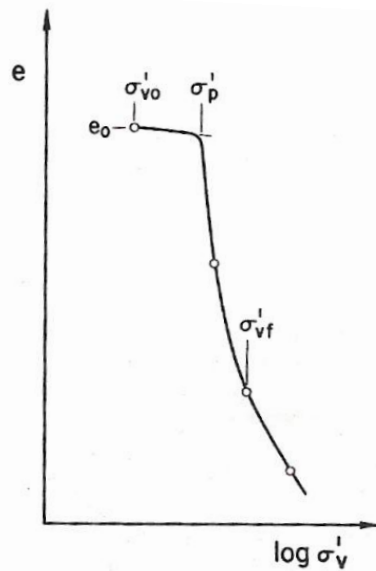


Figure 2.10: General Features of an e - $\log \sigma'_v$ Curve (Mesri and Choi 1985)

The section of the curve corresponding to stresses above the preconsolidation pressure is called the compression region and is also known as the virgin consolidation line. The dramatic increase in the slope of the curve in this region corresponds to a restructuring of the clay fabric. In this region interparticle bonds are broken and the result is high compressibility (Mesri and Choi 1985). The slope of the virgin consolidation line is the compression index (C_c), which is used in settlement calculations. The following empirical equations have been proposed to estimate C_c using the Liquid Limit (LL) of the clay:

$$C_c = 0.009(LL - 10\%) \quad (2.13)$$

for undisturbed clays (Terzaghi and Peck 1967), and

$$C_c = 0.007(LL - 10\%) \quad (2.14)$$

for remoulded clays (Skempton 1944 vide. Terzaghi and Peck 1967)

However, for many clays this curve is highly non-linear, and expressing C_c as a single value is inaccurate. Mesri and Choi (1985) proposed a new parameter to replace C_c in settlement calculations. The new parameter C'_c is the slope of the line joining the point P, where a

recompression line extending from the point (e_0, σ_{v0}') reaches σ_p' , and the point on the $e - \log \sigma_v'$ curve corresponding to the final effective stress.

In Figure 2.10 there is a well defined point (σ_p') which separates the compression and recompression regions. Results of laboratory oedometer tests often do not show the preconsolidation pressure so clearly. Disturbance in the sample, which can occur during sampling, preservation, storage and sample preparation, has been found to flatten the $e - \log \sigma_v'$ curve (Leonards 1962), refer to Figure 2.11. As the value of σ_p' has a significant effect on the predicted settlement, as will be discussed later, work has been done to predict the field value of σ_p' and the corresponding $e - \log \sigma_v'$ curve. The earliest and most popular method for determining σ_p' is a graphical procedure, which was proposed by Casagrande in 1936. Methods have also been proposed by Burmister (1942, 1951) and Schmertmann (1955) (Leonards 1962).

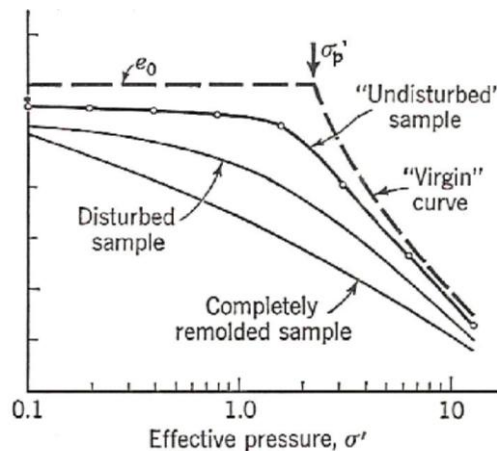


Figure 2.11: Effect of Disturbance on $e - \log \sigma_v'$ Curve (Leonards 1962)

Total Settlement Calculations using $e - \log \sigma_v'$ Curve

To determine the total consolidation settlement the values of C_c , C_r and σ_p' from the $e - \log \sigma_v'$ curve are used to evaluate the term Δe in Equation (2.12). However, the calculation used is dependent on the stress history of soil, which determines whether the clay is in a normally consolidated or overconsolidated state.

Normally Consolidated Clays

A clay which in its in-situ state has consolidated and is under the maximum stress it has ever been exposed to, is known as a normally consolidated (*NC*) clay. For clays which have only recently reached this equilibrium state, this means that the current overburden pressure

(σ_{v0}') is equal to the preconsolidation pressure (σ_p') (Bjerrum 1973). By inspection of Figure 2.11 it is clear that the change in void ratio for an increase in stress will follow the Virgin Consolidation line. Therefore:

$$\Delta e = C_c \log \frac{\sigma_{v0}' + \Delta\sigma_v}{\sigma_{v0}'} \quad (2.15)$$

and

$$\text{sett} = \frac{H}{(1 + e_0)} C_c \log \left(\frac{\sigma_{v0}' + \Delta\sigma_v}{\sigma_{v0}'} \right) \quad (2.16)$$

Overconsolidated Clays

Overconsolidated clays, are clays which have fully consolidated at a pressure, σ_p' , greater than their current overburden pressure (σ_{v0}') . Overconsolidation is the result of factors including erosion, desiccation of surface layers, tectonic forces, sustained seepage forces and temporary overloading arising from conditions such as an overriding ice sheet (Leonards 1962). When determining the settlement of overconsolidated clays, the value of σ_p' is highly important, as the compressibility of clay is about ten times greater for pressures above σ_p' than for pressures below σ_p' (Duncan 1993). Also the process required to determine the consolidation settlement is dependent on whether or not the final effective stress $(\sigma_{v0}' + \Delta\sigma)$ exceeds σ_p' .

If the final effective stress does not exceed the preconsolidation pressure (σ_p') then the $e - \sigma_v'$ relationship is characterised by the recompression part of the $e - \log \sigma_v'$ curve. The settlement is therefore:

$$\text{sett} = \frac{H}{(1 + e_0)} C_r \log \left(\frac{\sigma_{v0}' + \Delta\sigma_v}{\sigma_{v0}'} \right) \quad (2.17)$$

On the other hand if the final effective stress of the clay does exceed the preconsolidation pressure then the $e - \sigma_v'$ relationship first follows the recompression curve and then follows the virgin consolidation line. For this case the total consolidation settlement is

$$\text{sett} = \frac{H}{(1 + e_0)} \left[C_r \log \left(\frac{\sigma_p'}{\sigma_{v0}'} \right) + C_c \log \left(\frac{\sigma_{v0}' + \Delta\sigma_v}{\sigma_p'} \right) \right] \quad (2.18)$$

Quasi Preconsolidation Pressure

If a normally consolidated clay remains at a constant effective stress for hundreds or thousands of years then the effective σ_p' becomes larger than σ_{vo}' (Bjerrum 1973; Leonards 1962). This phenomenon is the result of the clay continuing to settle after primary consolidation has finished. As the clay settles the particles are rearranged into a more stable configuration, resulting in higher strength and lower compressibility. If an oedometer test is then performed on a sample of the clay, the sample will appear to be overconsolidated, as shown in Figure 2.12 (Bjerrum 1973). If a small additional load is applied to the aged clay, so that the quasi-preconsolidation pressure is not exceeded, the settlements will be small. However, conventional settlement analysis is unable to predict the settlements in this case. In contrast, if a larger load is applied, so that the quasi-preconsolidation pressure is exceeded then the settlements will be large and can be predicted using conventional settlement analysis (Bjerrum 1973). This preconsolidation pressure effect also occurs in over consolidated clays. A similar effect can also be the result of water table variations, thixotropic effects or cementation (Bjerrum 1973; Leonards 1962).

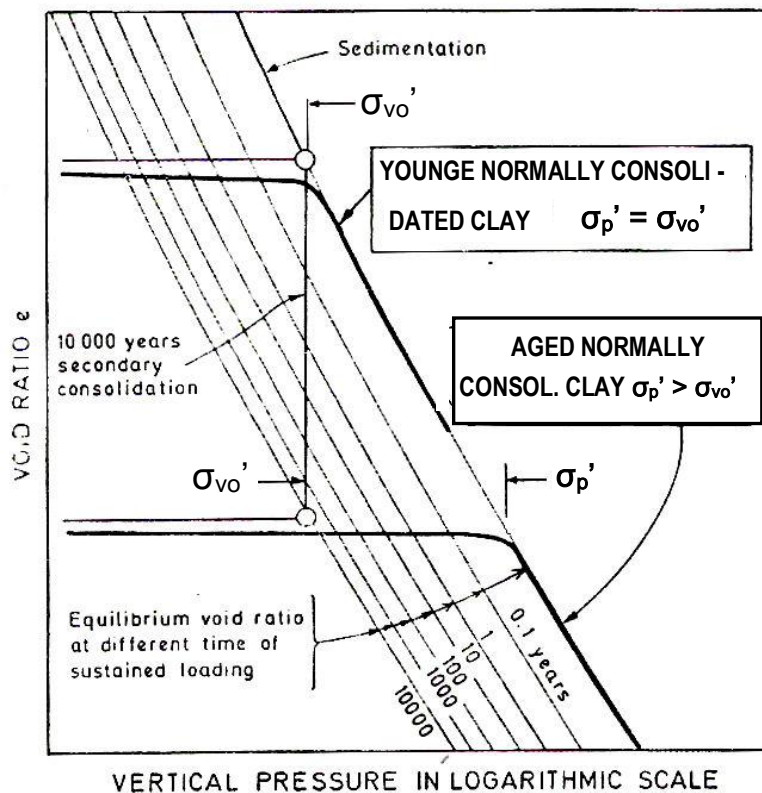


Figure 2.12: Effect of Aging on σ_p' (Bjerrum 1973)

Total Consolidation Settlement Calculations using Coefficient of Compressibility

An alternative method for determining the total consolidation settlement when a clay layer is subjected to an increase in stress involves the use of the following equation:

$$\text{sett} = \Delta H = m_v \Delta \sigma H \quad (2.19)$$

where m_v is the coefficient of volume compressibility, which is defined as the volumetric strain per unit increase in effective stress. For one dimensional consolidation this is:

$$m_v = \frac{\Delta H / H}{\Delta \sigma} \quad (2.20)$$

This is a much simpler calculation than using the $e - \log \sigma'_v$ curve, but it is not as accurate because m_v varies with σ'_v . To get the most accurate result using this method it is necessary to use the value of m_v appropriate to the stress level in the clay.

The value of m_v is related to the oedometer modulus (D) also known as the constrained modulus, and this is related to Young's modulus and poisons ratio via:

$$D = \frac{1}{m_v} = \frac{(1 - \nu)}{(1 + \nu)(1 - 2\nu)} E \quad (2.21)$$

The values of D and m_v can be determined from an oedometer test, with the values of m_v usually in the range 0.05 MPa^{-1} to 1.5 MPa^{-1} , the lower values corresponding to very stiff clays, and the higher values corresponding to soft clays and peats (Sivakugan 2008a).

Time Rate of Consolidation

The settlement calculations described in the previous sections all determine the final consolidation settlement; that is the settlement after a significantly long period of time when the stresses and pore pressures have reached equilibrium. Often in practice, it is important to know the settlement at a given time much less than the required time to complete consolidation. Terzaghi (1925) developed a method for determining this, for the case of one-dimensional consolidation. Theoretically the same can be done for three dimensions however, the problem is so complex that a generally accepted solution has still not been determined. The assumptions upon which Terzaghi's theory is based are:

1. The pressure increment is applied instantaneously.
2. The soil is homogeneous and saturated.
3. The water and soil grains are incompressible.
4. Both drainage and strains occur only in one direction.
5. Strains are small in comparison to the initial height.
6. Darcy's Law,

$$v = ki \quad (2.22)$$

where v is the pore water velocity, k is the coefficient of permeability and i is the hydraulic gradient, is valid.

7. The coefficients of permeability and volume compressibility are constant during consolidation.

Using conservation of mass (change in volume = flow out – flow in), Darcy's law, and phase relations for V_v and V_s , the governing differential equation for consolidation can be shown to be:

$$c_v \frac{\partial^2 u}{\partial z^2} = \frac{\partial u}{\partial t} \quad (2.23)$$

where c_v is the coefficient of consolidation, which is defined as.

$$c_v = \frac{k}{m_v \gamma_w} \quad (2.24)$$

The solution to this equation for the conditions, where the clay layer is drained from both the top and bottom (at $z = 0$ and $2H_{dr}$; $u = 0$) and where the initial distribution of excess pore water pressure is uniform (at $t = 0$, $u = u_0$), is:

$$u(z, t) = u_0 \sum_{m=0}^{m=\infty} \frac{2}{M} \sin(MZ) e^{-M^2 T} \quad (2.25)$$

where $u(z, t)$ is the change in pore pressure due to the applied load at depth z and time t , u_0 is the initial pore pressure increase (which is equal to the applied load),

$$M = \frac{(2m + 1)\pi}{2}, \quad m = 0, 1, 2, 3, \dots \quad (2.26)$$

$$T = \frac{c_v t}{H_{dr}^2} \quad (2.27)$$

and

$$Z = \frac{z}{H_{dr}} \quad (2.28)$$

T and Z are dimensionless time and depth factors, and H_{dr} is the longest drainage distance, which is half of the clay layer thickness for a doubly drained layer. In order to relate the changes in pore pressure u , gained from equation (2.25), to the settlement, the percentage consolidation, or consolidation ratio is used. The percentage consolidation U_z , at depth z and time t , can be shown to be:

$$U_z = \left(1 - \frac{u}{u_0}\right) \times 100 \quad (2.29)$$

By combining equations (2.25) and (2.29) a relationship between the consolidation ratio and the time factor can be obtained. This relationship is show in Figure 2.13.

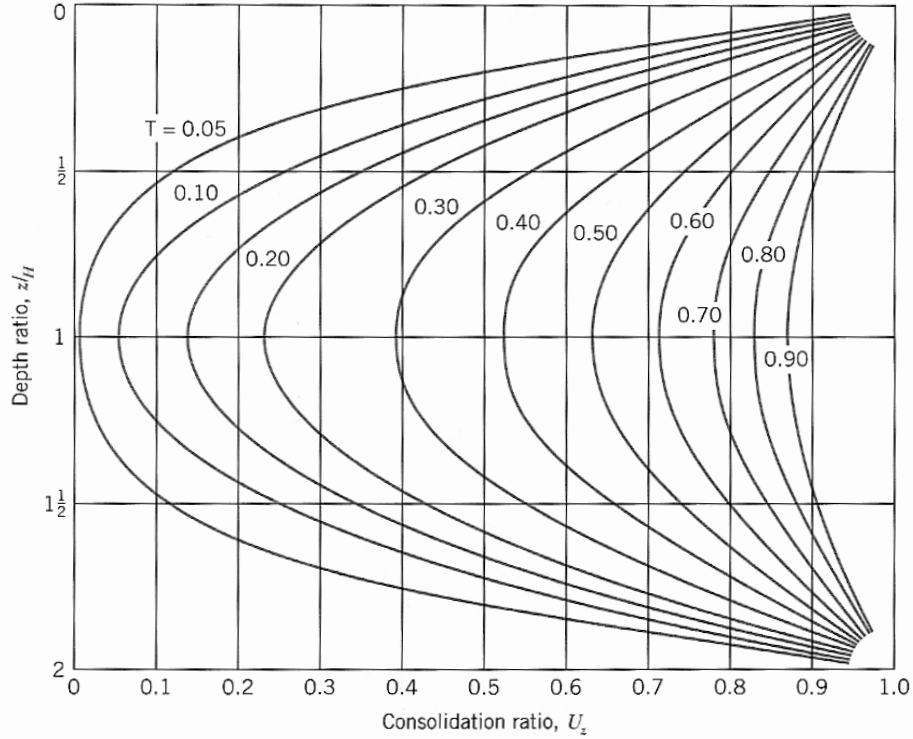


Figure 2.13: Consolidation Ratio as a Function of Depth and Time Factors, for Uniform Initial pore pressure in a Doubly Drained Layer (Cernica 1995)

It is in practise more relevant to find the average degree of consolidation for the entire depth of the clay layer, at a given time. This is defined as the total volume change (or height change for 1D consolidation) at time t , divided by the ultimate total volume (or height) change, and is the average value of U_z . This average value can be determined by dividing the area of the dissipated excess pore water pressure in Figure 2.13 by the initial area of excess pore water pressure (Sivakugan 2008a). Mathematically this involves integration of equation

(2.29), with equation (2.25) substituted in for u , and results in the equation:

$$U_{avg} = 1 - \sum_{m=0}^{m=\infty} \frac{2}{M^2} e^{-M^2 T} \quad (2.30)$$

This is graphed in Figure 2.14. By multiplying the value of U_{avg} obtained from Figure 2.14, for a given time, by the total settlement calculated in accordance with sections 3.3.4 or 3.3.5, the overall settlement at any given time can be determined.

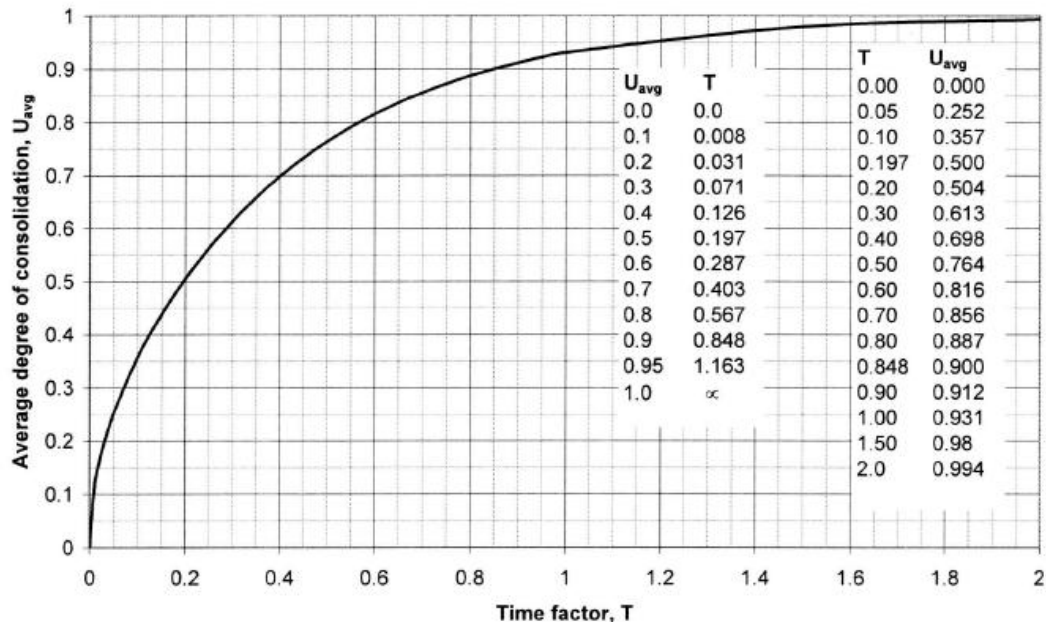


Figure 2.14: Average Degree of Consolidation (U_{avg}) - Time Factor (T)

Relationship (Sivakugan 2008a)

Equations (2.25) and (2.30) along with Figure 2.13 and Figure 2.14 are all derived for the case where the initial excess pore water pressure distribution with depth is uniform. In many practical situations this is not the case as the stress increase due to an applied load decreases with depth (as discussed in Chapter 2) and the clay compressibility sometimes decreases with depth (Duncan 1993). Terzaghi and Frolich (1936) and Janbu (1965) (vide. Duncan 1993) considered solutions to equation (2.23), the governing equation for one-dimensional consolidation, for cases where the initial pore water pressure decreased with depth. They found that, for such distributions, if drainage occurred only at the top of the layer, consolidation would proceed more rapidly than if the initial distribution were linear, this finding is shown in Figure 2.15. In spite of these findings, Curve A in Figure 2.15 which is

equivalent to Figure 2.14 is almost always used when calculating settlements in practice, even when curve B or C may be more appropriate. This can lead to a reduction in the accuracy of settlement predictions (Duncan 1993).

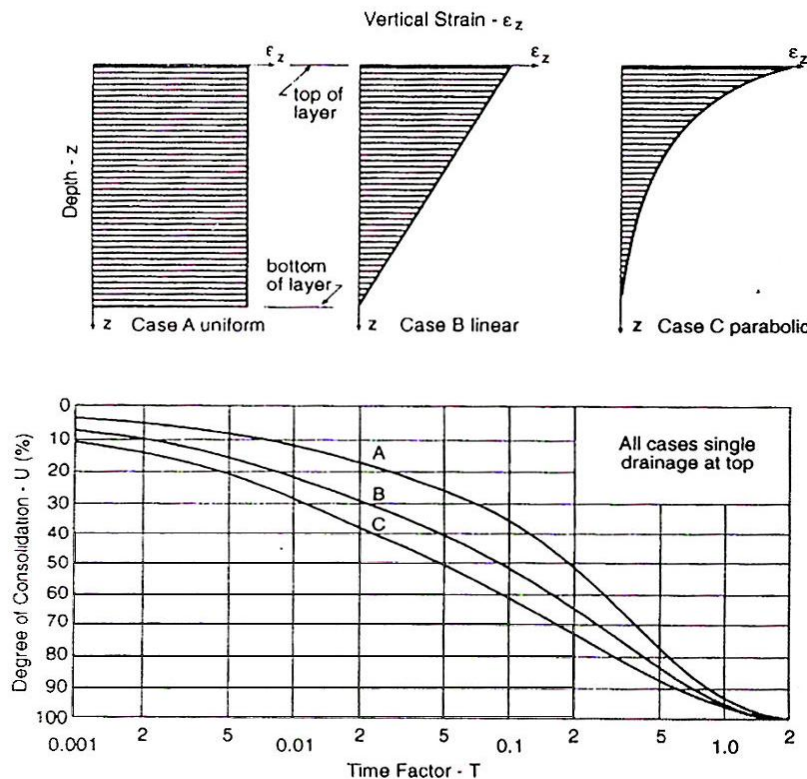


Figure 2.15: The Influence of Strain Profile on the Rate of Consolidation (After Terzaghi and Frolich (1936) and Janbu (1965) vide. Duncan 1993)

Determination of c_v

There are two procedures currently in widespread use for the determination of c_v , Casagrande's logarithm of time method and Taylor's square root of time method. Both methods require measurement of the time rate of consolidation in an oedometer test.

In Casagrande's method the settlement readings (R) are plotted against the logarithm of time see Figure 2.16. The idea of the method is to determine the time corresponding to 50% consolidation (t_{50}), which can then be used in equation (2.27) to find c_v . Firstly, R_{100} the settlement corresponding to 100% consolidation is taken to be point where the tangent of the curve at the point of inflection meets the back extension of the straight line portion of the curve corresponding to secondary compression, refer to Figure 2.16. R_0 the dial reading corresponding to zero consolidation, is found by choosing any two times such that $t_2 = 4t_1$, and then marking the point a distance $R_2 - R_1$ above R_1 . R_{50} is then given by:

$$R_{50} = \frac{1}{2}(R_0 - R_{100}) \quad (2.31)$$

and t_{50} is the time corresponding to R_{50} .

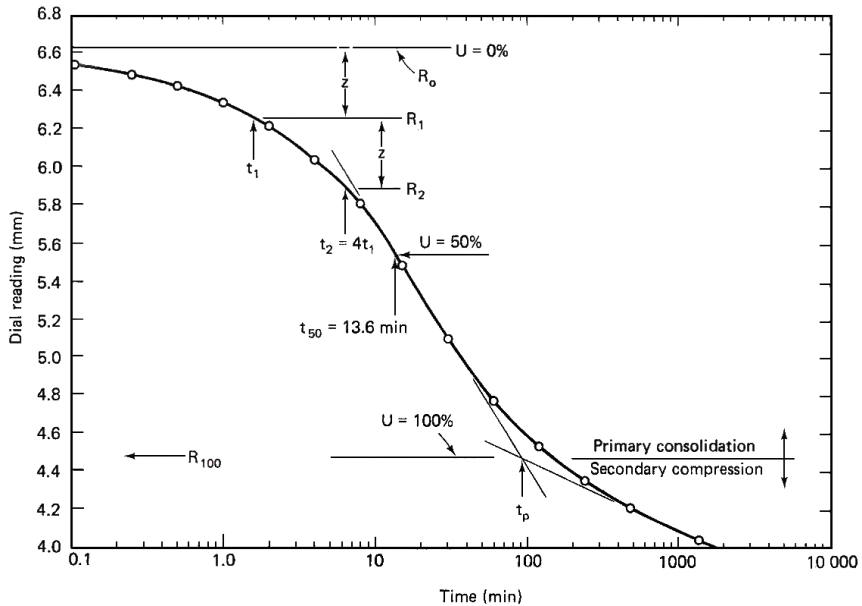


Figure 2.16: Casagrande's Logarithm of Time Method (Holtz and Kovacs 1981)

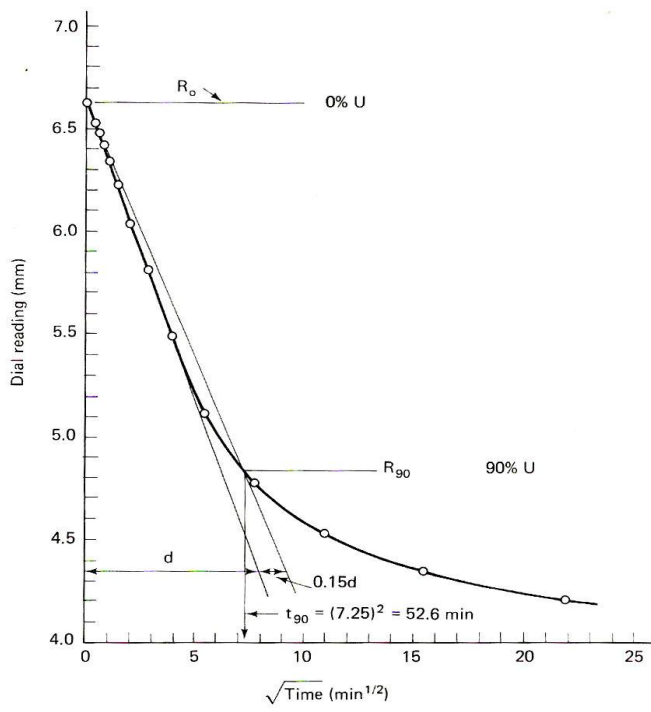


Figure 2.17: Taylor's Square Root of Time Method (Holtz and Kovacs 1981)

Taylor's method requires the dial gauge settlement reading to be plotted against the square root of time, refer to Figure 2.17, from which the value t_{90} and subsequently c_v can be found. Firstly, R_0 is found by extending the initial straight line section of the curve back to the point

where $t = 0$. A second straight line is then drawn from R_0 so that the time at each point on this curve is 1.15 times as large as the time at the corresponding point of the first line. The point where this second line intersects the laboratory curve corresponds to 90% consolidation, and t_{90} can be read directly off the graph. By substitution of t_{90} into equation (2.27) c_v can be found.

Difficulties in Accurately Determining Consolidation Settlement

In the 27th Terzaghi Lecture, presenter J. Michael Duncan (1993) discussed a number of factors affecting the accuracy of settlement calculations, including determination of the preconsolidation pressure σ_p' , the value of c_v , embedded sand layers and consolidation theory itself.

As discussed previously the value of σ_p' used has a significant effect on the settlement calculated due to the considerable difference in clay compressibility before and beyond σ_p' . Determining an appropriate value to use for σ_p' can be difficult as it often varies with depth. Also, there is often much scatter in the σ_p' determined from multiple laboratory tests on samples from the same region even when care is taken to avoid sample disturbance.

There are many factors which complicate the selection of an appropriate value for c_v , some of which stem from the incorrect assumption that c_v is a constant throughout consolidation. Firstly, c_v is an order of magnitude greater below σ_p' than it is above σ_p' , which is a problem when the stress increase takes the clay from an overconsolidated state to an underconsolidated state. Secondly, the two commonly used methods for laboratory determination of c_v , Cassagrande's method and Taylor's method, generally give differing values of c_v . The two methods would give the same results if laboratory consolidation curves matched theoretical curves, but in most cases this does not occur and Taylor's method gives a higher c_v value. Another difficulty is that the value of c_v is dependant on the drainage path length (H_{dr}) which decreases as consolidation proceeds. The use of initial or final H_{dr} should be the same in both laboratory determination of c_v and field calculations. If the initial H_{dr} is used then c_v will generally increase as the consolidation pressure increases, even if the soil is normally consolidated to begin with. Also test data indicates that c_v may increase as the initial drainage path length increases.

Whether embedded sand layers are just lenses or whether they are capable of facilitating drainage is of great importance in the determination of settlement. If there is a sand layer in the centre of a clay layer this can halve the drainage length which in turn speeds

consolidation by four times. Unfortunately there currently is no quantitative method to determine if a sand layer can provide drainage.

Finally, the accuracy of settlement calculations is limited by the assumptions upon which conventional consolidation theory is based. As previously mentioned c_v is not a constant as assumed by the theory. The other main problem is that consolidation theory assumes that the stress strain behaviour of soils is linear and elastic, neither of which are true, as evidenced by the $e - \log \sigma'_v$.

2.2.4. Secondary Compression Settlement

Secondary compression or creep is time dependant settlement which occurs at a constant value of stress. In the 1920's Terzaghi conducted experiments involving hydraulic conductivity which concluded that secondary compression effects occur both during and after primary consolidation. However, for simplicity many engineers assume that this secondary settlement occurs only after primary consolidation has finished (Olson 1998). Mersi (1985; 2005) goes as far as to define secondary settlement as settlement that occurs after primary consolidation has ended, and it is this definition which is used in the following section for the purpose of secondary settlement calculations, see Figure 2.18.

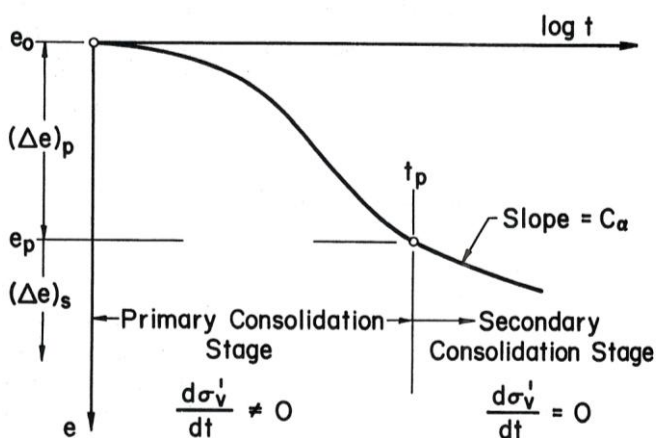


Figure 2.18: Void Ratio - Log Time Graph Showing the Definition of Secondary Compression used in Calculations

Calculation of Secondary Compression

The secondary settlement of soft clays can be described well using the secondary compression index:

$$C_\alpha = \frac{\Delta e}{\Delta \log t} \quad (2.32)$$

which is the slope of a Void ratio – Log time graph in the region where the time is greater than the end of primary consolidation time (t_p), see Figure 2.18. The value of C_α can be obtained from a standard oedometer test described previously, and this value can be used directly for calculations of the secondary settlement in the field (Mesri and Choi 1985). An alternative way of determining C_α is to use an empirical correlation relating C_c to C_α . Mesri and Godlewski (1977, vide Mesri and Choi 1985) observed that for a wide variety of natural soils the value of C_α/C_c ranged between 0.02 and 0.10. More specifically, for most inorganic soft clays:

$$\frac{C_\alpha}{C_c} = 0.04 \pm 0.01 \quad (2.33)$$

and for highly organic plastic clays:

$$\frac{C_\alpha}{C_c} = 0.05 \pm 0.01 \quad (2.34)$$

Using C_α a prediction of secondary compression in the field can be calculated using:

$$s_s = \frac{C_\alpha}{1 + e_p} H \log \frac{t}{t_p} \quad (2.35)$$

where e_p is the void ratio at the end of primary consolidation.

2.3 Deformations Beneath Embankments on Soft Soils

2.3.1. Introduction

Construction of embankments on soft ground often results in large foundation deformations, which can leave the embankments unserviceable (Hsi and MacGregor 1999) and can also cause damage to piles supporting surrounding structures (Poulos 1999). Due to the common occurrence of this problem, a large number of case studies are present in the literature in which the vertical and horizontal deformations beneath trial embankments have been monitored and compared with the predictions from numerical models. In many of the studies (Hsi and MacGregor 1999; Indraratna et al. 1997; Oh 2006; Rankine et al. 2005) different ground improvement techniques have been implemented and modelled to determine their efficiency in speeding the settlement, thereby reducing the magnitude of post construction settlement and lateral displacement. Despite the large number studies documented in the literature on foundation deformations, it appears that there is little research into the effects that these deformations have on the embankments themselves. The following section summarises the three key parameters which characterise the foundation deformation beneath an embankment at a certain time; the settlement, lateral displacements, and excess pore pressure.

2.3.2. Settlement Patterns

The pattern of settlement beneath an embankment can be classified as one of four types based on the embankment's dimensions (Zhang 1999). These are shown in Figure 2.19 and are:

1. One-Dimensional,
2. Typical Settlement Basin,
3. Transitional Settlement Pattern, and
4. Sagged Settlement Pattern.

Zhang (1999) developed these classifications, and determined the conditions under which they occur and how the position of maximum settlement can be determined. The patterns were developed based on the distribution of shear stresses beneath an embankment founded on elastic material, where consolidation was not considered. As such the distributions shown in Figure 2.19 are for short-term undrained conditions, however a review of a number of trial embankment deformations indicated that while settlement is time dependant settlement

patterns do not change significantly during consolidation. A slight shift of the maximum settlement towards the centre of the embankment is what, in some cases occurs.

The results of the study found that the typical settlement basin, which is generally taken for granted to be the settlement pattern occurring in the field, only occurs when the crest width to height ratio is less than three. The sagged settlement pattern occurs under very wide embankments where the crest width to height ratio is greater than five, and for ratios of between three and five a transitional pattern is formed. The one-dimension pattern could only occur beneath an infinitely wide embankment.

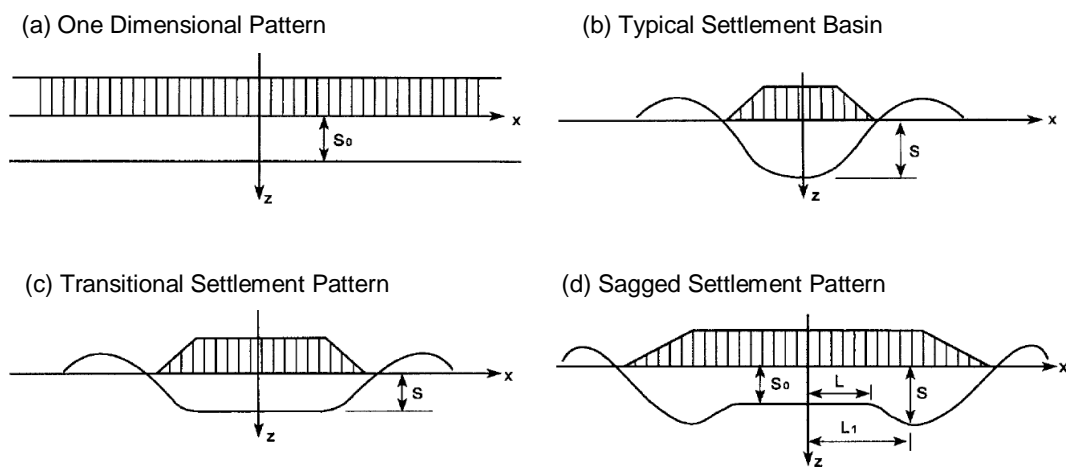


Figure 2.19: Settlement Patterns beneath Embankments on Soft Ground (Zhang 1999)

In the following paragraphs the settlement patterns beneath a number of trial embankments are discussed and compared with the patterns Zhang identified.

A series of 15 thoroughly instrumented embankments were constructed in Malaysia, on soft marine Maur clay, and some of the settlement records with respect to position are documented in the literature. In particular, a study into the foundation deformation of one of the embankments, which was rapidly constructed on an untreated foundation till it failed, was reported by Indraratna and Balasubramaniam (1992). This embankment, which had a crest width of 20 m and a total width at the base of 40 m reached a height of 5.5 m before it failed with a tensile crack forming in the embankment combined with shear slip failure in the foundation. For this embankment the settlement patterns were measured and compared with numerical predictions at heights of 2, 3, 4 and 5 metres. The measured settlement patterns for heights of 3 and 4 metres clearly show the sagged settlement pattern and the pattern for a height of 5 metres shows a transitional pattern. Zhang (1999) predicted the location of the maximum settlement for each height and the predictions matched the measured results well, as is shown in Figure 2.20. It should be noted however, that Zhang did not develop a method

to determine the magnitude of these maximum settlements. The numerical models created by Indraratna and Balasubramaniam (1992) did not predict the pattern of settlement well. They created models using the modified Cam-clay and hyperbolic stress-strain models in the Finite Element packages CRISP and ISBILB respectively. However, all the numerical models, which included both drained and undrained conditions, predicted settlements in a typical basin pattern. Based on the results it was not conclusive which model best predicted the settlement behaviour of the foundation, though it was clear that the hyperbolic model gave better predictions of heave beyond the toe of the embankment.

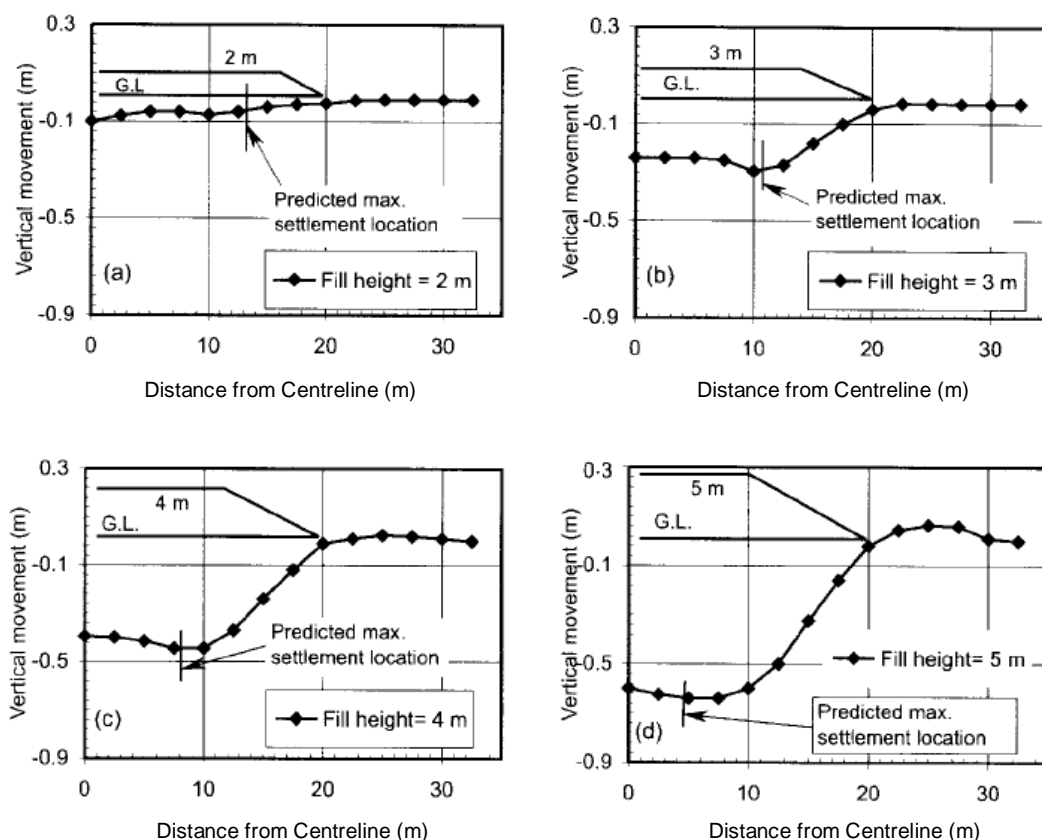


Figure 2.20: Measured Settlements beneath the Embankment Constructed to Failure on Maur Clay, Showing Position of Maximum Settlement Predicted by Zhang (Zhang 1999)

Similar settlement pattern data is also available in the literature for another Malaysian test embankment, which had a foundation treatment that included geogrids and vertical drains (Indraratna et al. 1997). Despite being a very wide embankment, with a crest width of 72.8 metres, after the first 4 metre high stage of construction, the measured and numerically predicted settlement patterns had the shape of a typical settlement basin rather than a sagged settlement pattern. This is probably a result of the shear stress being transferred to the geogrids rather than to the foundation. For this embankment, the numerical settlement predictions which were made using a modified Cam-clay model in CRISP were significantly

smaller than the measured settlements for all stages except for the first. The likely cause of this is the effect of creep not being accounted for in the Cam-clay model. Indraratna et al. (1997) also produced settlement versus time results which were corrected for creep and these matched the measured data very well.

A number of trial embankments, where settlement patterns have been monitored, have also been built in conjunction with major road works in Australia. As part of the construction of an eight kilometre section of the Pacific Highway in New South Wales a 55 metre wide, 5.5 metre high trial embankment was built on a foundation improved by the installation of wick drains (Hsi and MacGregor 1999). The measured settlement profile and the settlement profile predicted numerically using a Cam-clay model in the program COFEA are shown in Figure 2.21. Despite the large base width of this embankment the settlement pattern is a typical settlement basin. This is most likely due to the particularly flat batters of the embankment which leave the crest width at only about 15 metres. Another factor which would also contribute to the settlement pattern being more like a typical settlement basin, is that the hydro-static profile gauge which was used to measure the settlement pattern was only installed after the first 0.9 metres of fill was placed. From Figure 2.21 it is clear that a numerical model can, very accurately predict the settlement pattern beneath an embankment.

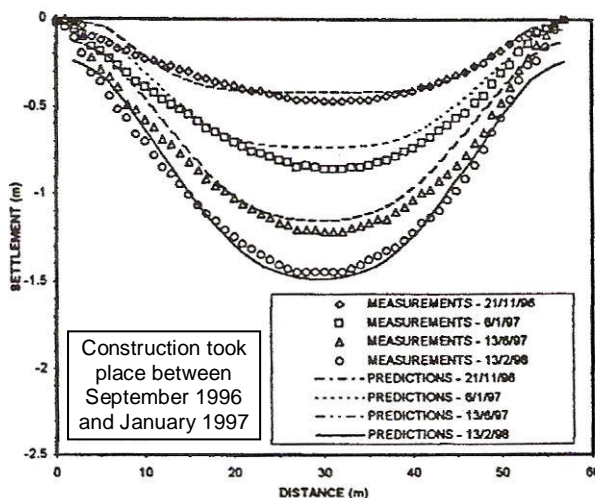


Figure 2.21: Settlement Pattern beneath Trial Embankment on Pacific Highway NSW at Four Different Times (Hsi and MacGregor 1999)

Oh (2006) analysed another three trial embankments constructed in Southeast Queensland; the Sunshine Motorway embankment, the Brisbane Motorway Embankment and the Gold Coast Highway Embankment (Oh 2006). Each of these embankments was split into three sections with different foundation improvement techniques used in each section. For the Sunshine Motorway and the Gold Coast Highway embankments, which would both be considered to be wide embankments, the settlement patterns for all sections were typical

settlement basins. This settlement pattern can be attributed to the use of geogrids at the base of the embankments. For the Brisbane Motorway embankment the settlement pattern varied for different sections. One of the patterns produced was a typical settlement basin whilst the other was initially a sagged settlement basin but with time changed as shown in Figure 2.22.

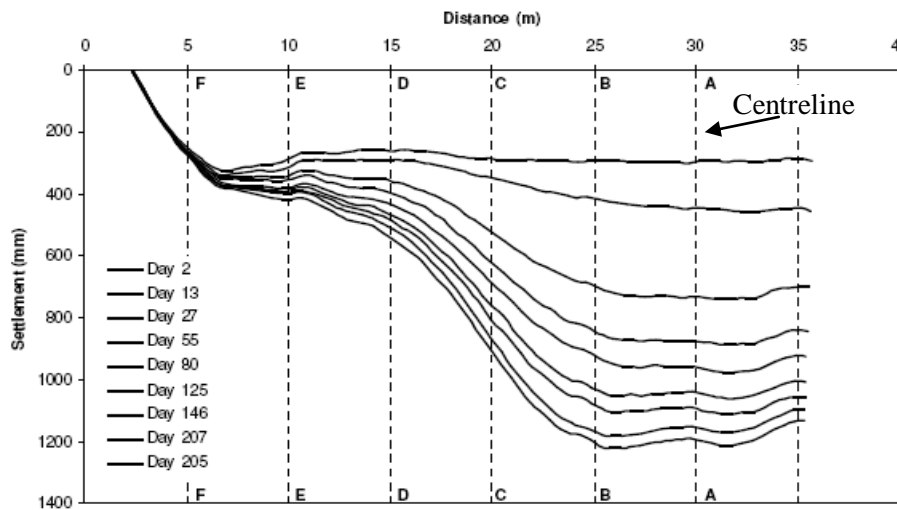


Figure 2.22: Settlement Pattern beneath the Brisbane Motorway Embankment (Oh 2006)

It is clear from the case studies reported in the literature that the settlement pattern beneath an embankment is dependent on factors including its width to height ratio and the use or otherwise of geogrids in the foundation. Numerical models developed indicate that the settlement of embankments can be accurately modelled and predicted, provided the appropriate constitutive model is used with realistic values for the model parameters.

2.3.3. Lateral Displacements

Lateral displacements occurring within embankment foundations can have significant detrimental effects on surrounding structures (Tavenas et al. 1979), and have also been found to be useful for predicting the impending failure of embankments (Hunter and Fell 2003). In this thesis it was envisaged that a connection between lateral displacements and the onset of pavement cracking could be established. In many of the trial embankment case studies in the literature, including those discussed in section 2.3.2, lateral displacement profiles at the toe of the embankments have been measured and numerical models have been made to predict them. In many cases the results of lateral displacement predictions have lead to the conclusion that predictions are highly sensitive to the quality of input variables and are thus difficult to predict (Indraratna and Balasubramaniam 1992; Indraratna et al. 1997). This difficulty in predicting the lateral displacements with such models has lead to studies into empirical methods for determining these displacements, which relate the maximum lateral displacement to the maximum settlement. The sections below summarise the lateral

displacement results of some of the case studies as well as the empirical correlations developed.

Short-Term Lateral Displacements in the Construction Phase

The principal assumption made in many numerical models where foundation deformation during the construction phase is considered, is that construction takes place so rapidly that the clay can be considered to be undrained. It is also a common assumption that the undrained behaviour of clays can be best described using elastic analysis, with a Poisson's ratio of $\nu = 0.5$. Numerous case studies have shown, that with these assumptions settlements can be predicted well, but that lateral displacements and profiles are not predicted well (Tavenas et al. 1979). Poulos (1972 vide. Tavenas et al. 1979) suggested some possible causes for the poor predictions of short-term lateral displacement including; the anisotropy of soil, the non-linear stress-strain behaviour of soil and the nonhomogeneity of soil. By 1979 a number of these issues had been addressed in Finite Element models, including the anisotropy and stress-strain behaviour, but even with these improvements Tavenas (1979) noted the apparent inability to accurately predict both settlement and lateral displacement in the one model. More recent studies indicate that this is still a problem. Lateral displacement predictions for the first stage of the Malaysian embankment with geogrids and vertical drains (Indraratna et al. 1997), were of about the right magnitude but did not match the profile particularly well. In contrast, Hsi and MacGregor (1999) were able to roughly predict the profile for the Pacific Highway two months into construction, including the position of the maximum lateral displacement, but the predicted magnitude of displacement was about three times larger than measurements. For the Sunshine Motorway embankment the profiles predicted by Oh (2006) were again similar to measurements in shape but the predicted magnitudes were up to two and a half times too large.

Tavenas et al. (1979) studied the lateral displacements beneath 21 different trial embankments and suggested correlations between the centreline settlement and maximum lateral displacement. For foundations which become normally consolidated very early in the construction phase, the deformations are governed by the undrained shear distortion of the clay and the maximum lateral deformation (y_m) is approximately equal to the central settlement (s) (see Figure 2.23). For the more common case where the foundation is overconsolidated the y_m/s ratio is initially between about 0.06 and 0.36, but undergoes an abrupt change after which $\Delta y_m/\Delta s$ is approximately equal to 1. Tavenas and Leroueil (1979 vide. Tavenas et al. 1979) suggested that this change may be a result of the clay reaching a normally consolidated state.

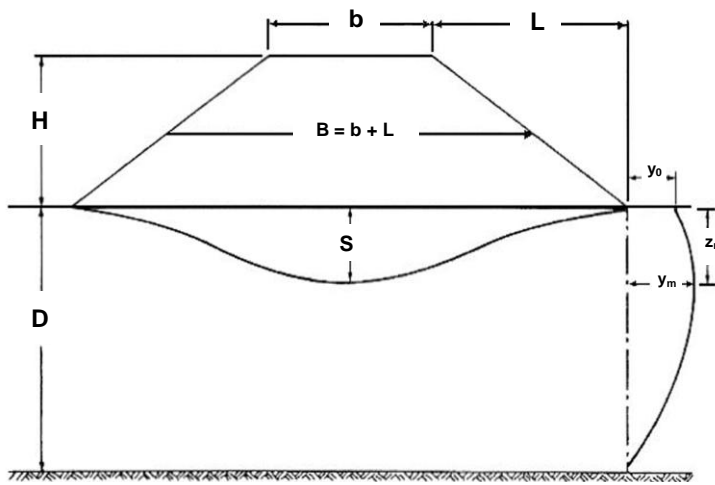


Figure 2.23: Definition of the geometry and Deformation Parameters (Tavenas et al. 1979)

The shape of the short-term lateral displacement profile is also dependant on whether a normally consolidated state is reached throughout the clay layer. In the case that one is, the shape of the profile will match the common theoretical predictions shown in Figure 2.24. Alternatively, if only part of the foundation becomes normally consolidated then the normally consolidated section may have a profile similar to a theoretical one corresponding to the height which is normally consolidated, and in the overconsolidated regions the lateral deformations will be smaller than the theoretical predictions.

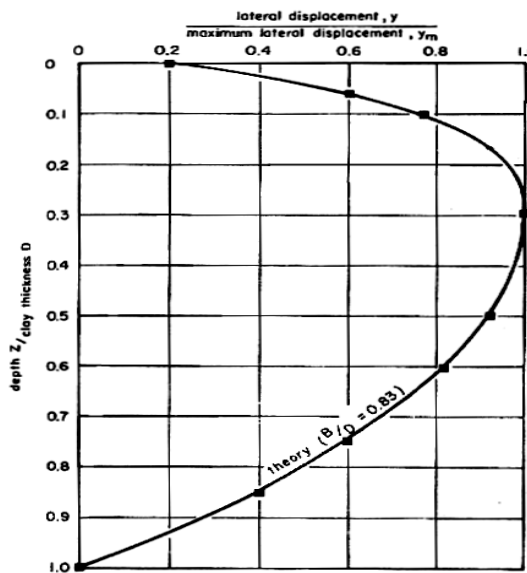


Figure 2.24: Theoretical Lateral Displacement Profile beneath an Embankment Toe (Tavenas et al. 1979)

Long-Term Lateral Displacements

A major difference between the prediction of short-term and long term lateral deformations is that for long term displacements the foundation is generally considered to be fully drained. In older FEM models this would sometimes result in the predicted long term deformations being less than the end of construction deformations, due to the use of a drained Poisson's ratio of $\nu = 0.3$ as opposed to 0.5 for undrained conditions. This is an occurrence which is contrary to most field observations (Tavenas et al. 1979). This problem however, is not present in the more recent case studies, though there are still difficulties in accurately predicting lateral displacements. In the Malaysian embankment with geogrids and vertical drains (Indraratna et al. 1997) the displacement measurements for the later stages of construction were all 2 – 2.5 times larger than the predicted ones. For the Sunshine Motorway embankment (Oh 2006) neither the profiles nor the displacement magnitudes were predicted particularly well. In one case the predicted displacements were approximately 100% larger than measurements, though in other cases predictions were more accurate, being only 20% larger than the measurements. In contrast some of the long term predictions for the Pacific Highway embankment (Hsi and MacGregor 1999) agreed with measured values quite well.

Tavenas et al. (1979) observed that, in the long term the change in lateral displacement is proportional to the change in settlement. An analysis of six trial embankments resulted in the average relationship being $\Delta y_m = 0.16\Delta s$ where Δy_m is the change in the maximum lateral displacement beneath the toe and Δs is the corresponding change in settlement beneath the centre of the embankment. However it was concluded that too few case histories were studied to give a clear definition of all the parameters controlling the $\Delta y_m/\Delta s$ ratio. The distribution of lateral displacements with depth beneath the toe of an embankment was found to remain constant with time if the whole clay layer remained in either a normally consolidated or over consolidated state throughout loading. If, on the other hand, the clay initially consisted of sections which were normally consolidated and sections which were over consolidated and the over consolidated sections became normally consolidated during loading, then the distribution of lateral displacements and position of the maximum lateral displacement varied with time.

Based on the results of Tavenas' study and data presented by Stewart in 1992, an idealised relationship between the maximum settlement and lateral displacement was developed by Stewart et al. (1994). This relationship is shown in Figure 2.25.

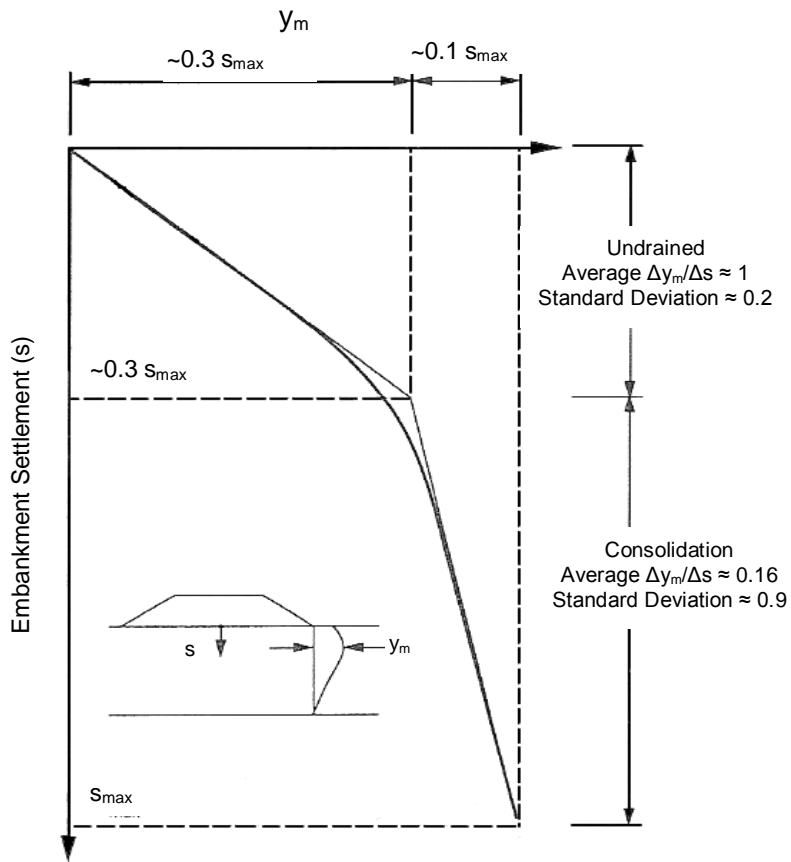


Figure 2.25: Idealised relation between embankment settlement and maximum lateral displacement beneath the toe (Stewart et al. 1994)

2.3.4. Pore Water Pressure

The dissipation of excess pore water pressure beneath an embankment is important as it gives a measure of how far the consolidation has progressed. In case studies in the literature it is common to measure the pore pressure at several depths beneath the embankment using piezometers, and in some cases compare these measurements with the results of numerical models. In general the results of such models indicate that the variation of pore pressure with time can be predicted well using coupled consolidation models (Hsi and MacGregor 1999; Indraratna and Balasubramaniam 1992; Oh 2006; Rankine et al. 2005). The variation of pore pressure with depth is also considered in the study of the Malaysian embankment constructed to failure (Indraratna and Balasubramaniam 1992). For this case the predictions were in good agreement with the measurements.

2.4 Geotechnical Site Investigations

2.4.1. Introduction

A factor of key importance to the success of the models created in this and any geotechnical modelling project is the appropriate assignment of soil properties. To obtain these soil parameters there are numerous different field and laboratory tests which can be used. In this chapter the tests which were used in the Tully Project to obtain this data will be discussed. These include the use of boreholes, from which samples can be taken for laboratory tests, and in which standard penetration tests can be performed, and piezocones. The laboratory tests conducted include consolidation or oedometer tests which have been discussed previously in section 2.2.3 and triaxial tests.

2.4.2. Boreholes

Bore holes are narrow holes, the diameter of which is dependent on the equipment used to create them, which can extend to depths up to 60 metres. From boreholes disturbed or undisturbed samples may be extracted for identification of soil strata and their properties. In situ standard penetration tests (SPTs) can also be conducted at various depths. The subsections below discuss SPTs and some of the correlations used to obtain soil properties from them, and triaxial tests and the soil properties which are obtained from these. Oedometer tests which have also been conducted on borehole samples in the Tully project are not discussed here as they have been described previously in section 2.2.3.

Standard Penetration Test

SPTs are one of the oldest and most popular in situ tests (Sivakugan 2008a). They produce results in the form of an N value which is the number of blows required to make a split-spoon sampler penetrate 300 mm into the soil (Barnes 2000). One blow consists of dropping a 63.5 kg weight freefall through a distance of 760 mm onto an anvil which is attached to the sampler through stiff drill rods. This N value can then be correlated to the relative density, friction angle and Young's modulus of sands, though it must first be corrected for overburden and hammer efficiency. The corrected blow count is given by:

$$(N_1)_{60} = C_N E_h N \quad (2.36)$$

where C_N is the correction for overburden which can be given by:

$$C_N = 0.78 \sqrt{\frac{1}{\sigma_{v0}' (kPa)}} \quad (2.37)$$

(Liao & Whitman 1986 vide. Sivakugan 2008a) and E_h is the hammer efficiency which converts N value to one which would be obtained if the hammer was 60% efficient. E_h is given by:

$$E_h = \frac{\text{Hammer Efficiency}}{60} \quad (2.38)$$

A number of correlations between $(N_1)_{60}$ and friction angle (ϕ) have been developed for granular soils these include:

Peck et. al. (1974 vide. Sivakugan 2008a):

$$\phi = 27.1 + 0.3(N_1)_{60} - 0.00054[(N_1)_{60}]^2 \quad (2.39)$$

Hatanaka and Uchida (1996 vide. Sivakugan 2008a):

$$\phi = \sqrt{20(N_1)_{60}} + 20 \quad (2.40)$$

Kulhawy and Mayne (1990) based on a graphic relation by Schmertmann (1975 vide. Sivakugan 2008a):

$$\phi = \tan^{-1} \left[\frac{N_{60}}{12.2 + 2.3 \left(\frac{\sigma_{v0}'}{P_a} \right)} \right] \quad (2.41)$$

where $P_a=101.3\text{kPa}$ is atmospheric pressure.

SPT results can also be used to determine Young's Modulus using the following correlations:

Leonards (1986 vide. Sivakugan 2008a), for normally consolidated sands:

$$E \left(\frac{kg}{cm^2} \right) = 8N_{60} \quad (2.42)$$

Kulhawy and Mayne (1990 vide. Sivakugan 2008a):

$$E = \alpha P_a N_{60} \quad (2.43)$$

where $\alpha = 5$ for sands containing fines, $\alpha = 10$ for clean normally consolidated sands and $\alpha = 15$ for clean overconsolidated sands.

The above correlations are all for granular soils as SPT has been found to be unreliable in cohesive soils. However, a rough estimate of undrained shear strength (c_u) can be obtained from Kulhawy and Mayne (1990 vide. Sivakugan 2008a):

$$\left(\frac{c_u}{P_a}\right) = 0.29(N_{60})^{0.72} \quad (2.44)$$

As c_u can be obtained more accurately from piezocene tests this correlation will only be required if there are no piezocones in the area of interest.

Triaxial Tests

Triaxial tests are laboratory tests conducted to determine the cohesion (c , c' , or c_u) and friction angle (ϕ , ϕ' or $\phi_u = 0$) of a soil sample, where the prime indicates effective stresses, the u indicates undrained conditions and no additional annotation indicates total stresses. They are carried out on undisturbed clay samples or reconstituted sand samples, which are cylindrical in shape with a length to diameter ratio of two. The samples are encased in an impermeable rubber membrane and placed in a triaxial cell, which is filled with water and pressurised to apply a uniform confining pressure to the specimen (see Figure 2.26). Additional vertical stress is then applied until the specimen fails. This is repeated for at least three samples with different confining pressures. The Mohr circles for the stresses at

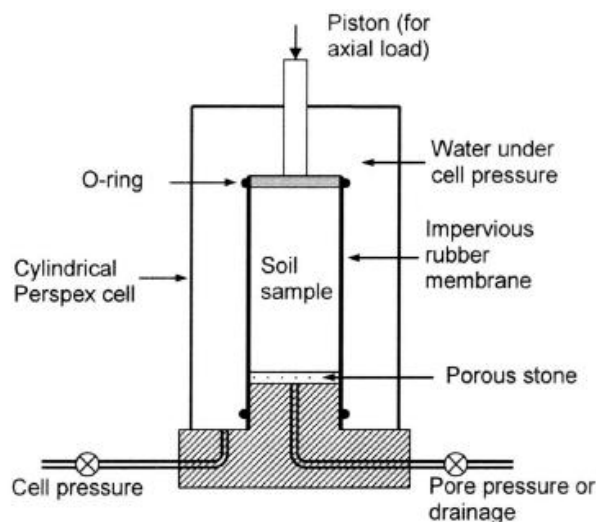


Figure 2.26: Triaxial Test Apparatus (Sivakugan 2008a)

failure are drawn assuming that the vertical stress ($\sigma_{cell} + \Delta\sigma$) is the major principal stress and that the horizontal stress (σ_{cell}) is the minor principal stress. The failure envelope is obtained by drawing a line tangential to all the Mohr circles, and the friction angle is the angle between this line and the horizontal, as shown in Figure 2.27. Cohesion is the shear stress defined by the failure envelope when the normal stress is zero. This test can be conducted under consolidated drained (CD) conditions, consolidated undrained (CU) conditions and unconsolidated undrained (UU) conditions, where consolidated indicates that the specimen is allowed to consolidate under the confining pressure alone, and drained or undrained refers to the specimen's drainage conditions when the additional stress is applied.

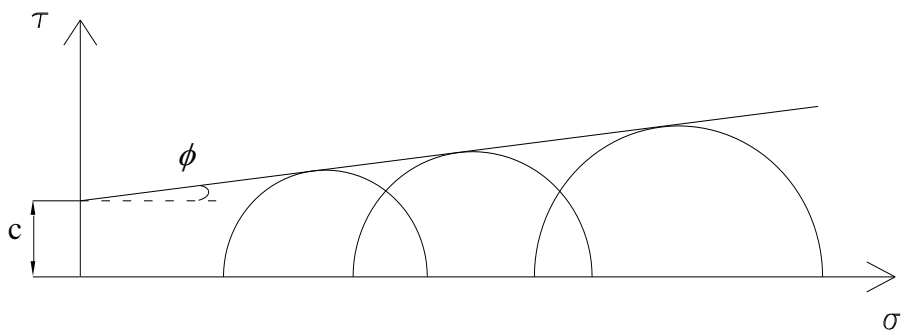


Figure 2.27: Mohr-Coulomb Failure Envelope

2.4.3. Piezocone Tests

A piezocone test (CPTU) is a type of cone penetration test (CPT) or Dutch cone test, in which pore water pressure (u) can be measured, as well as, the cone resistance (q_c) and sleeve friction (f_s) which are measured in CPT tests. A cone penetration test involves a probe which consists of a solid cone with a 60° apex, and a base diameter of 35.7 mm, corresponding base area of 1000 mm^2 . This is attached to a cylindrical friction sleeve with a surface area of $15\,000 \text{ mm}^2$. This probe is pushed into the soil at a constant rate of 20 mm/s by a hydraulic force. The resistant force acting on the cone, and on the sleeve of the probe, expressed as pressures, are the cone resistance and sleeve friction respectively. In a piezocone test the pore pressure is also measured continuously as the cone is advanced into the soil, and dissipation tests can be conducted where the change in pore pressure with time is measured while the piezocone is held stationary at a given depth (Brouwer Accessed: 28.05.2007).

The ratio of the sleeve friction to the cone resistance is a useful parameter for the identification of soil type and is known as the friction ratio. It generally has a value between 0 and 10% with granular soils having the lower ratios and cohesive soils having the higher values (Sivakugan 2008a). Figure 2.28 can be used to identify the soil type, and has been used in the determination of soil strata in this thesis.

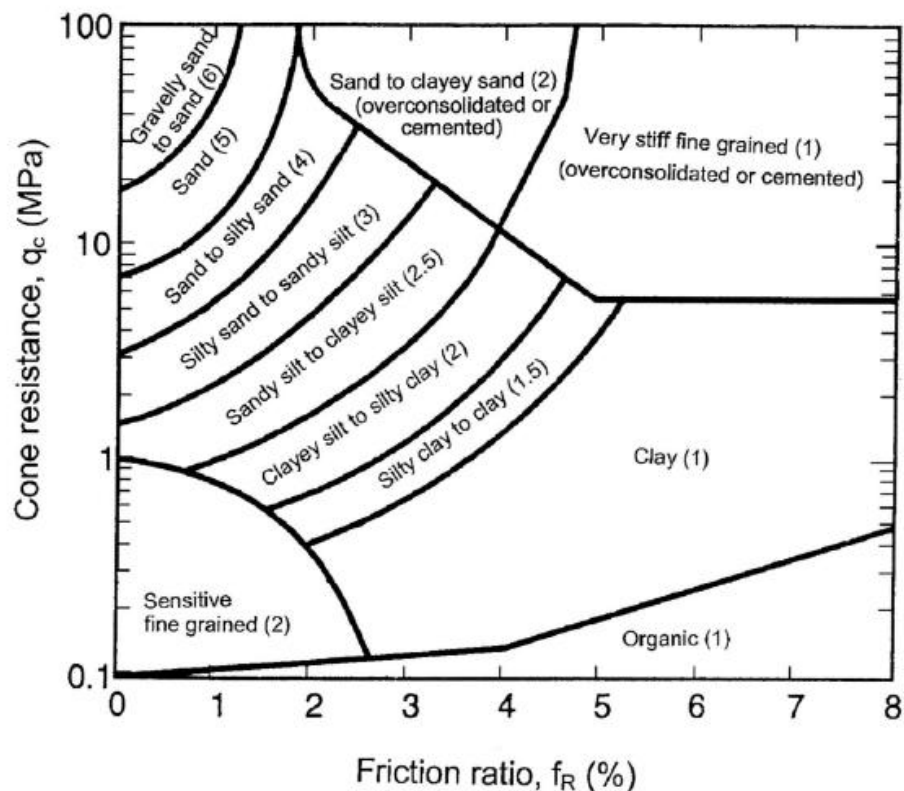


Figure 2.28: Soil Classification based on Cone Penetration Test (Sivakugan 2008a)

Many empirical correlations have been developed to correlate the tip resistance from a CPT test with soil properties including undrained shear strength (c_u), Young's modulus (E) and effective friction angle (ϕ'). Schmertmann (1975, vide. Sivakugan 2008a) estimated the undrained shear strength to be:

$$c_u = \frac{q_c - \sigma_{vo}}{N_k} \quad (2.45)$$

where N_k is the cone factor and can be estimated by:

$$N_k = 13 + 0.11PI \pm 2 \quad (2.46)$$

where PI is the plasticity index of the soil.

A review of published correlations between q_c and E for sands and clays indicate a wide range of variability in the correlations for both. In clays the published correlations tend to range between $E = 3q_c$ and $E = 7q_c$. In sands, most published values are in the range $E = 1.5$ to $3.5 q_c$ (Ground Test Pty Ltd - Now Douglas Partners 1981). Schmertmann (1978, vide. Sivakugan 2008a) suggested the correlations below for sands:

For axisymmetric loadings:

$$E = 2.5q_c \quad (2.47)$$

For plane strain loadings:

$$E = 3.5q_c \quad (2.48)$$

Meyerhof and Fellenius (1985 vide. Sivakugan 2007) suggested the following correlations for various classifications of sands:

For silts and sands:

$$E = 1.5q_c \quad (2.49)$$

For compact sands:

$$E = 2q_c \quad (2.50)$$

For dense sands:

$$E = 3q_c \quad (2.51)$$

For sands and gravels:

$$E = 4q_c \quad (2.52)$$

For this thesis, correlations in the ranges specified above will be used initially, and a relation more appropriate to the soils at the site will be obtained by calibration of the trial embankment models with measured data.

The effective friction angle of a soil can be determined from a correlation by Robertson and Campanella (1983) which relates the effective friction angle to tip resistance and effective overburden pressure, see Figure 2.29 and Equation (2.53)

$$\phi' = \tan^{-1} \left[0.1 + 0.38 \log \left(\frac{q_c}{\sigma_{vo}'} \right) \right] \quad (2.53)$$

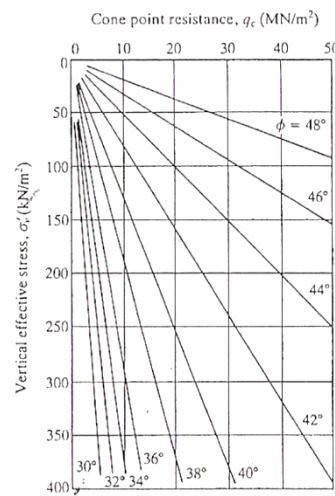


Figure 2.29: Correlation Between Cone Tip Resistance and Effective Friction Angle (Robertson and Campanella 1983)

From a piezocone dissipation test the horizontal coefficient of consolidation (c_h), and permeability or hydraulic conductivity (k) for the soil can be determined. To determine the permeability the time, t_{50} , which is the time for 50% of the pore water pressure to be dissipated, is obtained and used in Figure 2.30 (Mayne 2002 Accessed: 31.05.07). Obtaining c_h is a more laborious process which will not be discussed here as the coefficients of consolidation and permeabilities used in this thesis will be obtained from oedometer tests.

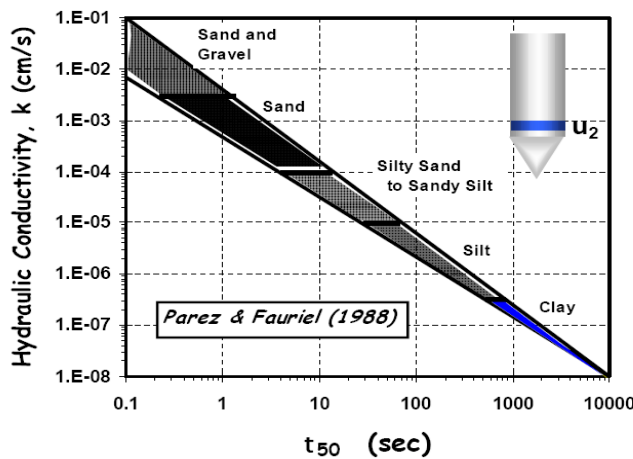


Figure 2.30: Determination of Hydraulic Conductivity or Permeability from a Piezocone Dissipation Test (Mayne 2002 Accessed: 31.05.07)

2.5 Geotechnical Monitoring Equipment

Due to the high degree of uncertainty involved with geotechnical predictions and designs it is often considered beneficial to monitor the state of a foundation after an embankment or other form of load has been constructed on top of it. In larger projects, providing monitoring equipment in areas which are constructed first can provide useful information regarding the validity of assumptions upon which designs were made and can allow for compensation to be made in parts of the construction occurring later. Monitoring data can also give early warning if failure of a foundation is eminent.

The measurements of most interest when embankments are being built include settlement, pore pressure dissipation and horizontal movement. There are many different systems and types of equipment which can be used to measure these parameters, but in this section only the equipment used in the Tully trial embankments will be discussed, that is settlement plates, piezometers, and inclinometers.

2.5.1. Settlement Plates

Settlement plates are pieces of equipment which measure the settlement at a particular location. The settlement plates used on site at Tully are simply plates on the ground attached to rods of known length which extend vertically upwards. These vertical rods are encased in other rods to isolate the settlement plate from the soil being placed around it (see Figure 2.31). Settlements at given times are determined by taking the level of the top of the inner rod. The difference between the initial rod level and the level after a given amount of time is the settlement which has occurred during that period of time. The actual level of the settlement plate can also be obtained by subtracting the length of the inner rod from the level of the top of the rod.

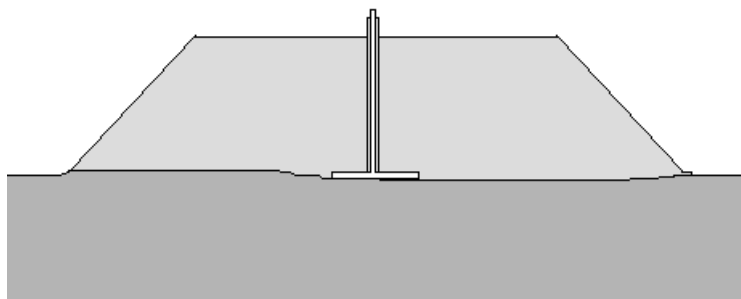


Figure 2.31: Diagram of a Settlement Plate

2.5.2. Piezometers

Piezometers are devices used to measure the pore pressure at a given location within a foundation. In the Tully project vibrating wire piezometers were used. This type of piezometer converts the water pressure surrounding the device into a frequency signal which is transmitted to a recording device.

The piezometer contains a diaphragm attached to a tensioned wire in a manner which results in a change in tension in the wire when the water pressure changes, as shown in Figure 2.32. An electromagnetic coil is used to excite the wire causing it to oscillate at its natural frequency, which is dependent on its tension. The vibrations in the wire then generate a frequency signal in the electromagnetic coil which is transmitted to the recording device. The frequencies recorded can then be converted back to pore water pressures by the application of calibration factors (Durham_Geo-Enterprises 2006).

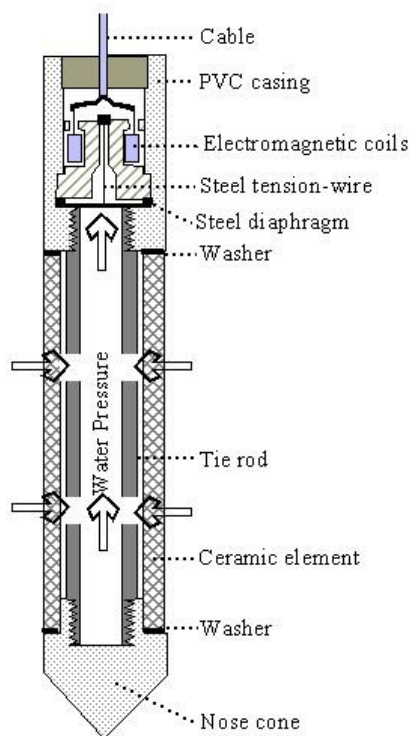


Figure 2.32: Diagram of a Vibrating Wire Piezometer (Canterbury_City_Council 2007)

2.5.3. Inclinometers

Inclinometers are typically used to measure horizontal displacements along a vertical line, though they can be set up with other orientations. An inclinometer probe has the form of a rod with wheels attached on the sides at both ends as shown in Figure 2.33. This device is

passed down inclinometer casing and measures its own tilt or inclination at various depths. Assuming that the base of the inclinometer casing is fixed in stiff material which will not move, the displacement normal to the casing, at locations along the rest of the casing can be determined from the tilt of the probe.



Figure 2.33: Inclinometer Probe (Durham_Geo-Enterprises 2006)

Inclinometer casing is either metal or plastic tubing which contains four longitudinal grooves spaced equally around the inside of the tubing. These grooves are tracks for the inclinometer probe's wheels, which control the orientation of the probe when it is lowered down the casing for measurements. Inclinometer casing is generally installed in vertical boreholes and grouted into place. The strength and stiffness of the grouting should be similar to that of the surrounding soil profile to ensure that the casing moves as an integral part of the soil mass making the measurements an accurate representation of the soil mass movement (Hines 1985).

Once the casing is installed measurements should be taken to determine the initial profile of the casing. This involves lowering the probe to the bottom of the casing and taking measurements at 0.5 meter intervals as the probe is raised back to the surface. At each height the output from the inclinometer is two measurements which are functions of the angle of tilt in the plane of the wheels and the angle of tilt in the plane perpendicular to the wheels (Lei et al. 2006). From these angles the position of the top of the inclinometer probe relative to the bottom of the inclinometer probe can be determined. Figure 2.34 shows the calculation for the simplified case where the inclination is only in the plane of the wheels. With the set of measurements at 0.5 meter intervals the position of the entire length of inclinometer casing relative to the base of the casing can be determined. The same process of taking measurements at 0.5 metre intervals is used each time measurements are required and by comparing the new profile of the casing to the initial profile, the profile of displacements normal to the casing is calculated (Durham_Geo-Enterprises 2006).

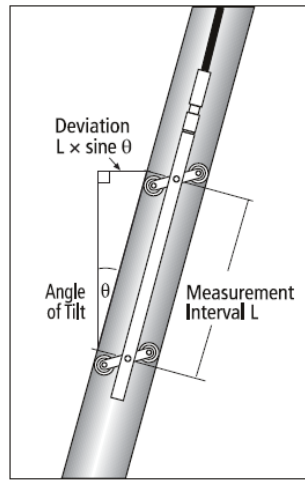


Figure 2.34:Simplified Example of Calculations Required to Determine Inclinometer Casing Profile
(Durham_Geo-Enterprises 2006)

2.6 ***Summary of the Literature Review***

This literature review covered an extensive range of topics relating to this thesis. It began by summarising some of the methods which can be used to determine the increase in stress at a given position within a foundation due to the application of a surface load. This was followed by a section containing methods for the determination of settlement as well as some of the theory associated with these methods. In particular this section focused on the consolidation of clays as this was the process causing the majority of settlement and settlement related issues on the Tully project. Following this was a summary of published literature which dealt with foundation deformations caused by embankments. The settlement, lateral displacement and pore pressure results from the literature were analysed to determine the nature and accuracy of results which could be expected in the trial embankment modelling stage of this thesis. Information regarding the site investigation techniques which were used on the Tully project was then presented along with correlations some of which were used to obtain the required model input parameters from the collected site data. Finally, the geotechnical monitoring equipment used to measure settlement, pore pressure and lateral displacements on the trial embankments was discussed.

Chapter 3: Numerical Modelling and FLAC

3.1 *Introduction*

Before a numerical modelling program such as FLAC is chosen for use in a study, it is necessary to gain an idea of what methods the program implements to solve models and how these methods compare with the methods used by other programs. With this knowledge a more informed choice can be made as to which program is best suited to the modelling task. The first four sections of this chapter deal with these issues, summarising why FLAC was chosen, the differences in modelling techniques employed by FLAC and other programs and some of the features of FLAC. This is followed by a review and explanation of the different constitutive models which can be used in FLAC to model soils. As an important aspect of this thesis is the modelling of consolidation processes the next section in this chapter summarises some of the key principles which must be understood to create effective coupled consolidation models. Finally, a FLAC model which validates that FLAC can model 1-D consolidation accurately is included and discussed.

3.2 *Numerical Modelling Software*

FLAC (Fast Lagrangian Analysis of Continua) is one of a number of different numerical modelling programs available which are suitable for use in the modelling of embankment deformations. It is a two-dimensional explicit finite difference program which was specifically designed for use in geotechnical engineering (Itasca 2005b). Being a finite difference program FLAC differs from most of the other widely used programs in geotechnical engineering such as PLAXIS, ABAQUS, ANSYS and CRISP, all of which use a finite element method (FEM) of solution. A review of the literature indicates that there is not a generally preferred program and that each of these programs are equally capable of modelling embankment deformation. However, individual programs do have different advantages and disadvantages which may make them better suited to particular situations or users. PLAXIS for example, is quite user friendly and can be run on portable computers, but is perhaps not as versatile as some programs. Whereas ABAQUS is quite powerful but requires more powerful computers to run it and was not designed specifically for geotechnical engineering applications (Sivakugan 2006). James Cook University currently has licences to ABAQUS, PLAXIS and FLAC, and FLAC was chosen for use in this study due to its versatility and comparatively minimal hardware requirements, as well as its suitability for modelling the situations necessary for the completion of this thesis.

3.3 Finite Element versus Finite Difference

Both the Finite Difference Method (FDM) and the Finite Element Method (FEM) are numerical methods used to solve sets of differential equations, such as those governing the stress-deformation relationships of materials, using initial and/or boundary values. The finite difference method is the older of the two, but as computing power has advanced FEM programs have dominated the market.

The finite difference method uses the numerical approach of replacing derivatives with algebraic expressions involving variables at discrete points in space, known as nodes. Between these nodes the variables are not defined. In contrast the finite element method requires that field variables vary in a predefined fashion (e.g. linearly or parabolically) within elements. The variation of these variables within the elements is used in the solution process which involves minimising either the error or energy terms in the problem.

Despite the different ways of formulating the problems it can be shown that the resulting algebraic equations which are to be solved are equivalent (Itasca 2005c).

3.4 Explicit and Implicit Solution Techniques

FLAC uses an explicit solution technique known as time marching to solve the algebraic equations derived in the finite difference method. While this method could be used in conjunction with FEM, in general FEM programs use an implicit matrix-orientated solution scheme, which likewise could also be used with a finite difference method.

The explicit calculation process used in FLAC first uses the equations of motion to determine nodal velocities and displacements from the state of stress in the model and then uses the constitutive equation (stress/strain relationship) to calculate the new state of stress from the velocities and displacements. This loop represents one time step, and within the time step, variables remain constant. This means that within a time step the change in stress of one element will not affect the velocity or displacement of another element. As a result the time step must be kept smaller than the physical time it takes for information to be passed from one element to another, so that systems are modelled realistically. The main advantage of this technique is that no iteration is required to calculate the stresses from the strains within an element even when the constitutive relation is highly nonlinear. This differs from an implicit technique where significant iteration is required within each solution step to allow every element to affect every other element. Overall, it is most efficient to use an explicit method to solve “ill-behaved” problems, for example when nonlinearity, large-strains or physical instability are present. On the other hand it is more efficient to use an

implicit method to model linear, small strain problems (Itasca 2005c). Another advantage of using an explicit time marching technique is that it allows problems which consist of several stages, such as staged construction or excavation to be modelled with ease. Table 3-1 shows a comparison of implicit and explicit solution methods.

Table 3-1: Comparison of Explicit and Implicit Solution Methods (Itasca 2005c)

Explicit	Implicit
The timestep must be below a critical value for the solution to be stable.	Solution is stable even for large timesteps.
Little computational effort is required for each timestep.	Significant computational effort is required for each timestep
Significant numerical damping is not required for dynamics solution.	With unconditionally stable schemes, numerical damping is dependant on timestep.
Nonlinear constitutive relations can be followed without requiring additional iterations.	An iterative procedure is required to implement nonlinear constitutive relations.
Memory requirements are at a minimum, because matrices are not formed.	Stiffness matrices can be large and require large amounts of memory.
Large displacements and strains are accommodated without additional computing effort	Additional computing effort is required to accommodate large displacements and strains.

3.5 *FLAC Features*

One excellent feature of FLAC is that it contains a powerful in-built programming language called FISH (short for FLACish). This allows the user to write additional functions to be run as part of the model. FISH can be used to specify alternative constitutive models, to define, manipulate and print or plot user defined variables, to automate parameter studies and for many more purposes.

Another feature of FLAC Version 5.0, which was not in Version 4.0, is that it can be run in either a command-driven mode or a menu-driven mode. The menu driven mode allows users to control all the basic functions in FLAC with the point-and-click of a mouse within an interactive windowed environment. Alternatively, in command-driven mode, models are created and analysed from a command prompt, using word commands. Command-driven mode can be more difficult to learn, as knowledge of the commands and keywords is required, however, it does have some advantages over menu-driven mode. These include:

1. Engineering problems usually involve a number of sequential operations. Using a series of commands to model this corresponds closely with the physical sequence being represented.

2. A FLAC data file (model file) can be easily created and modified in a text editor (eg. Notepad). Any number of these files can then be loaded into FLAC to run in sequence, which is ideal for parametric investigations.
3. The word –orientated input file is an excellent record of analyses performed and can easily be included as is in an engineering report.
4. The command driven structure allows user written functions to be incorporated in an appropriate sequence easily.

For this thesis command driven mode has been used. Other FLAC features include the ability to specify either velocity boundary conditions or stress boundary conditions, the ability to specify a water table and the ability to model coupling between a deformable porous solid and a viscous fluid flowing within the pore space (eg. consolidation), which is critical for this thesis.

3.6 Constitutive Models

One major difficulty in the numerical modelling of soils is applying a constitutive relation which realistically represents the stress-strain behaviour of the soil. Since numerical methods were introduced, a number of different soil models have been proposed and utilized. Initially, basic linear elastic models were used, but since then nonlinear elastic models such as Duncan and Chang, elastic-plastic models such as Mohr-Coulomb, and critical state models such as Cam Clay have been developed and implemented to better approximate the stress-strain behaviour of different soils. Most of the software packages mentioned in the previous section now come with many different soil models inbuilt, allowing the user to just select a model rather than having to define and program the model. FLAC comes with a choice of eleven soil models, including; elastic isotropic, elastic transversely isotropic, Drucker-Prager, Mohr-Coulomb, strain hardening/softening and modified Cam-clay (Itasca 2005c). Høeg (1977) noted the importance of the choice of model after comparisons of numerical analyses with various material models showed that while the vertical stresses beneath loaded areas were not highly sensitive to the model used, the same was not true of horizontal and shear stresses. Therefore, the strain distribution in the soil is sensitive to the material model used (Høeg 1977). In the next few sections the constitutive models of relevance to this thesis are discussed.

3.6.1. Elastic Models

The defining feature of an elastic model is that all strains resulting from an applied load are recoverable (Lewis and Schrefler 1987). In other words when a soil deforms from the application of a load, the soil will return to its original shape if the load is removed. The most basic type of elastic model is the linear elastic model, see Figure 3.1. In one dimension,

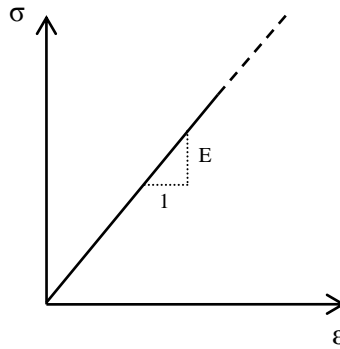


Figure 3.1: Linear Elastic Stress-Strain Relation

this model relates stress to strain via a constant value of Young's Modulus, regardless of the magnitude of the stresses and strains. In two or three dimensions a second parameter is also required to describe the elastic behaviour of a material, this parameter is usually Poisson's ratio (ν) which relates the strain in one direction to that in an orthogonal direction. Alternatively, the elastic behaviour of a material can be expressed in terms of a bulk modulus (K) and shear modulus (G). The bulk modulus relates changes in pressure to volume changes, and the shear modulus relates the changes in shear strain to changes in shear stress. Bulk modulus and shear modulus can be calculated from Young's modulus and Poisson's ratio using equations (3.1) and (3.2) and are the required input parameters for the isotropic elastic model in FLAC.

$$G = \frac{E}{2(1 + \nu)} \quad (3.1)$$

$$K = \frac{E}{3(1 - 2\nu)} \quad (3.2)$$

Despite the simplicity of this model it can be used to give good approximations in over consolidated soils where only small strains occur (Høeg 1977). Linear elastic models are often used to approximate undrained loading, although in modern numerical analyses non-linear elastic models are sometimes used for this purpose (Tavenas et al. 1979). A popular non-linear elastic model is the hyperbolic model which was originally proposed by Kondner, but has been extensively developed by Duncan and Chang and is often called the Duncan-Chang model (Naylor and Pande 1981). This model uses the stress-strain relation:

$$\sigma_1 - \sigma_3 = \frac{\varepsilon_1}{a + b\varepsilon_1} \quad (3.3)$$

where $\sigma_1 - \sigma_3$ is the principle stress difference and ε_1 is the major principle strain, refer to Figure 3.2.

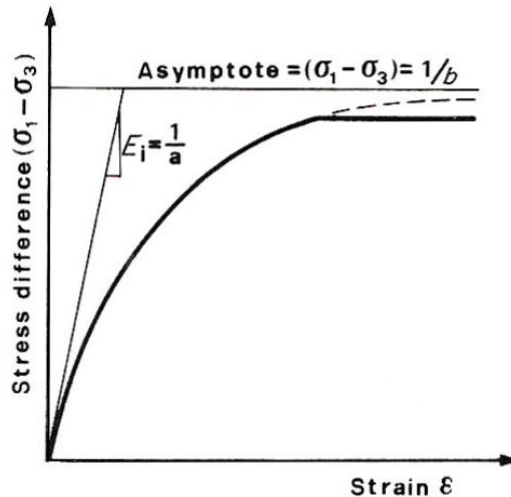


Figure 3.2: Hyperbolic Stress-Strain Curve (Lewis and Schrefler 1987)

FLAC has two inbuilt elastic models, the elastic isotropic model, and the elastic transversely isotropic model, where elastic moduli are different for directions normal and parallel to the soil layers. Both of these models are linearly elastic, however, a non-linear model such as the hyperbolic model, can easily be programmed into FLAC using FISH (Itasca 2005c). In this thesis the elastic isotropic model is used for the preliminary runs to develop an understanding of the process.

3.6.2. Elastic-Plastic Models

The next level of sophistication is achieved by allowing plastic strains, which are not recoverable on unloading, to occur in the stress-strain model. The basic elastic-plastic models work on the basis that the stress-strain relationship is elastic until the stress state reaches a yield condition. Once the stress reaches this yield condition any further strains are made up of a combination of elastic and plastic strains, with only the elastic strains contributing to the new stress state. To clarify this consider a one dimensional loading situation; Figure 3.3 (a) shows an idealised elastic-perfectly plastic stress-strain relation. The relation is elastic until the yield stress σ_y is reached, after this if even an infinitesimal increment of stress is added the strains will increase indefinitely, and these strains occurring after the yield point is reached are not recoverable on unloading, that is they are plastic strains. It is clear from this behaviour that it is not possible for the stress in the material to exceed the yield stress. Figure 3.3 (b) is the stress-strain relation for an elastic plastic

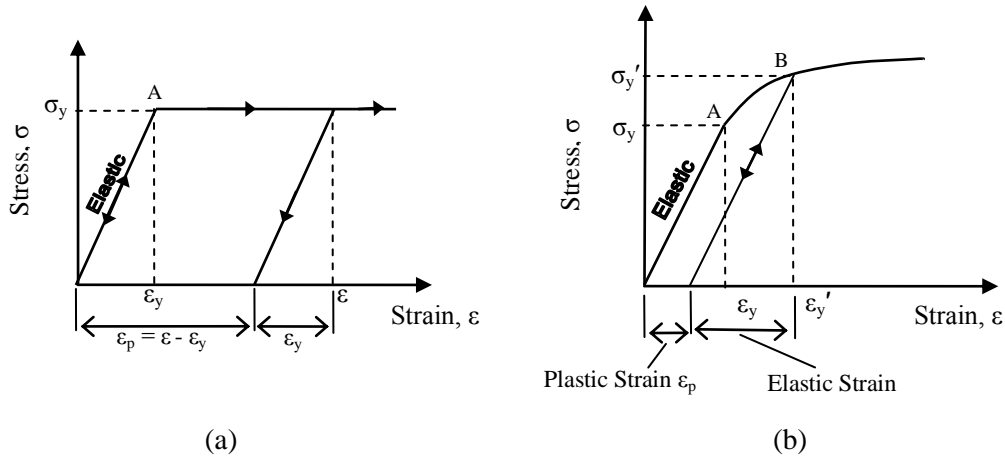


Figure 3.3: Ideal stress strain relations for (a) an elastic-perfectly plastic material and (b) an elastic-plastic material

material where some strain hardening occurs. In this case like in Figure 3.3 (a) the relation is elastic up to point A. However, beyond this point a combination of elastic and plastic strains occur. If the material is unloaded from the point B, only the elastic strains will be recoverable, and if it is then reloaded the material will behave elastically till point B is reached. Point B can therefore be considered as the new yield point. As such the yield stress itself can again not be exceeded, because once the original elastic limit is reached (point A) the yield stress increases as plastic strain hardening occurs.

Now in three dimensions the yielding is not dependant on a single stress, but the stresses in three perpendicular directions. As these stresses will change depending on how you chose to orientate the soil element, the yield condition is written in terms of the principal stresses which do not depend on the orientation of the soil element. When written in this form the yield condition is called a yield function and represents a surface in stress space. As was discussed in the one dimensional examples, this yield surface cannot physically be exceeded; it separates elastic behaviour from impermissible states of stress (Lewis and Schrefler 1987).

Much of the early work in soil mechanics, which incorporated plasticity theory, used the two dimensional Mohr-Coulomb strength relationship as a yield criterion, as shown in Figure 3.4 (Høeg 1977). In 1952, Drucker and Prager developed a three dimensional representation of the Mohr-Coulomb yield criterion as shown in Figure 3.5. However, experience has shown that the Drucker-Prager approximation gives poor results and offers no real advantage in terms of numerical computations (Naylor and Pande 1981).

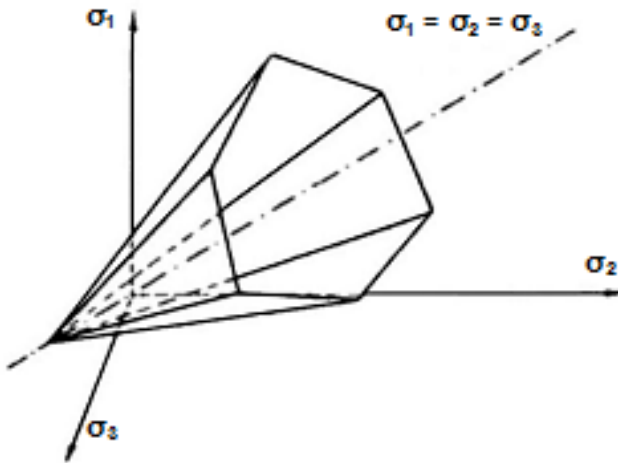


Figure 3.4: Mohr-Coulomb Failure Surface (Høeg 1977)

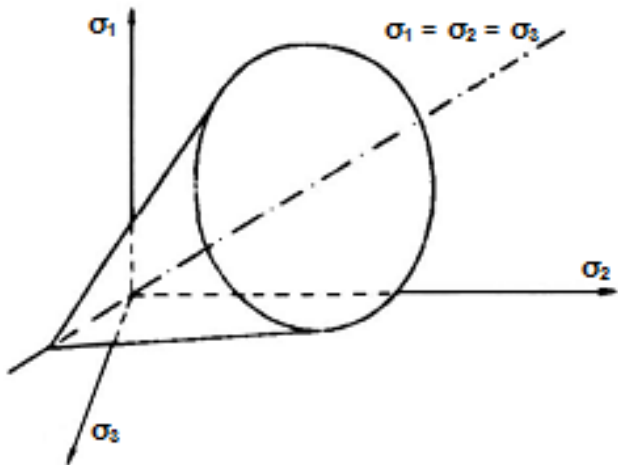


Figure 3.5: Drucker-Prager Failure Surface (Høeg 1977)

Now once the state of stress in the material reaches the yield surface the calculation of the material's plastic deformation behaviour is dependant on what is known as the plastic potential surface. This is just another surface in stress space like the yeild surface, except that instead of defining the points at which the material will yield, it determines the direction in which plastic deformations occur. For a given state of stress which lies on the plastic potential surface the direction of the plastic strains which occur is defined as the outward normal to the surface at that stress point. This is called the normaility condition. To graphically represent this the stress axes must also correspond to the plastic strain increment axes, see Figure 3.6 (Naylor and Pande 1981). The mathematical representation of the normal to the plastic potential surface, which defines the relationship between the plastic strain increments and the stress and stress increments is called the plastic flow rule (Høeg 1977) and generally has the form:

$$d\boldsymbol{\varepsilon}^p = \lambda \frac{\partial g(\sigma)}{\partial \sigma} \quad (3.4)$$

where $d\boldsymbol{\varepsilon}^p$ is the incremental strain vector, $g(\sigma)$ is the plastic potential surface and λ is a constant. This flow rule and the condition that the state of stress must lie on the yield surface are used in the computation of plastic deformations.

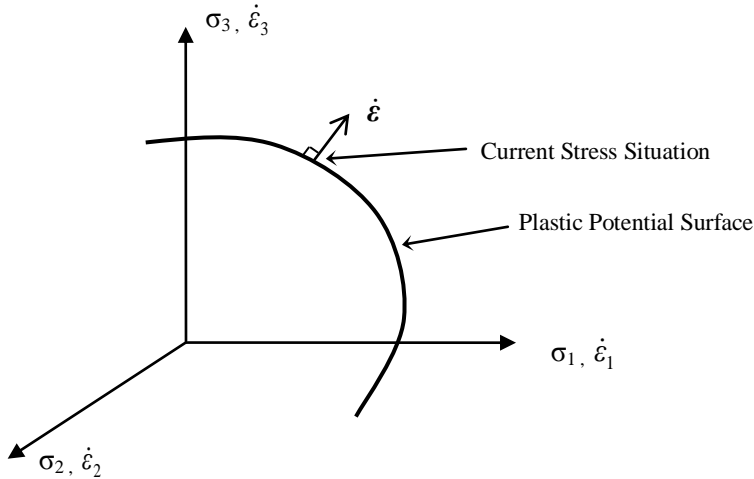


Figure 3.6: Plastic Potential Surface and the Normality Condition

For many materials, metals for example, the plastic potential surface is identical to the yeild surface. When this is the case the flow rule is said to be associated. If the yeild function and plastic potential function are not the same the flow rule is termed as non-associated. In soil mechanics non-associated flow rules are usually used in elastic-plastic soil models, because it was found that using the Mohr-Coulomb relationship as both the yeild surface and the plastic potential surface, resulted in unrealistically large plastic strains (Høeg 1977).

The process used by FLAC to calculate stresses and strains once yeilding occurs is outlined below.

1. The total incremental displacements are calculated from the equations of motion, which are extensions of Newton's second law: $\sum F = ma$, where F is force, m is mass and a is acceleration .
2. The resulting change in stress ($\Delta\sigma$) is calculated using Hooke's law.
3. If $\Delta\sigma$ causes the overall stress state to violate the yield condition, the strain increment is divided into plastic and elastic strains and the new $\Delta\sigma$ will be based only on the elastic part of the strains.
 - i. The elastic strain can be calculated using:

- Elastic deformation = Total deformation – Plastic deformation
- ii. The plastic strain required for input into the above expression is determined by applying the plastic flow rule and the condition that the new stress point must still lie on the yield surface. In FLAC the plastic flow rule has the form: $\Delta\varepsilon_i^p = \lambda \frac{\partial g}{\partial \sigma_i}$ for $i = 1,3$, where $\Delta\varepsilon_i^p$ is the plastic strain in the i principal stress direction, g is the plastic potential function, and λ is a constant, the value of which is determined when the condition that the new stress point be on the yield surface is applied. The plastic potential surface used in FLAC for shear (Mohr-Coulomb) yielding is: $g = \sigma_1 - \sigma_3 N_\psi$ where σ_1 and σ_3 are the major and minor principle stresses respectively and $N_\psi = \frac{1+\sin\psi}{1-\sin\psi}$, where ψ is the dilation angle.
 - iii. The new stress state is then calculated by using Hooke's law on the elastic strains.

For the purpose of this thesis FLAC's inbuilt Mohr-Coulomb model has been used to model the embankment material. In FLAC this model incorporates a tensile failure criterion as well as the Mohr-Coulomb failure criteria into the yield criterion. It should also be noted that if the soil yields due to the tensile criteria, a different, associated flow rule is applied for plastic strains rather than the shear one specified above. The parameters required to specify a Mohr-Coulomb material in FLAC are: bulk modulus (K), shear modulus (G), cohesion (c), friction angle (ϕ), dilation angle (ψ) and tension limit (σ^t) (Itasca 2005a).

Elastic-plastic models can also be varied to incorporate strain hardening or softening into the model (see Figure 3.7). This is done by making the yield surface a function of the plastic strain and the principal stresses. Thus, if the soil has a strain hardening behaviour then the volume enclosed by the yield surface will increase as straining occurs.

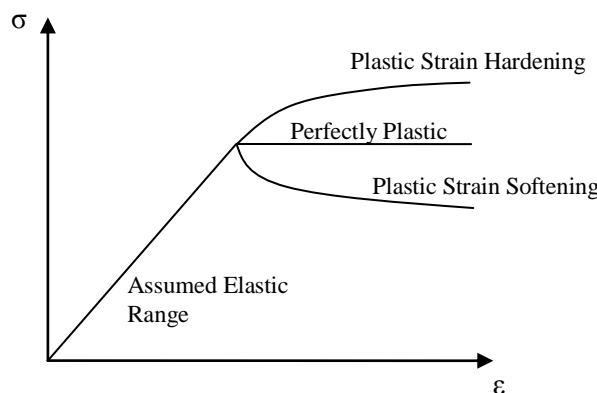


Figure 3.7: Plastic Strain Hardening and Softening

3.6.3. Critical State Models

A critical state model is a further development to the basic elastic-plastic models. These models differentiate between yielding and ultimate collapse by using a strain-dependant yield surface in conjunction with a critical state line. As such a critical state model allows a soil to yield and continue to deform until a critical state line is reached, at which point perfect plasticity is achieved (Lewis and Schrefler 1987). Cam-clay and modified Cam-Clay are two critical state models commonly used to model soft clay.

3.7 Consolidation – Modelling A Coupled Problem in FLAC

To consider the time-dependence associated with the fluid flow and mechanical deformation in consolidation of clays, a coupled numerical model is required. A coupled model uses a constitutive model as discussed in Section 3.6 and adds to this model fluid flow characteristics. The pore pressures and flow of the fluid are then calculated as functions of time. This will affect the rate at which the stress is transferred to the soil skeleton and therefore the rate at which deformations take place. However, it should not affect the overall deformations as the water or other fluid can drain and therefore will not affect the eventual stiffness of the soil. As this project consists of embankments being built on layers of soft clay, a coupled model will be used.

Modelling consolidation in FLAC is a challenging task. There are numerous different methods which can be implemented depending on the situation being modelled and the purpose of the analysis. In addition to this there are three different numerical schemes which can be used; basic-flow, saturated fast flow and unsaturated fast flow. The choice of an appropriate modelling approach should be made based on three main factors:

1. The ratio of the characteristic time scale of the diffusion process (t_c) to the actual time scale of interest (t_s),
2. The ratio of fluid stiffness to soil skeleton stiffness, characterised by R_k , and
3. Whether the perturbation to the system is primarily mechanical or pore water pressure driven.

These factors should be used in conjunction with Table 3-2 to determine the most appropriate solution method for the task.

The characteristic time scale of the process (t_c) is given by:

$$t_c = \frac{L^2}{c_v} \quad (3.5)$$

Where L is the average flow path length and c_v is the coefficient of consolidation which can be calculated using:

$$c_v = \frac{k_{FLAC}}{\left[\frac{n}{K_w} + \frac{1}{(K + \frac{4}{3}G)} \right]} \quad (3.6)$$

where n is porosity, K_w is the bulk modulus of water ($= 2 \times 10^9$ Pa), K is the bulk modulus of the soil (Pa), G is the shear modulus of the soil (Pa) and k_{FLAC} is the FLAC permeability ($\text{m}^2/\text{Pa.s}$) which is related to geotechnical permeability (k) in m/s and the unit weight of water ($\gamma_w = 9810 \text{ N/m}^3$) by:

$$k_{FLAC} = \frac{k}{\gamma_w} \quad (3.7)$$

The fluid to soil stiffness ratio is evaluated in terms of R_k which is defined as:

$$R_k = \frac{K_w}{n(K + \frac{4}{3}G)} \quad (3.8)$$

The situations modelled in this thesis all involve soft clays, and as a result have very large values of R_k . In such cases the stable explicit flow time step calculated and used by FLAC in the basic flow scheme is small compared to the time scale of the consolidation process, which can result in large computational times. This problem of small time steps compared with the consolidation time is accentuated if there are multiple soil layers with different bulk moduli and or permeabilities.

There are three solution methods outlined in Table 3-2, which deal with the case of a large value of R_k . These are; to use the basic flow scheme and reduce the bulk modulus of water so that $R_k \leq 20$ or to use the fast flow scheme, either saturated or unsaturated, with the correct bulk modulus of water. Each of these methods result in a larger time step than if the correct value for the bulk modulus of water was used with the normal flow scheme. Itasca, the developers of FLAC, recommend the use of the fast flow logic scheme, and in most models created as part of this thesis the fast flow logic was used.

Table 3-2: Different Solution Methods for Modelling Coupled Fluid-Mechanical Problems (Itasca 2005d)

Time Scale	Imposed Process Perturbation	Fluid vs. Solid Stiffness	Modelling Approach and Main Calculation Commands	Adjusted Fluid Bulk Modulus, K_w^a
$t_s \ggg t_c$ (steady-state analysis)	Mechanical or pore pressure	any R_k	1. Effective Stress with no fluid flow	no fluid
$t_s \ggg t_c$ (steady-state analysis)	Mechanical or pore pressure	any R_k	2. Effective Stress CONFIG gw SET flow off SET mech on <i>If flow is unsaturated use:</i> SET funsat on SET fast wb on to speed the solution.	$K_w^a = 0.0$
$t_s \lll t_c$ (undrained analysis)	Mechanical or pore pressure	any R_k	3. Pore Pressure Generation CONFIG gw SET flow off SET mech on <i>If flow is unsaturated use:</i> SET funsat on SET fast wb on to speed the solution.	Realistic value for K_w^a
t_s in the range of t_c	Pore pressure	any R_k	4. Uncoupled Flow-Mechanical CONFIG gw	
			Step 1: SET flow on SET mech off	$K_w^a = \frac{n}{\left[\frac{n}{K_w} + \frac{1}{(K + \frac{4}{3}G)} \right]}$
t_s in the range of t_c	Mechanical	any R_k	Step 2: SET flow off SET mech on	$K_w^a = 0.0$
			5. Coupled Flow-Mechanical CONFIG gw SET flow on SET mech on	Adjust K_w^a so that $R_k \leq 20$

t_s in the range of t_c	Mechanical	$R_k \gg 1$	<p>6. Coupled Saturated Fast Flow</p> <p><i>This can only be applied for fully saturated flow</i></p> <p>CONFIG gw SET flow on SET mech on SET fastflow on</p>	Realistic value for K_w^a
t_s in the range of t_c	Mechanical	$R_k \gg 1$	<p>7. Coupled Unsaturated Fast Flow</p> <p><i>This can only be applied for partially saturated flow</i></p> <p>CONFIG gw SET flow on SET mech on SET funsat on</p>	Realistic value for K_w^a

When modelling consolidation in FLAC with the grid configured for groundwater flow, which is the case for all methods in Table 3-2 except for the first, all soil parameters specified should be drained parameters. For a Mohr Coulomb model, these parameters are drained bulk and shear moduli (or Young's modulus and Poisson's ratio), dry density, effective cohesion and effective friction angle. In areas where the saturation is not zero FLAC will calculate the apparent properties automatically (Itasca 2005d).

It is also important when developing a model to avoid sudden changes in loadings and where possible application of loads, additional material or excavations should be made gradually. If sudden loadings cannot be avoided it is recommended that the undrained response of the system be generated first before the coupled process is modelled. This is achieved by setting flow off and running the model to equilibrium and then setting flow on and running the model as intended (Itasca 2005d).

3.8 Validation of FLAC Solution to a Simple 1-D Consolidation Problem

As part of the process of learning to use FLAC a number of basic models including non-coupled deformation only problems and coupled deformation and flow problems were created and studied. In this section one of these examples, a coupled 1-dimensional consolidation problem, is shown and the FLAC results are compared with values calculated using Terzaghi's time rate of consolidation theory.

3.8.1. Problem Definition

A 100 kPa pressure of infinite extent is applied vertically on the surface of a 20 metre thick layer of soft clay. The clay layer is underlain by a very stiff impervious material and is thus singly drained. The initial state of the problem corresponds to an undrained equilibrium in which a uniform pore pressure of 100 kPa exists. The time rate of settlement is to be modelled, as well as the pore pressure distribution with depth at different times.

Properties of the clay layer are:

$$\begin{aligned} \text{Bulk Modulus: } K &= 2 \times 10^6 \text{ Pa} \\ \text{Shear Modulus: } G &= 1 \times 10^6 \text{ Pa} \\ \text{Porosity: } n &= 0.3 \\ \text{Permeability: } k_{\text{FLAC}} &= 1 \times 10^{-10} \text{ m}^2/\text{Pa.s} \text{ corresponding to } k_{\text{Geotech}} = 98.1 \times 10^{-6} \text{ cm/s} \end{aligned} \quad \left. \begin{array}{l} \text{corresponding to} \\ \left. \begin{array}{l} E = 2.5 \text{ MPa} \\ v = 0.3 \end{array} \right. \end{array} \right\}$$

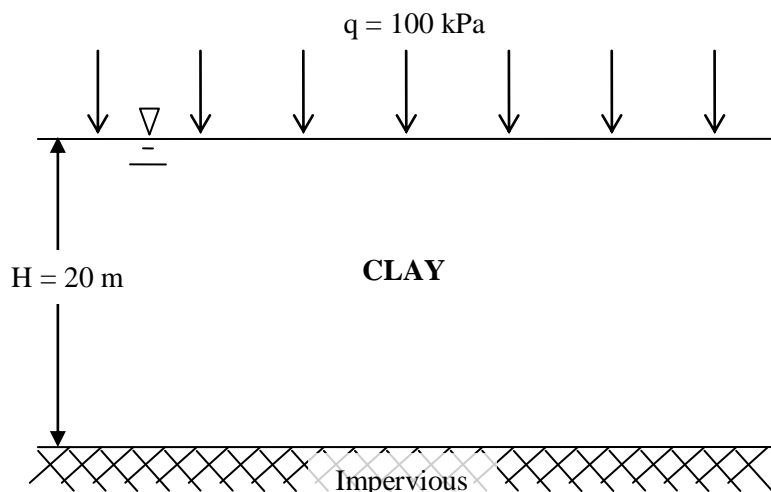


Figure 3.8: One-Dimensional Consolidation Problem

3.8.2. FLAC Model

The FLAC code used to model this problem is displayed below, and commented to describe the steps involved in the modelling process. Import parameters to observe in the problem are the boundary conditions used to simulate the one dimensional situation. All grid points are fixed against movement in the horizontal direction and the base of the clay layer is also fixed against vertical movement. There are no-flow conditions on both sides and at the base of the grid, creating the condition that the layer singly drained with drainage only allowed at the surface. This example also highlights the value of having the FISH programming language incorporated into FLAC.

;This program runs a classical 1-d consol problem with 20 m singly-drained
;clay layer. Pore pressure, effective stress variations are plotted at various
;times, and the consolidation settlement with time is plotted at the end.

new ; This tells FLAC that this is a new model unrelated to anything done previously, it is required if FLAC has been used to model another problem before this.

;This section between the Def and the End is a FISH function in which all the soil and water
;properties required for the model are specified. It will not execute until it is called in
;the FLAC commands. The last three lines before the end calculate parameters not required
;for the simulation but which are required for the theoretical calculations done separately

Def soil_properties

```
bulk1 = 2e6           ; drained (dry) bulk modulus, Pa
shear1 = 1e6          ; shear modulus, Pa
perm1 = 1e-10         ; mobility coefficient, m2/(Pa.s)
poros1 = 0.3          ; porosity
waterbulk = 2e9        ; bulk modulus of water, Pa
thickness = 20         ; layer thickness (drained only from top), m
app_pressure = 1e5      ; vertical pressure applied at top, Pa
ini_porepressure = 1e5; initial pore pressure, Pa
ini_verticalstress = -1*app_pressure
```

```
alpha1 = bulk1 + 1.333*shear1 ; Pa
Storativity = poros1/waterbulk + 1/alpha1    ; 1/Pa (this is equivalent to mv)
diffusivity = perm1/storativity             ; coefficient of consolidation cv in m2/s
```

End

soil_properties ;this calls the FISH function soil_properties so that it runs
set log on

print diffusivity ;prints value of diffusivity (cv) to the screen and records it in flac.log
print storativity ;prints value of storativity (mv) to the screen and records it in flac.log
set log off

config gw extra 2 ;sets the model to include groundwater flow, and allows for one
;extra 'vector timeseries' to be created

set flow on

set mech on

set fastflow on ;This changes the solution procedure to use fastflow logic. This is
;done because the stiffness of the water is much greater than
;the stiffness of the soil skeleton, and as such solution under the
;standard scheme would be particularly slow.

set nmech 100 ;sets nmech so that when the model is solved there will be a maximum
;of 100 mechanical timesteps for each flow timestep

grid 5 20

generate 0,0 0,thickness 5,thickness 5,0 ratio 1,1

;the above commands specify the grid, its dimensions and the mesh ratio

model elastic

```

prop dens=2000 bulk = bulk1 shear = shear1
plot grid hold

prop perm = perm1 porosity = poros1
water bulk=waterbulk den=1000

set large      ;this causes the gridpoint coordinates to be recalculated after each
                ;timestep taking account of the displacements

ini pp=ini_porepressure      ;sets initial pore pressure for whole grid
ini syy= ini_verticalstress  ;sets initial total vertical stress for whole grid

fix x           ;fixes the grid so no velocity is allowed in the x direction
fix x y j=1    ;stops movement in the x and y directions at the base of the clay layer
apply pressure=app_pressure j=21      ;applies the 100kPa load at the surface

ini pp=0 j=21   ;these two lines fix the pore pressure at the surface to be zero
fix pp j=21

;-----
;The FISH function below calculates the theoretical (Terzaghi Theory) pore pressure,
;allowing plots at four different depths within the soil layer, to be made and
;compared against the values calculated in FLAC. This function will run each time
;history values are recorded (once every 10 timesteps).

define theory
tt=diffusivity*gwtime/thickness^2      ; T=cv*t/Hdr^2
i=3

loop j(1,jgp)                         ;this cycles through all the grid point depths
zz=(thickness-y(i,j))/thickness        ; Z=z/h
sumpore=0
section
loop m (1,100000)                    ;inside this loop the summation is calculated
mmm=0.5*pi*(2*m-1)                  ;M
suminc=sin(mmm*zz)*exp(-mmm^2*tt)/mmm
sumpore=sumpore+suminc
if abs(suminc/(sumpore+1)) < 1e-5 then ;this stops the summation if an adequate
  exit section                         ;accuracy is obtained - saving
  end_if                                ;computational time
end_loop
end_section
ex_1(1,j)= sumpore*2*ini_porepressure ;stores the theoretical pp in a vector
                                         ;timeseries
end_loop

grpp1=ex_1(1,1)                      ;these extract the theoretical pore pressures at four depths
grpp6=ex_1(1,6)                      ;from the vector ex_1 and saves them separately so they can
grpp11=ex_1(1,11)                    ;be plotted or exported for comparison with FLAC results
grpp16=ex_1(1,16)
grpp21=ex_1(1,21)

theory=1
end

```

```

;-----

Define tot_vert_stress
tot_vert_stress=-syy(3,1)
porepress=pp(3,1)
eff_vert_stress=-syy(3,1)-porepress
time_days=gwtime/(60*60*24)
end

;-----

;these save the variables named after each 10 timesteps
his gwtime      ;1
his tot_vert_stress ;2
his porepress    ;3
his eff_vert_stress ;4
his ydis i=3 j=21 ;5

his gpp i=3 j=1   ;6          -> FLAC pore pressures at depths of 5, 10,
his gpp i=3 j=6   ;7          15, and 20 m
his gpp i=3 j=11  ;8
his gpp i=3 j=16  ;9
his gpp i=3 j=21  ;10

his theory       ;11         -> Theory pore pressures at depths of 5, 10,
his grpp1        ;12
his grpp6        ;13         15, and 20 m
his grpp11       ;14
his grpp16       ;15
his grpp21       ;16
his time_days    ;17

;-----


;Below is another FISH function which creates tables of pore pressure, effective stress
;and total stress with depth at various stages during the analysis and plots them.
;It also prints the time of consolidation which the plots correspond to, and the
;settlement at this time
Def pptable
i=3
loop j (1,jzones)
ytable(1,j)=j
xtable(1,j)=pp
effstress = app_pressure - pp
ytable(2,j) = j
xtable(2,j) = effstress
ytable(3,j) = j
xtable(3,j) = -1.0*syy
end_loop
consolidation_time = gwtime ;is the flow time
settlement = ydisp(4,21)
currentsteps = step
nextcyclesteps=currentsteps + varstep
command
plot hold table 1 2 3

```

```

set log on
print consolidation_time settlement currentsteps table 1
set log off
endcommand
end
;
```

;Below is another FISH function which controls the solution process. It sets the
;number of time steps between each generation and plot of stresses with depth,
;and makes the model run for this amount of steps, a number of times (specified
;on the loop line). Note that a variable step is used, so that the number of
;steps between each plot increases as consolidation progresses. This was done
;so that points on the settlement time graph were more evenly spaced. In this
;function the total settlement at each graphed time interval is also recorded
;in a table.

```

def solution ; To run "pptable" several times till consolidation is over
loop k (1,8)
varstep=500+200*k
command           ;need this since within FISH
set step varstep ;tells FLAC to compute 'varstep' number of timessteps when solved
solve auto on      ;gets FLAC to solve the model, the auto on command lets
endcommand         ;FLAC vary the number of mechanical steps for each flow
                   ;timestep. This is required as the procedure of using one
                   ;mechanical step for each flow step is not effective as
                   ;the mechanical timestep required for numerical stability is much
                   ;less than the fluid timestep required for stability.
pptable
ytable(4,k)=-1.0*settlement
xtable(4,k)=consolidation_time
end_loop
end
;
```

solution;makes the FISH solution function run

```

plot hold table 4      ;To plot settlement with time
plot hold his 2 3 4 vs 1 ;To plot total, effective, and pore pressures with time
plot hold his 6 skip 20 cross 12 7 skip 20 cross 13 8 skip 20 cross 14 9 skip 20 cross 15 vs 1
                   ;plots pore pressures at varying depths with time against theory
```

;The lines below save the values in each of the tables to a text file so that
;they can be imported into EXCEL for comparison.

```

set log on
print table 1
print table 2
print table 3
print table 4
set log off
```

;these lines save the FLAC and theory pore pressure values to a text file
set hisfile solvetocompvphis280507.txt
his write 1 skip 20

```

his write 6 skip 20
his write 7 skip 20
his write 8 skip 20
his write 9 skip 20
his write 16 skip 20
his write 11 skip 20
his write 12 skip 20
his write 13 skip 20
his write 14 skip 20
set hisfile his.txt

```

Figure 3.9 is one of the graphs produced by FLAC in the process of solving the model. It shows the distribution of effective stress, pore pressure and total stress with depth, 2 days four hours and 15 minutes after the 100 kPa load is applied. Table 1 corresponds to pore water pressure; Table 2 corresponds to effective stress and Table 3 corresponds to total stress.

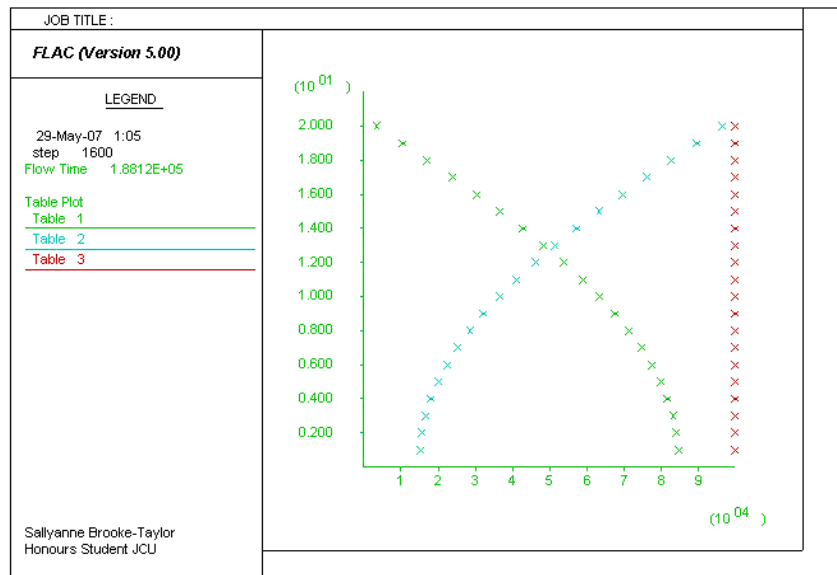


Figure 3.9: Plot in FLAC of the Distribution of Effective stress and Pore Pressure after 188 120 seconds (2days, 4hrs and 15mins)

The variation of these quantities with time was also plotted in FLAC and is shown in Figure 3.10. To get these results the model was solved using the ‘SOLVE auto on’ command. In initial runs of the model a different command ‘STEP’ was used. This command executes the specified number of time steps using one mechanical step for each fluid step. Considering the almost instantaneous timescale of mechanical deformations as opposed to the often lengthy consolidation processes, it can be expected that having equal numbers of mechanical and flow time steps would result in reduced accuracy. When the SOLVE auto on command is used, FLAC automatically adjusts the number of mechanical or fluid time steps ensuring that the solution is stable. Figure 3.11 shows the distribution of stresses with time when the

STEP command is used to solve the model. The inaccuracies caused by using equal mechanical and fluid time steps are clearly shown by the perturbations in the three curves of Figure 3.11, which are significantly smaller and hardly noticeable in Figure 3.10. Given the noticeable difference in the results shown in Figure 3.10 and Figure 3.11 future models will be solved using the SOLVE auto on command rather than the STEP command to ensure the highest possible accuracy can be achieved.

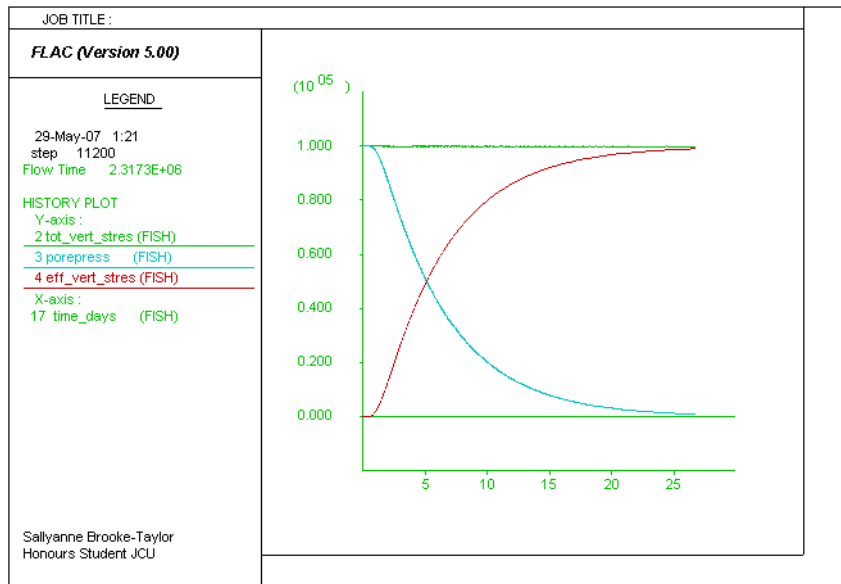


Figure 3.10: Variation of Pore Pressure, Effective Stress and Total Stress with Time

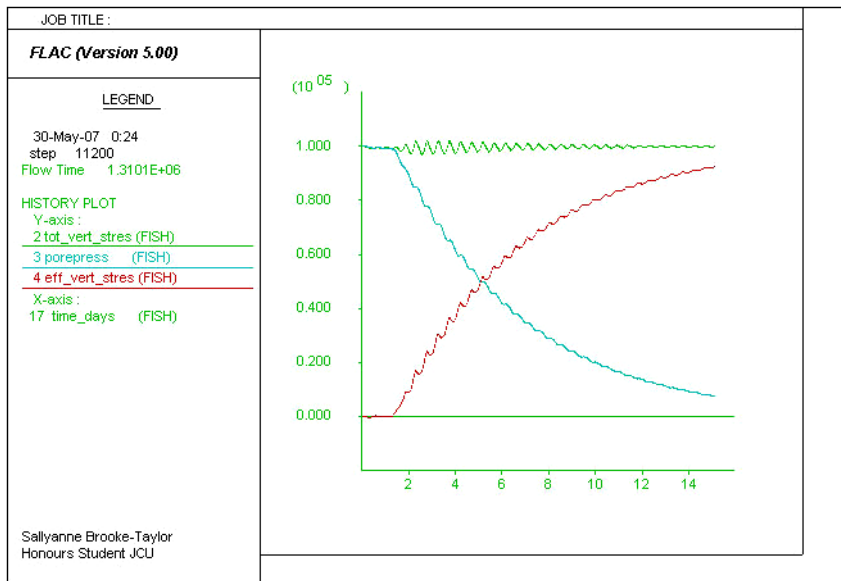


Figure 3.11: Variation of Pore Pressure, Effective Stress and Total Stress with Time, when the Model is Solved Using the STEP Command

3.8.3. Theoretical Calculation

The same problem was analysed using Terzaghi's one dimensional time rate of consolidation theory, which is summarised in Section 2.2.3: Consolidation - Time Rate of Consolidation. To use this theory a value for m_v and c_v were required. These were calculated in the FLAC program above and are:

$$m_v = \frac{n}{K_w} + \frac{1}{K + 4/3 G} = 0.3002 \text{ MPa}^{-1} \quad (3.9)$$

$$c_v = \frac{k}{m_v} = 3.331 \times 10^{-4} \text{ m}^2/\text{s} \quad (3.10)$$

Where K_w is the bulk modulus of water and is equal to 2×10^9 Pa. Equations (3.9) and (3.10) are taken from an example problem in the FLAC manual. They are based on Biot's consolidation theory which is a three dimensional consolidation theory.

From equations (2.19) and (3.9) the total settlement is:

$$\text{Sett} = m_v \Delta \sigma H = 0.3002 \times 0.1 \times 20 = 0.6\text{m}$$

The theoretical settlement with respect to time curve was then created in Excel using Figure 2.14 and a settlement of 0.6 metres.

3.8.4. Comparison of FLAC Results with Theory

A graph showing the settlement with respect to time results from both the FLAC simulation and the theoretical calculation is shown in Figure 3.12.

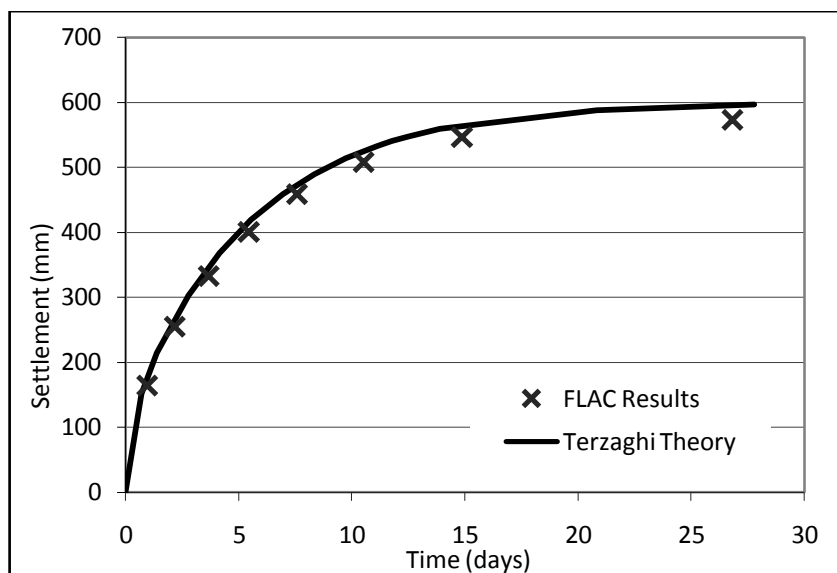


Figure 3.12: Settlement with Time Comparison

The difference between the two sets of values is minimal, with the FLAC results being approximately 4% smaller than theoretical values. This indicates that the FLAC model accurately simulates the settlement–time relationship of this one-dimensional problem.

The variation of pore pressure with time at four different depths was also recorded in the FLAC model and compared with the results predicted from Terzaghi's one dimensional consolidation theory. Figure 3.13 shows the two sets of results, and it is clear that the agreement between FLAC and theory is good. However, what may not be noticeable from Figure 3.13 is that the relative error in the FLAC results increases with time, from less than 1% initially up to 25% in some measurements towards the end. This is likely to be the result of a combination of two factors. Firstly, that the magnitude of pore pressure decreases with time, therefore an equally small absolute error will become a larger relative error, and secondly, that FLAC uses an explicit time-marching solution technique, and in any such numerical technique the errors will always increase as the number of solution steps increase.

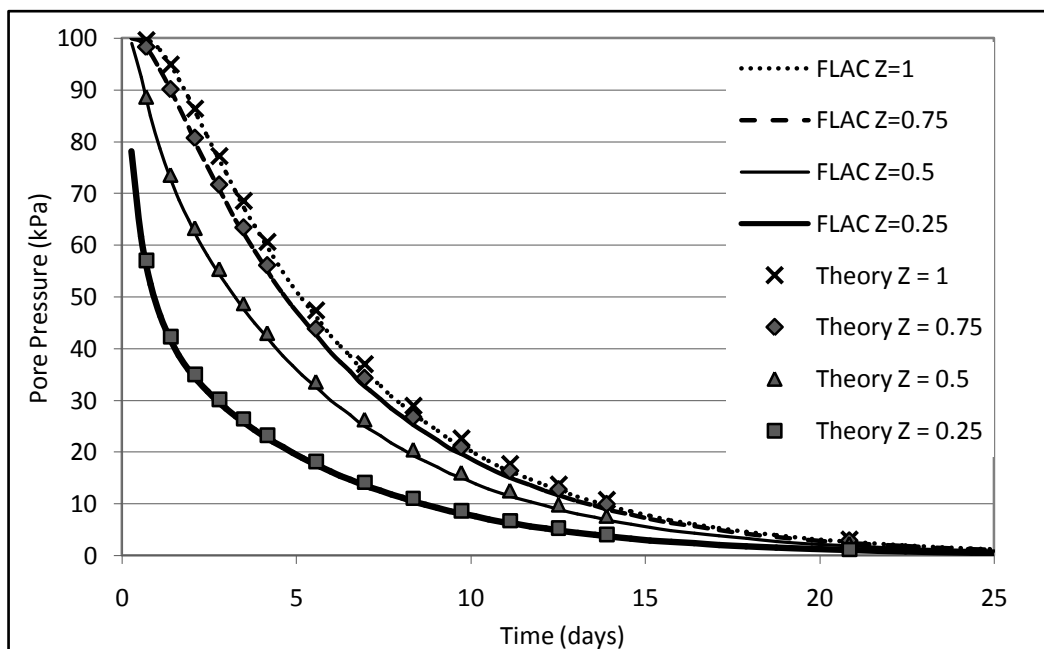


Figure 3.13: Comparison of FLAC Results and Theory for Pore Pressure with Time at Four Depths

3.8.5. Conclusions from the 1-D Consolidation Problem

The results of this simple consolidation problem validate that FLAC can be used to accurately model one dimensional consolidation problems. It should, however be noted that while the theory that the results were compared to is widely used and accepted in the geotechnical community, it is based on a number of assumptions, some of which are not realistic, as discussed in the Time Rate of Consolidation and Difficulties in Accurately Determining Consolidation Settlement parts of section 2.2.3. As such a better validation of

the capabilities of FLAC to model consolidation in the field will be the results of the trial embankment models. Although, these will be subject to other complications such as accurate determination of soil properties, variations of soil strata along the length of the embankments and the assumption that the embankments can be modelled as two dimensional plain strain situations.

3.9 *Summary*

This chapter briefly discussed why FLAC was chosen to be the program used for the numerical modelling in this thesis. It then went on to explain how the Finite Difference Method used by FLAC differs from the Finite Element Method (FEM) used by a number of other numerical modelling programs. It also outlined how the implicit solution technique used by most FEM programs differs from the explicit solution technique employed by FLAC. Some of the features of FLAC were then discussed. This was followed by an explanation of some of the different stress-strain relationships inbuilt in FLAC which can be used to model soils. Both elastic and plastic constitutive relations were discussed. Following this was an overview of how consolidation can be modelled in FLAC, in particular this section focused on how to chose the most effective modelling procedure for a problem. The chapter was concluded with the discussion of a FLAC model which validated that FLAC can be used to accurately model one-dimensional consolidation problems.

Chapter 4: The Tully Project

4.1 Introduction

The Tully project is a 14.7 km stretch of highway being constructed to improve the flood immunity of the Bruce Highway in North Queensland. It is being delivered under an “alliance” contractual arrangement between the Department of Main Roads, Maunsell and BMD, with Maunsell undertaking the design work and BMD the construction work. This arrangement allows the project to be completed in a much shorter timeframe as the construction is able to begin on some sections while other sections are still in the design phase. Currently the project is in the first year of a two year construction program.

The new section of highway will span from Corduroy Creek in the South to Tully High School in the North as shown in Figure 4.1. It is single lane in each direction and includes 59 culverts, 6 bridges, and embankments ranging up to 7.5m high. This section of highway is situated in a flood plain, and the natural ground is highly stratified and contains some very soft layers. In addition the soil profile varies significantly along the alignment. Based on geotechnical investigations conducted along the proposed new road alignment settlement predictions were made, which included total settlement expected and time to achieve that settlement. The most up to date predictions as at July 2007 had settlements ranging from less than 40mm up to 300mm in some sections, and allowed settlement periods of up to six months.

For areas where large settlements were predicted and the time for the settlements to take place was also large, preloading and in some cases surcharging was included in the construction process. Preloading is where the embankments are constructed to the required road height and left for a predetermined length of time to allow settlement to take place. After the preload period an amount equal to the pavement thickness is removed from the top of the embankment and the pavement is placed. Surcharging is the same as preloading except that an additional height of fill is added above the finished road height to reduce the time for the required amount of settlement to take place. Preloading is also required in many of the culvert locations, and in these locations the process is similar to other areas except that after the preload period the entire embankment is removed and a culvert is placed. The settlement predictions and proposed preloading treatment for the entire alignment is included in Table A-1 in Appendix Appendix A: Tully Data.

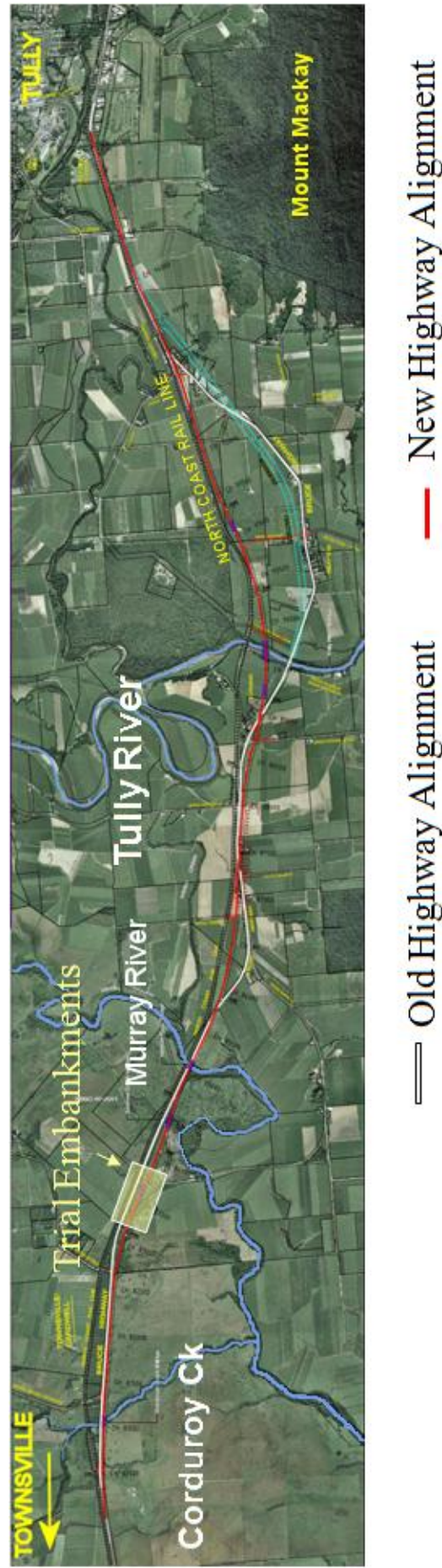


Figure 4.1: Alignment of the New Highway Showing the Location of the Trial Embankments

4.2 The Trial Embankments

In the area surrounding the Lagoon Creek South Bridge (CH83330 – CH83740) three trial embankments were constructed. The site was chosen due to land availability and because some of the highest settlements were predicted in part of this area. The trial embankments are located along the alignment and will form part of the highway when it is completed, Figure 4.2 shows the locations.

Each of the three embankments was instrumented with settlement plates placed at the centre of the embankments at longitudinal intervals of 20 or 25 metres. Piezometers were also placed in the foundations of each of the embankments with one in trial embankment 1, two at each of two locations in trial embankment 2 and another two at a location in trial embankment 3. Where two piezometers were used at the same location, they were placed at different depths, 1.5 metres apart within the foundation. Additionally, inclinometers were used in trial embankments 1 and 2, with one inclinometer about one metre from the toe in embankment 1, one about one metre from the toe in the culvert section of embankment 2 and a third inclinometer at the toe in the other section of embankment 2. No inclinometers were placed near embankment 3 because this embankment was constructed with berms for the preloading stage which will be removed when the highway is completed. The temporary widening of the embankment due to these berms meant that there was not an appropriate location for inclinometer casing to be installed. The positioning of this instrumentation as well as the geometry of trial embankments 1 and 2 is shown in Figure 4.3 and Figure 4.4 respectively.

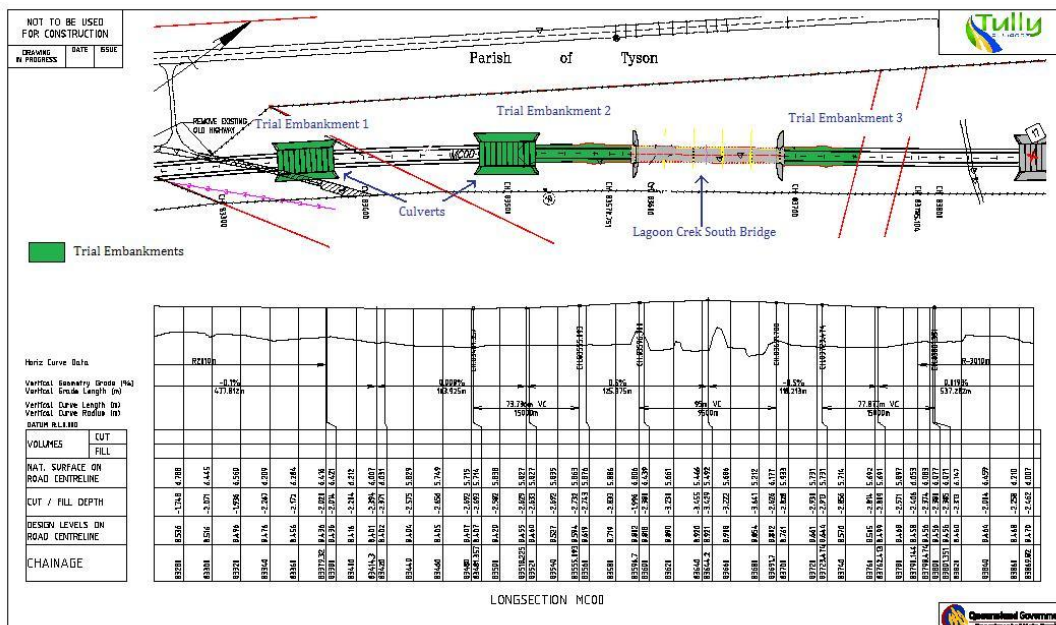


Figure 4.2: Location of the Three Trial Embankments (Modified from a drawing provided by the Tully Alliance)

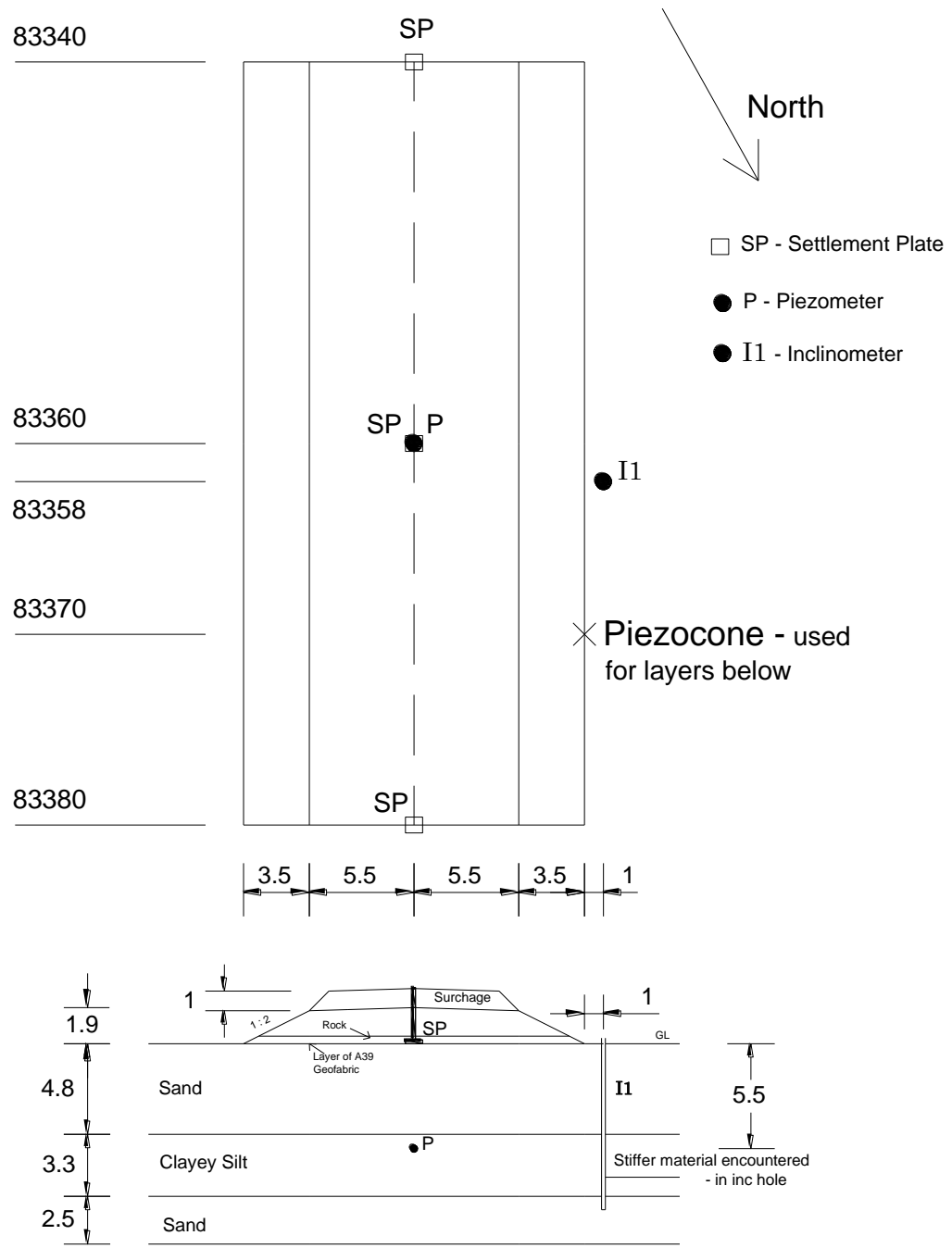


Figure 4.3: Location of Instrumentation and Geometry of Trial Embankment 1

Figure 4.5 is a photograph taken of trial embankment 2 looking towards Lagoon Creek. It shows the different batter slopes present over the culvert section, closest to the camera, and the road embankment section. The location of some of monitoring equipment is also visible in this photograph. A closer view of the top of the inclinometer casing and the piezometer monitoring box located in the culvert section of Trial Embankment 2 is shown in Figure 4.6.

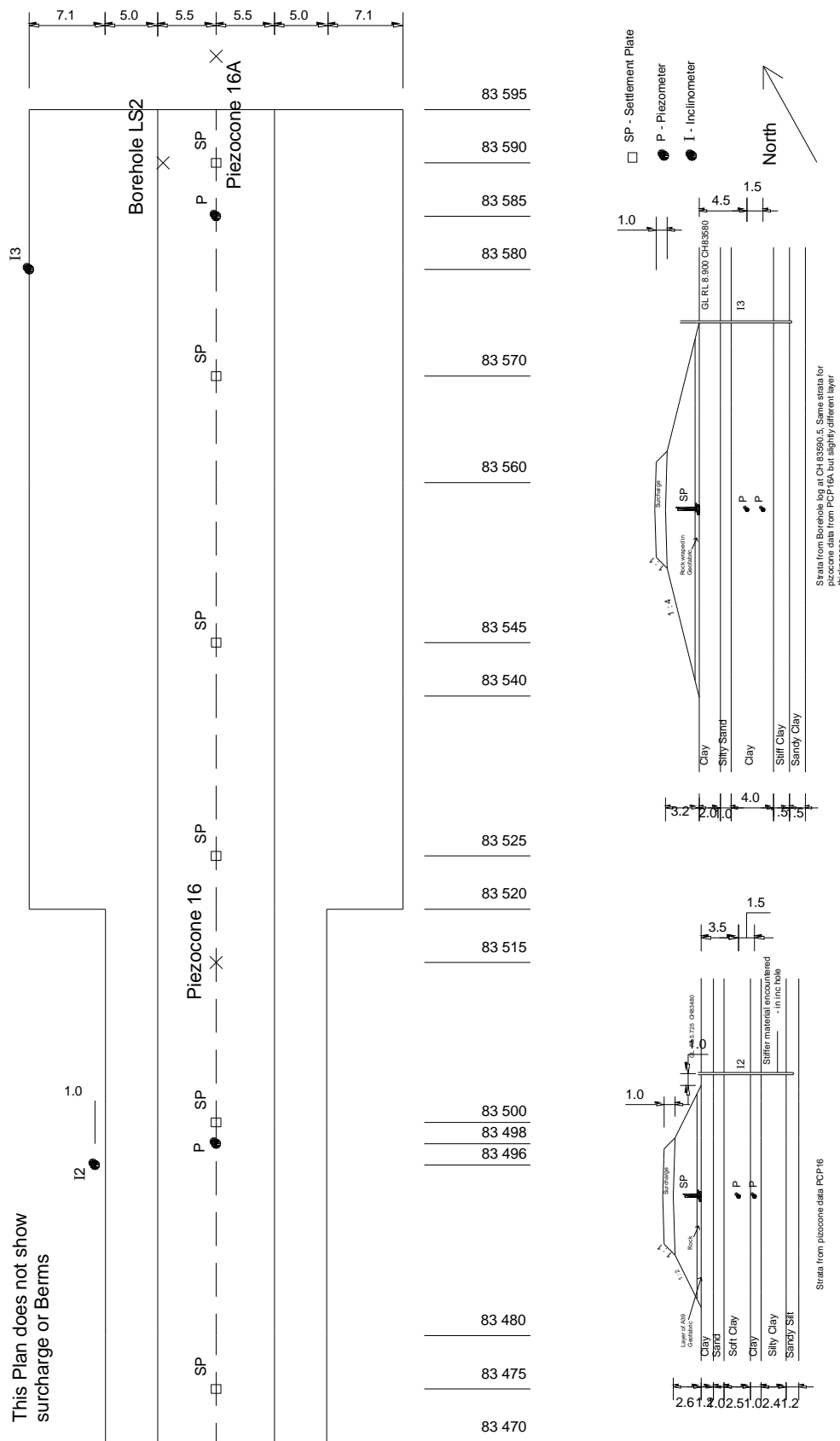


Figure 4.4: Location of Instrumentation and Geometry of Trial Embankment 2



Figure 4.5: Embankment 2, Looking Towards Lagoon Creek

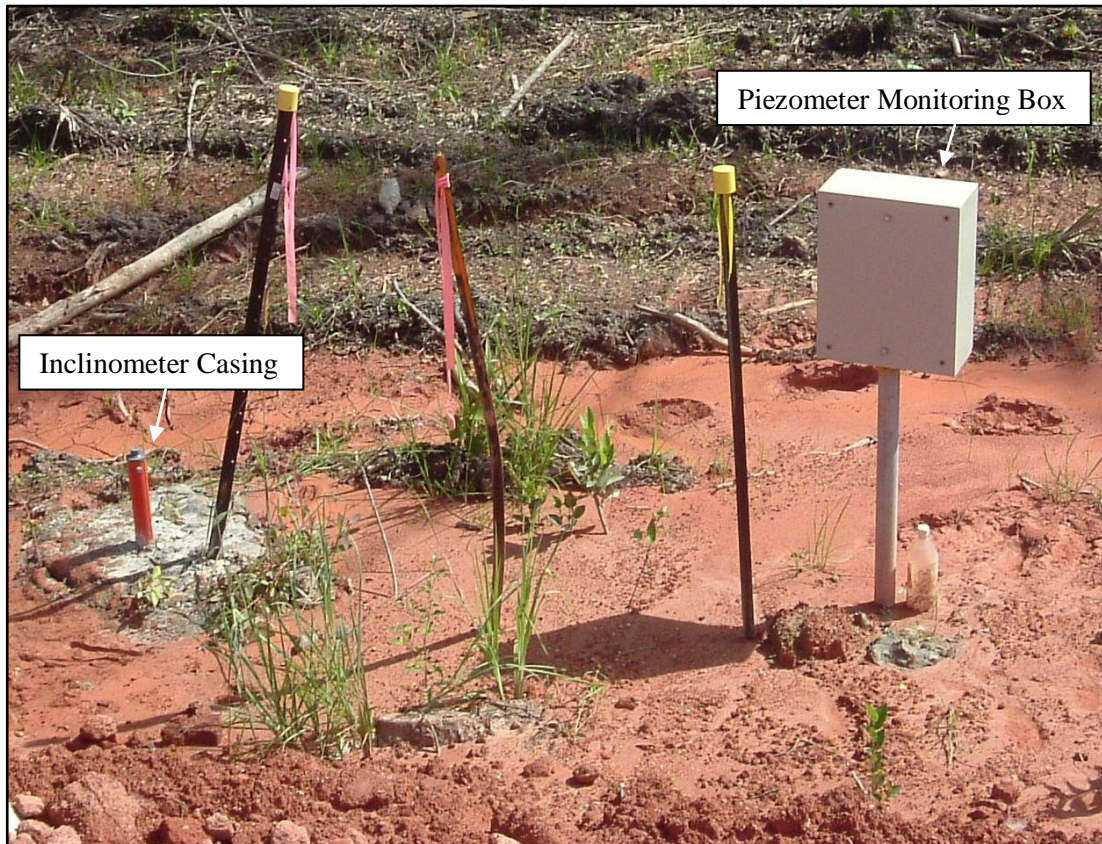


Figure 4.6: Top of Inclinometer Casing and Piezometer Monitoring Box next to the Culvert Section of Trial Embankment 2

Construction began on the trial embankments in March 2007, and was not completed until July due to five weeks of wet weather halting progress from mid May till early June. Another unfortunate occurrence was that construction began before all the instrumentation was in place. This made the process of matching model predictions with measurements more difficult as an unknown amount of settlement resulting from the embankments took place before any settlement was recorded.

Settlement readings were taken by surveyors at intervals of between 3 and 7 days, along with the corresponding height of the embankment. The piezometers recorded a continuous stream of data, which was downloaded at regular intervals. Inclinometer data was also collected manually on a regular basis, however, this was not made available for use in this thesis, due to difficulties encountered by the project team when converting the raw data to actual lateral displacements.

4.3 Geotechnical Investigations

The geotechnical investigations that were conducted on the Tully project included boreholes in which SPT's were done and from which samples were taken as well as piezocone tests.

Several boreholes were drilled at each bridge location, spanning the length of the bridges. These boreholes were extended to depths of between 31.2 and 41.2 meters, with SPT tests conducted at intervals of 1.5 metres and samples also taken at intervals of 1.5 metres. Borehole logs from the Lagoon Creek South area that were used in determining soil layers and properties for the trial embankment foundations are included in Appendix A-2.2: Borehole Logs and the locations of these boreholes are shown in Appendix A-2.1: Map Showing the Location of the Boreholes and Piezocone Tests. Additional boreholes were conducted at other locations which extended only to depths of 10 to 15 metres. Samples were also taken from these and consolidation tests were conducted on the clay samples, refer to Appendix A-2.3: Consolidation Test Results, for the test results used to determine foundation properties for the trial embankment modelling. The results from the consolidation tests were used to determine the permeability of the clay layers as well as the dry densities of these layers.

In addition to the boreholes, piezocone tests were conducted at each of the culvert or potential culvert locations. These extended to depths of between 2 and 20 metres, and at some of the locations dissipation tests were also conducted. The piezocone data was the main source of information used for determining the foundation soil layers and assigning values to the parameters required for the models. The test data used is included in Appendix A-2.4: Piezocone Results.

Samples of the material being used for the embankments were also taken. Triaxial tests and consolidation tests were conducted on this material. However the results were not made available to the writer for use in this thesis.

4.4 Summary

In this chapter a brief overview of the Tully Project was given. It covered general details about the 15 km stretch of highway being constructed and the geotechnical conditions of the area. As well as this the trial embankments which form part of the project were discussed. Within this trial embankment section the location of the monitoring equipment was the focus. Finally, details of the geotechnical investigations undertaken by the Tully Alliance team to determine the nature of the natural foundation of the embankments were presented.

Chapter 5: Preliminary Consolidation Models

5.1 *Introduction*

This chapter is divided into two sections. The first section discusses a sensitivity analysis conducted, in which the effects of variations in a number of soil properties and also in the initialisation process are studied. During this analysis a problem with the timing of the settlement results was observed and the second part of this chapter outlines part of the process used in an attempt to isolate and fix the problem.

5.2 *Sensitivity Analysis*

A number of preliminary models were created to gain an understanding of how the values of permeability, Young's modulus, density, effective cohesion, effective friction angle and model initialisation conditions affected the foundation deformations and stresses associated with consolidation resulting from an embankment load. In these models the embankment was simulated by an applied load at the surface of the model and the foundations consisted of only one or two different soil layers as opposed to the six distinct layers evident beneath the second trial embankment.

5.2.1. Model Geometry and Soil Properties in the Basis Model

One of the main objectives when creating the preliminary models was to create models which would solve quickly, but would still give useful results. As such the model geometries were made as simple as possible with as few elements as were required for accuracy. The main simplification made to achieve this purpose was to replace the embankment with an embankment shaped applied stress at the surface of the foundation. This meant that the actual model was just the rectangular shaped foundation. The symmetry of the embankment was also taken advantage of and only one half of the embankment and foundation was modelled.

There were two model geometries used in the preliminary modelling stage, one for the single layer models and another for the two layer models. In both models the total depth of the foundation was 5 metres and the width of the foundation modelled was 15 metres. The finite difference mesh in both cases had 8 zones vertically and 15 zones horizontally, and was graded so that the elements near the applied load were slightly smaller (see Figure 5.1 and Figure 5.2 for the two grids used). Grading the mesh in this way was done to improve the accuracy of the model as the required element size for a given accuracy is inversely proportional to the stress gradient in the area, which in the problem modelled was highest near the embankment loading.

In the single layer models the entire foundation had the properties of a soft clay. The properties in the original model were chosen to be similar to the properties of the 2.5 metre thick soft clay layer beneath the culvert section of the second trial embankment (refer to section 6.3). In the two layer models the top 1.5 metre layer had the properties of a sand similar to the second top layer beneath the culvert section of the second trial embankment and the bottom 3.5m layer had the same properties as used in the one layer model. The properties used in the original models are listed below.

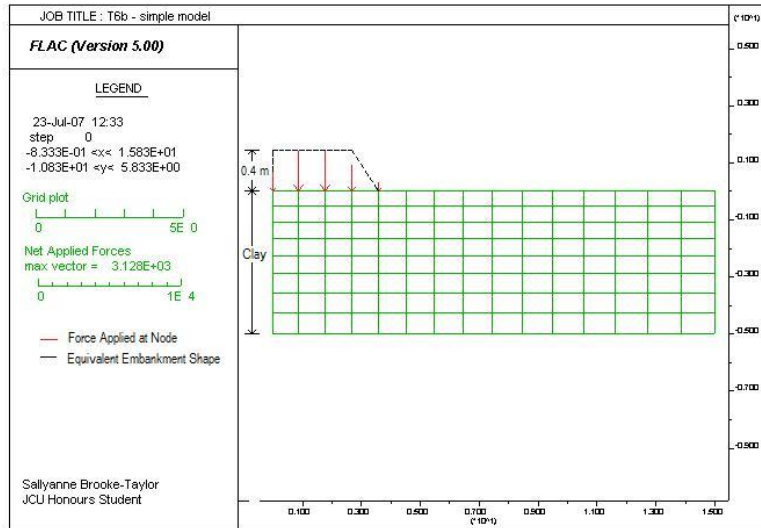


Figure 5.1: Mesh for the Single Layer Models

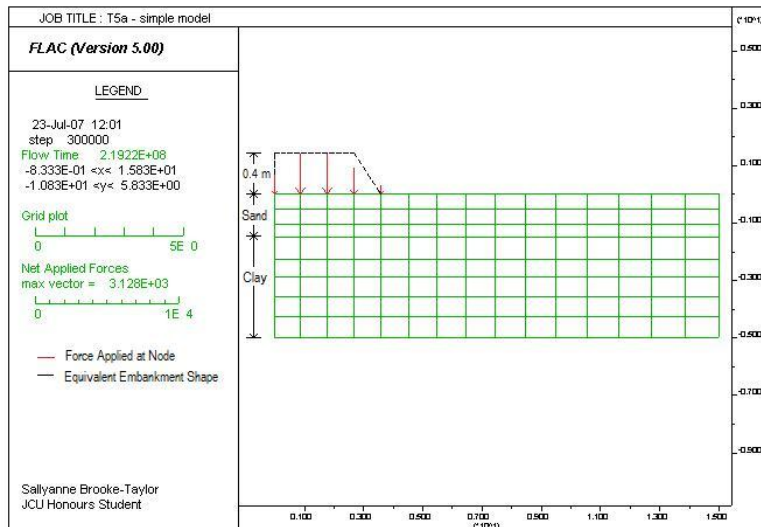


Figure 5.2: Mesh for the two Layer Model

Sand Layer (Two Layer Model only):

Young's Modulus	$E = 19.3 \times 10^6 \text{ Pa}$
Poisson's ratio	$\nu = 0.4$
Dry Density	$\rho = 1480 \text{ kg/m}^3$
Permeability	$k = 500 \times 10^{-9} \text{ cm/s}$
	$k_{FLAC} = 500 \times 10^{-15} \text{ m}^2/\text{Pa.s}$
Effective Cohesion	$c' = 0 \text{ kPa}$
Effective Friction Angle	$\phi' = 35^\circ$

Clay Layer (Both Single Layer and Two Layer Models):

Young's Modulus	$E = 1 \times 10^6 \text{ Pa}$
Poisson's ratio	$\nu = 0.4$
Dry Density	$\rho = 650 \text{ kg/m}^3$
Permeability	$k = 30 \times 10^{-9} \text{ cm/s}$
	$k_{FLAC} = 30 \times 10^{-15} \text{ m}^2/\text{Pa.s}$
Effective Cohesion	$c' = 0 \text{ kPa}$
Effective Friction Angle	$\phi' = 25^\circ$

The original applied stress used in each model is equivalent to a small embankment 0.4 metres high and 2.65 metres wide at the crest from the centre to one edge with batters at a slope of 1 metre vertically for every 2.3 metres horizontally. This is only a very small load however significant failures occurred if the load was increased in the single layer models.

5.2.2. Boundary Conditions

When modelling coupled problems there are two sets of boundary conditions which need to be considered; those relating to the soil skeleton, that is the mechanical boundary conditions, and those relating to the fluid.

Mechanical boundary conditions can be one of two forms, a stress boundary condition or a velocity boundary condition. From experience, predicted stresses and displacements tend to be overestimated in models using stress boundary conditions and underestimated in models using fixed or velocity boundary conditions (Coetzee et al. 1998). In the preliminary models created the velocities perpendicular to the boundaries were fixed at zero for both of the vertical boundaries and also at the bottom of the model. This results in a condition of no horizontal displacements at either side of the model and no vertical displacements at the base of the model. The horizontal displacements were also fixed at the base of the model.

In FLAC fluid boundary conditions are applied by fixing or freeing the pore water pressure and or saturation at the boundaries. There are therefore four possible fluid boundary conditions. If both pore pressure and saturation are free the boundary is impermeable. If the pore pressure is fixed and saturation is free, fluid can flow into or out of the model. The saturation can also vary but only if the pore pressure is fixed to zero. This is the normal boundary condition for a free surface. Fixing the saturation but keeping the pore pressure free is the condition used when there is an applied discharge at the boundary, and fixing both the pore pressure and the saturation, is the normal condition used when a pore pressure distribution is fixed, this condition allows flow to occur across the boundary (Coetzee et al. 1998).

In the preliminary models the boundary along the line of symmetry (the left vertical boundary in Figure 5.1) and the bottom boundary were made impermeable. The top boundary had a pore pressure fixed to zero and the saturation fixed to 1 to force the water table to remain at the surface, though a model having the pore pressure fixed to zero and the saturation free was found to produce exactly the same results. At the other vertical boundary a pore pressure distribution representing the hydrostatic pore pressures resulting from a water table at ground level was fixed. Fixing the pore pressure distribution at this boundary is appropriate as long as the boundary is far enough from the embankment that the load does not affect the stresses in this area, otherwise the boundary condition will have an effect on the results obtained. Observation of the stress contours in the preliminary models indicated that this condition was satisfied.

5.2.3. The Solution Process

There were three main stages to the solution process used in the preliminary models; initialisation of the stresses in the foundation before the embankment load was applied, undrained analysis and coupled drained analysis.

Initialisation can be performed in a number of ways including:

- (a) Specifying the expected stress distributions within the foundation due to gravity,
- (b) Allowing the model foundation with no embankment load to run until it reaches equilibrium,
- (c) Allowing the model foundation with no embankment load to run until it reaches equilibrium but with higher than actual strength parameters to stop yielding from occurring in the convergence process and
- (d) Making the model elastic and allowing it to run until it reaches equilibrium, to avoid yielding in the convergence process, then changing it back to Mohr-Coulomb.

Methods (b), (c) and (d) above can be performed either with or without specifying estimated stresses prior to running the model, however, specifying estimated stresses reduces the computational time required for the model to reach equilibrium. Equilibrium in this case is defined as the state when the unbalanced force ratio is below a specified value, the default value for example is 0.001.

Determining which method was most effective was the first factor investigated with the preliminary models, but after this all models were initialised by first specifying the expected stress distributions and then allowing the model to run (with flow on) to equilibrium with the correct strength parameters. As this process resulted in displacements which were not in any way related to the embankment, the horizontal and vertical displacements were reset to zero after equilibrium was reached. Similarly, yielding occurred in some models during the initialisation process, and as this would not actually happen in the field and again was not related to the embankment loads, the yielding history was reset by changing the model to be elastic and then back to being Mohr-coulomb. In most models this was done after the undrained analysis so that it was obvious which elements were failing during the consolidation process.

The undrained analysis was a necessary part of the solution procedure because the embankment load was applied instantaneously rather than gradually. In this stage of the solution procedure flow was turned off and the stresses were allowed to come to equilibrium. As there was no flow, and the stiffness of water was significantly higher than that of the soil the majority of the applied embankment load should have been transferred to pore pressure during this phase. This stage was assumed to occur instantaneously and the FLAC model did not associate any time with it, because the time scale of mechanical deformations is generally significantly smaller than that of flow related deformations.

The final stage of the solution process was the drained or consolidation stage. In this part of the analysis flow was turned back on and water was allowed to escape from the modelled foundation where the boundary conditions allowed it to. During this stage, the pore pressure would decrease as the water drained and the stress was transferred to the soil skeleton. This analysis was run for a period long enough to allow the consolidation process to finish, at which point the pore pressure distribution had reached a uniform hydrostatic profile. In FLAC this stage was run using the ‘SOLVE auto on’ command. As discussed in section 3.8.5 this command allows FLAC to control the number of mechanical steps for each fluid step and vice-versa to ensure that the unbalanced forces remain below a specified value and the solution is stable. Due to the way this command works the model could not just be run until it reached equilibrium instead it was run until a specified time in seconds was reached.

This time was the time which it would take for the process to be completed in the field not the time taken for the computer to solve it. This value was different for each of the models run as the time of consolidation is dependent on some of the soil properties varied in the models.

For both the initialisation and drained analysis the inbuilt fast flow logic method was used to solve the models, as it was considerably faster than the normal solution scheme.

5.2.4. Required Output

To observe the effects of variations of different properties a number of different types of results were output. The output observed included the settlement versus time graph for the location at the surface beneath the centre of the embankment, which was the vertical displacement at the top left corner of the grid. The pore pressure distribution, the vertical displacement distribution and the state of the elements (either elastic, at yield in tension, at yield in shear or elastic but yielded in the past) were also recorded after each stage of the solution process.

As well as this the models were programmed to also calculate the theoretical one-dimensional settlement, to give some basis to compare the results against. To determine the theoretical settlement m_v was calculated for each layer using equation (3.9) and this was used in equation (2.19) along with the height of each layer and the applied stress, as shown in equation (5.1).

$$\text{sett} = m_{v1} \times (\text{Applied Stress}) \times H_1 + m_{v2} \times (\text{Applied Stress}) \times H_2 \quad (5.1)$$

This will not be exactly what you would expect the settlement to be beneath the centre of the embankment as the Applied Stress in equation (5.1) should be the effective stress at depth, which if used would give a smaller theoretical settlement. Also settlement beneath an embankment does not fall into the category of one dimensional consolidation and according to Zhang's work (refer to Section 2.3.2) the settlement beneath the centre of the embankment should be equal to or greater than the one dimensional settlement depending on the embankment width, due to shear stress developed in the foundation. As such the theoretical calculation is just an approximation of what the settlement should be.

5.2.5. Results

This section outlines the results obtained and conclusions drawn from the multiple models which were run. The code for the basis two layer model and basis one layer model are included in Appendix B-1.1: Original Two Layer Model and Appendix B-1.2: Original Single Layer Model.

Results of the Original Two Layer Model

The graphs output from this model are shown from Figure 5.3 through to Figure 5.8. Figure 5.3 shows the settlement versus time graph for two locations beneath the centre of the embankment, one at the surface and one at a depth of 1.5 metres where the two layers meet. From this graph it can be seen that the total settlement was 5.71mm and that almost all of that settlement (5.52 mm of it) occurred in the bottom layer which was the soft clay layer. This magnitude of settlement compares reasonably well with the theoretical calculation of 6.48 mm, of which 6.34 mm was from the clay layer and 0.14 mm was from the sand layer. The unexpected result shown in Figure 5.3 is the ratio of initial settlement to total settlement. In this model this ratio had a value of 0.45 which is very high. For embankments on soft clays it generally does not exceed 0.15 (Balasubramaniam 2007). The effect of each of the soil properties on this ratio was observed during this preliminary modelling stage and is discussed in the following sections along with the conclusions regarding sensitivity.

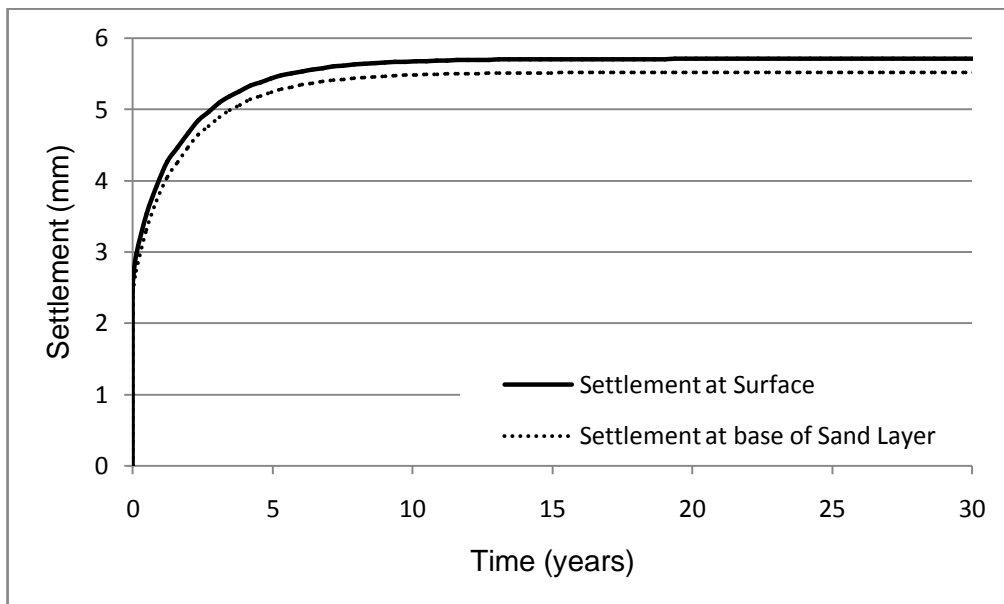


Figure 5.3: Vertical Displacement beneath the Centre of the Embankment against Time

Figure 5.4 shows the pore pressure distribution after the undrained analysis. The pore pressure contours at the right side of the model correspond to the fixed hydrostatic distribution. The way that these contours extend horizontally for some distance indicates that the width of the modelled area is wide enough for the boundary conditions at this point to be not affecting the result, as the embankment is not changing the pore pressures in this region.

The slight raising of the contours towards the left side of the model is due to the embankment load being transferred to the pore pressure as expected. However, the top

contour is horizontal across the whole model indicating that in this region the embankment load may have been transferred to the soil skeleton as opposed to the water. This assumption is confirmed by observation of the effective stress contours shown in Figure 5.5. This is another unexpected result given the low stiffness of the sand in comparison to water, but it does to some degree explain why the immediate settlement may be excessively high.

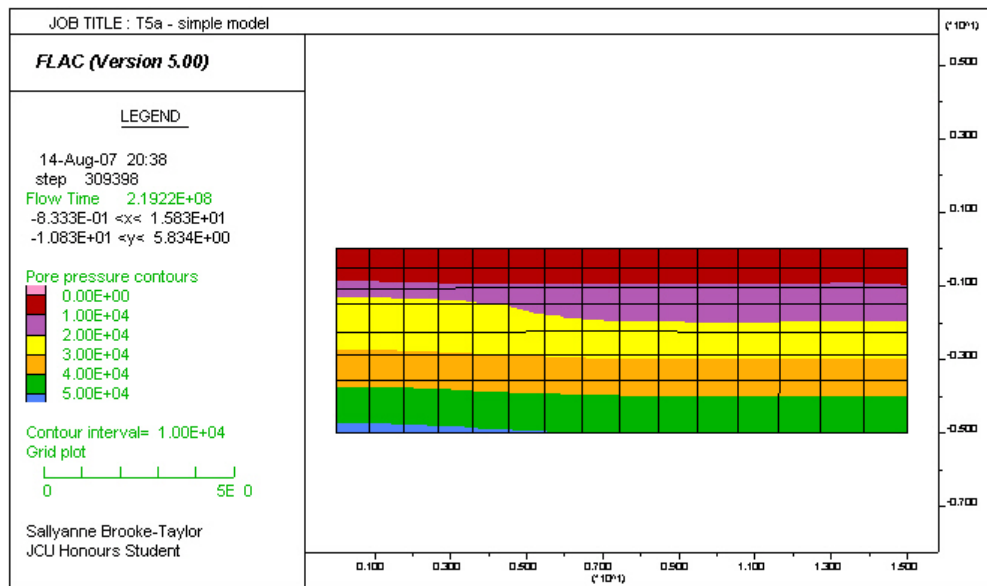


Figure 5.4: Pore Water Pressure Distribution in Two Layer Model after Undrained Analysis

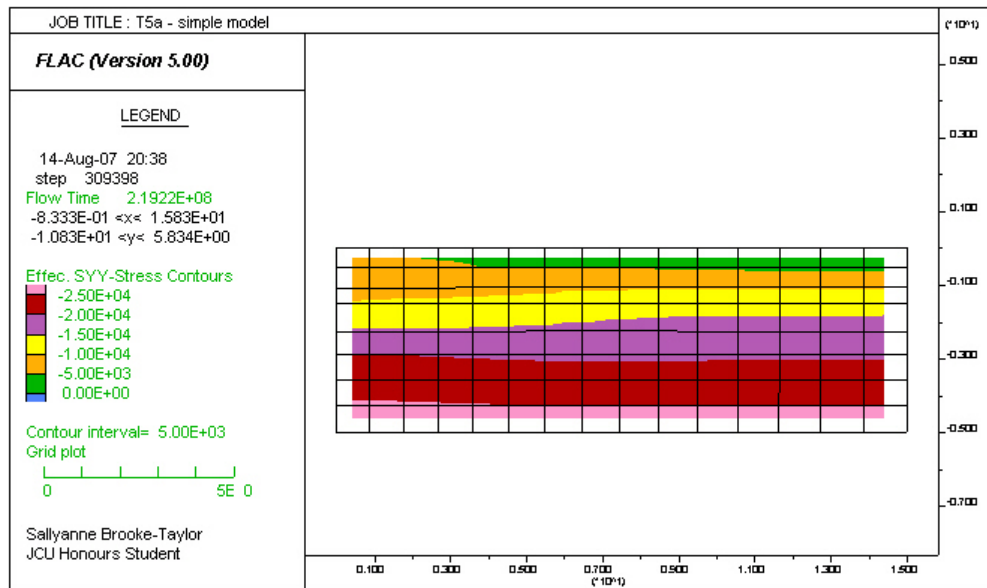


Figure 5.5: Vertical Effective Stress Distribution in Two Layer Model after Undrained Analysis

Figure 5.6 is the vertical displacement distribution in the foundation after the undrained analysis. It is a typical vertical displacement plot showing settlement beneath the embankment and heave next to the toe of the embankment.

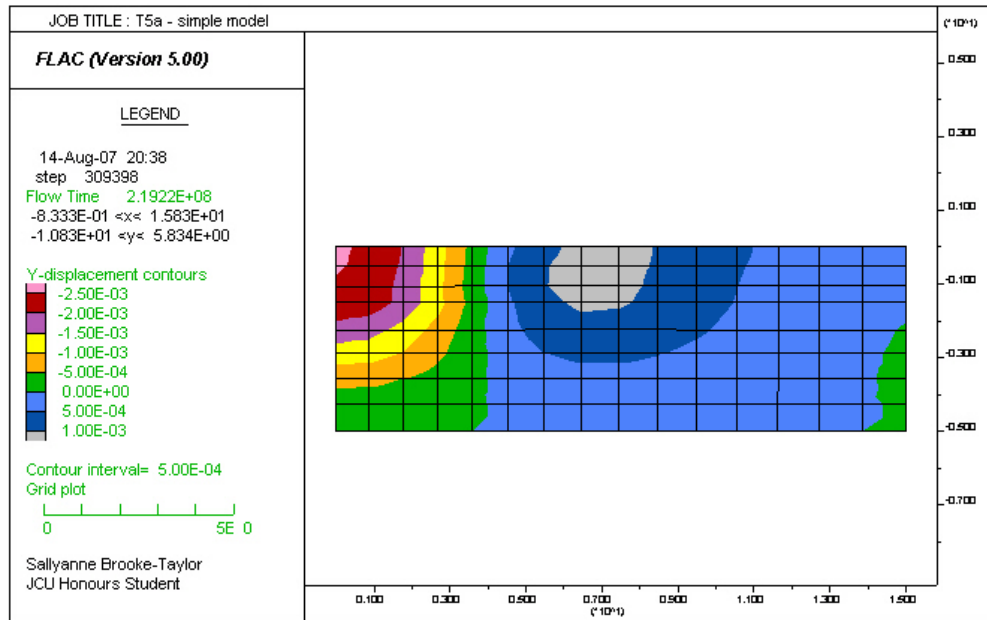


Figure 5.6: Vertical Displacement Distribution in Two Layer Model after Undrained Analysis

In Figure 5.7, which shows the pore pressure distribution after the drained analysis, the pore pressure contours have returned to being horizontal contours showing a hydrostatic pore pressure distribution across the model. This indicates that the consolidation process has finished. Finally, it can be seen from Figure 5.8 that the heave shown in Figure 5.6 has settled as water was allowed to drain leaving only settlement in the foundation which was highest at the surface beneath the centre of the embankment.

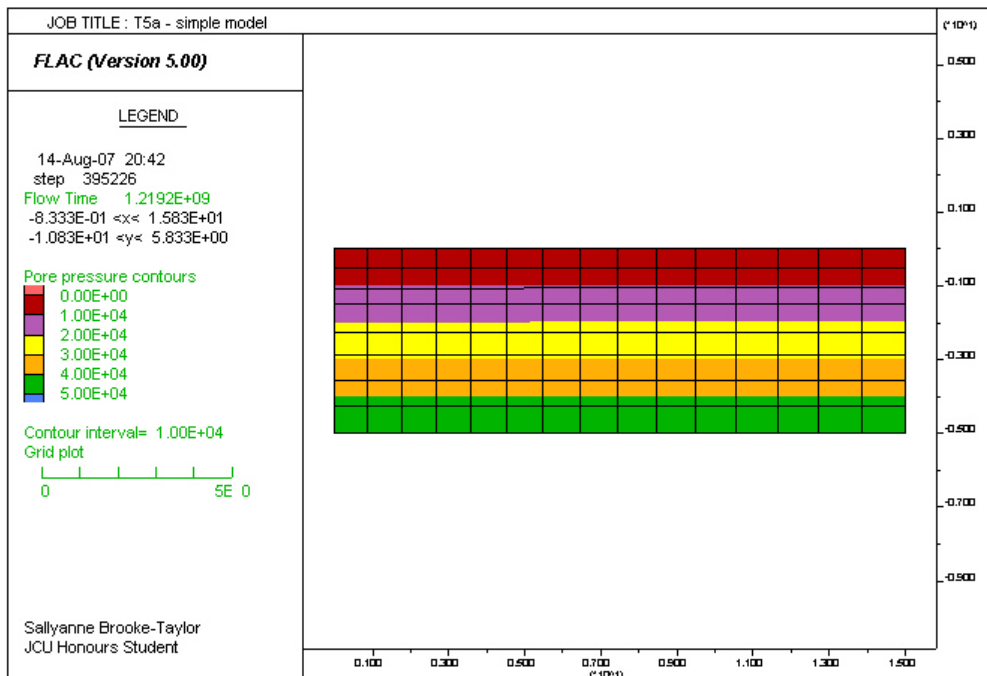


Figure 5.7: Pore Water Pressure Distribution in Two Layer Model after Drained Analysis

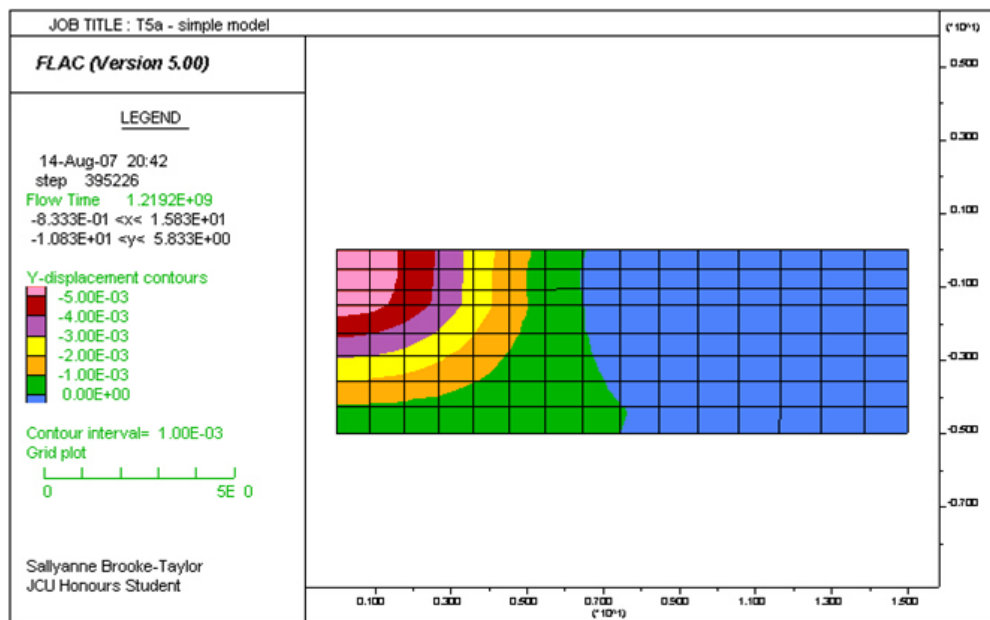


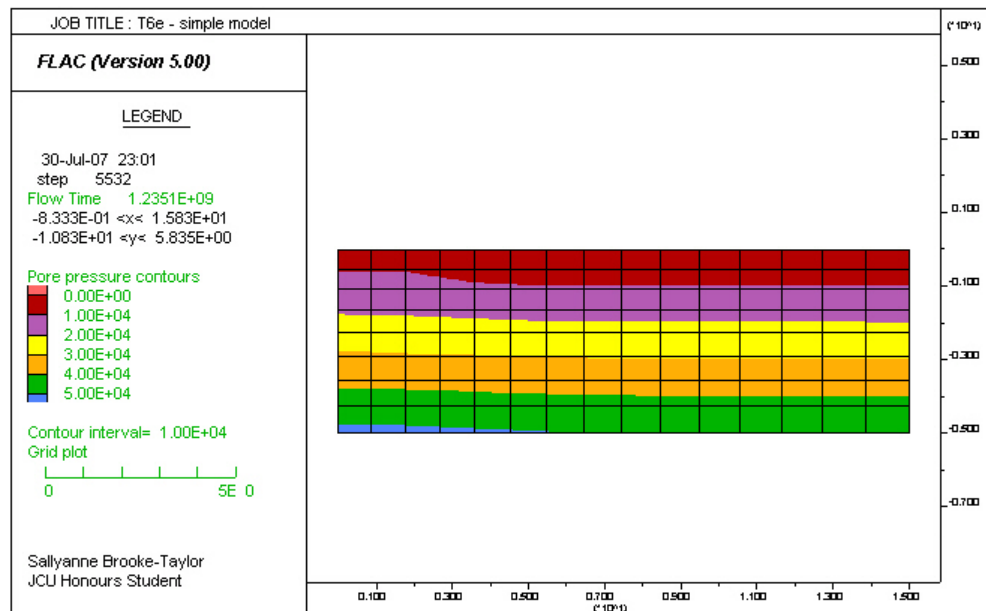
Figure 5.8: Vertical Displacement Distribution in Two Layer Model after Drained Analysis

Effect of Initialisation Conditions

The majority of models run to test the effects of different initialisation conditions were single layer models. Six variations of the initialisation and solution procedure were tested, of which only two models produced settlements close to the theoretical prediction of 9.05 millimetres. The main reason for trialling different initialisation procedures is that when a Mohr-Coulomb model is initialised by running it until equilibrium, elements of the model foundation often yield, which does not happen in practice. To avoid this problem the FLAC manual suggests either using higher than normal strength parameters (c' and ϕ') for the initialisation stage or making the model elastic for the initial stage and then in both cases converting the model back to Mohr-Coulomb with the correct strength properties for the analysis. Alternatively, the initial stress distribution can be inputted to the model by the user if known, to avoid running the model to equilibrium. Each of these options was tested including using the normal strength parameters for initialisation, and the resulting settlements and indications as to whether the pore pressure graphs after the undrained analysis were as expected are recorded in Table 5-1. Where the pore pressure distribution is classed as realistic the distribution took on a form similar to that shown in Figure 5.9, and in all cases where it was classed as unrealistic the distribution had a form similar to that shown in Figure 5.10.

Table 5-1: Results from Single Layer Models with Different Initialisation Procedures

Initialisation/Solution Process	Pore Pressure Distribution After Undrained Analysis	Immediate Settlement (mm)	Consolidation Settlement (mm)	Total Settlement (mm)
Normal c' and ϕ' for all three stages	Realistic	6	4	10
High c' and ϕ' for initialisation, normal c' and ϕ' for undrained and drained	Unrealistic	13	16	29
Elastic for initialisation, normal c' and ϕ' for undrained and drained	Unrealistic	33	18	51
Elastic for initialisation and undrained, normal c' and ϕ' for drained	Realistic	16	20	36
Initial stresses approximated but not run to equilibrium, normal c' and ϕ' for undrained and drained	Unrealistic	22	20	42
Normal c' and ϕ' for all three stages, but state (i.e. yielding) reset after undrained	Realistic	6	4	10

**Figure 5.9:** Pore Pressure Distribution after Undrained Analysis for Single Layer Model where Actual c' and ϕ' values were used for all three stages

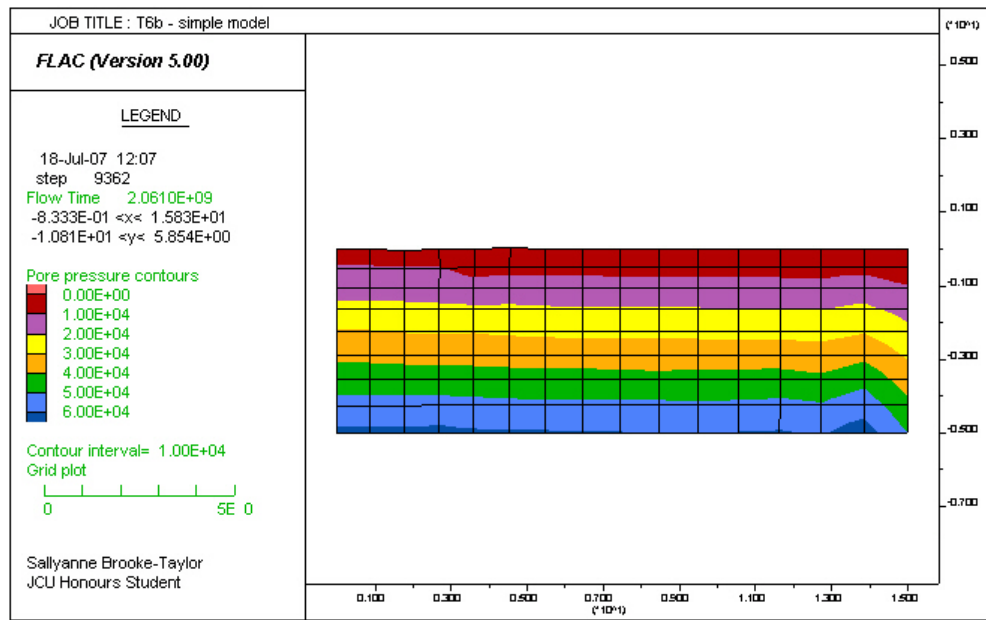


Figure 5.10: Pore Pressure Distribution After Undrained Analysis for Single Layer Model where High c' and ϕ' values were used for the Initialisation Stage

In the fifth model shown in Table 5-1 where initial stresses were simply input, the reason for the unrealistic settlements and pore pressure distribution was that the estimated horizontal stresses were significantly smaller than the ones calculated when the model was run to equilibrium with normal strength parameters. The estimates were calculated using:

$$\sigma_h = K_o \sigma_v \quad (5.2)$$

where:

$$K_o = \frac{v}{1-v} \quad (5.3)$$

is the coefficient of earth pressure at rest. There are several different expressions for K_o throughout the literature for different types of soil, and Equation (5.3) is based on an assumption that the soil is elastic (Barnes 2000). Another model was run with the initial horizontal stress distribution set equal to that calculated by FLAC in the run to equilibrium with normal strength parameters, and this model had the normal pore pressure distribution and initial and consolidation settlements of 6 mm and 4 mm respectively.

The models described in Table 5-1 were each repeated but with a higher applied embankment pressure of 10 kPa as opposed to 3.5 kPa. The results were similar except that all models significantly overestimated the settlements due to yielding occurring in the foundations. It is believed that the yielding occurring was to a large extent the result of having the tensile capacity of the foundation set to zero. A tensile capacity of zero is a decent

assumption for sands, however, for natural clays specifying some tensile capacity is more realistic.

Based on these results it was decided that future models would be run with the correct strength properties for all three stages of the solution process, but that the state of the model would be reset after the undrained analysis so that it was clear which elements failed during the consolidation process. The two layer model was then run with this solution method to confirm that it was suitable and the results which were discussed in Section 5.2.5 under the heading Results of the Original Two Layer Model confirmed it to be acceptable. It should also be noted that none of the alternative initialisation methods significantly reduced the ratio of immediate to total settlement.

Effect of Permeability, k

Three single layer models were run with different permeabilities of $k_{FLAC} = 30 \times 10^{-14} \text{ m}^2/\text{Pa.s}$, $30 \times 10^{-15} \text{ m}^2/\text{Pa.s}$ and $30 \times 10^{-16} \text{ m}^2/\text{Pa.s}$. The results of these models showed that permeability did not affect the magnitude of settlement, the ratio of initial settlement to total settlement or which elements yielded. The only factor it affected was the time for consolidation to occur. If the permeability was reduced by a factor of 10 then the time for consolidation to occur increased by approximately a factor of 10. This was as expected, and in accordance with Equations (2.24) and (2.27) which combine to give the relationship:

$$t = \frac{T(H_{dr})^2 m_v}{k_{FLAC}} \quad (5.4)$$

i.e.

$$t \propto \frac{1}{k_{FLAC}}$$

A number of two layer models were also created in which the permeability of each of the layers was varied separately. As in the single layer models, varying the permeability did not affect the magnitude of settlement, the ratio of initial settlement to total settlement or which elements yielded. It did affect the time of consolidation, though, as there were two layers the ratio of times was not simply the inverse relation of Equation (5.4). The other factor that permeability affected in the two layer model was the computational time and number of steps required for the initialisation stage to reach equilibrium. As the difference in permeability of the two layers increased the time required to solve the model also increased.

Effect of Young's Modulus, E

Four single layer models were run with Young's Moduli of $E = 1 \times 10^5 \text{ Pa}$, $1 \times 10^6 \text{ Pa}$, $2 \times 10^6 \text{ Pa}$ and $1 \times 10^7 \text{ Pa}$. From these models it was determined that Young's Modulus not only affected the amount of settlement as expected, but also had a slight affect on the ratio of initial settlement to total settlement. The results showed that as the value of Young's Modulus increased the magnitude of settlement decreased in inverse proportion, and the ratio of initial settlement to total settlement increased slightly.

A number of two layer models were also run with varying values of Young's Modulus, a summary of the results is recorded in Table 5-2. From these results a number of conclusions were drawn regarding the effect of Young's Modulus on the ratio of initial settlement to total settlement. Firstly, as the moduli of two adjacent layers approach each other the ratio of initial to total settlements increases. However, the ratio cannot be reduced much below 0.5 by increasing the difference between moduli of different layers as the grid failed due to numerical problems. The numerical problems were believed to be associated with the use of Lagrangian analysis, and based on the results in Table 5-2 occurred when the ratio of moduli of adjacent layers was greater than 40. Also, in contrast to what was found in the single layer models if the ratio of the moduli of adjacent layers was held constant but the moduli were increased there was no significant change in the settlement ratio.

Table 5-2: Results From Two Layer Models Where Young's Modulus was Varied

Model Number	Young's Modulus (MPa)		Applied Stress (kPa)	Approximate Settlement (mm)				Initial Sett / Total Sett
	Layer 1	Layer 2		Initial	Consolidation	Total	Theoretical	
5a	19.3	1	3.5	2.9	2.9	5.8	6.48	0.5
9d	19.3	10	3.5	0.55	0.33	0.88	0.78	0.63
9e	19.3	0.1	3.5	Grid Crashed				
9f	19.3	0.5	3.5	Grid Crashed				
9h	193	1	3.5	Grid Crashed				
9i	193	10	3.5	0.3	0.3	0.6	0.65	0.5
9j	600	30	3.5	0.1	0.09	0.19	0.22	0.53
9k	600	30	35	3	0.6	3.6	2.2	0.83
9l	19.3	19.3	3.5	0.36	0.17	0.53	0.475	0.68
9m	1930	100	3.5	0.03	0.029	0.059	0.071	0.51
9n	60	3	3.5	0.95	0.95	1.8	2.2	0.53

Based on the results, the effect on settlement of varying the Young's Modulus was generally similar to that predicted by the theoretical calculations and when the ratio of the moduli of adjacent layers was held constant the inverse relation between Young's Modulus and settlement could clearly be seen. An interesting effect noticed was that when the ratio of adjacent moduli was higher (19.3 or more) the modelled settlement was less than the theoretical settlement and when the ratio was 2 or less the modelled settlement was more than the theoretical settlement. This may be due to the relative stiffness of the layers affecting the distribution of stresses which was not accounted for in the theoretical calculation.

Another important effect discovered during the running of these models, which was found to be independent of the value of Young's Modulus, was that if the applied stress was high enough to cause large areas of yielding in the model then the immediate to total settlement ratio increased dramatically.

Effect of Density, ρ , Effective Cohesion c' , and Effective Friction Angle, ϕ'

Three two layer models were run where the density of the clay layer took on values of 650 kg/m³, 1000 kg/m³ and 1480 kg/m³ respectively. The results showed that density did not have any significant effect on the magnitude of settlement, the ratio of initial settlement to total settlement, the pore pressure distributions or which elements yielded. Similarly a number of models were run where the cohesion and friction angle were varied independently between values of 0 – 50 kPa and 10° – 45° respectively. As with the density these parameters did not significantly affect any of the parameters observed, though it is believed that if the applied stress was higher, they may have affected the number of elements that yielded and based on this the magnitude and ratio of settlements.

5.2.6. Conclusions Drawn from the Sensitivity Analysis

The conclusion that came out of the sensitivity analysis which had most effect on later models was the discovery of how sensitive the predicted settlements were to differences in the initialisation process. It was determined that the only form of initialisation which produces settlement magnitudes close to theoretical predictions involves the model foundation being solved to equilibrium with its correct strength properties. Generally, all of the soil properties tested had the theoretically expected effects on the magnitude and time of settlement. The model results were found to be insensitive to density, and at low stresses also to the Mohr Coulomb strength parameters. None of the properties had any significant effects on the ratio of initial to total settlement, other than that if the soil yielded the initial

settlement increased dramatically. Observation of the pore pressure and effective stress distributions immediately after the undrained analyses indicated that the high immediate settlements encountered could be a result of a higher than expected proportion of the embankment load being transferred to the soil grains during the undrained analysis. However, the results of this sensitivity analysis did not uncover any way of reducing the ratio to the values believed to be realistic.

5.3 *Investigation into the Problem of High Immediate Settlements*

In all of the preliminary models created as part of the sensitivity analysis a high proportion, of the total settlements modelled occurred instantaneously. This behaviour is contrary to that normally observed in the field and also contrary to theoretical expectations. Under undrained conditions settlement should be comparatively small as the apparent bulk modulus of a soil is increased due to the high bulk modulus of the water compared to the soil. In FLAC this apparent bulk modulus is given by:

$$K_u = K + \frac{K_w}{n} \quad (5.5)$$

Where K_u is the apparent bulk modulus of soil under undrained conditions, K is the bulk modulus of soil under drained conditions, K_w is the bulk modulus of water and n is the porosity of the soil (Itasca 2005d). In the soft soils considered in this thesis the bulk modulus of water is orders of magnitude larger than that of the soil, therefore from equation (5.5) the apparent bulk modulus of the soil should be orders of magnitude larger under undrained conditions than under drained conditions. Following on from this the immediate settlement should be orders of magnitude smaller than the drained settlement.

Given that the purpose of this thesis was to investigate the potential for pavement cracking to occur in the embankments on the Tully project, and that pavement cracking was only a concern because of the high settlements expected to occur after construction due to consolidation, finding a solution to this problem was considered of high importance and a thorough investigation was conducted. Parts of this investigation are summarised in the following sections.

5.3.1. Modifying the One-Dimensional Model

The approach used to isolate the problem was to make use of the one dimensional consolidation model discussed in section 3.8, by modifying it until it started to produce the large immediate settlements. Very minor modifications were made between each rerunning of the model so that if the large immediate settlement occurred it was clear what commands had caused it.

Varying the Grid

The one dimensional model discussed in section 3.8, consisted of a 5 x 20 element grid representing a foundation, 5 metres wide and 20 metres deep. These dimensions do not lend themselves well to embankment modelling as the narrow width would cause significant boundary effects in a two dimensional situation. Therefore the first modification was to make the grid 20 metres wide and 10 metres deep. Running the model with this and other grid geometries indicated the grid shape was not causing the problem.

Including Generation of Foundation Stresses

In the one dimensional model the pore water pressure and total vertical stress distribution within the foundation, caused by the applied load, were set in the model before it was solved. This was easily done in the one dimensional model because firstly it was one dimensional and secondly there was no gravity so the total vertical foundation stresses and pore water pressure were uniform and equal to the applied stress. The lines of code setting these initial conditions were removed in the next modification so that the undrained pore pressure and stress distribution were calculated by FLAC as part of the consolidation process. This made no noticeable difference to the results of the model.

Reducing the Load Width

The next logical modification was to make the model two dimensional by reducing the load width. Instead of having the load applied across the whole surface, the load was restricted to one quarter of the surface. The load was applied next to one of the vertical boundaries with the implication that the boundary was a symmetry boundary. Running this model resulted in the large immediate settlements recorded in the earlier two dimensional models. Figure 5.11 shows the settlement versus time results for both the one dimensional model and the two dimensional variation of the same model. The difference in overall magnitude of settlement shown in Figure 5.11 is not a major concern, because in the two dimensional model, the stress in the soil attenuates with depth due to the finite width of the load, and the expected settlement would therefore be less. The magnitude of immediate settlement cannot so easily

be explained, and is not in accordance with the settlement time curves observed in the literature or on site in Tully. Some increase in the early rate of settlement of the two dimensional model compared with the one dimensional model would be expected as pore water would be able to drain both vertically and horizontally, compared with purely vertical drainage in the one dimensional model. However, the magnitude of settlement which occurs effectively immediately is believed to be significantly larger than could be explained by the previous statement. The code for the two dimensional model from which the settlement results in Figure 5.11 come is included in Appendix B-1.3: Code for the Two Dimensional Consolidation Model Created by modifying the One Dimensional Consolidation Model.

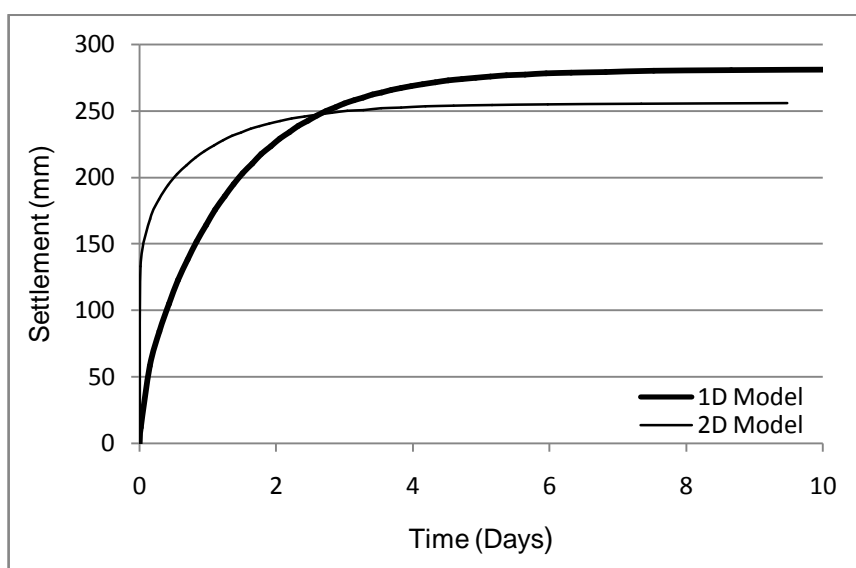


Figure 5.11: Comparison of Settlement Versus Time for 1-Dimensional Model and 2-Dimensional Variation of the Same Model

Given that the change in code required to change the model from one dimensional to two dimensional, was half a line of code, it is believed that the problem is not due to an error in the code written, but perhaps a problem relating to the physics of the problem not being suited to the numerical solution procedure used. To confirm this belief and obtain advice on how to overcome the issue, a number of people were consulted for advice including my supervisors, Mr Michael Matheson, and Associate Professor Nagaratnam Sivakugan, Dr Briony Rankine who previously used FLAC to model embankments on soft clays, Dr. John McLellan a regular user of FLAC from the JCU Geology Department, Dr Bruce Hobbs a long time user of FLAC from CSIRO in Perth and Dr Christine Detournay the code developer for the Fluid-Mechanical Interaction aspects of FLAC from Itasca USA. No one who looked at the code written found any problems in the code, however, suggestions were made of further investigations which could be conducted.

In addition to this models were also created which included gravity, and in which an embankment was actually placed rather than just a load. The large immediate settlements were found to be present in these models as well, whether or not the embankment was placed instantaneously or incrementally.

5.3.2. Investigations Conducted on a Basic Two Dimensional Consolidation Model

A number of investigations were conducted on the basic two dimensional consolidation model, which was created by modifying the one dimensional model that matched theory. The two dimensional model investigated was the most basic model that could be created which produced the large immediate settlement issue. It did not include gravity, there was only a single layer of soil, 10 metres deep by 20 metres wide, and the embankment was simulated by a 100 kPa load applied to the surface of the grid. Soil properties for the foundation are listed below.

Foundation Properties:

Bulk Modulus	$E = 2 \times 10^6 \text{ Pa}$
Shear Modulus	$K = 1 \times 10^6 \text{ Pa}$
Dry Density	$\rho = 2000 \text{ kg/m}^3$
Permeability	$k = 1 \times 10^{-4} \text{ cm/s}$
	$k_{FLAC} = 1 \times 10^{-10} \text{ m}^2/\text{Pa.s}$

Some of the investigations conducted are documented in the following sections.

Bulk Modulus of Water

Given the close link between the relative magnitude of undrained settlements and the bulk modulus of water, as indicated by equation (5.5) a number of models were created in which the bulk modulus of water was varied. Models were created in both the normal flow scheme and the fast flow scheme. The results of this investigation are shown in Figure 5.12.

Figure 5.12 indicates that variations in the bulk modulus of water have very little effect on the settlement-time relationship when Fast Flow is used. The modulus does however appear to have a notable affect on the overall relationship when the normal flow scheme is used, but does not greatly affect the magnitude of immediate settlements. This is contrary to what was expected, as from equation (5.5) it was expected that at least in the normal flow scheme a decrease in the bulk modulus of water would result in a notable increase in the immediate settlement but would have little effect on the final settlement. From these results it appeared that varying the bulk modulus of water was not the key to solving the issue.

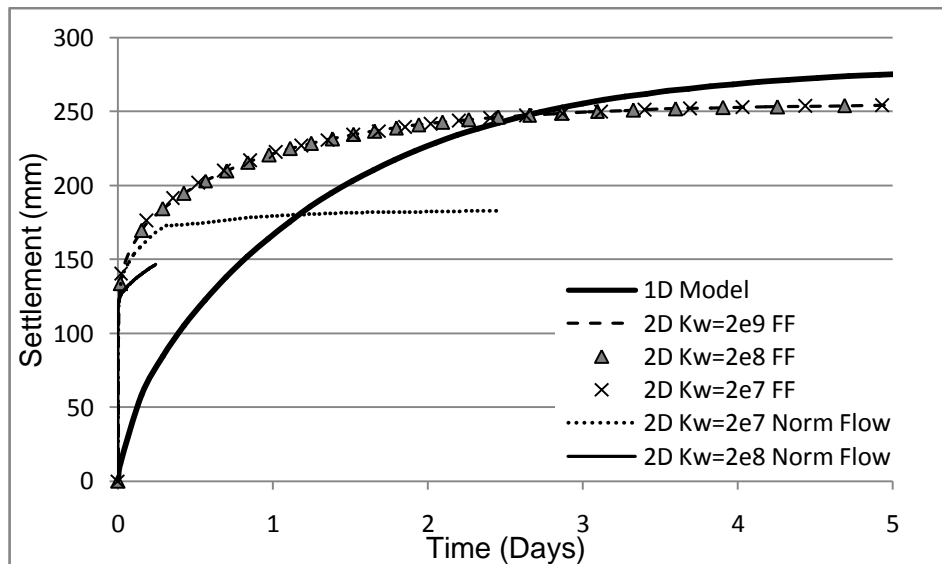


Figure 5.12: Effect of Bulk Modulus of Water on the Settlement versus Time Relationship for the Two Dimensional Models

Boundary Conditions and Symmetry

No boundary conditions were changed between the one dimensional model which worked and the two dimensional model with high immediate settlements. However, given the differing nature of stress and displacement distributions between the one and two dimensional models, it was conceivable that boundary conditions may have had a different effect on the different models. To investigate whether boundary conditions may have affected the results a model in which symmetry was not used and in which the boundaries were made to be further from the areas of interest was created. The grid including boundary conditions and applied stresses is shown in Figure 5.13. The settlement versus time results for this model, which are shown in Figure 5.14, indicated that the boundary conditions were not causing the problem.

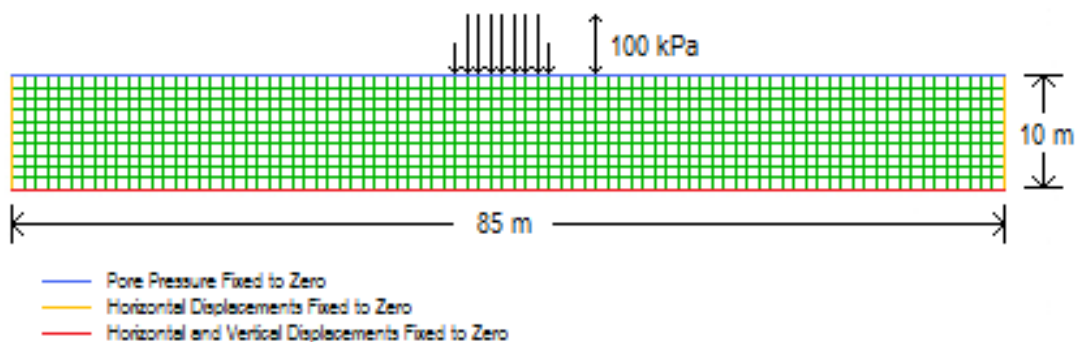


Figure 5.13: Grid Showing Applied Stress and Boundary Conditions For Two Dimensional Model without Symmetry

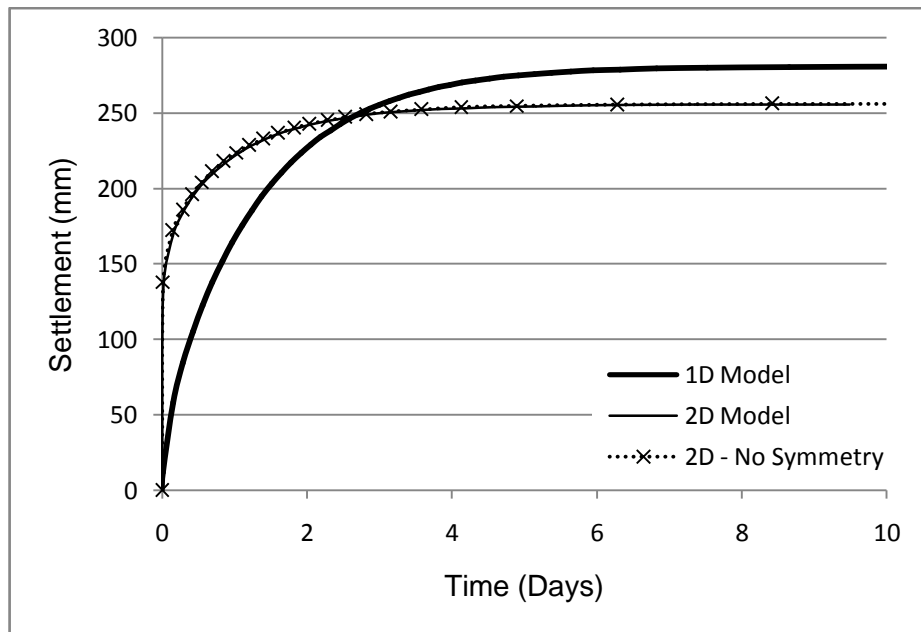


Figure 5.14: Settlement Results of the Two Dimensional Model which did not use Symmetry Compared with Previous Models

Grid Size

Another factor investigated was the size of the grid used for the model. Whilst the grid size and density was the same in both models, the more complicated stress distribution associated with the two dimensional model may not have been captured effectively by the same sized grid. Additionally, the timestep used by FLAC is proportional to the smallest zone size, therefore by increasing the mesh density the very early settlements could be observed more clearly to see whether the problem was in fact due to instantaneous settlements or due to very rapid settlements, which could conceivably be realistic. The results, which are shown in Figure 5.15 indicate that the 20x10 zone grid was not fine enough to get an accurate value for the final settlement. Additionally, it is seen that the increase in accuracy of using a 60x30 or 100x50 element grid compared with a 48x24 element grid is insignificant. Figure 5.15 also indicates that using a finer grid does not resolve the issue of large immediate settlements. The first hour of each of the settlement curves is shown more clearly in Figure 5.16. In this graph it can be seen that the first data point in each case corresponds to a settlement greater than 90mm, which for the 100x50 zone grid corresponds to a time of just 48 seconds. Even though the specified permeability of the foundation was quite high this value is believed to be unrealistic.

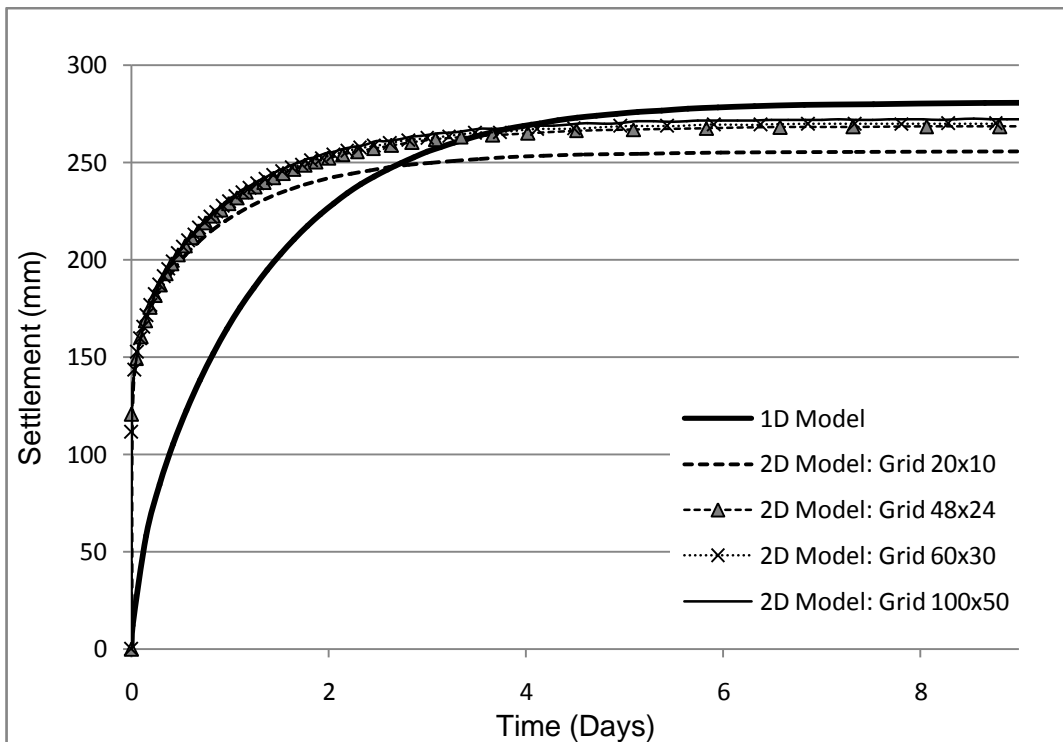


Figure 5.15: Variation of Settlement – Time Curves with Grid Density

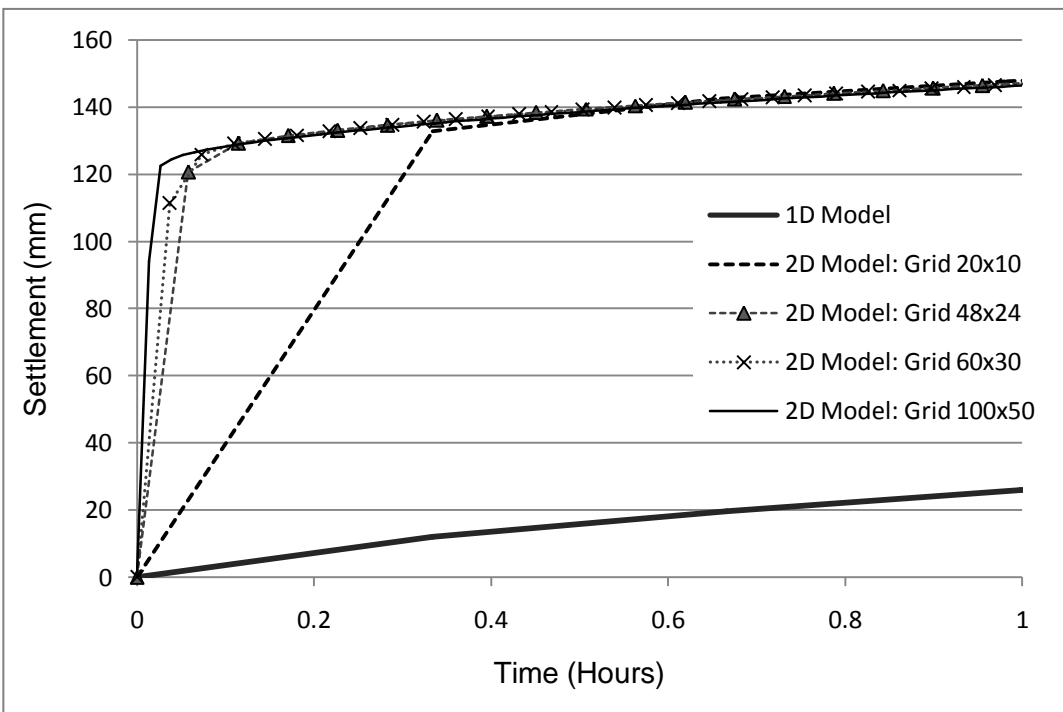


Figure 5.16: Variation of Settlement - Time Graphs with Grid Density Early in the First Hour of the Consolidation Process

5.3.3. Conclusions from the Investigations into the Problem of High Immediate Settlements

Based on the investigations conducted it was determined that the high immediate settlements relative to the total settlements were a result of a difference between modelling a one dimensional situation compared with a two dimensional situation. Despite numerous investigations into factors which may have been affected by a change from a one dimensional to a two dimensional model, in addition to communication with numerous other users of FLAC, the cause of the problem was not found.

5.4 Summary of the Preliminary Modelling

From the preliminary modelling conducted the effect of variation on a number of the soil properties required for the modelling was observed and in most cases was found to have a similar effect to what would be expected from one dimensional theory. In addition an issue of an excessively high ratio of immediate to total settlement was observed and thoroughly investigated. Despite the investigation a viable explanation of the behaviour was not found.

This phenomenon of immediate settlement being quite significant in proportion to the total settlement was also seen in a similar example published in the FLAC 5.0 user manual (Example 13 from the Example Applications Volume), where an embankment built on a cam-clay foundation had approximately the same abnormally high initial to total settlement ratio as the ones encountered during this preliminary modelling. Personal communications with Itasca (Detournay 2007) revealed that the results are in line with their expectations for such problems in soft clays.

If these results are in fact realistic then delayed consolidation settlement would not be an issue on the Tully Project. It is therefore believed that an error of some form has caused the high immediate settlements. Despite this it was decided that the trial embankment modelling would still be completed using a coupled consolidation model, which would help confirm whether or not the high immediate settlements observed were realistic.

Chapter 6: Numerical Modelling of the Trial Embankments near Tully

6.1 *Introduction*

This chapter outlines the process involved and the results obtained from the modelling of a section of one of the trial embankments near Tully. Unfortunately, the quality of data received from site was compromised by some of the construction procedures used. Due to this and some of the difficulties encountered during the modelling process only one location was modelled.

6.2 *Selection of the Location to Model*

The location which was modelled in this thesis was chainage 83500 which was part of the second trial embankment, in the section which had batter slopes of 1:2, refer to Figure 4.4. The reasons behind this choice were as follows.

1. Locations along trial embankment 1 (CH83340-CH83380) were ruled out after determination of the foundation profile revealed that there was not a significant clay layer beneath this embankment. This meant that settlements were expected to be smaller and to occur rapidly and as such would not be representative of the majority of sections along the proposed new alignment.
2. Locations along trial embankment 3 were ruled out because there were berms on this embankment, there were no inclinometers and also because geogrids were used in the foundation. Berms complicate the model geometry slightly but more importantly are not representative of the majority of the embankments in the project. Geogrids would add a significant level of complexity to the model, as they would need to be modelled as structural elements embedded in the soil. Modelling this would require many assumptions regarding the frictional properties between the geogrids and the soil. As no such information could be obtained from site it was believed that there was little point in modelling these sections. Additionally, as at July geogrids were not in the designs for anywhere else along the alignment.
3. Out of the remaining locations, CH 83500 was chosen for three reasons. Firstly, there were piezometers, a settlement plate and an inclinometer all within close proximity as shown in Figure 4.4. Secondly, the location was also close to one of the Piezocone test locations (Piezocone 16) which meant that there was information about the foundation soil profile available. Finally, this location was at the centre of the section with 1:2 batter slopes, rather than at one end of the embankment or near where the embankment geometry changed. This was important as the model created

was two-dimensional, and was therefore based on the assumption that the geometry modelled in two dimensions extended indefinitely in the third dimension, which would be a very poor assumption if the location modelled was near an end of the embankment.

6.3 Assignment of Foundation and Embankment Properties

The assignment of foundation properties was an evolutionary process mainly due to a lack of information. The only sources of data about the foundation layers in the area modelled were the results of a piezocone test and the results of oedometer tests from samples at two different heights within the main clay layer. Requests were made for additional samples to be obtained when the inclinometer casing was installed, so that laboratory tests could be conducted at the university to gather more information, however any samples which may have been obtained did not reach the university. As such many parameters used in the models were initially estimated based on published correlations involving piezocone tests or CPTs, and were later modified to give a better correspondence between the modelled and measured settlements. By comparing the modified parameters with the CPT test results, relations were determined which were more representative of the particular soil near Tully. The values of soil properties used in the final model as well as the value of the piezocone tip resistance (q_c) from which some of the properties were determined are shown in Table 6-1.

Table 6-1: Soil Properties Used in Model of Trial Embankment 2

Layer	Depth of Base of Layer (m)	q_c (MPa)	E (MPa)	Dry Density (kg/m ³)	ϕ' (degrees)	c' (kPa)	k_{FLAC} (m ² /Pa.s)	n
Embankment Material	-	-	30	1960*	28	5	-	-
Rock Layer	-	-	80	1700*	38	0	-	-
1. Clay	1.2	0.5	2	1200	25	3	5×10^{-13}	0.52
2. Sand	2.2	5.5	8.3	1480	35	0	5×10^{-12}	0.44
3. Soft Clay	4.7	0.2	0.8	650	25	0	2×10^{-13}	0.75
4. Clay	5.7	0.5	2	500	25	7	1.5×10^{-13}	0.81
5. Silty Clay	8.1	2	6	1380	28	21	2×10^{-12}	0.48
6. Sandy Silt	9.3	10	15	1450	38	7	1.2×10^{-12}	0.45

*These are moist densities not dry densities (see Section 6.3.5)

6.3.1. Layer Classification

The classification of the layers, for instance as sand or clay, was determined using the piezocone results shown in Appendix A-2.4: Piezocone Results, in conjunction with Figure 2.28. Areas on the piezocone results chart where the tip resistance and friction ratio remained approximately constant were grouped as layers, and for each layer an average tip resistance and friction ratio were determined and used on Figure 2.28. These average tip resistance values, which are recorded in Table 6-1 were also used to determine Young's Modulus (E) and initial estimates for the effective friction angle (ϕ') of each layer.

6.3.2. Bulk and Shear Moduli

For all the materials in the model, the bulk and shear moduli were calculated from Young's modulus and Poisson's ratio using Equations (3.1) and (3.2). Poisson's ratio was taken to be 0.4 for all foundation layers and 0.3 for the rock and embankment material. Young's Modulus for each layer was determined from the correlations discussed in section 2.4.3. In the earliest models created, Schmertmann's 1978 relation $E = 3.5q_c$, for plain strain loadings was used for layers identified as sands or silty sands, and $E = 5q_c$ was used for clay layers. However, as these moduli produced model settlements which were significantly less than those measured on site, the relations used were changed. In the final model Meyerhof and Fellenius' 1985 correlation $E = 1.5q_c$, was used for the sand layers and $E = 4q_c$ was used for clay layers.

6.3.3. Dry Density

The density value for the embankment material was the average value obtained from laboratory tests on a number of samples. For reasons explained below in section 6.3.5 the bulk density as opposed to the dry density was specified for the embankment and rock material. The dry densities specified for the soft clay and clay layer beneath it were based on results obtained in conjunction with the oedometer tests (refer to Appendix A-2.3: Consolidation Test Results). However, there was no density information for any of the other layers, and as a result all the other densities were estimates. This was not considered to be a major problem in terms of the accuracy of the model created as preliminary modelling showed that foundation deformations were insensitive to variations in the dry density of the foundation layers.

6.3.4. Effective Friction Angle, Effective Cohesion and Tensile Strength

For the original model the effective friction angles were determined from the piezocone tip resistance using Robertson and Campanella's 1983 chart shown in Figure 2.29. These values were later modified slightly based on the recommendations of an engineer familiar with the area. Effective cohesion for the foundation layers was originally estimated based on soil type and whether or not layers were believed to be overconsolidated. These values were again modified in later models to match settlement results and avoid the occurrence of slope failure in the models, given that no such failures were observed in the field. The tensile strength of each foundation layer was calculated using equation (6.1), which was the tensile capacity recommended in the FLAC user manual (Itasca 2005a)

$$\sigma_t = \frac{c'}{\tan\phi'} \quad (6.1)$$

At the outset of the project it was believed that the strength parameters for the embankment material would be based on the results of triaxial tests. However, despite the tests being conducted by the Department of Main Roads, the results were not made available at the time during which models were being developed. As such strength properties of the embankment and rock layer were estimates.

6.3.5. Permeability, Porosity and Saturation

The permeability of the clay layers within the foundation was determined from the results of oedometer tests. Oedometer test results, which included m_v and c_v values for different applied pressures, were available for two depths within the main soft clay layer, see Appendix A-2.3: Consolidation Test Results. Equation (2.24) was used to convert the test results to permeability values, and based on the range of permeabilities calculated for different pressures appropriate values were chosen for each of the clay layers in the model. For the other foundation layers permeability was assigned based on the soil classification.

In contrast the embankment and rock layer were not given permeabilities or porosities. Not specifying these properties allowed free drainage from the foundation into the unsaturated embankment, as occurred from the foundation in areas not beneath the embankment. This was done because the actual rock permeability was several orders of magnitude greater than the permeability in any other layer. Using such a different permeability in FLAC would cause the stable explicit time step to be excessively small. In some initial models where an appropriate rock permeability was specified the timestep used by FLAC was in the order of

1×10^{-6} seconds, which given the time required to compute each timestep, would have resulted in the model taking several years to run.

An alternative solution to this problem would be to specify a much lower permeability for the rock layer, which was done in some earlier models. However, models where no rock permeability was specified ran significantly faster than those where a lower permeability was specified and were found to be of equal if not greater accuracy. Therefore the method of not specifying rock or embankment permeabilities and porosities was adopted.

Porosity values for all foundation layers were calculated from the soil densities using equation (6.2) below

$$n = 1 - \frac{\rho_d}{G_s \times \rho_w} \quad (6.2)$$

Where ρ_d is the dry density, G_s is the specific gravity of the soils grains which was assumed and ρ_w is the density of water.

The entire foundation was specified as fully saturated, indicating a water table at ground level. This was not considered an unrealistic assumption, given the wet conditions experienced on site during construction. Tests from site indicated that the saturation level of the embankment material was 0.85. However, as no porosity was specified for the embankment, FLAC would not be able to compute the actual embankment density from the dry density and saturation. To overcome this, the bulk density was specified for the embankment along with a saturation of zero.

6.4 Model Geometry and Boundary Conditions

The finite difference grid used for the model is shown in Figure 6.1. The foundation layers shown are those determined from the piezocone data. They have the same locations and thicknesses as shown in Figure 4.4 and the properties shown in Table 6-1. In contrast the embankment profile does not match that in Figure 4.4, as the numerical model was based on embankment height measurements taken during the construction process as opposed to the design heights.

The depth of the model was restricted to 9.3 metres as this was the depth to which piezocone data was available. This was considered to be a suitable depth as the bottom layer was significantly stiffer than the clay layers and was underlain by even stiffer layers. The width of the foundation was chosen to be five times the height of the foundation. This large width to height ratio was used to minimise boundary effects on the model, and was the minimum ratio used in similar models in the literature (Indraratna et al. 1997; Rankine et al. 2005).

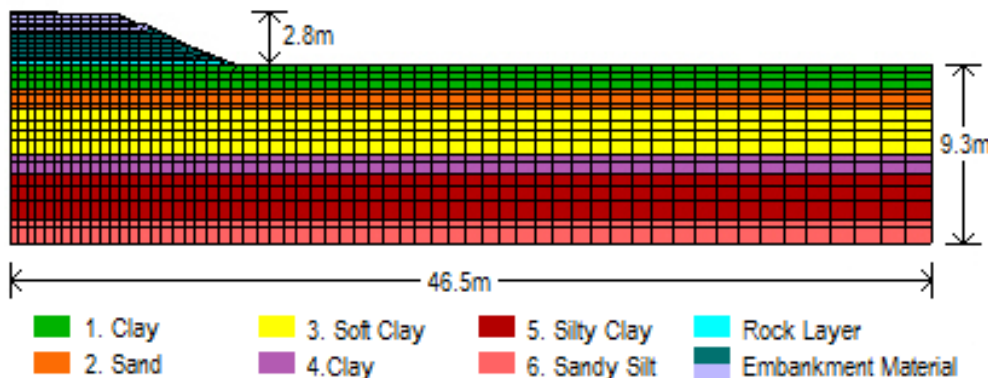


Figure 6.1: Finite Difference Grid for Trial Embankment Model Showing Different Soil Layers

The choice of mesh size was largely controlled by the geometry of the problem, and the coarsest grid acceptable was used to minimise run times of the model. It was mainly the thin soil layers which reduced the required grid size. Soil layers which were one element deep and had a significantly different stiffness to surrounding layers were found in early models to produce anomalies in the pore water pressure and stress distributions around the layer boundaries. The cause of the anomalies was numerical and associated with the use of Lagrangian analysis which does not handle differences in stiffness of much more than an order of magnitude well. To reduce the errors associated with having layers of highly contrasting stiffnesses, a minimum of three rows of elements was used where a layer was surrounded on both sides by materials with highly contrasting stiffnesses and a minimum of two rows of elements was used where the high stiffness contrast was only on one side. Ideally a much finer grid should be used, and sub layers with intermediate stiffnesses should be employed between layers of highly contrasting stiffness. However the time constraints associated with this project did not allow for such a model to be created.

In the model, horizontal velocities and displacements were fixed to zero at both vertical boundaries and at the base of the model. The stiffness of the underlying layers, depth below ground surface and the friction between these and the bottom layer in the model were considered to be enough to justify fixing horizontal motion at the bottom to zero. Vertical motion was also fixed to zero at the base of the model. The vertical symmetry boundary was made impermeable as was the base of the model. A hydrostatic pore pressure distribution, corresponding to a water table at the surface was fixed at the other vertical boundary as this boundary was deemed to be far enough away that the embankment load would not affect the pore water pressure at this location. A pore pressure of zero was fixed all along the surface of the model to represent the surface of the water table.

6.5 Modelling Procedure

The first step in the modelling procedure was the initialisation of stresses within the foundation. This was done in a method similar to that used in the preliminary models, in which expected overburden stresses and hydrostatic pore pressures were input into the model. Then the model, consisting of only the foundation at this point, was solved with flow on until equilibrium was reached. This state was then considered to represent the initial conditions on site, although as soil properties and insitu stresses are highly dependent on the foundation's stress history, there was no way to confirm that this state did actually replicate the initial insitu stresses.

Once the initial state was established placement of the embankment began. To ensure the results of the numerical model could be compared with results from the corresponding trial embankment, the model embankment was placed incrementally, with the timing and height of each increment corresponding closely to the construction sequence measured in the field. This was particularly important as wet weather halted the progress on site resulting in the actual construction taking place over a period of three months, which given the timescale of the consolidation process could not be considered to be instantaneous. Figure 6.2 shows both the modelled and actual construction sequences.

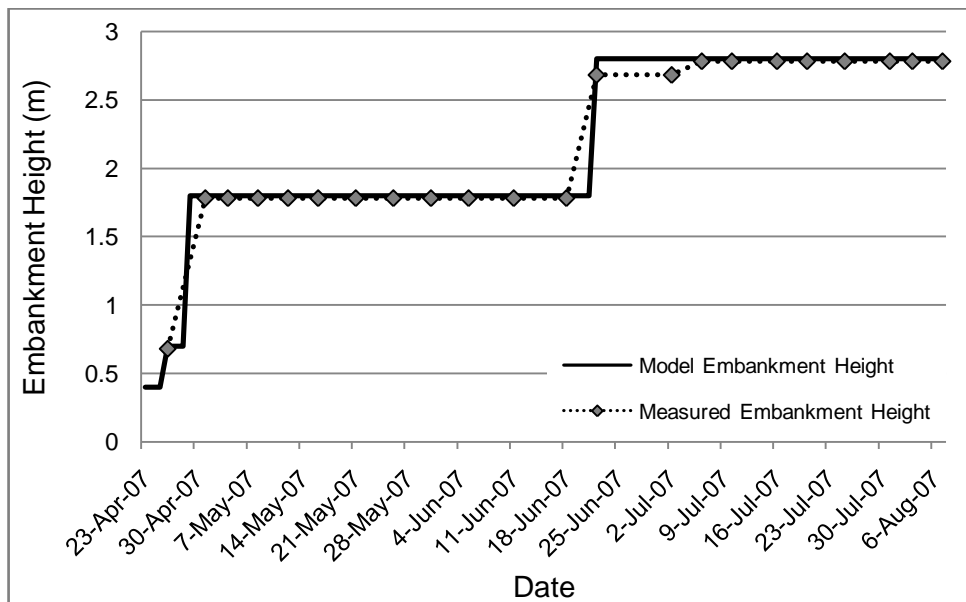


Figure 6.2: Embankment Construction Sequence

One aspect which can be seen in Figure 6.2 that made comparisons between model and field data more difficult was that information regarding the actual embankment height was only available after the settlement plates had been installed which occurred on the 26th April 2007. Despite enquires being made to the engineers on site the actual start date and rate of

construction prior to this was not made available to the writer, and it is unknown whether such information was actually recorded.

With each addition of a section of embankment the model was solved firstly with flow turned off to develop the undrained response and then solved with flow set on till the desired time was reached.

6.6 *Trial Embankment Data from Site*

The data obtained from site consisted of settlement plate heights and piezometer pressures. Inclinometers were also installed and data was collected, however, interpretation of the measurements and conversion into actual lateral displacements by the project design team was not achieved within a timeframe that allowed them to be exploited for this study. Whilst this is unfortunate, based on the difficulties in matching field and model lateral displacements discussed in the literature (refer to section 2.3.3), as well as the difficulties encountered in matching the pore pressure and settlement data for the Tully embankments discussed below, there would likely be a difficulty in matching the data, and the value in attempting to do so would be limited.

Figure 6.3 shows the data recorded from the settlement plate at the location which was modelled. The first point to notice was that on three occasions the settlement plates were knocked by construction equipment. Observation of the data recorded after the settlement plate was knocked the second time, clearly shows that knocking the plate significantly affected the subsequent settlement results. Also no settlement reading was taken on the day that the plate was knocked for the second time. Given that it would be impossible as well as pointless to try and match the data as recorded, corrections were made to the data collected after the settlement plate was knocked for the second time. This involved adding a data point where there was one missing, modifying the next point, and adding 188 millimetres of settlement to all of the data points after the plate was knocked for the third time, to remove the sudden drop in settlement. The corrected data is also shown in Figure 6.3.

The other main issue to note from Figure 6.3 is that the rate of settlement noticeably increased around the 1st of June. Such a phenomenon should only occur as the result of an increase in loading or embankment height. However, the recorded embankment height did not increase until after the 18th of June. This anomaly was believed to be a result of a construction practice used on site of stockpiling excess embankment material around the settlement plates. Whilst it could not be confirmed, the results indicate that the embankment

height measured by the surveyors was the general embankment height as opposed to the height of the stockpile around the settlement plate. It is therefore concluded that a stockpile was placed near the settlement plate around the first of June, but that further construction at the location did not take place until after the 18th of June. This practice of stockpiling brings the accuracy of all of the results into question, because it means that the settlement plates are measuring settlement resulting from a localised load above them as opposed to just a general embankment load which could be considered to be two dimensional.

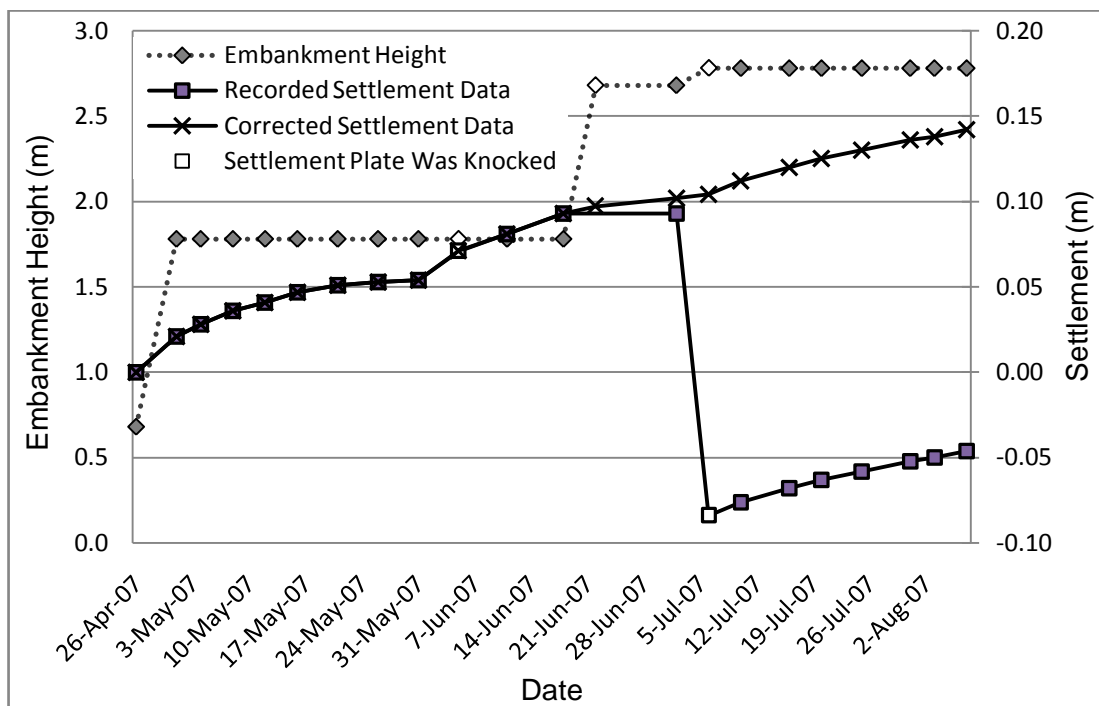


Figure 6.3: Settlement Plate Results for CH83500

The piezometer results, shown in Figure 6.4, also indicate increases of embankment height prior to the 18th of June. However these results tend to indicate a gradual increase of embankment height between the 24th May and the 28th of June. This does not correspond particularly well with the sudden increase in settlement rate occurring around the 1st of June. However, this may be explained as a combination of the inaccuracies in the settlement readings discussed previously and the rain that occurred during this period temporarily raising the water table and resulting in slightly higher measured pressures, prior to the 1st of June.

Another point to note when regarding Figure 6.4, is that the readings from the piezometer at 3.5 metres depth do not show any jump in pore pressure corresponding to the first major increase in embankment height. This could be explained by the stockpiling of embankment material above the piezometer prior to the increase in overall embankment height on the 26th

of April. To illustrate how stockpiling could explain why the top piezometer did not experience an increase in pore pressure when the bottom piezometer did, consider the 2:1 stress distribution discussed in section 2.1.2. Figure 6.5 is a diagram showing the region of stress increase based on the 2:1 distribution, when an embankment is placed around a pre-existing stockpile. From this diagram it can be seen that it is plausible that the top piezometer may not have experienced a notable increase in pressure with the application of the embankment, but whether this is the actual explanation is not known. The lack of settlement data prior to this date makes it more difficult to confirm or disprove the explanation.

Given that it appears that stockpiling of embankment materials has occurred and affected the piezometer results, and also that the exact depths of the piezometers and the water table are not known, accurately matching the model data to the site data is not feasible.

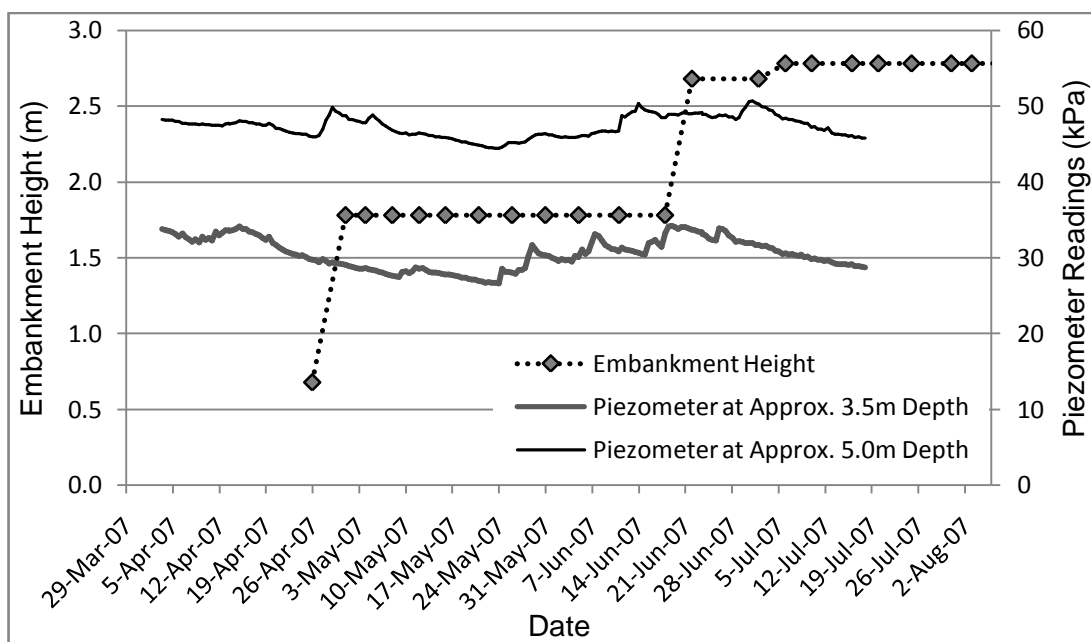


Figure 6.4: Piezometer Data at CH83500

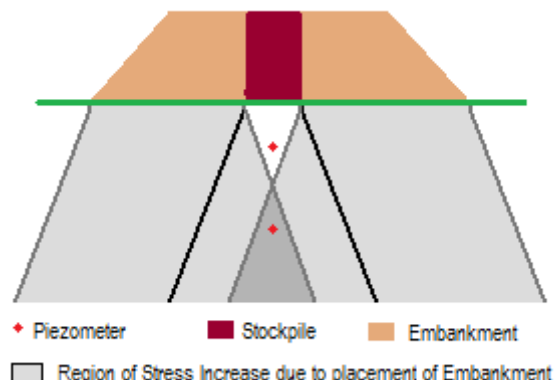


Figure 6.5: Diagrammatic Explanation of Reason for the Lack of an Increase in Pore Pressure in the Top Piezometer

6.7 Model Results and Comparisons with Field Results

The following section contains results output from the numerical model of CH83500 a location on the second trial embankment at Tully. The program code for this model is included in Appendix C: Trial Embankment Code.

6.7.1. Settlements

Figure 6.6 shows the settlement-time curves for both the model and field data. From this figure it is clear that the issue of high immediate settlements observed, investigated and discussed in Chapter 5: Preliminary Consolidation Models, was still an issue in the trial embankment model. Apart from this issue the magnitudes of the model settlements matched the field data quite well until the time when the settlement plates were knocked. Given the uncertainties in the true field settlement after this time the slight discrepancies between model and field results after this time are not a major concern. The difference in the timing of the increased settlement rate corresponding to the placement of the final layer of the embankment is due to the field data not matching the measured loading curve as discussed in Section 6.6.

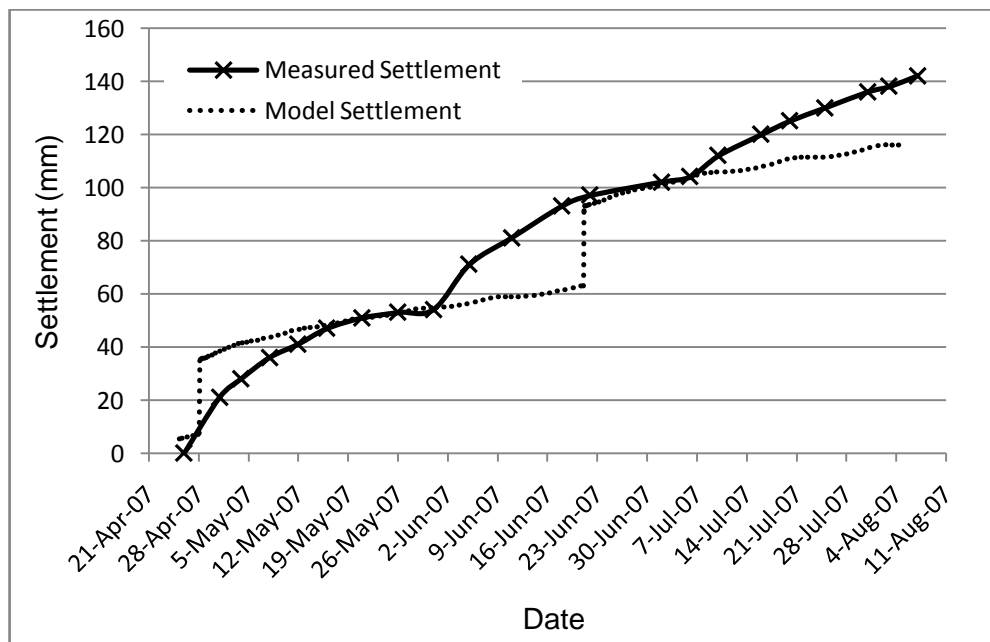


Figure 6.6: Comparison of Model and Field Settlement Versus Time Curves

The vertical displacement contours within the embankment and foundation immediately before the placement of each layer of embankment and at the end of the simulation are shown in Figure 6.7. These plots clearly show that during the construction stages the settlement profile was not a typical settlement basin but rather a sagged settlement profile in accordance with the research conducted by Zhang (1999), which is discussed in Section

2.3.2. Assuming that this model is an accurate representation of what is occurring in the field, the settlement measured by the settlement plates and shown in Figure 6.6 will not be the maximum settlement in the foundation, during the construction period. This would tend to indicate that settlement should be measured at several lateral positions at each monitored cross-section, if an accurate picture of the settlement magnitude and profile is required.

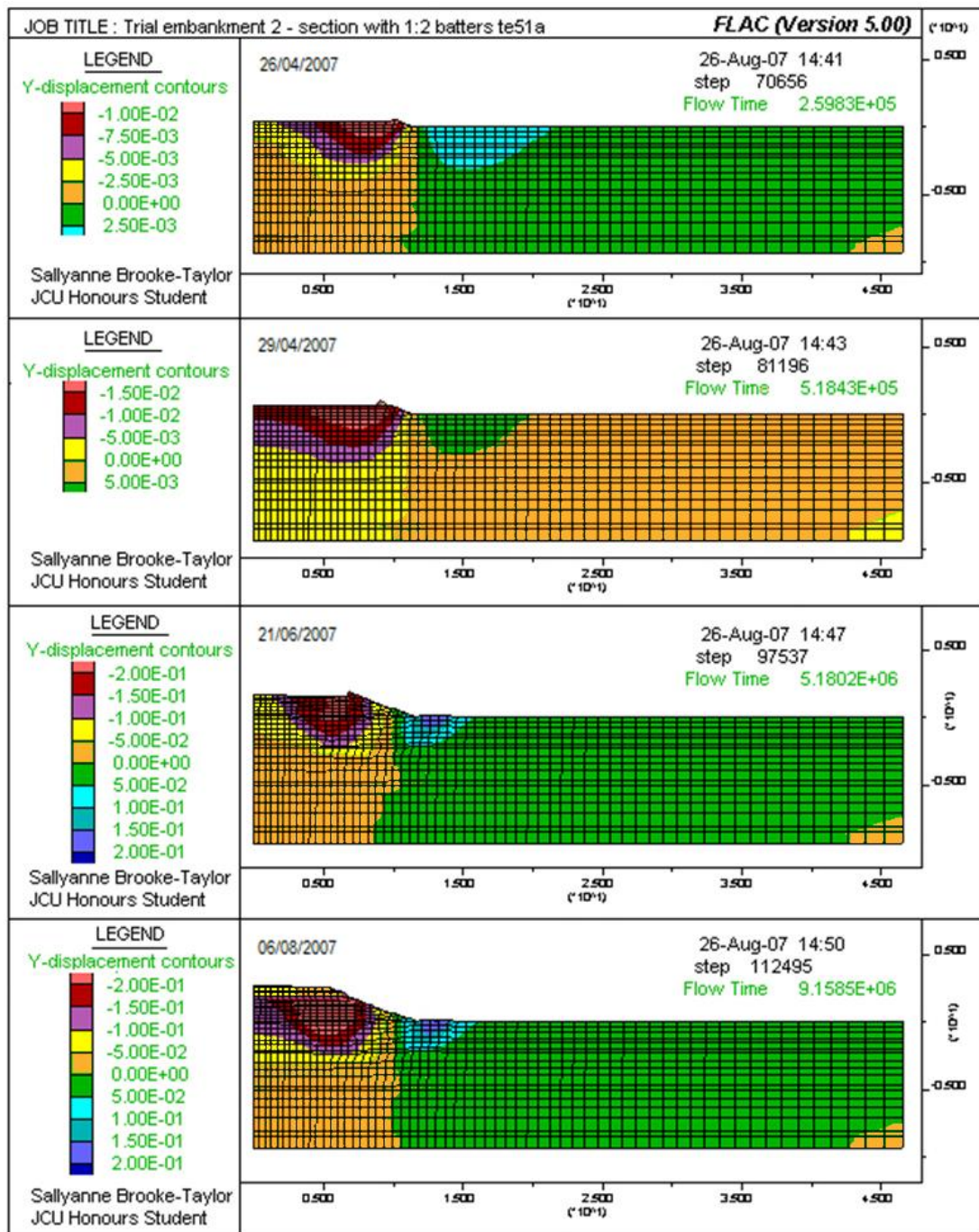


Figure 6.7: Vertical Displacement Contours after each Stage of Construction

Comparing the first and second contour plots and the third and fourth contour plots it can be seen that as the embankment crest width to height ratio decreases with the increasing height

of the embankment, the location of the maximum settlement moves towards the centre. This is again in accordance with Zhang's work. There is however, a distinct change in the shape of the displacement contours between the second and third plots. This can be explained as the result of significant plastic displacements occurring after the embankment reached a height of 1.8 metres. The presence of plastic deformations is also indicated by the significant distortion in the grid, and was confirmed by a plot from FLAC showing which elements had yielded. Finally, in the last contour plot it appears that the top of the embankment has settled much less than the rest of the embankment. This is because the displacements shown in these zones are only the displacements that occur after the zones have been added to the model. The comparatively small displacements in these zones are therefore not an indication of arching or any similar phenomenon.

6.7.2. Pore Water Pressure

Both the pore pressures predicted by the numerical model and the pore pressures measured by piezometer on site are shown in Figure 6.8. The most obvious difference between the modelled and field pressures is that the model data is characterised by a few large sudden increases followed by gradual decreases, whilst the site data consists mostly of smaller increases and subsequent decreases. The most likely explanation for this difference is that on site each increment of embankment would have been placed over a number of days rather than instantaneously as in the model. Therefore some of the pore pressure would have dissipated before the entire increment was placed, meaning that the actual pressure never reached the extremes shown in the model. This effect would also be accentuated by the stockpiling of material above the monitoring equipment.

The other main discrepancy between the model and field data is the magnitude of pore pressures for each depth. Theoretically, the model pressures corresponding to a depth of 3.4 metres should correspond closely to the field pressures at a depth of 3.5 metres, and likewise the model pressures for a depth of 5.1 metres should correspond closely to the field pressures at 5 metres depth. However, Figure 6.8 shows the field's 5 metre depth piezometer matching the pressure at 3.4 metres depth in the model more closely, and the 3.5 metre depth piezometer corresponding to a depth of approximately 2.3 metres in the model. Given that the piezometer pressures for each depth drop below the hydrostatic pore water pressure of the intended depth, based on the water table being at the surface as in the model, it has been concluded that either the piezometers were not installed as deep as was intended or the water table was 1 to 1.5 metres below the surface. It may also have been that the piezometers were not working, not calibrated correctly or were not installed such that they accurately measured the inherent pore pressures in the adjacent soil.

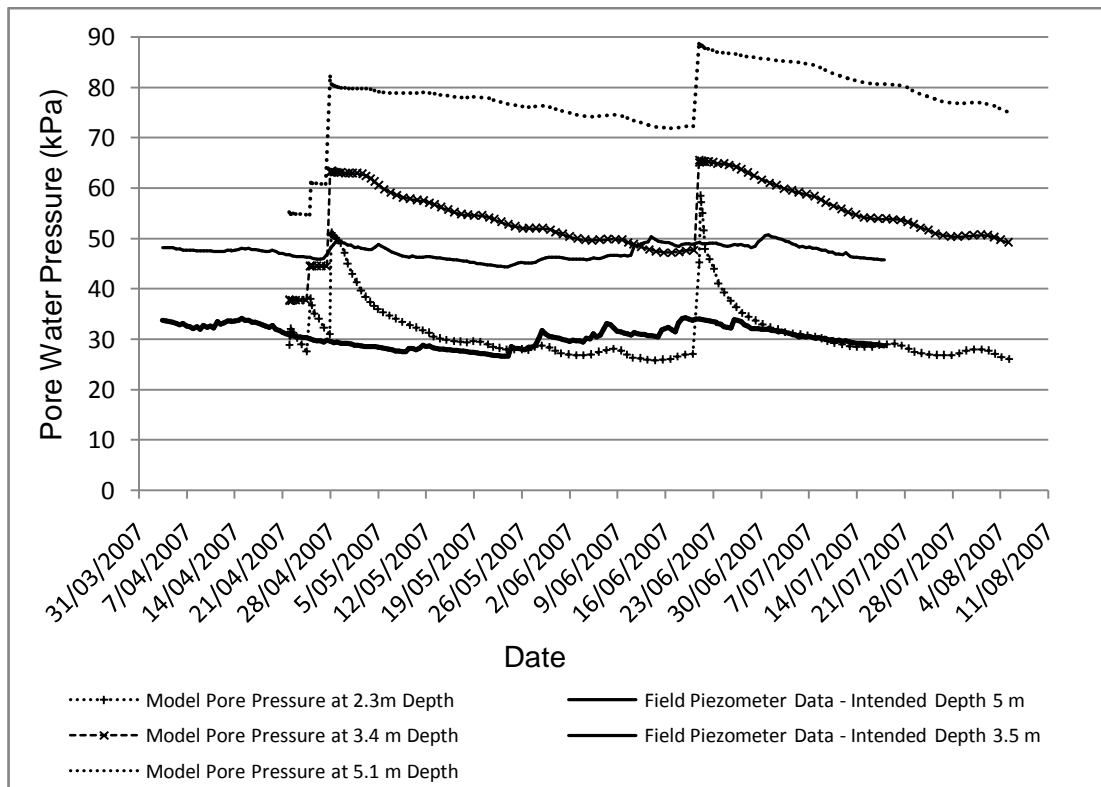


Figure 6.8: Comparison of Model and Field Pore Water Pressure Versus Time Results

The significant discrepancy between the field and model data could also be partially due to differences between the modelled and actual foundation permeabilities. If the actual permeabilities were higher than those modelled, then more of the excess pore water pressure would dissipate during the construction period resulting in lower overall pressures in the field compared to the model. A similar effect would also be noticed if the thickness of the clay layers or positions of the piezometers within the layers, were different in the model and on site. If for example the piezometer happened to be closer to a sand layer on site than in the model, drainage and therefore pore pressure dissipation would be faster, and excess pore pressure at the end of construction would be lower. This phenomenon is clearly shown in the model pore pressure time curves for depths of 2.3 metres and 3.4 metres. The curve for 2.3 metres depth shows the pore pressure dropping very rapidly immediately after additional load is applied, as it is just 0.1 metres beneath a sand layer with high permeability. As such for most of the simulated period the pore pressure is not much above the hydrostatic pore pressure. In contrast the curve for 3.4 metres depth only decreases slowly initially, because it is closer to the centre of the same clay layer meaning that water cannot drain from this location until some of the water near the edges of the layer has drained. The pore pressure for this location therefore remains higher for much longer.

Finally, analysis of Figure 6.8 indicates that the instantaneous increase in pore pressure associated with each increment of embankment matches what would theoretically be expected. As discussed in Section 2.2.3, when a load is applied to a foundation the applied stress is initially transferred to the pore pressure, and with time the stress is transferred from the pore water to the soil grains, which causes the consolidation settlement. Therefore, in the model's pore pressure data, the increase occurring when each layer of embankment is applied should be approximately equal to the weight of the layer of embankment applied. In fact, the instantaneous increase in pore pressure should actually become less with depth in the foundation because the total stress in a foundation caused by an applied load decreases with depth as discussed in section 2.1. The modelled data shows this result well. For example when the last 1 m layer of embankment is applied, the weight of the additional layer is 19.2 kPa. The corresponding increases in pore pressure are 18.2 kPa, 17.8 kPa and 16.4 kPa for depths of 2.3 m, 3.4 m, and 5.1 m respectively. This theoretically expected result tends to indicate that the high immediate settlements observed in the models are not the result of the applied stressed being incorrectly distributed to the soil skeleton rather than to the pore water.

6.8 *Summary and Conclusions from the Trial Embankment Modelling*

In this chapter the details and results of the trial embankment model created were covered. The reasons behind the choice of location to model and how the various model input parameters were determined were covered first. These sections were followed by details of the numerical model and the modelling procedure used. A discussion of the data and quality of data obtained from site was then presented, followed by a comparison of the model and field results.

The time rate of settlement and dissipation of pore pressure results from the trial embankment model generally, did not match the site data particularly well. In the case of the pore pressure dissipation, discrepancies resulted from uncertainties in the location of the piezometers and water table as well as the construction practice of stockpiling excess material above the monitoring equipment causing differences in the actual and modelled construction sequence. For the settlement results it was the practice of stockpiling in combination with the unresolved issue of high immediate settlements occurring in the numerical model that detracted from the accuracy of the model compared with the field. However, the eventual magnitudes of settlement produced in the model did match the field data quite well, and as such, relationships suitable for the Tully project, between CPT tip

resistance and Young's Modulus were developed and could be used for modelling other sections of the highway. The relationships found to be acceptable were, Meyerhof and Fellenius' 1985 correlation $E = 1.5q_c$ for the sand layers and $E = 4q_c$ for the clay layers. Similarly the correlations between cohesion, friction angle and the CPT results could be used in other models of the highway for layers where the CPT results were similar to layers in the trial embankment model. To confirm these correlations at least one other embankment model should have been created, but due to the inaccuracy of the data obtained from site and the high immediate settlements occurring in the numerical models it was decided that little would be gained by modelling another location. For these same reasons, particularly the problem with high immediate settlements, it was decided that a model of another section of the highway would not replicate the actual field situation closely enough to accurately determine whether pavement cracking was a potential problem. Instead it was concluded that more value would be obtained by conducting a parametric investigation into pavement cracking and using the results of this investigation to determine if there is potential for cracking to occur on the Tully project.

Chapter 7: Investigation into Pavement Cracking

7.1 Introduction

The parametric investigation into pavement cracking is summarised in this chapter, along with the implications of the results regarding the chances of pavement cracking on the Bruce Highway upgrade near Tully.

Due to the large number of parameters which could potentially affect the deformations of an embankment, it was decided that the simplest possible model should be used as a basis so that meaningful results could be obtained. This meant a single layered foundation modelled as elastic and an embankment with only a single pavement layer.

The parameters in this model expected to have the most effect on pavement cracking were:

- Embankment Height
- Young's Modulus of the Foundation
- Young's Modulus of the Embankment
- Young's Modulus of the Pavement
- Batter Slope of the Embankment
- Poisson's Ratio of the Foundation
- Poisson's Ratio of the Embankment , and
- Poisson's Ratio of the Pavement.

At the beginning of this study it was intended that each of these parameters would be varied in the parametric investigation, however, due to the initial results obtained not all of the parameters were tested.

7.2 Determination of a Failure Criterion for Pavement Cracking

The first stage in this modelling problem was to determine how a pavement crack could be defined in terms of outputs from the model. Two different approaches were considered, one based on whether the elements in the pavement of the model had yielded and the second based on the stresses and strains measured in the pavement.

7.2.1. Approach 1: Yielding of Pavement Zones

In this approach both the pavement and embankment would be modelled as Mohr-Coulomb materials with appropriate stiffness, cohesion, friction angle and tension capacities specified.

After running the model, the current state of each of the zones in the embankment and pavement would be output from FLAC, as shown in Figure 7.1. Note that Figure 7.1 is included as it shows all of the possible states that elements in a Mohr – Coulomb model can have. It was obtained during the solution process of a preliminary pavement model and thus the results shown have no relevance to the actual situation.

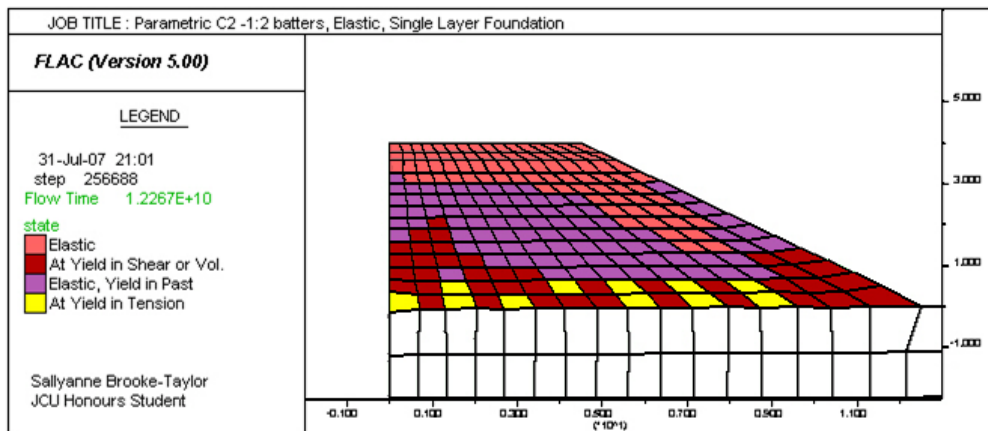


Figure 7.1: Element States During the Solution Process of a Preliminary Pavement Model

From an output such as Figure 7.1 a crack could be defined to have occurred if an element in the pavement was ‘at yield in tension’, ‘at yield in shear or volume’ or ‘elastic, yield in past’. However, investigation into the meaning of these possible states, particularly ‘elastic, yield in past’ indicated that such a simplistic definition of cracking would be inaccurate. Firstly, ‘elastic, yield in past’ simply means that at some point in the solution process the element reached the failure criterion. This could be caused by redistribution of stresses once an element reached yield causing the element to return to an elastic state, or could also be caused artificially by transient loads due to sudden placement or removal of large portions of the grid (Sainsbury 2007). As such it is only a useful representation of yielding in the past if the embankment is placed in small increments so that unrealistic transient loads are not developed, and even if this realistic loading is achieved it does not give an indication of whether or not plastic flow occurred while the element was at yield.

This ambiguity regarding the meaning of ‘elastic, yield in past’ poses a significant problem as it is believed that in most cases if pavement cracking or slip failure occurred most zones would be shown as ‘elastic, yield in past’ at the end of the simulation as opposed to ‘at yield’. This is because at the end of the simulation the model should be in equilibrium and the model could not be in equilibrium if significant plastic deformations were occurring. However, it would still be possible for some elements to be at yield if the conditions around the element were such that plastic flow could not occur in the yielded element, or if the plastic flow occurring was smaller than the maximum allowed for the system to be

considered at equilibrium as defined by the user specified force ratio.

Given this uncertainty associated with whether yielding and plastic flow has occurred when an element is ‘elastic, yield in past’ and the required reliance on this resulting from elements not being at yield when in equilibrium, it was decided that this approach should not be used.

7.2.2. Approach 2: Measurement of Stresses and Displacements

The second approach, which was the approach used in the investigation, was to output the horizontal stresses, horizontal displacements, and vertical displacements, that occurred at the base of the pavement. These values would then be compared to values that would indicate that cracking had occurred.

Ideally, plastic strains should be output rather than displacements, as these would be the strains occurring after yielding had occurred and would therefore correspond loosely to a crack width. However, plastic strains could not be output in FLAC for a Mohr-Coulomb model, only the total volumetric or shear strains. Given the difficulty associated with interpreting such information, it was decided that horizontal and vertical displacements would be output instead.

Also, as the plasticity indicators (the first approach) could not be used effectively, and plastic strains could not be determined directly, it was decided that the embankment and pavement would be modelled as elastic without a Mohr-Coulomb failure criterion. Another reason for this approach is that accurate strength parameters were not known for either the embankment or the pavement material used on the Tully project, so using a Mohr-Coulomb model would add six more variables to the parametric study.

Whilst treating the embankment and pavement as elastic would slightly reduce the magnitude of settlements observed, the uncertainty this might cause was alleviated by monitoring the stresses obtained from the model as well. Stresses in an elastic model would be expected to be higher than those in a Mohr-Coulomb model as they are not restricted by a failure criterion, and any tensile stresses which were higher than an acceptable value, at the end of a simulation when the model was in equilibrium, were considered to indicate a possibility of cracking. Maximum induced tensile stresses between about 375 and 500 kPa were considered acceptable for the pavements designed for the Tully Project (as advised by the Tully Alliance Design Team). Therefore, any tensile stresses greater than this were considered to be indicators of a potential for pavement cracking. In general different pavements will have different strengths and a different criterion may need to be applied for different projects. However, in this investigation the stresses were output from the model,

not, whether or not yielding had occurred, therefore the results of this investigation could be used for other projects.

7.3 Modelling Strategies Devised and Attempted

A number of modelling strategies were considered before the procedure used was accepted.

These included:

1. a fully coupled model with the embankment placed incrementally,
2. a model without flow with the embankment placed incrementally,
3. a model without flow with the embankment placed instantaneously and
4. the use of two models both without flow, the first with the embankment built incrementally and the second with the displacements measured in the first model being applied incrementally to a fully built embankment.

Each of these models is discussed in the following section with the reasons why they were or were not used. The method adopted for the analysis was the fourth option listed above.

7.3.1. Option 1: Fully Coupled Model with Embankment Placed Incrementally

If this modelling strategy could have been implemented successfully it would have been the preferred option, as it would most realistically represent the construction process of an embankment on soft clay. However, due to the issue of high immediate settlements discussed in Chapters 5 and 6, if the embankment was built incrementally then the majority of settlement would have occurred prior to the placement of the pavement. As it is the settlement occurring after the placement of the pavement which is of concern when considering pavement cracking, it was deemed that a fully coupled model could not effectively be used for this analysis.

Variations of this model were also considered, including building the model with flow turned off, to simulate undrained conditions, and then allowing flow, however, the high immediate settlements occurred even under undrained conditions.

7.3.2. Option 2: Model without Flow with the embankment placed incrementally

In this model the embankment would be placed incrementally with it being run to equilibrium after each increment. An undrained bulk modulus would be specified for the foundation whilst the embankment was constructed, and then changed to a drained bulk modulus once the final embankment increment was placed. The intention of this was that

only small settlements would be experienced during the construction phase, and the consolidation settlements would occur after construction when the bulk modulus was changed. However, further research into this option revealed that the elastic moduli used in FLAC are tangent moduli as opposed to secant moduli. This means that strain increments are a result of stress increments rather than the total magnitude of stress (Itasca 2005b). As such changing the bulk modulus after the entire embankment and pavement are constructed would not result in any additional settlement, and changing it just before the placement of the pavement would only result in settlements due to the weight of the pavement not the whole embankment. As this model could not be modified to produce realistic consolidation settlements, it was rejected.

7.3.3. Option 3: Model without Flow with the embankment placed instantaneously

This option was not a preferred option due to the unrealistic nature of placing an entire embankment instantaneously. However, after options 1 and 2 had to be rejected it needed to be considered. A number of preliminary models based on this approach were created to test the validity of the approach and from these it was determined that this approach also should be rejected, as the results of the models showed the phenomenon of arching occurring within the embankment. Figure 7.2 shows the vertical displacement contours for one of these models and clearly shows the edge of the batter and pavement settling much less than the rest of the embankment, which is not a realistic situation.

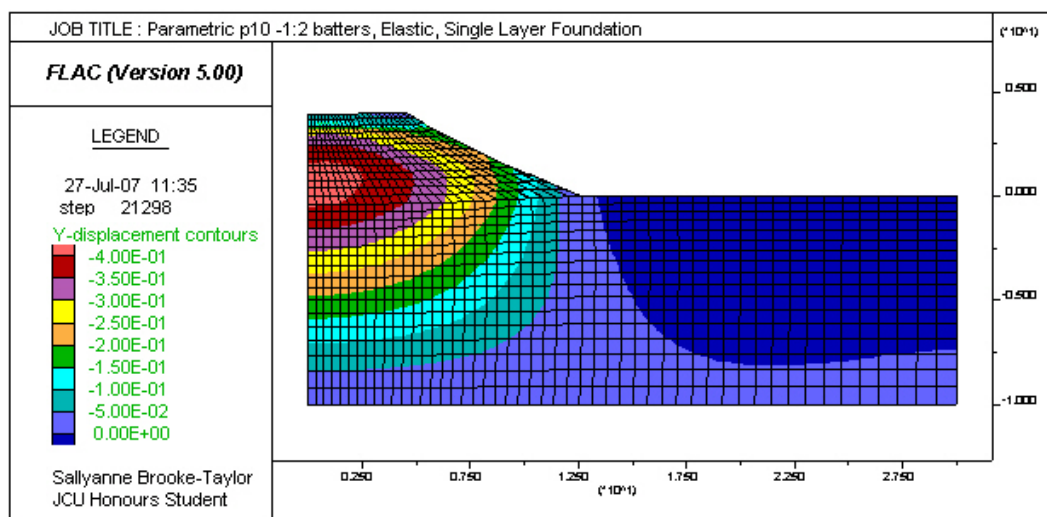


Figure 7.2: Vertical Displacement Contours for a Model with the Embankment Placed Instantaneously

7.3.4. Option 4: The Two Stage Model

This final option was the modelling approach used for the parametric investigation. The first stage consisted of an embankment being placed incrementally onto the foundation, with equilibrium being reached after the placement of each increment. The horizontal and vertical displacements at each gridpoint along the base of the embankment were then output from this model for use in the second model. The second model consisted solely of the embankment with no foundation but with an identical grid to that used in the first model. The displacements from the first model were then applied gradually to the base of this model over a 10000 timesteps.

Whilst this was chosen as the best method to use there were a number of simplifying assumptions upon which it was based. The first is that all settlement occurred after the entire embankment was placed. This could have been modified so that only a proportion of the total settlement was applied to the second model. However, the fraction of post construction settlement is highly dependent on the time of construction, which would vary from embankment to embankment, so the chosen fraction of post construction settlement to total settlement would just be a different assumption, which was not worst case in terms of settlement. Another assumption was that the rate at which displacements were applied would not affect the resulting stress and displacement distribution. For simplicity, in the second models the settlement was increased linearly over the 10000 timesteps to reach the displacements of the first models, whereas in reality settlement would increase as a plateauing exponential function. Finally, observation of the settlement pattern in the first models after each load increment indicated that the pattern changed as the embankment was built, as shown in Figure 7.3.

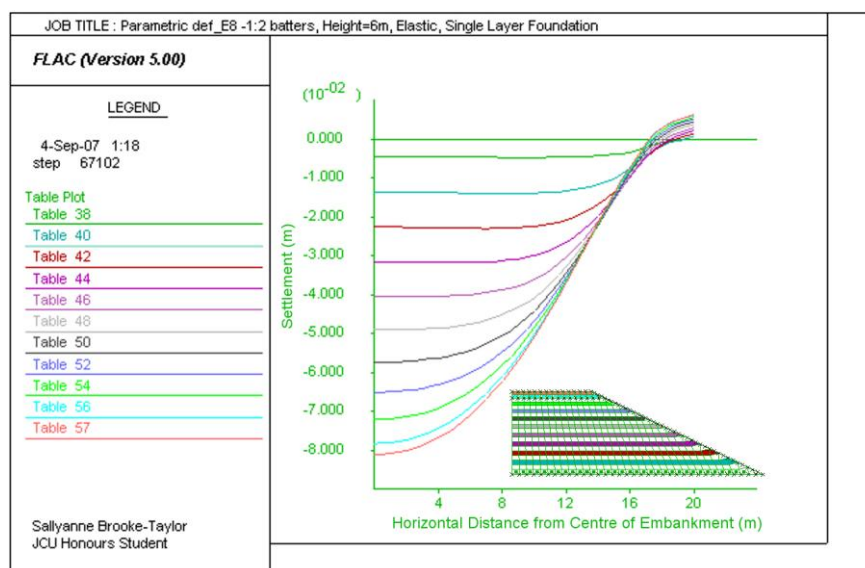


Figure 7.3: Settlement Pattern beneath a 6m High Embankment during Construction

These patterns are based on the assumption that all settlement associated with each layer has taken place before the next layer is added. Due to consolidation occurring in the field, this is not realistic, and as the actual settlement patterns allowing for consolidation were not known variations of the settlement pattern with time or embankment height could not be incorporated into the model.

7.4 Parameters Investigated and Models Created

The first series of models created were used to determine the effect of variations in foundation stiffness and embankment height. For all models the boundary conditions were kept the same, with the bottom boundary fixed for both horizontal and vertical movement and the two vertical boundaries fixed for horizontal movement. The batter slopes were kept at 2 (horizontal) : 1 (vertical) and the other parameters which were kept constant are shown in Table 7-1.

Table 7-1: Properties Held Constant Whilst Height and Foundation Stiffness were Varied

	Young's Modulus, E (MPa)	Poisson's Ratio, v	Density, ρ (kg/m ³)
Pavement	200	0.2	2170
Embankment	20	0.3	1960
Foundation	varied	0.4	1590

Heights of 3, 4.5 and 6 metres were modelled and for each of these, Young's Modulus values of 5, 8 and 10 MPa were trialled for the foundation. For the 3 metre high embankment Young's Modulus values of 3, 4 and 6 MPa were also modelled so that a similar range of settlements were achieved for each model. The dimensions and grids for each of the three heights are shown in Figure 7.4.

The next series of models created were to determine the effect of changes in the ratio of embankment and pavement stiffness. For this investigation all the models discussed above, except for the additional stiffnesses trialled only on the 3 metre high embankment, were repeated for an embankment stiffness of $E = 40$ MPa. Ideally the models should have been repeated for much higher pavement stiffnesses as the value of 200 MPa is at the lower end of the possible range for pavement stiffness. However, due to the Lagrangian formulation that FLAC uses to solve the models, stiffness ratios for adjacent soil layers of much greater than

10 cause numerical errors. As such the embankment stiffness was increased to reduce the ratio, and it is assumed that increasing the ratio would have the opposite effect.

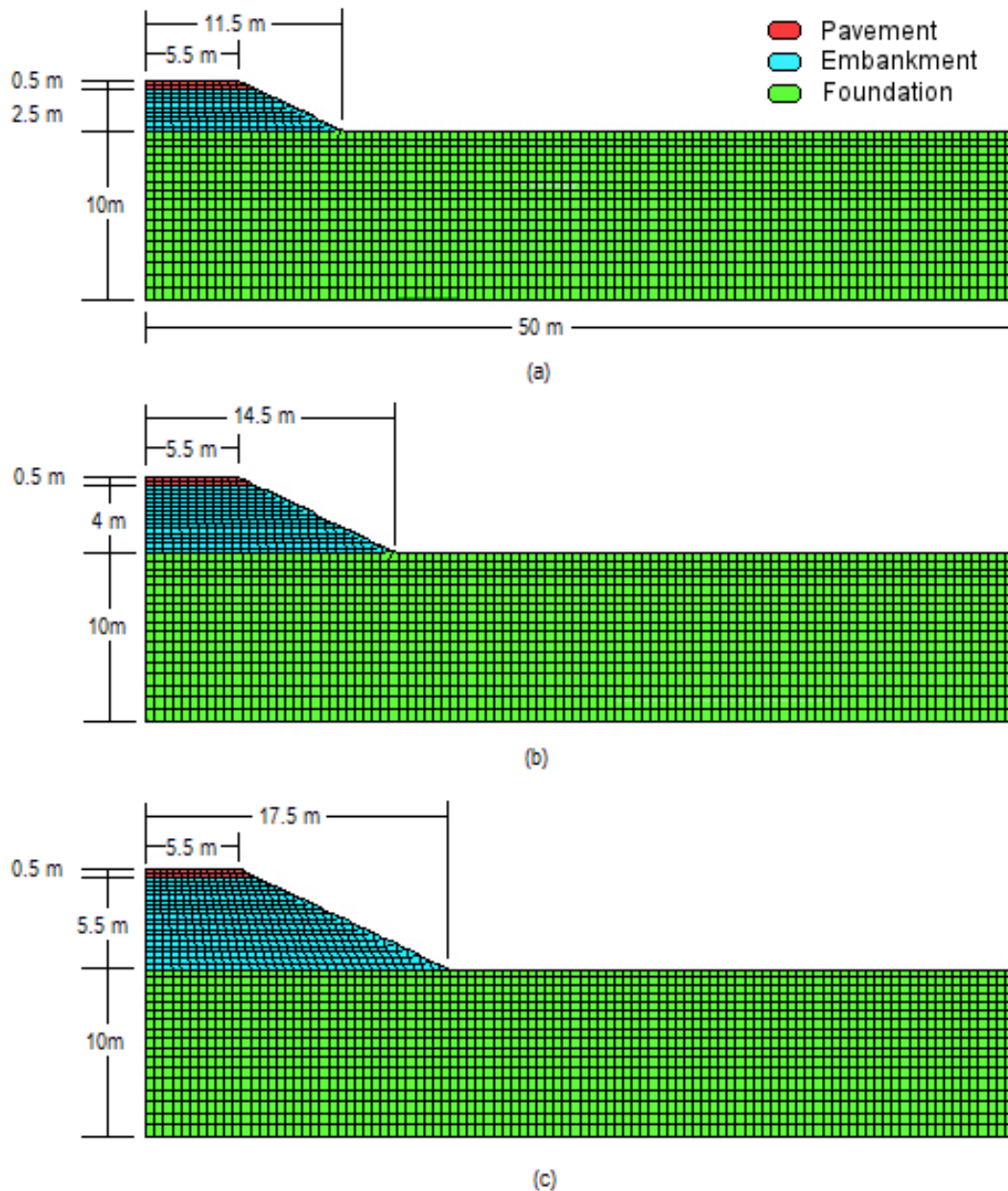


Figure 7.4: Dimensions and Grids for (a) the three metre high embankment, (b) the 4.5 metre high embankment and (c) the 6 metre high embankment

The other parameters listed in the introduction to this section which were believed to potentially have an effect on pavement cracking were not investigated. The results of the above investigation made it clear that varying these properties would not induce pavement cracking in the models. The code for one of the 3 m high embankments is included in Appendix D-1: Code for Pavement Cracking models.

7.5 Results

Contrary to the original expectations that high settlements would be accompanied by high differential displacements which could cause tension cracks to form in the pavement, all of the models created were found to have compressive forces in the pavement. Figure 7.5 shows the maximum horizontal pavement stresses plotted against Young's Modulus of the foundation for the first set of models in which the embankment stiffness was $E = 20$ MPa. As there was no tension achieved in the pavement of any of the models it was the minimum compression at the underside of the pavement which was recorded and is plotted in Figure 7.5. This minimum compression was found to occur at or near the edge of the pavement, as shown in Figure 7.6 which is a plot of the horizontal stress profile at the base of the pavement for a foundation Young's Modulus of 8 MPa and embankment heights of 3, 4.5 and 6 metres.

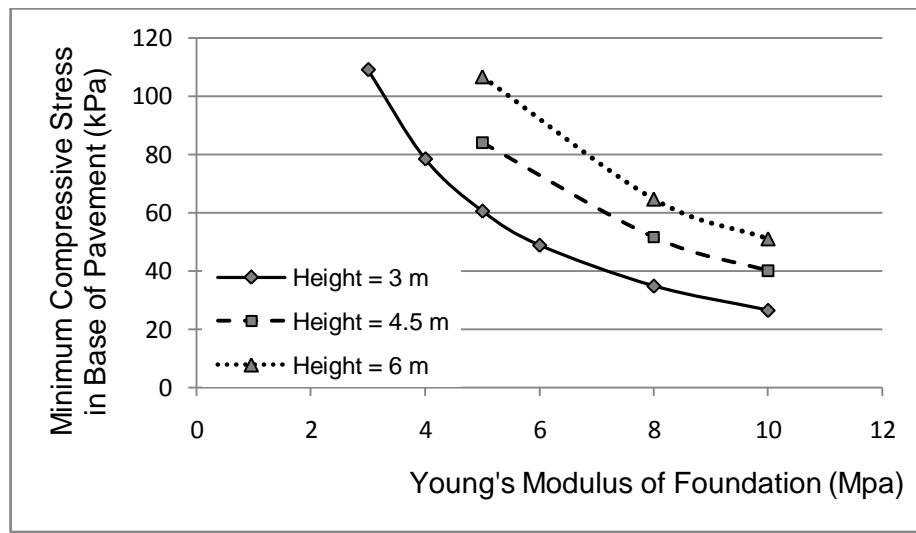


Figure 7.5: Effect of Embankment Height and Young's Modulus on the Pavement Stresses

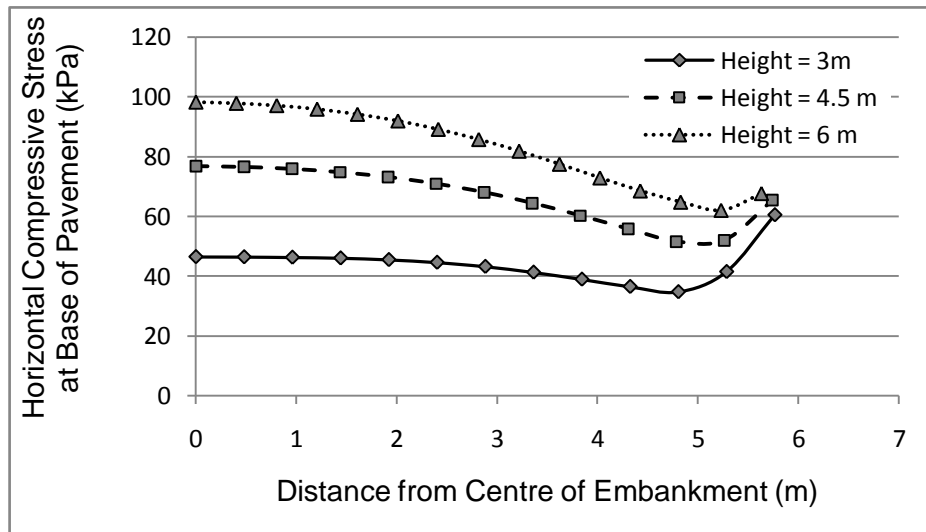


Figure 7.6: Horizontal Stress Profile at Base of the Pavement for Models with $E_{\text{foundation}} = 8$ MPa

From Figure 7.5 it is clear that the minimum horizontal compression in the pavement is a function of both foundation stiffness and embankment height.

The minimum compressive stresses as shown in Figure 7.5 are shown in Figure 7.7 plotted against the maximum settlement beneath the embankment. This graph also shows the results of the second stage of the modelling where the embankment stiffness was changed to $E = 40$ MPa. In all models this maximum settlement was found to be at the centre of the embankment. These results show the minimum compression in the pavement to be proportional to the maximum settlement. That is, higher settlements result in higher compressive stresses, which would indicate that higher settlements reduce the chances of pavement cracking. Also for both values of embankment stiffness modelled, the difference in embankment height between 4.5 m and 6 m had very little effect on the stress versus settlement curve. This indicates that in this height range, settlement and height are not independent variables. In contrast, the pavement stress – settlement curve for the 3 m high embankment had a different slope to the curves for the other two heights, for both the values of embankment stiffness modelled. To understand the reason for this different slope more models would need to be created to determine whether the slope changes gradually with height or whether there are two distinct slopes the curves can have, with a critical height at which the slope changes. Due to time constraints and the fact that the results indicated that variations in embankment height would not result in tension in the pavement and a potential for cracking, further investigation into this particular matter was not conducted.

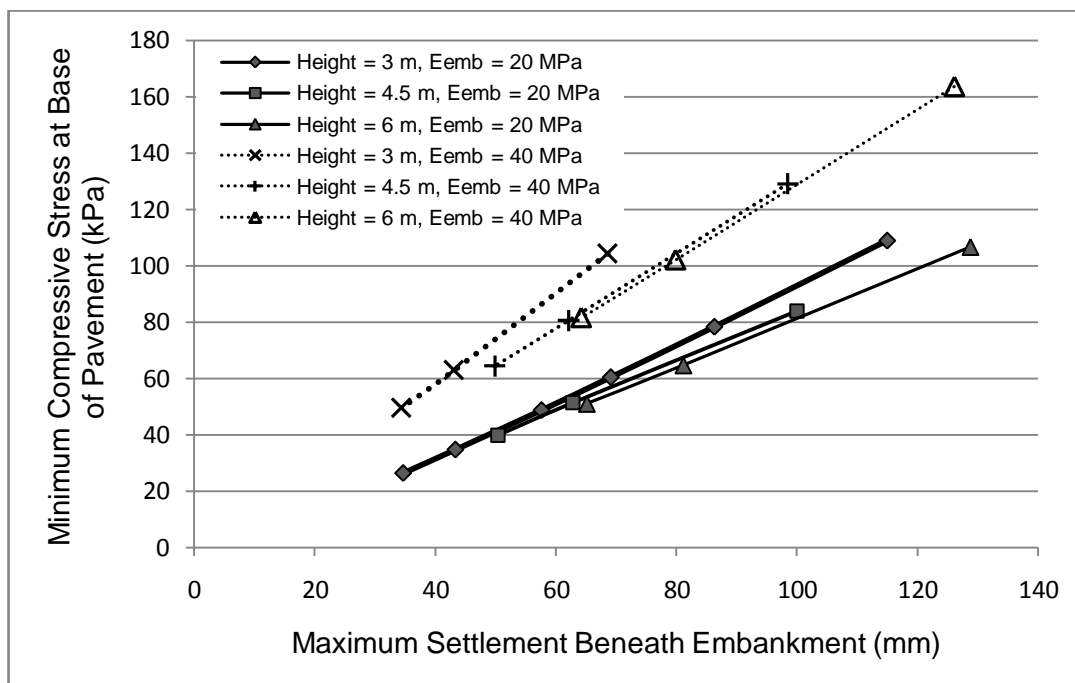


Figure 7.7: Effect of Settlement beneath the Embankment on Pavement Stresses

The minimum compressive stresses were also plotted against the maximum lateral displacement beneath the toe of the embankment. However, the graph was almost identical to Figure 7.7 as the ratio of maximum lateral displacement to maximum settlement was almost constant at about 0.34 for all models. This ratio is consistent with the ratios observed in the literature and the idealised relationship developed by Stewart et al. (1994) which is shown in Figure 2.25. A table of all these results as well as the pavement stress – lateral displacement graph are included in Appendix D-2: Data from Pavement Cracking Models.

In addition to the horizontal stress, the horizontal and vertical displacements at the base of the pavement were also output from the models. Analysis of the horizontal displacements indicated that whilst the horizontal displacements at the base of the models were all away from the centre of the embankment, the displacements at pavement level were all towards the centre of the model. This agrees with the stress results that have the pavement in compression. As the horizontal displacements are showing how much pavement elements are being squashed not how much they are being stretched, which could correspond to crack widths, no further analysis was done on them.

Vertical displacements recorded along both the bottom and top of the pavement were almost identical to the settlement beneath the embankment as shown in Figure 7.8. The lack of any significant differential vertical displacements along the pavement is in agreement with all the previous results in which no potential for cracking is present, and as such no further analysis was conducted on the vertical displacements.

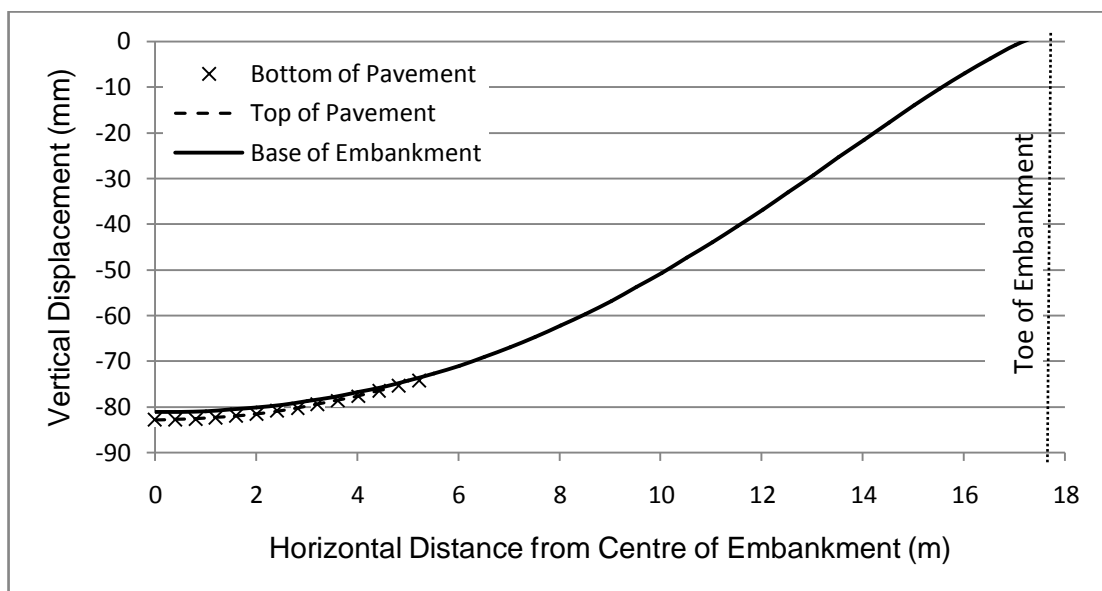


Figure 7.8: Vertical Displacements at Top and Bottom of Pavement Compared with Settlement beneath the Embankment for 6m High Embankment with $E_{\text{foundation}} = 8 \text{ MPa}$, $E_{\text{Embankment}} = 20 \text{ MPa}$, $E_{\text{pavement}} = 200 \text{ MPa}$

7.6 Discussion and Interpretation

From the results presented in section 7.5 it is clear that pavement cracking is not a concern for any of the situations modelled, and that the chances of pavement cracking actually decrease as the settlement beneath the embankment increases. This result is consistent with simple bending theory as detailed below.

Ignoring the foundation for the moment, consider the cross-section of the embankment and pavement together as a beam, for example a concrete beam, which is supported at both ends. Under its own weight this beam will deform into a curved shape. Assuming that the beam is strong enough to support its own weight without cracking or yielding it will remain in equilibrium in the curved shape unless another force is applied to it. For this to be the case the net force within the beam must be zero, therefore any tension in the underside of the beam caused by the curvature must be balanced by an equal amount of compression in the top of the beam. The case is similar for the embankment and pavement, by statics they must deform in a way which puts the top of the pavement into compression.

The analogy can however be taken further in order to explain the trends in the horizontal stress results shown in Figure 7.7. Within a beam there must be a depth where the horizontal stress is zero, this is known as the neutral axis and at this depth the length of a horizontal strip does not change due to the deformation. The depth of the neutral axis is dependent on the geometry of the cross section and in the case of a composite beam also on the stiffness of the different materials that form the beam. In the case of a beam made of a single type of material the neutral axis passes through the centroid of the beam. In a composite beam the effective cross section used for determining the neutral axis of the beam is modified to account for the differing stiffness (Hibbeler 2003). Materials with higher stiffness are given a larger area, therefore if there are two materials with the stiffer one on top, for example a pavement on an embankment, the neutral axis will be moved higher.

This can be used to explain why the compressive pavement stresses were higher in models where the ratio of pavement to embankment stiffness was lower, refer to Figure 7.7. The lower ratio meant that the ‘neutral axis’ of the embankment-pavement system was lower, meaning that there was a greater distance between the bottom of the pavement and the ‘neutral axis’. Now, as the strain in a deformed beam increases with the distance from the neutral axis the stress must also increase with distance. Therefore, the greater the distance between the bottom of the pavement and the neutral axis the higher the compressive stress in the pavement. The reverse of all this should also hold true, that if the ratio of pavement to embankment stiffness was increased the neutral axis would move higher and the

compressive stress in the bottom of the pavement would decrease. Given this it may be possible to have the ratio of pavement to embankment stiffness so high that the neutral axis is actually within the pavement and the bottom of the pavement is therefore in tension. Unfortunately, this option could not be explored using FLAC as numerical problems occur when the stiffness ratio of adjacent layers is increased above about 10. However, even if this could be achieved the bottom of the pavement would be very close to the neutral axis and therefore the tension in it would be small making the chances of pavement cracking also small.

Another factor which may affect the position of the neutral axis and therefore the stresses in the pavement would be the occurrence of cracks or yielding in the embankment material. Consider the analogy of a concrete beam again. When the load applied to the beam is such that the tension in the bottom fibres is greater than the tensile capacity of the material, cracks begin to form. Once cracks have formed there is no longer any tensile capacity across those cracks. Now, because the cracked region does not support any load the effective cross-sectional area reduces and the neutral axis moves away from the cracked area. Therefore, going back to the models, if enough of the embankment material yielded then the neutral axis might be pushed high enough to put it within the pavement and make the base of the pavement go into tension.

To test whether allowing the embankment material to yield would have an effect on the pavement stresses an additional model was created. This model was of a 3m high embankment, and had a foundation with stiffness $E_{foundation} = 4 \text{ MPa}$. It was identical to one of the earlier models except that both the embankment and pavement were Mohr-Coulomb materials with appropriate strength properties. The maximum settlement of the two equivalent models was almost identical with the Mohr-Coulomb model reaching a maximum settlement of 86.6 mm compared with the elastic model reaching 86.3 mm. There was however, a noticeable decrease in the minimum compressive stress which was 55.5 kPa as opposed to 78.4 kPa in the elastic model. Whilst this indicates that allowing the embankment to yield does affect the pavement stresses, further research would need to be conducted to determine if it is actually possible for this to cause pavement cracking. Based on the results of this Mohr-Coulomb model as well as the trends in the elastic model results, it is believed that the chances that this mechanism could cause pavement cracking are very small.

In addition the chances of pavement cracking due to these mechanisms are reduced further by the fact that the deformation of the pavement and embankment is restricted by the foundation. In the analogy so far the effect of the foundation has been ignored, but the foundation could affect the problem in a couple of ways. First, the foundation could be

considered as analogous to having a spring as a third support beneath the centre of the centre of the beam. In this way the amount of deformation allowed to take place would be controlled by the stiffness of the spring. Alternatively, the foundation itself could be considered as part of the beam. In this case the neutral axis would be much lower, and whilst variations in the relative stiffness and strength properties of the pavement and embankment would affect the neutral axis, no realistic values of these parameters could conceivably cause pavement cracking.

The way in which the models were created in FLAC makes these analogies particularly appropriate. For example all materials are treated as being continuous mediums rather than particulate materials, so in the simulations the embankment and pavement would distribute forces as if they were a continuous beam. Whether modelling the embankments in this way had a significant effect on the results is not known. It would be a useful exercise if this topic was researched further, to use a different program and create equivalent models which treated the soils as a collection of discrete particles to see the effect on the results. Even more useful would be an experimental investigation which monitored the deformations and stresses within the embankment and pavement not just within the foundation.

Two other aspects of the models have been identified as areas in which more research might lead to the discovery of situations which may cause pavement cracking. The first involves the interaction between the pavement and embankment. In all models created as part of this thesis project the pavement and embankment have been modelled as being rigidly connected. This rigid connection however, may not necessarily be the best representation of the connection between the two different materials. For instance some frictional slip may take place along the interface due to the significant difference between the stresses in each material for the same deformation. The most extreme case would be if there was slip with no friction. In this case the pavement by itself would effectively act as a beam with the bottom going into tension and the top into compression. Whilst this is unrealistic, investigation into this case would show whether, in a worst case scenario, pavement cracking was possible. If cracking was not present in this model, one could be very confident that pavement cracking would not be a problem in a realistic situation involving embankments of similar dimensions to those studied in this investigation resting on uniform foundations. If the results of the extreme case indicated a potential for cracking, then more research into the actual nature of the connection between embankments and pavements could be conducted and models could be created with a more realistic, possibly frictional, connection between the different materials.

The other variable which could be modified to potentially cause pavement cracking is the width of the embankment. In all models created as part of this investigation the same half crest width of 5.5 m was used as this was the standard width of the embankments in the Tully project. This comparatively narrow width compared with the embankment heights resulted in settlement profiles taking the form of typical settlement basins in all of the models. However, if the width of the embankment was increased to the extent that the settlement profile beneath the embankment was a sagged settlement profile, as discussed in Section 2.3.2, then the resulting embankment deformation might put parts of the pavement into tension. To test this theory, five 3 m high embankments were modelled with a crest half width of 20 m, and different values for foundation stiffness. The results showed that when the settlement profile beneath the embankment was a sagged settlement pattern the centre of the pavement was put into tension which increased with the magnitude of settlement, as shown in Figure 7.9. This indicates that if wide enough, embankments could be at risk of pavement cracking due to high settlements. However, further investigation into this potential cause of pavement cracking was not conducted as the embankment width required to achieve a sagged settlement pattern was far greater than any of the embankment widths on the new section of the Bruce Highway near Tully. In addition to this, it should be noted that in general for an embankment to have the high crest width to height ratio required to cause the sagged settlement pattern, the embankment would need to be very low, and if the embankment is low then the settlement and resulting tensile stress in the pavement will in most cases be small.

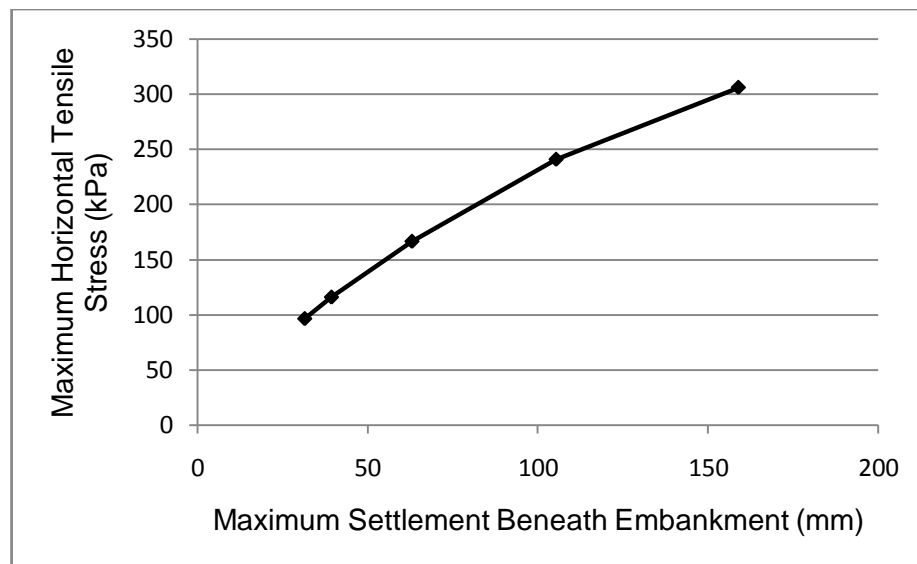


Figure 7.9: Variation of Maximum Horizontal Tensile Stress in a Pavement with Settlement for a Wide Embankment

Despite these other areas for further research which have been discussed above, the results presented in Section 7.5 quite clearly show that pavement cracking due to excessive settlement is not a problem in realistic situations involving embankments of dimensions similar to those modelled which rest on uniform foundations.

7.7 Implications of Results for the Tully Project

The results of this investigation quite clearly indicate that pavement cracking due to excessive settlements should not be a problem for any of the embankments on the Bruce Highway upgrade near Tully. Embankments modelled as part of the investigation were chosen to have heights spanning the expected range of embankment heights on the project, to have a half crest width of 5.5m which is the standard width used on the project, and to have batter slopes of 1:2 which is the slope to be used in the sections with the highest embankments. Additionally, the various values for foundation stiffness used in the models were chosen to give settlements in the range of the settlements expected on sections of the highway where no preloading was done. The results of this investigation can therefore be related to the embankments of the Tully project, and those working on the project can have confidence that pavement cracking will not occur as a result of the excessive deformations associated with building on soft ground.

This result, however, should be treated with caution, as it does not rule out the possibility of pavement cracking resulting from other factors not investigated in this project. For example in all models created the foundation profile was the same over the entire width of the embankment and surrounding area modelled. This may not be an accurate representation of the foundation for the whole length of the new stretch of highway. In some areas soil layers may not be uniform and horizontal or there may be a stiff material beneath one side of an embankment which doesn't extend the full width of the embankment, as shown in Figure 7.10. In these cases the deformation profile beneath the embankments would not be the typical settlement basin developed in the models created, but may be one which causes the embankment to deform in a way that results in tension not compression in the pavement.

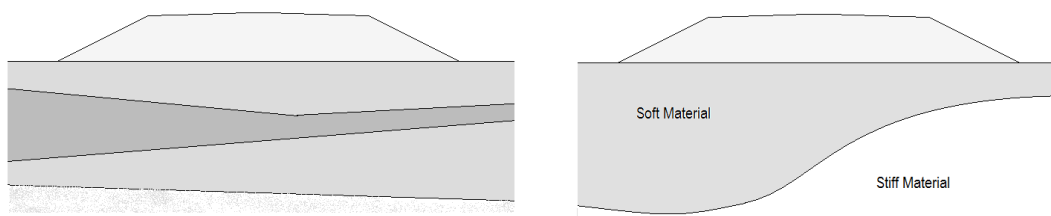


Figure 7.10: Possible Foundation Profiles

Another factor which could result in the post construction cracking of pavement is water. If the pavement was sufficiently water proof so that during rainfall the embankment material beneath it did not get wet whilst the batters and a small region adjacent to them but beneath the embankment did, then depending on the nature of the embankment and foundation material, swelling could occur in the wet areas. This localised swelling may be enough to cause stresses in the pavement which could cause pavement cracking. Cracking as a result of this wetting of the soil, could be of concern for the long term maintenance of the highway, as it is situated in an area prone to regular wetting. However, the soils in the Tully region do not tend to be highly prone to shrink-swell movements, and in addition the extremely high rainfall in the Tully region means that the soils are generally wet, with extreme drying rarely occurring.

7.8 Summary and Conclusions of the Investigation into Pavement Cracking

To investigate what factors affect the chances that pavement cracking will occur on a road embankment a number of models were created. Parameters including; embankment height, foundation stiffness and embankment stiffness were varied. Each run actually consisted of two models being solved in sequence. The first was a model of pavement, embankment and foundation in which the embankment was placed incrementally. The second used the vertical and horizontal displacements from the base of the embankment in the first model and applied them gradually to just the embankment and pavement. Whilst not ideal, this approach in which all materials were modelled as elastic was found to be the most appropriate way to account for consolidation without using a coupled model. Potential for pavement cracking was assessed by comparing the stresses in the pavement to values representing the maximum tensile stress the pavement could sustain without cracking. Displacements in the pavement were also monitored; however, as both the stresses and displacements showed the pavement to be in compression rather than in tension, little analysis was done on them. These results showing compression in the pavements of all models, quite definitively indicated that pavement cracking due to large settlements was not a concern for road embankments in general and particularly those on the Bruce Highway upgrade near Tully.

Chapter 8: Summary, Conclusions and Recommendations for Further Research

8.1 *Introduction*

The intent of this thesis was twofold:

1. to determine the potential for pavement cracking to occur as a result of large foundation deformations in the pavements of the Bruce Highway upgrade near Tully and
2. to determine under what conditions pavement cracking is likely to occur in road embankments and what variables have the most influence on the probability of it occurring

These aims were addressed by using FLAC (Fast Lagrangian Analysis of Continua) to numerically model a section of a trial embankment built as part of the Tully Project, as well as numerous generalised embankments. Difficulties with getting the numerical models to match the timing of the deformations that were measured in the trial embankment on site were encountered when using a coupled consolidation model. As a result an alternative modelling approach was developed to account for the delayed settlement associated with consolidation. This approach was used for the parametric investigation and the results of this investigation were used to assess the potential for pavement cracking to occur in the embankments of the new section of the Bruce Highway. The conclusions drawn from each of the modelling stages along with recommendations for further research are discussed in the remainder of this Chapter.

8.2 *Preliminary Modelling*

The preliminary modelling which is discussed in Chapter 5 consisted of a sensitivity analysis and an investigation into an issue involving the timing of settlements which was encountered during the sensitivity analysis. For the sensitivity analysis a number of coupled embankment models were created in which the values of foundation permeability, Young's modulus, density, effective cohesion and effective friction angle as well as the initialisation process were varied. The models were found to be insensitive to density, and for the low forces applied also to effective cohesion and friction angle. All other parameters were found to affect the models as would be predicted by theory.

The two most important discoveries from this modelling were that the models are particularly sensitive to the initialisation process used and also that there was a problem with

the timing of settlements in the models. A thorough investigation was conducted into the timing issue, which was that too high a proportion of the settlement was occurring instantaneously. However, despite this the cause of the problem and a solution were not found.

8.3 Trial Embankment Modelling

A section of one of the trial embankments built near Tully was modelled using a coupled consolidation model and the results were compared with the settlement plate and piezometer readings recorded at the location on site. This modelling confirmed that the large immediate settlements encountered during the preliminary modelling were a problem in the modelling rather than a misconception regarding what the time rate of consolidation beneath an embankment should be. As a result of this rate of consolidation problem and the poor quality of the data received from site the model created did not match the field data well. For this reason, it was concluded that an accurate picture of the chances of pavement cracking on the new section of Bruce Highway could not be obtained by creating coupled consolidation models of the critical embankment sections. As the original purpose of the trial embankment modelling was to refine the correlations between the geotechnical information available for the foundations and the model input parameters these corresponded to, it was pointless to create more than one embankment model given that the calibration information would not be used for modelling other sections of the highway.

Despite the lack of success of the trial embankment modelling, much was learnt from the exercise. The most important point being that whilst numerical modelling can be a very powerful tool, the quality of the results which are produced are highly sensitive to the quality of data input into the model. If too many assumptions are required to determine the inputs into a model it cannot be assumed that the results of the model will be accurate and a valid representation of the system even if the model is working correctly. Given this it is recommended that before attempting to numerically model a particular system, the extent and quality of information available should be assessed, and only if the information is good, should numerical modelling be used over other perhaps less accurate but faster methods.

8.4 Parametric Investigation into Pavement Cracking and Implications for the Tully Project

In the parametric investigation into pavement cracking the effect of varying the embankment height, foundation stiffness and embankment stiffness were studied. Investigation into other

variables was also intended; however the results of the first sets of models so conclusively indicated that pavement cracking was not a problem that further investigation was deemed unnecessary.

To avoid the problem of high immediate settlements that was encountered in the other modelling phases a new two stage approach was developed for this study. Instead of using a coupled model, two mechanical only models were created, the first to determine the final distribution of horizontal and vertical displacements at the base of the embankment and the second to apply these displacements gradually to the embankment. The potential for pavement cracking was assessed based on the stresses occurring in the pavement compared to a maximum acceptable tensile stress.

The results of the study indicated that the embankment – pavement system acted much like a beam which bends under its own weight, putting the base into tension and the top into compression. As the pavement is at the top of the embankment all the models put the pavement into compression, which increased as the amount of settlement increased. The only way which was found to induce tension into the pavement was to make the crest width to height ratio of the embankment high enough that it caused a different deformation profile beneath the embankment. However, based on research in the literature review, the crest width to height ratio to cause this alternative profile is five, which is higher than any of the ratios on the Tully Project.

Based on the results of the study and the dimensions of the embankments in the new section of the Bruce Highway near Tully, it was concluded that pavement cracking as a result of large consolidation settlements would not be a problem on the Tully project. However, it is possible that pavement cracking may occur as a result of a non-uniform foundation profile, or in the long term as a result of the wetting and drying cycles associated with the high amount of rainfall to which the region is exposed.

8.5 Recommendations for Further Research

During the completion of this project a number of areas for further research presented themselves. Some of these are listed below.

1. Further investigation to determine the cause of the high ratio of immediate to total settlement in two-dimensional coupled consolidation FLAC models could be done with the aim of finding a solution to the problem and subsequently refining the trial embankment model created.

2. Trial embankment models could be created in a different numerical modelling program such as PLAXIS or ABAQUS. These could be compared with the FLAC model to determine whether the issue of the large immediate settlements was only apparent in the FLAC models created in this thesis or whether it is a more general problem found in other numerical modelling packages. If the issue did not occur in the chosen package, additional trial embankment models could be created to refine the correlations between field data and input values for FLAC, and critical sections of the new highway could be modelled to predict their deformations.
3. An experimental investigation could be conducted to determine how to correlate the output from JCU's inclinometer probe to actual displacements. Known displacements could be induced on a piece of inclinometer casing and measured using the inclinometer to achieve this. The results could be applied to the data collected from the trial embankment sites, to produce lateral displacement results for the trial embankments which could be compared to the results of numerical models.
4. Extensive investigation of road embankments which currently have pavement cracking problems could be conducted. Numerous locations could be visited and data including embankment height, crest width, batter slope, pavement thickness embankment stiffness, pavement stiffness, foundation properties and batter irrigation and rainfall patterns could be collected and collated. This information could be used to determine what factors cause pavement cracking from experience and would also provide data to validate numerical models.
5. An experimental investigation could be carried out, where the deformations and stresses in the pavements of real or model embankments are be monitored. This would provide useful information to assess the validity of the results of the pavement cracking investigation.
6. The pavement cracking investigation could be extended by creating a model with an interface between the embankment and pavement to allow for slippage at the interface. The model could then be run with various different frictional relations between the two materials to determine whether slippage at this interface would cause pavement cracking. It would be beneficial to couple this modelling with an experimental investigation to determine when slippage might occur, and the nature of the interaction between pavement and embankment when it does occur.

7. The pavement cracking investigation could also be extended by creating a number of models in which all the materials were modelled as Mohr-Coulomb with varying strengths. Alternatively, the embankment and pavement could be modelled as Mohr-Coulomb and the foundation modelled as Cam-Clay. This could lead to the discovery of a condition which causes pavement cracking. However, based on the results of this thesis it is believed that this is unlikely and the results would just serve to further confirm that pavement cracking due to large deformations is not a problem.
8. The pavement cracking investigation could be repeated using a model which treats the soil as a particulate media rather than a continuous media. The results of this could be compared with the results from the investigation in this thesis to determine whether treating soil as a continuous media is an acceptable approximation for this type of investigation.
9. An investigation could be conducted to determine whether repeated wetting and dry cycles can cause pavement cracking and if so under what conditions. This would be particularly useful information for engineers designing roads and pavements.

References

- Balasubramaniam, A. (2007). "Personal Communication."
- Barnes, G. E. (2000). *Soil Mechanics - Principles and Practice*, Macmillan Press LTD, London.
- Bjerrum, L. "Embankments on Soft Ground." Oslo.
- Brouwer, J. J. M. (Accessed: 28.05.2007). "Guide to Cone Penetration Testing." <http://www.conepenetration.com/cpt4.html#cptu>.
- Canterbury_City_Council. (2007). "The Management of Coastal Erosion - Report 2." <http://www.canterbury.gov.uk/buildpage.php?id=705>.
- Cernica, J. N. (1995). *Geotechnical Engineering: Soil Mechanics*, John Wiley & Sons, Inc., New York.
- Coetzee, M. J., Hart, R. D., Varona, P. M., and Cundall, P. A. (1998). *FLAC Basics: An Introduction to FLAC and a guide to its Practical Application in Geotechnical Engineering*, Itasca Consulting Group Inc., Minnesota.
- Detournay, C. (2007). "Personal Communication with Itasca."
- Duncan, J. M. (1993). "Limitations on Conventional Analysis of Consolidation Settlement (The Twenty-Seventh Karl Terzaghi Lecture)." *Journal of Geotechnical Engineering*, 119(9), 1332-1359.
- Durham_Geo-Enterprises. (2006). "Slope Indicator 2006 Catalog." <http://www.slopeindicator.com/pdf/slope-indicator-2006-catalog.pdf>.
- Fadum, R. E. "Influence Values for Estimating Stresses in Elastic Foundations." *Proceedings of the Second International Conference on Soil Mechanics and Foundation Engineering*.
- Ground Test Pty Ltd - Now Douglas Partners, G. C. A. (1981). "Promotional brochure titled: Dutch Cone Test."
- Hibbeler, R. C. (2003). *Mechanics of Materials*, Pearson Education, Inc., New Jersey.
- Hines, N. K. (1985). "Installationtion of Inclinometer Casing in Small Boreholes." *Australian Geomechanics News - News Journal of the Australian Geomechanics Society*, Number 9.
- Høeg, K. "Deformation Computations in Geotechnical Engineering." *The Second Laurits Bjerrum Lecture*, Norwegian Geotechnical Institute, Oslo.
- Holtz, R. D., and Kovacs, W. D. (1981). *An Introduction to Geotechnical Engineering*, Prentice Hall, New Jersey.

- Hsi, J. P., and MacGregor, J. P. "Prediction and Monitoring of Embankment Performance." *Proceedings of 8th ANZ Conference on Geomechanics*, Hobart, Tasmania.
- Hunter, G., and Fell, R. (2003). "Prediction of impending failure of embankments on soft ground." *Canadian Geotechnical Journal*, 40(1), 209-220.
- Indraratna, B., and Balasubramaniam, A. S. (1992). "Performance of Test Embankment Constructed to Failure on Soft Marine Clay." *Journal of Geotechnical Engineering-Asce*, 118(1), 12-33.
- Indraratna, B., Balasubramaniam, A. S., and Sivaneswaran, N. (1997). "Analysis of settlement and lateral deformation of soft clay foundation beneath two full-scale embankments." *International Journal for Numerical and Analytical Methods in Geomechanics*, 21(9), 599-618.
- Itasca, C. G. (2005a). "FLAC Manual." Command Reference, Itasca Consulting Group, Inc., Minneapolis.
- Itasca, C. G. (2005b). "FLAC Manual." User's Guide, Itasca Consulting Group, Inc., Minneapolis.
- Itasca, C. G. (2005c). "FLAC Manual." Background - The Explicit Finite Difference Method, Itasca Consulting Group, Inc., Minneapolis.
- Itasca, C. G. (2005d). "FLAC Manual." Fluid-Mechanical Interaction, Itasca Consulting Group, Inc., Minneapolis.
- Lei, G. H., Ai, Y. B., and Shi, J. Y. (2006). "The Interpretation of Pendulum-Type Inclinometer Readings." *Canadian Geotechnical Journal*, Vol 43(2), pg 210-216.
- Leonards, G. A. (1962). "Foundation Engineering." McGraw-Hill Civil Engineering Series, McGraw-Hill, New York.
- Lewis, R. W., and Schrefler, B. A. (1987). *The Finite Element Method in the Deformation and Consolidation of Porous Media*, John Wiley & Sons, Brisbane.
- Mayne, P. W. (2002 Accessed: 31.05.07). "Flow Properties from Piezocone Dissipation Tests." <http://geosystems.ce.gatech.edu/Faculty/Mayne/papers/PiezoDissipation.pdf>.
- Mesri, G., and Choi, Y. K. (1985). "Settlement Analysis of Embankments on Soft Clays." *Journal of Geotechnical Engineering-Asce*, 111(4), 441-464.
- Mesri, G., and Vardhanabhuti, B. (2005). "Secondary compression." *Journal of Geotechnical and Geoenvironmental Engineering*, 131(3), 398-401.
- Murthy, V. N. S. (2003). *Geotechnical Engineering: Principles and Practices of Soil Mechanics and Foundation Engineering*, Marcel Dekker, Inc., New York.
- Naylor, D. J., and Pande, G. N. (1981). *Finite Elements in Geotechnical Engineering*, Pineridge Press, Swansea, UK.

- Oh, E. (2006). "Geotechnical aspects of motorway embankments on soft clays in Southeast Queensland," PhD Thesis, Griffith University.
- Olson, R. E. (1998). "Settlement of embankments on soft clays." *Journal of Geotechnical and Geoenvironmental Engineering*, 124(8), 659-669.
- Osterberg, J. O. "Influence Values for Vertical Stresses in a Semi-infinite Mass Due to an Embankment Loading." *Proceeding of the Fourth International Conference on Soil Mechanics and Foundation Engineering*, London, 393-394.
- Poulos, H. G. (1999). "Approximate Computer Analysis of Pile Groups Subjected to Loads and Ground Movements." *International Journal for Numerical and Analytical Methods in Geomechanics*, 23, 1021-1041.
- Rankine, B., Sivakugan, N., and Wijeyakulasuriya, V. "Observed and predicted behaviour of clay foundation response under the Sunshine Motorway Trial Embankment." *Proceedings of the 16th International Society for Soil Mechanics and Geotechnical Engineering*, Osaka, 951-954.
- Robertson, P. K., and Campanella, R. G. (1983). "Interpretation of Cone Penetration Tests .1. Sand." *Canadian Geotechnical Journal*, 20(4), 718-733.
- Sainsbury, D. (2007). "Personal Communication with Itasca."
- Sivakugan, N. (2006). "A FLAC Primer." James Cook University.
- Sivakugan, N. (2007). "CS4001: Foundation Engineering - Lecture Notes." James Cook University.
- Sivakugan, N. (2008a). "Chapter 1: Review of Soil Mechanics." *Geotechnical Engineering Handbook*, B. M. Das, ed., J. Ross Publishing, Inc.
- Sivakugan, N. (2008b). "Chapter 3: Designs of Shallow Foundations." *Geotechnical Engineering Handbook*, B. M. Das, ed., J. Ross Publishing, Inc.
- Stewart, D. P., Jewell, R. J., and Randolph, M. F. (1994). "Design of Piled Bridge Abutments on Soft Clay for Loading from Lateral Soil Movements." *Geotechnique*, 44(2), 277-296.
- Tavenas, F., Mieussens, C., and Bourges, F. (1979). "Lateral Displacements in Clay Foundations under Embankments." *Canadian Geotechnical Journal*, 16(3), 532-550.
- Terzaghi, K., and Peck, R. B. (1967). *Soil Mechanics in Engineering Practice*, John Wiley & Sons, New York.
- U.S.Navy. (1971). "Soil Mechanics, Foundations, and Earth Structures " NAVFAC Design Manual DM-7, Washington, D.C.
- Zhang, L. M. (1999). "Settlement patterns of soft soil foundations under embankments." *Canadian Geotechnical Journal*, 36(4), 774-781.

Appendix A: Tully Data

A-1: Settlement Predictions and Preloading and Surcharge Requirements

Table A-1: Settlement Predictions and Preloading Designations (Produced by the Alliance)

CONTROL LINE CHAINAGE	START	FINISH	PREDICTED SETTLEMENT (mm%%P50%)	HEIGHT OF SURCHARGE (m)	SETTLEMENT PERIOD (MONTHS)	TYPE SECTION	MONITORING EQUIPMENT
80010.414	80420		40	-	<1	A	MONITORING PLATES @ 50.000 CENTRES
80420	80480	80451		-		A	
80480	80540		40	-	<1	A	1 MONITORING POINT AT CH 80510.000 1 SETTLEMENT POINT AT CH 80570.000
80540	80600	80568	50	-	1	B	
80600	81000		40	-	<1	A	MONITORING POINT @ 50.000 CENTRES
81000	81030.747		40	-	<1	C	1 MONITORING POINT AT CH 81020.000
81030.747	81090.397	CORDUROY CREEK BRIDGE					
81090.397	81125		40	-	<1	C	1 MONITORING POINT AT CH 81110.000
81125	81135		40	-	<1	A	1 MONITORING POINT AT CH 81130.000
81135	81530		40	-	<1	A	MONITORING POINTS @ 50.000 CENTRES
81135	81530		40	-	<1	A	MONITORING POINTS @ 50.000 CENTRES
81530	81555	81544.6	<40	-	-	A	1 SETTLEMENT PLATE AT CH 81545
81530	81555	81544.6	<40	-	-	A	1 SETTLEMENT PLATE AT CH 81545
81555	81610		40	-	<1	A	1 MONITORING POINT AT CH 81580
81555	81610		40	-	<1	A	1 MONITORING POINT AT CH 81580
81610	81650	81630	<40	-	-	A	1 SETTLEMENT PLATE AT CH 81630
81610	81650	81630	<40	-	-	A	1 SETTLEMENT PLATE AT CH 81630
81650	81665		100	-	3	B	1 SETTLEMENT PLATE AT CH 81660
81650	81665		100	-	3	B	1 SETTLEMENT PLATE AT CH 81660
81665	81710	81690	100	-	3	B	1 SETTLEMENT PLATE AT CH 81690
81665	81710	81690	100	-	3	B	1 SETTLEMENT PLATE AT CH 81690

CONTROL LINE CHAINAGE			PREDICTED SETTLEMENT (mm%%P50%)	HEIGHT OF SURCHARGE (m)	SETTLEMENT PERIOD (MONTHS)	TYPE SECTION	MONITORING EQUIPMENT
START	FINISH						
81710	81865		50	-	1	A	MONITORING POINTS @ 50.000 CENTRES
81710	81865		50	-	1	A	MONITORING POINTS @ 50.000 CENTRES
81865	81915	81889.5	50	-	1	B	1 SETTLEMENT PLATE AT CH 81890
81865	81915	81889.5	50	-	1	B	1 SETTLEMENT PLATE AT CH 81890
81915	81955		50	-	1	A	1 MONITORING POINT AT CH 81940
81915	81955		50	-	1	A	1 MONITORING POINT AT CH 81940
81955	82000	81980	<40	-	-	A	1 SETTLEMENT PLATE AT CH 81980
81955	82000	81980	<40	-	-	A	1 SETTLEMENT PLATE AT CH 81980
82000	82080		50	-	1	B	1 MONITORING POINT AT CH 82040.000
82080	82140	82111	200	-	3	B	1 SETTLEMENT PLATE AT CH 821000.000
82140	82240		100	-	2	B	MONITORING POINTS @ 50.000 CENTRES
82240	82300	82270	50	-	1	B	1 SETTLEMENT PLATE AT CH 82270.000
82300	82375		100	-	2	B	SETTLEMENT PLATES @ 50.000 CENTRES
82375	82430	82405	200	-	6	B	1 SETTLEMENT PLATE AT CH 82400.000
82430	82460		200	-	5	B	1 SETTLEMENT PLATE AT CH 82445.000
82460	82510	82485	200	-	5	B	1 SETTLEMENT PLATE AT CH 82490.000
82510	82565		40	-		B	1 MONITORING POINT AT CH 82540.000
82565	82615	82590	<40	-	-	A	1 SETTLEMENT PLATE AT CH 82585.000
82615	82665		100	-	1	A	1 SETTLEMENT PLATE AT CH 82640.000
82665	82695	82680	100	-	1	B	1 SETTLEMENT PLATE AT CH 82675.000
82695	82820		100	-	1	A	SETTLEMENT PLATES @ 50.000 CENTRES
82820	82900		100	-	1	A	1 SETTLEMENT PLATE AT CH 82880.000
82900	82940	82920	100	-	1	B	1 SETTLEMENT PLATE AT CH

CONTROL LINE CHAINAGE	FINISH		PREDICTED SETTLEMENT (mm%%P50%)	HEIGHT OF SURCHARGE (m)	SETTLEMENT PERIOD (MONTHS)	TYPE SECTION	MONITORING EQUIPMENT
START							
							82920.000
82940	83030		100	-	1	A	SETTLEMENT PLATES @ 50.000 CENTRES
83030	83080	83050	100	-	1	B	1 SETTLEMENT PLATE AT CH 83025.000
83080	83140		100	-	1	B	1 SETTLEMENT PLATE AT CH 83110.000
83140	83200	83170	150	-	3	D	1 SETTLEMENT PLATE AT CH 83170.000
83200	83315		150	-	3	B	SETTLEMENT PLATES @ 50.000 CENTRES
83315	83375	83345	40	-		D	1 SETTLEMENT PLATE AT CH 83340.000
83375	83470		250	-	6	B	1 SETTLEMENT PLATE AT CH 83430.000
83470	83530	83500	250	-	6	D	1 SETTLEMENT PLATE AT CH 83500.000
83530	83563.68		250	-	6	B	1 SETTLEMENT PLATE AT CH 83550.000
83563.68	83587.68		250	-	6	D	1 SETTLEMENT PLATE AT CH 83580.000
83587.68	83690.64	LAGOON SOUTH BRIDGE					
83690.64	83714.64		250	-	6	J	1 SETTLEMENT PLATE AT CH 83700.000
83714.64	83840		250	-	6	H	SETTLEMENT PLATES @ 50.000 CENTRES
83840	83885	83865	100	-	1	B	1 SETTLEMENT PLATE AT CH 83860.00
83885	84050		100	-	1	A	SETTLEMENT PLATES @ 50.000 CENTRES
84050	84100	84073	50	-	1	B	1 SETTLEMENT PLATE AT CH 84080
84050	84100	84073	50	-	1	B	1 SETTLEMENT PLATE AT CH 84080
84100	84125		50	-	1	B	1 MONITORING POINT AT CH 84110
84100	84125		50	-	1	B	1 MONITORING POINT AT CH 84110
84125	84185	84155	50	-	1	B	1 SETTLEMENT PLATE AT CH 84150
84125	84185	84155	50	-	1	B	1 SETTLEMENT PLATE AT CH 84150
84185	84240		50	-	1	A	MONITORING POINTS @ 50.000 CENTRES

CONTROL LINE CHAINAGE			PREDICTED SETTLEMENT (mm%%P50%)	HEIGHT OF SURCHARGE (m)	SETTLEMENT PERIOD (MONTHS)	TYPE SECTION	MONITORING EQUIPMENT
START	FINISH						
84185	84240		50	-	1	A	MONITORING POINTS @ 50.000 CENTRES
84240	84300	84270	50	-	1	B	1 SETTLEMENT PLATE AT CH 84280
84240	84300	84270	50	-	1	B	1 SETTLEMENT PLATE AT CH 84280
84300	84342.452		50	-	1	A	1 MONITORING POINT AT CH 84310
84300	84342.452		50	-	1	A	1 MONITORING POINT AT CH 84310
84342.452	84366.452		50	-	1	C	1 MONITORING POINT AT CH 84340
84342.452	84366.452		50	-	1	C	1 MONITORING POINT AT CH 84340
84366.452	84510.062	LAGOON CREEK BRIDGE					
84366.452	84510.062	LAGOON CREEK BRIDGE					
84510.062	84534.062		100	-	2	C	1 SETTLEMENT PLATE AT CH 84530
84510.062	84534.062		100	-	2	C	1 SETTLEMENT PLATE AT CH 84530
84543.062	84605	84575	100	-	6	B	SETTLEMENT PLATES @ 25.000 CENTRES
84543.062	84605	84575	100	-	6	B	SETTLEMENT PLATES @ 25.000 CENTRES
84605	84675		100	-	6	B	SETTLEMENT PLATES @ 25.000 CENTRES
84605	84675		100	-	6	B	SETTLEMENT PLATES @ 25.000 CENTRES
84675	84735	84705	100	-	6	B	SETTLEMENT PLATES @ 25.000 CENTRES
84675	84735	84705	100	-	6	B	SETTLEMENT PLATES @ 25.000 CENTRES
84735	84805		100	-	6	B	SETTLEMENT PLATES @ 50.000 CENTRES
84735	84805		100	-	6	B	SETTLEMENT PLATES @ 50.000 CENTRES
84805	84865	84835	100	-	2	B	1 SETTLEMENT PLATE AT CH 84830
84805	84865	84835	100	-	2	B	1 SETTLEMENT PLATE AT CH 84830
84865	84970		200	1	6	F	SETTLEMENT PLATES @ 50.000 CENTRES
84865	84970		200	1	6	F	SETTLEMENT PLATES @ 50.000 CENTRES
84970	85044.912	85000	200	1	6	F	1 SETTLEMENT PLATE AT CH 85000
84970	85044.912	85000	200	1	6	F	1 SETTLEMENT PLATE AT CH 85000

CONTROL LINE CHAINAGE	FINISH	PREDICTED SETTLEMENT (mm%%P50%)	HEIGHT OF SURCHARGE (m)	SETTLEMENT PERIOD (MONTHS)	TYPE SECTION	MONITORING EQUIPMENT
START						
85044.912	85072.37	40	-	<1	C	1 MONITORING POINT AT CH 85050
85044.912	85072.37	40	-	<1	C	1 MONITORING POINT AT CH 85050
85072.37	85137.37	MURRAY RIVER BRIDGE				
85072.37	85137.37	MURRAY RIVER BRIDGE				
85137.37	85164.601	40	-	<1	C	1 MONITORING POINT AT CH 85165
85137.37	85164.601	40	-	<1	C	1 MONITORING POINT AT CH 85165
85164.601	85200	40	-	<1	A	1 MONITORING POINT AT CH 85190
85164.601	85200	40	-	<1	A	1 MONITORING POINT AT CH 85190
85200	85245	85225	<40	-	A	1 SETTLEMENT PLATE AT CH 85225
85200	85245	85225	<40	-	A	1 SETTLEMENT PLATE AT CH 85225
85245	85305	50	-	<1	A	MONITORING POINTS @ 50.000 CENTRES
85245	85305	50	-	<1	A	MONITORING POINTS @ 50.000 CENTRES
85305	85365	85335	50	-	1	1 SETTLEMENT PLATE AT CH 85330
85305	85365	85335	50	-	1	1 SETTLEMENT PLATE AT CH 85330
85365	85485	50	-	1	A	MONITORING POINTS @ 50.000 CENTRES
85365	85485	50	-	1	A	MONITORING POINTS @ 50.000 CENTRES
85485	85555	85521	100	-	B	1 SETTLEMENT PLATE AT CH 85520
85485	85555	85521	100	-	B	1 SETTLEMENT PLATE AT CH 85520
85555	85610		50	-	<1	1 MONITORING POINTS AT CH 85590
85555	85610		50	-	<1	1 MONITORING POINTS AT CH 85590
85610	85675	85643	<40	-	A	1 SETTLEMENT PLATE AT CH 85640
85610	85675	85643	<40	-	A	1 SETTLEMENT PLATE AT CH 85640
85675	85915		50	-	<1	MONITORING POINT @ 50.000 CENTRES
85675	85915		50	-	<1	MONITORING POINT @ 50.000 CENTRES
85915	85975	85945	<40	-	A	1 MONITORING POINT AT CH 85940
85915	85975	85945	<40	-	A	1 MONITORING POINT AT CH 85940
85975	86150		40	-	<1	MONITORING POINTS @ 50.000 CENTRES
85975	86150		40	-	<1	MONITORING POINTS @ 50.000

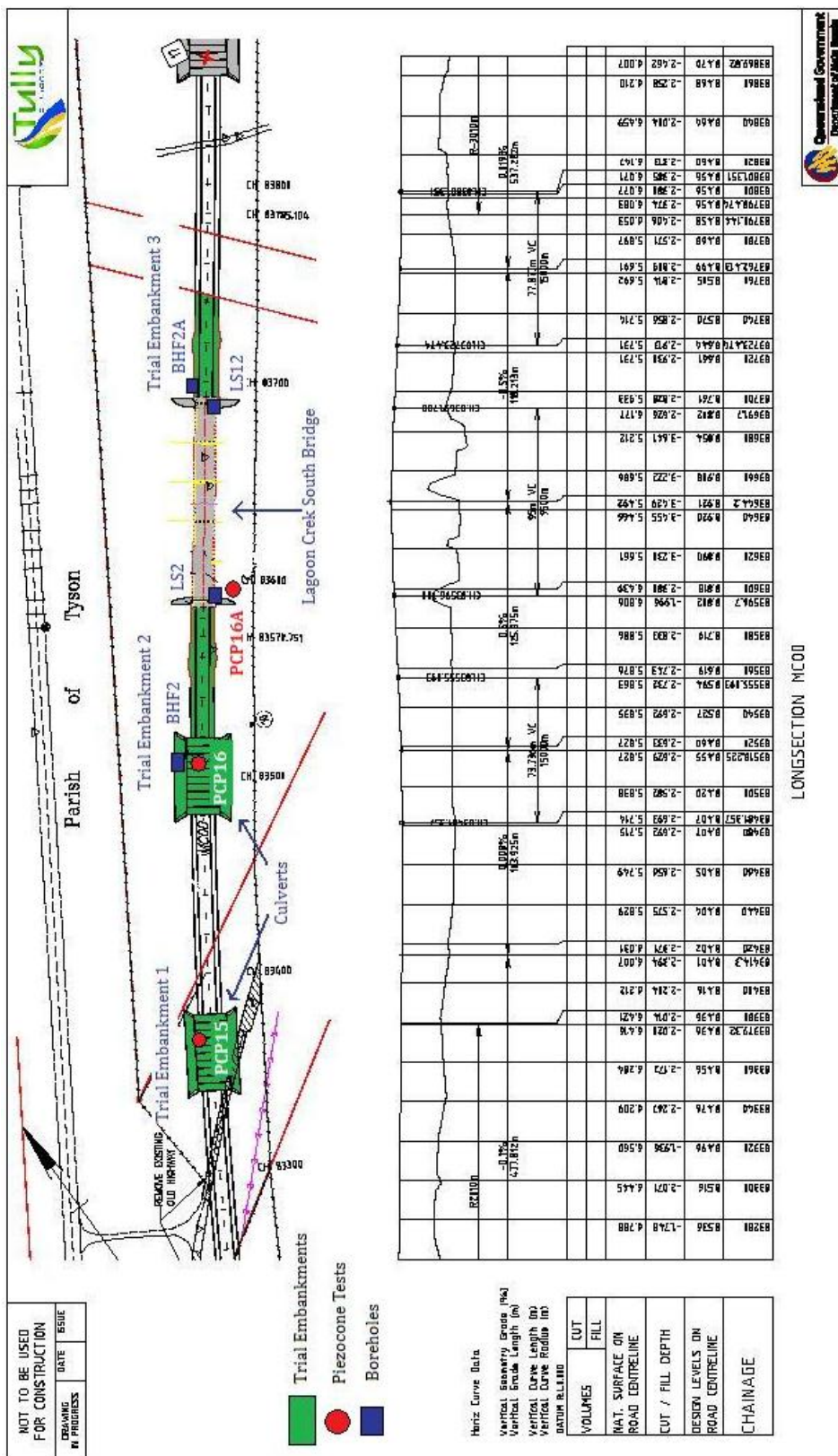
CONTROL LINE CHAINAGE			PREDICTED SETTLEMENT (mm%%P50%)	HEIGHT OF SURCHARGE (m)	SETTLEMENT PERIOD (MONTHS)	TYPE SECTION	MONITORING EQUIPMENT
START	FINISH						
							CENTRES
88710	88840		100	-	3	B	SETTLEMENT PLATES @ 50.000 CENTRES
88840	88900	88870	100	-	3	D	1 SETTLEMENT PLATE AT CH 88870.000
88900	89010		50	-	3	B	MONITORING POINTS @ 50.000 CENTRES
89010	89070	89040	100	-	3	D	1 SETTLEMENT PLATE AT CH 89040.000
89070	89100		100	-	3	B	1 SETTLEMENT PLATE AT CH 89085.000
89100	89145		150	-	2	B	SETTLEMENT PLATES AT 25.000 CENTRES
89145	89190	89165	150	-	2	B	1 SETTLEMENT PLATE AT CH 89170.000
89190	89221.28		150	-	2	D	1 SETTLEMENT PLATE AT CH 89210.000
89221.28	89307.89	TULLY OVERFLOW BRIDGE					
89283.89	89307.89	WICK AREA	250	-	<6	J	SETTLEMENT PLATES @ 25.000 CENTRES
89307.89	89360	WICK AREA	250	-	<6	H	SETTLEMENT PLATES @ 25.000 CENTRES
89360	89510	WICK AREA	100-200	-	<6	H	SETTLEMENT PLATES @ 25.000 CENTRES
89510	89545		100-200	-	<6	H	SETTLEMENT PLATES @ 25.000 CENTRES
89545	89578.69	89560	<40	-	<1	B	1 MONITORING POINT AT CH 89560.000
89578.69	89602.69		40	-	<1	C	1 MONITORING POINT AT CH 89590.000
89602.69	89781.991	TULLY RIVER BRIDGE					
89781.991	89805.991		40	-	<1	C	1 MONITORING POINT AT CH 89790.000
89805.991	89820		40	-	<1	A	1 MONITORING POINT AT CH 89815.000
89820	89860	89840	<40	-	-	A	MONITORING POINT AT CH 89830.000
89860	89870		50	-	1	A	1 MONITORING POINT AT CH 89865.000
							1 SETTLEMENT PLATE AT CH 89880.000
89870	89905	89885.565	50	-	1	D	1 MONITORING POINT AT CH 89920.000
89905	89930		50	-	1	D	1 SETTLEMENT POINT AT CH
89930	89970	89950	200	-	5	D	

CONTROL LINE CHAINAGE			PREDICTED SETTLEMENT (mm%%P50%)	HEIGHT OF SURCHARGE (m)	SETTLEMENT PERIOD (MONTHS)	TYPE SECTION	MONITORING EQUIPMENT
START	FINISH						
							89950.000
89970	90030		200	-	5	D	1 SETTLEMENT POINT AT CH 90000.000
90030	90070		100	-	3	B	1 SETTLEMENT POINT AT CH 90050.000
90070	90120	90095	50	-	3	B	1 SETTLEMENT POINT AT CH 90090.000
90120	90250		40	-	<1	B	MONITORING POINT @ 50.000 CENTRES
90250	90300		40	-	<1	A	1 MONITORING POINT AT CH 90280
90250	90300		40	-	<1	A	1 MONITORING POINT AT CH 90280
90300	90345	90323	100	-	1	B	1 SETTLEMENT PLATE AT CH 90320
90300	90345	90323	100	-	1	B	1 SETTLEMENT PLATE AT CH 90320
90345	90670		50-100	-	1-Feb	A	MONITORING POINT @ 50.000 CENTRES
90345	90670		50-100	-	1-Feb	A	MONITORING POINT @ 50.000 CENTRES
90670	90695	90683	<40	-	-	A	1 SETTLEMENT PLATE AT CH 90680
90670	90695	90683	<40	-	-	A	1 SETTLEMENT PLATE AT CH 90680
90695	90795		50	-	1	A	MONITORING POINT @ 50.000 CENTRES
90695	90795		50	-	1	A	MONITORING POINT @ 50.000 CENTRES
90795	90840	90820	50	-	1	B	1 SETTLEMENT PLATE AT CH 90820
90795	90840	90820	50	-	1	B	1 SETTLEMENT PLATE AT CH 90820
90840	91045		50-100	-	1-Feb	A	MONITORING POINTS @ 50.000 CENTRES
90840	91045		50-100	-	1-Feb	A	MONITORING POINTS @ 50.000 CENTRES
91045	91075	91060	100	-	2	B	1 SETTLEMENT PLATE AT CH 91060
91045	91075	91060	100	-	2	B	1 SETTLEMENT PLATE AT CH 91060
91075	91085		100	-	2	B	1 SETTLEMENT PLATE AT CH 91080
91075	91085		100	-	2	B	1 SETTLEMENT PLATE AT CH 91080
91085	91120	91103	100	-	2	B	1 SETTLEMENT PLATE AT CH 91100
91085	91120	91103	100	-	2	B	1 SETTLEMENT PLATE AT CH 91100
91120	91380		50	-	1	A	MONITORING POINTS @ 50.000

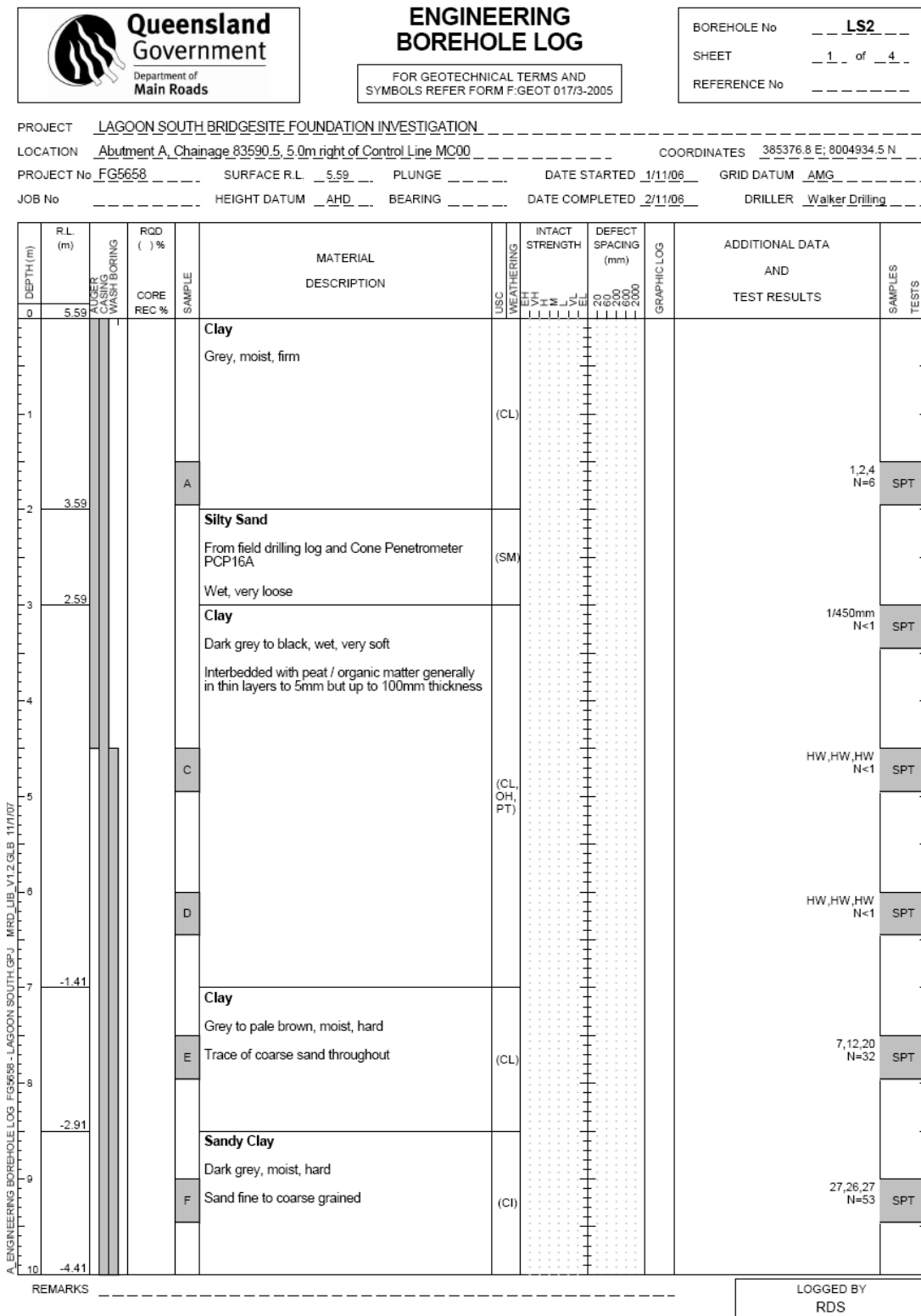
CONTROL LINE CHAINAGE			PREDICTED SETTLEMENT (mm%P50%)	HEIGHT OF SURCHARGE (m)	SETTLEMENT PERIOD (MONTHS)	TYPE SECTION	MONITORING EQUIPMENT
START	FINISH						
91120	91380		50	-	1	A	CENTRES MONITORING POINTS @ 50.000 CENTRES
91380	91390		50	-	1	A	
91380	91390		50	-	1	A	
91390	91410	91400	<40	-	-	A	MONITORING POINT AT CH 91400
91390	91410	91400	<40	-	-	A	MONITORING POINT AT CH 91400
91410	91420		40	-	<1	A	
91410	91420		40	-	<1	A	
91420	92095		40	-	<1	A	
91420	92095		40	-	<1	A	
92095	92130	92114	50	-	1	E	
92095	92130	92114	50	-	1	E	
92130	92200		50	-	1	E	MONITORING POINT @ 50.000 CENTRES
92200	92429		100	-	1	E	SETTLEMENT PLATES @ 50.000 CENTRES
92429	92481	92454.222	300	-	2	E	SETTLEMENT PLATES @ 50.000 CENTRES
92481	92620		50	-	1	E	MONITORING POINT @ 50.000 CENTRES
92620	92700		100	-	1	E	SETTLEMENT PLATES @ 25.000 CENTRES
92700	92730		100	-	4	E	1 SETTLEMENT PLATE AT CH 92715.000
92730	92800	92765	100	-	1	G	SETTLEMENT PLATES AT 25.000 CENTRES
92800	93040		50	-	1	A	MONITORING POINT @ 50.000 CENTRES
93040	93070	93055	N/A	-	N/A	TBA	
93070	93215		N/A	-	N/A	TBA	
93215	93240	93227.91	N/A	-	N/A	TBA	
93240	93280		N/A	-	N/A	TBA	

A-2: Geotechnical Site Investigation Data

A-2.1: Map Showing the Location of the Boreholes and Piezocone Tests



A-2.2: Borehole Logs



 Queensland Government Department of Main Roads				ENGINEERING BOREHOLE LOG <small>FOR GEOTECHNICAL TERMS AND SYMBOLS REFER FORM F:GEOT 017/3-2005</small>						BOREHOLE No <u>LS2</u> SHEET <u>2</u> of <u>4</u> REFERENCE No _____			
PROJECT		<u>LAGOON SOUTH BRIDGESITE FOUNDATION INVESTIGATION</u>		LOCATION		<u>Abutment A, Chainage 83590.5, 5.0m right of Control Line MC00</u>		COORDINATES		<u>385376.8 E, 8004934.5 N</u>			
PROJECT No		<u>FG5658</u>		SURFACE R.L.		<u>5.59</u>		PLUNGE		DATE STARTED <u>1/11/06</u>		GRID DATUM <u>AMG</u>	
JOB No				HEIGHT DATUM		<u>AHD</u>		BEARING		DATE COMPLETED <u>2/11/06</u>		DRILLER <u>Walker Drilling</u>	
DEPTH (m)	R.L. (m)	ALGER CASING WASH BORING	RQD () %	CORE REC %	SAMPLE	MATERIAL DESCRIPTION	WEATHERING USC	INTACT STRENGTH	DEFECT SPACING (mm)	GRAPHIC LOG	ADDITIONAL DATA AND TEST RESULTS		SAMPLES TESTS
10	-4.41				G	Clayey Sand Grey, wet, medium dense Sand fine to coarse grained	(SC)		200 600 200 600 200		7,12,14 N=26 SPT		
11	-5.91				H	Clay Grey to pale brown, moist, very stiff to hard Coarse sand band 12.0m - 12.1m	(CL)				11,10,15 N=25 SPT		
12					I						7,11,20 N=31 SPT		
13					J						8,13,21 N=34 SPT		
14					K	Clayey Sand Grey to pale brown, moist, medium dense to dense Sand fine to coarse grained Trace of gravel to 7mm throughout	(SC)				16,20,19 N=39 SPT		
15					L						14,9,10 N=19 SPT		
16	-10.41										4,4,6 N=10 SPT		
17													
18													
19	-13.41												
20													
REMARKS _____												LOGGED BY RDS	

 Queensland Government Department of Main Roads				ENGINEERING BOREHOLE LOG <small>FOR GEOTECHNICAL TERMS AND SYMBOLS REFER FORM F:GEOT 017/3-2005</small>				BOREHOLE No <u>LS2</u> SHEET <u>3</u> of <u>4</u> REFERENCE No _____				
PROJECT <u>LAGOON SOUTH BRIDGESITE FOUNDATION INVESTIGATION</u> LOCATION <u>Abutment A, Chainage 83590.5, 5.0m right of Control Line MC00</u> COORDINATES <u>385376.8 E; 8004934.5 N</u> PROJECT No <u>FG5658</u> SURFACE R.L. <u>5.59</u> PLUNGE _____ DATE STARTED <u>1/11/06</u> GRID DATUM <u>AMG</u> JOB No _____ HEIGHT DATUM <u>AHD</u> BEARING _____ DATE COMPLETED <u>2/11/06</u> DRILLER <u>Walker Drilling</u>												
DEPTH(m)	R.L. (m)	WELL CASING WASH BORING	RQD () %	CORE REC %	SAMPLE	MATERIAL DESCRIPTION	USC WEATHERING EFT 1 2 3 4 5 6 7 8 9 10 11 12 13 14 15 16 17 18 19 20 21 22 23 24 25 26 27 28 29 30	INTACT STRENGTH	DEFECT SPACING (mm) 200 400 600 800 1000 1200 1400 1600 1800 2000	GRAPHIC LOG	ADDITIONAL DATA AND TEST RESULTS	SAMPLES TESTS
	-14.41					Sand (cont'd) Trace of clay in parts						
	20				N							5,6,12 N=18 SPT
	21				O		(SW)					6,10,11 N=21 SPT
	22											3,6,9 N=15 SPT
	23											6,11,14 N=25 SPT
	24											6,16,21 N=37 SPT
	25				Q	GRANITE Coarse-grained, acid igneous rock Resembles a pale brown to orange brown, moist, medium dense to very dense with depth, clayey sand and gravel						7,18,24 N=42 SPT
	26				R	Sand medium to coarse grained, gravel to 5mm Rock texture visible	XW					
	27				S							
REMARKS _____ _____										LOGGED BY <u>RDS</u>		

 Queensland Government Department of Main Roads				ENGINEERING BOREHOLE LOG <small>FOR GEOTECHNICAL TERMS AND SYMBOLS REFER FORM F:GEOT 017/3-2005</small>						BOREHOLE No <u>LS2</u> SHEET <u>4</u> of <u>4</u> REFERENCE No <u>-----</u>	
PROJECT <u>LAGOON SOUTH BRIDGESITE FOUNDATION INVESTIGATION</u> LOCATION <u>Abutment A, Chainage 83590.5, 5.0m right of Control Line MC00</u> COORDINATES <u>385376.8 E; 8004934.5 N</u> PROJECT No <u>FG5658</u> SURFACE R.L. <u>5.59</u> PLUNGE _____ DATE STARTED <u>1/11/06</u> GRID DATUM <u>AMG</u> JOB No _____ HEIGHT DATUM <u>AHD</u> BEARING _____ DATE COMPLETED <u>2/11/06</u> DRILLER <u>Walker Drilling</u>											
DEPTH(m)	R.L. (m)	CASING WASH BORING	RQD () %	SAMPLE	MATERIAL DESCRIPTION	USC WEATHERING	INTACT STRENGTH	DEFECT SPACING (mm)	GRAPHIC LOG	ADDITIONAL DATA AND TEST RESULTS	SAMPLES TESTS
30	-24.41			T	GRANITE (cont'd)	XW				7,13,22 N=35 SPT	
31				U						7,16,23 N=39 SPT	
32				V						9,20,26 N=46 SPT	
33				W						11,21,31 N=52 SPT	
34				X						14,30/150mmHB N>50 SPT	
35										30/40mmHB N>50 SPT	
36										Drilling refusal at 38.2m	
37											
38	-32.61				Borehole terminated at 38.2m						
39											
40											
REMARKS _____										LOGGED BY RDS	

 Queensland Government Department of Main Roads				ENGINEERING BOREHOLE LOG <small>FOR GEOTECHNICAL TERMS AND SYMBOLS REFER FORM F:GEOT 017/3-2005</small>						BOREHOLE No <u>LS12</u> SHEET <u>1</u> of <u>4</u> REFERENCE No <u> </u>			
PROJECT		LAGOON SOUTH BRIDGESITE FOUNDATION INVESTIGATION											
LOCATION		Abutment B, Chainage 83690.5, 5.0m right of Control Line MC00										COORDINATES 385436.6 E; 8005014.7 N	
PROJECT No		FG5658 SURFACE R.L. <u>5.51</u> PLUNGE <u> </u> DATE STARTED <u>15/11/06</u> GRID DATUM <u>AMG</u>											
JOB No		HEIGHT DATUM <u>AHD</u> BEARING <u> </u> DATE COMPLETED <u>16/11/06</u> DRILLER <u>Walker Drilling</u>											
DEPTH (m)	R.L. (m)	RQD () %	SAMPLE REC %	MATERIAL DESCRIPTION	WEATHERING	INTACT STRENGTH	DEFECT SPACING (mm)	GRAPHIC LOGS	ADDITIONAL DATA AND TEST RESULTS			SAMPLES TESTS	
0	5.51				USC	EH VH H M L	200 600 2000						
1					(SC)								
2													
3	3.01			A								1,0,1 N=1 SPT	
4													
5				B								HW,HW,HW N=1 SPT	
6				C								HW,HW,HW N=1 SPT	
7	-1.49			D								RW,RW,RW N=1 SPT	
8				E								6,13,22 N=35 SPT	
9	-2.99			F								4,5,9 N=14 SPT	
10	-4.49												
REMARKS _____												LOGGED BY RDS	
Clayey Sand													
Grey, wet, very loose													
Sand fine to coarse grained													
Clay													
Dark grey to black, wet, very soft													
Interbedded with peat / organic matter generally in thin layers to 5mm but up to 100mm thickness													
Clay													
Brown mottled grey, moist, hard													
Clayey Sand													
Grey, moist, medium dense sand fine to coarse grained													

 Queensland Government Department of Main Roads				ENGINEERING BOREHOLE LOG <small>FOR GEOTECHNICAL TERMS AND SYMBOLS REFER FORM F:GEOT 017/3-2005</small>						BOREHOLE No <u>LS12</u> SHEET <u>2</u> of <u>4</u> REFERENCE No _____			
PROJECT		LAGOON SOUTH BRIDGESITE FOUNDATION INVESTIGATION											
LOCATION		Abutment B, Chainage 83690.5, 5.0m right of Control Line MC00										COORDINATES 385436.6 E; 8005014.7 N	
PROJECT No		FG5658 SURFACE R.L. 5.51 PLUNGE _____ DATE STARTED 15/1/06 GRID DATUM AMG											
JOB No		HEIGHT DATUM AHD BEARING _____ DATE COMPLETED 16/1/06 DRILLER Walker Drilling											
DEPTH (m)	R.L. (m)	RQD () %	CORE REC %	SAMPLE	MATERIAL DESCRIPTION		WEATHERING EHH VHH H M VLM EL	INTACT STRENGTH	DEFECT SPACING (mm) 200 600 2000	GRAPHIC LOG	ADDITIONAL DATA AND TEST RESULTS		SAMPLES TESTS
					10	-4.49					Sand	Grey, wet, medium dense	
11													
12													
13													
14													
15													
16													
17													
18													
19													
20													
REMARKS _____										LOGGED BY RDS			
10	-4.49				Sand	Grey, wet, medium dense	G	(SW)					
11													
12	-6.79				Clay	Brown mottled grey, moist, very stiff	H						
13													
14													
15													
16	-10.49				Sandy Clay	Brown mottled grey, wet, stiff sand fine to medium grained	K	(SC)					
17													
18													
19													
20							M						

 Queensland Government Department of Main Roads				ENGINEERING BOREHOLE LOG				BOREHOLE No <u>LS12</u> SHEET <u>3</u> of <u>4</u> REFERENCE No _____				
FOR GEOTECHNICAL TERMS AND SYMBOLS REFER FORM F:GEOT 017/3-2005												
PROJECT		<u>LAGOON SOUTH BRIDGESITE FOUNDATION INVESTIGATION</u>										
LOCATION		<u>Abutment B, Chainage 83690.5, 50m right of Control Line MC00</u>										
PROJECT No		<u>FG5658</u>										
JOB No		<u>Surface R.L. 5.51 PLUNGE</u>										
		<u>DATE STARTED 15/11/06 GRID DATUM AMG</u>										
		<u>HEIGHT DATUM AHD BEARING</u>										
		<u>DATE COMPLETED 16/11/06 DRILLER Walker Drilling</u>										
DEPTH (m)	R.L. (m)	RQD () %	CORE REC %	SAMPLE	MATERIAL DESCRIPTION	USC WEATHERING 	INTACT STRENGTH 	DEFECT SPACING (mm) 	GRAPHIC LOG	ADDITIONAL DATA AND TEST RESULTS		SAMPLES TESTS
20	-14.49				Sandy Clay (cont'd)	(SC)						
21	-15.49			N	Sand					7,16,16 N=32	SPT	
22					Yellow-brown and grey, wet, medium dense to dense Fine to coarse grained with trace of gravel to 5mm							
23				O						6,9,8 N=17	SPT	
24				P						8,8,7 N=15	SPT	
25	-19.94			Q	GRANITE Coarse-grained, acid igneous rock					5,9,13 N=22	SPT	
26				R	Resembles a pale brown to orange brown, moist, medium dense to very dense with depth, clayey sand and gravel Sand medium to coarse grained, gravel to 5mm Rock texture visible					4,9,15 N=24	SPT	
27				S		XW				4,6,8 N=14	SPT	
28												
29												
30												
REMARKS _____										LOGGED BY RDS		

 Queensland Government Department of Main Roads			ENGINEERING BOREHOLE LOG <small>FOR GEOTECHNICAL TERMS AND SYMBOLS REFER FORM F:GEOT 017/3-2005</small>						BOREHOLE No <u>LS12</u> SHEET <u>4</u> of <u>4</u> REFERENCE No <u>-----</u>		
PROJECT <u>LAGOON SOUTH BRIDGESITE FOUNDATION INVESTIGATION</u> LOCATION <u>Abutment B, Chainage 83690.5, 5.0m right of Control Line MC00</u> COORDINATES <u>385436.6 E; 8005014.7 N</u> PROJECT No <u>FG5658</u> SURFACE R.L. <u>5.51</u> PLUNGE <u>-----</u> DATE STARTED <u>15/11/06</u> GRID DATUM <u>AMG</u> JOB No <u>-----</u> HEIGHT DATUM <u>AHD</u> BEARING <u>-----</u> DATE COMPLETED <u>16/11/06</u> DRILLER <u>Walker Drilling</u>											
DEPTH(m)	R.L. (m)	RQD () %	CORE REC %	SAMPLE	MATERIAL DESCRIPTION	USC WEATHERING	INTACT STRENGTH	DEFECT SPACING (mm)	GRAPHIC LOG	ADDITIONAL DATA AND TEST RESULTS	SAMPLES TESTS
30	-24.49			T	GRANITE (cont'd)	XW		2000 1600 1200 800 400		4,8,13 N=21 SPT	
31				U						6,12,22 N=34 SPT	
32				V						11,20,31 N=51 SPT	
33				W						10,20,33 N=53 SPT	
34											
35											
36	-30.79			X	Borehole terminated at 36.3m					15,33/150mmHB N>50 SPT	
37											
38											
39											
40											
REMARKS -----											LOGGED BY RDS

A-2.3: Consolidation Test Results

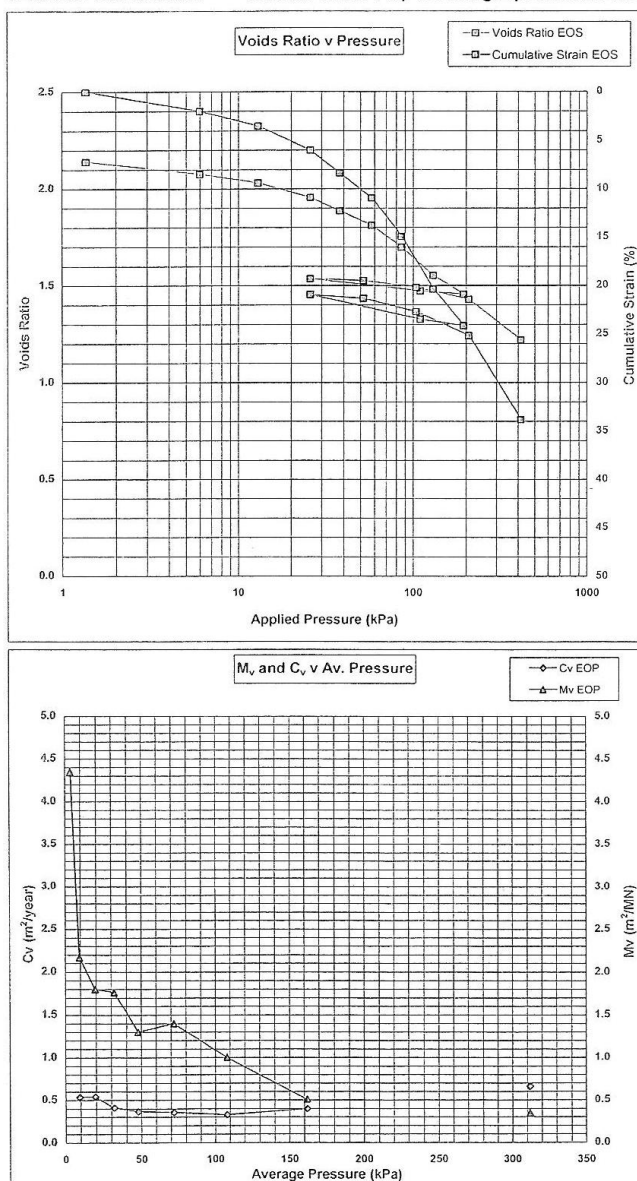
PAVEMENTS MATERIALS and GEOTECHNICAL DIVISION LABORATORY
Geotechnical Branch, 35 Butterfield Street Herston Qld 4006



REPORT ON OEDOMETER CONSOLIDATION TEST

Test Method: Q183/AS1289.6.6.1

PROJECT NAME BRUCE HIGHWAY REALIGNMENT
PROJECT NO FG5658
SOURCE BH F2
DETAILS 2.40m to 2.80m
DESCRIPTION Dark grey CLAY, traces of organic matter
SAMPLE NO GS06/857
TEST CONDITIONS Specimen inundated at commencement of test
DATE SAMPLLED 17-Nov-06
DATE TESTED 14-Dec-06
SPECIMEN PREPARATION Nominal 75mm Φ by 19mm high specimen sectioned from 100mm Φ undisturbed tube sample



Applied Pressure (kPa)	Voids Ratio		Cumulative Strain (%)	
	EOP*	EOS#	EOP*	EOS#
Void ratio at zero swell	1.4	2.14	2.14	0.00
6	2.08	2.08	2.02	2.02
13	2.03	2.03	3.53	3.53
26	1.96	1.95	5.87	6.01
38	1.89	1.88	7.99	8.38
58	1.81	1.81	10.59	10.98
86	1.70	1.70	14.50	14.95
130	1.58	1.55	18.92	20.39
194	1.47	1.45	22.18	24.18
110	1.47	1.47	21.61	23.50
26	1.53	1.53	19.11	20.93
52	1.52	1.52	19.52	21.33
104	1.49	1.49	20.84	22.71
208	1.43	1.43	23.08	25.19
416	1.25	1.22	30.29	33.84

Pressure Range (kPa)	Average Pressure (kPa)	M _v		C _v	
		EOP*	EOS#	EOP*	EOS#
1 - 6	4	4.35	4.35	0.41	0.41
6 - 13	10	2.17	2.17	0.53	0.53
13 - 26	20	1.80	1.90	0.54	0.54
26 - 38	32	1.76	1.97	0.41	0.41
38 - 58	48	1.30	1.30	0.36	0.36
58 - 86	72	1.40	1.42	0.35	0.35
86 - 130	108	1.00	1.24	0.32	0.32
130 - 194	162	0.51	0.59	0.40	0.39
194 - 110	152	0.07	0.08	4.07	4.08
110 - 26	68	0.30	0.31	1.19	1.19
26 - 52	39	0.16	0.15	2.11	2.11
52 - 104	78	0.25	0.27	1.71	1.71
104 - 208	156	0.22	0.24	1.69	1.69
208 - 416	312	0.35	0.42	0.66	0.65

* Calculated using e @ end of primary

Calculated using e @ end of stage

MOISTURE CONTENT (%)	85.0
WET DENSITY (l/m ³)	1.50
DRY DENSITY (l/m ³)	0.81
APPARENT PARTICLE DENSITY (l/m ³)	2.55
DEGREE OF SATURATION (%)	100

Checked by

Signatory

Mr P. Reynolds

Date reported 05/04/2007

Report No. FG5658/GS06/857/Q183/AS1289.6.6.1

Variations to Procedure: Cumulative strain results and Voids Ratio, M_v and C_v results derived from the determination of consolidation at the end of primary are not required by this method. These results are provided as additional information. Deformation Vs Time plots are available on request.

Remarks: C_{ac} = 0.7% for 130kPa applied pressure.

Client Details: Department of Main Roads
Townsville District



Accreditation Number: 2302
Accredited for compliance
with ISO/IEC 17025

This document is issued in
accordance with NATA's

F:GEOT 521/B

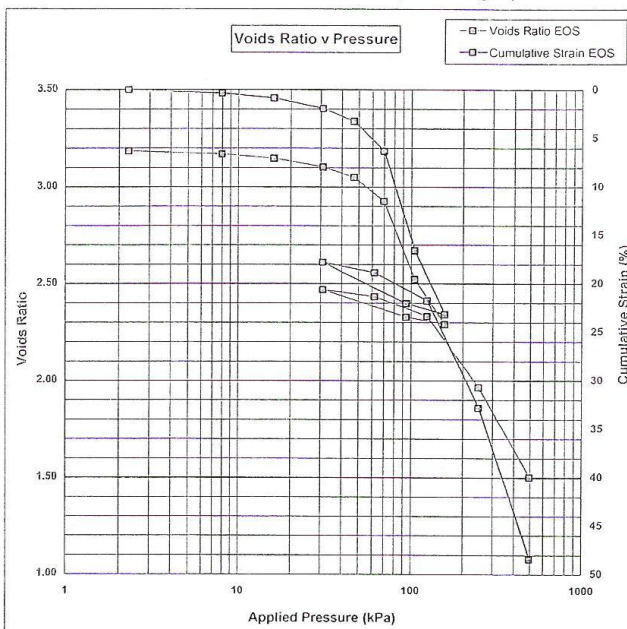
PAVEMENTS MATERIALS and GEOTECHNICAL DIVISION LABORATORY
Geotechnical Branch, 35 Butterfield Street, Herston, Qld. 4006



REPORT ON OEDOMETER CONSOLIDATION TEST

Test Method: Q183/AS1289.6.6.1

PROJECT NAME BRUCE HIGHWAY REALIGNMENT - TULLY
PROJECT NO FG5658
SOURCE BH F2
DETAILS 3.30m to 3.70m
DESCRIPTION Black ORGANIC CLAY with some dark grey clay bands
SAMPLE NO GS06/859
TEST CONDITIONS Specimen inundated at commencement of test
DATE SAMPLED 17-Nov-06
DATE TESTED 14-Dec-06
SPECIMEN PREPARATION Nominal 75mm Φ by 19mm high specimen sectioned from 100mm Φ undisturbed tube sample



Applied Pressure (kPa)	Voids Ratio		Cumulative Strain [%]	
	EOP*	EOS#	EOP*	EOS#
Void ratio at zero swell	2.3	3.18	3.18	0.00
8	3.17	3.17	0.32	0.37
16	3.15	3.15	0.81	0.90
31	3.11	3.10	1.72	1.97
47	3.06	3.05	2.80	3.27
70	2.95	2.93	5.26	6.33
105	2.67	2.52	11.75	16.60
157	2.33	2.29	17.10	23.20
94	2.32	2.33	16.12	22.06
31	2.46	2.47	12.23	17.80
62	2.44	2.43	13.17	18.88
124	2.35	2.33	15.50	21.79
248	2.04	1.96	24.21	32.83
496	1.57	1.50	37.51	48.45

Pressure Range (kPa)	Average Pressure (kPa)	Mv		Cv	
		EOP*	EOS#	EOP*	EOS#
2 - 8	5	0.55	0.65	11.04	11.03
8 - 16	12	0.62	0.66	10.39	10.38
16 - 31	24	0.61	0.71	12.00	11.98
31 - 47	39	0.67	0.81	9.05	9.03
47 - 70	59	1.07	1.33	3.25	3.23
70 - 105	88	1.85	2.93	1.13	1.09
105 - 157	131	1.03	1.27	0.75	0.74
157 - 94	126	0.15	0.18	4.52	4.53
94 - 31	63	0.62	0.68	1.73	1.73
31 - 62	47	0.30	0.35	5.14	5.14
62 - 124	93	0.37	0.47	3.60	3.58
124 - 248	186	0.70	0.89	1.17	1.14
248 - 496	372	0.54	0.63	0.70	0.68

* Calculated using e @ end of primary

Calculated using e @ end of stage

MOISTURE CONTENT (%)	157.4
WET DENSITY (t/m^3)	1.29
DRY DENSITY (t/m^3)	0.50
APPARENT PARTICLE DENSITY (t/m^3)	2.10
DEGREE OF SATURATION (%)	100

Checked by

Signatory M.P. Reynolds

Date reported 05/04/2007

Report No. FG5658/GS06/859/Q183/AS1289.6.6.1

Variations to Procedure: Cumulative strain results and Voids Ratio, Mv and Cv results derived from the determination of consolidation at the end of primary are not required by this method. These results are provided as additional information. Deformation Vs Time plots are available on request.

Remarks: $C_{ae} = 1.8\% \text{ for } 105\text{kPa applied pressure.}$

Client Details: Department of Main Roads
Townsville District

Accreditation Number: 2302
Accredited for compliance
with ISO/IEC 17025

This document is issued in accordance with NATA's accreditation requirements.

F:GEOT 521/8



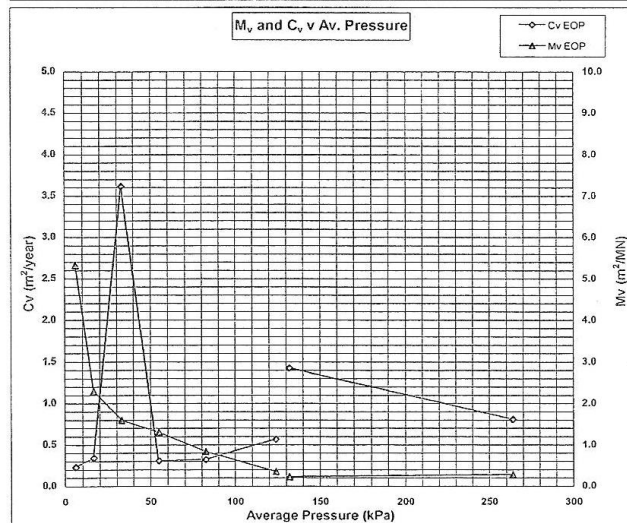
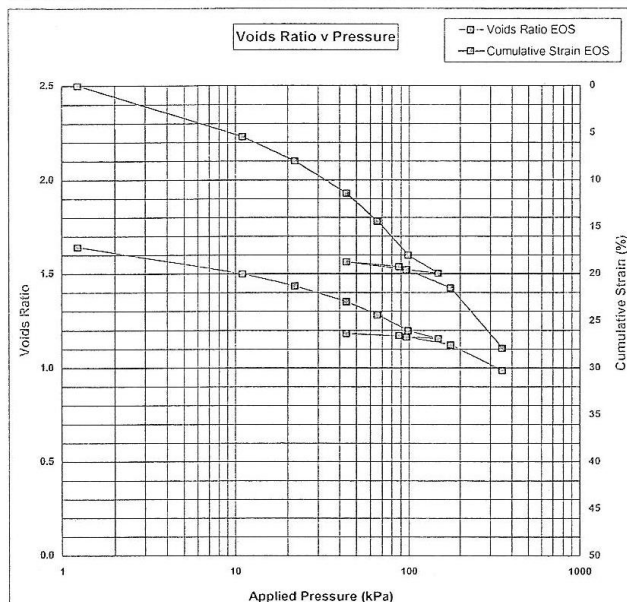
PAVEMENTS MATERIALS and GEOTECHNICAL DIVISION LABORATORY
Geotechnical Branch, 35 Butterfield Street Herston Qld 4006



REPORT ON OEDOMETER CONSOLIDATION TEST

Test Method: Q183/AS1289.6.6.1

PROJECT NAME Bruce Highway Realignment (Tully)
PROJECT NO FG5658
SOURCE BHF2A
DETAILS 5.5 - 5.9 m
DESCRIPTION Dark Grey CLAY
SAMPLE NO GS06/865
TEST CONDITIONS Specimen inundated at commencement of test
DATE SAMPLED 20-Nov-06
DATE TESTED 10-Jan-07
SPECIMEN PREPARATION Nominal 75mm Φ by 19mm high specimen sectioned from 100mm Φ undisturbed tube sample



Applied Pressure (kPa)	Voids Ratio		Cumulative Strain (%)	
	EOP*	EOS#	EOP*	EOS#
1.2	1.64	1.64	0.00	0.00
11	1.50	1.50	5.20	5.41
22	1.44	1.43	7.73	8.00
44	1.35	1.35	11.24	11.45
66	1.28	1.28	14.10	14.43
99	1.22	1.20	16.87	18.06
149	1.16	1.16	18.66	19.98
97	1.16	1.16	18.33	19.59
44	1.18	1.18	17.62	18.75
88	1.17	1.17	18.14	19.26
176	1.13	1.12	20.14	21.52
352	1.02	0.99	25.03	27.93

Pressure Range (kPa)	Average Pressure (kPa)	Mv (m²/MN)		Cv (m²/year)	
		EOP*	EOS#	EOP*	EOS#
1 - 11	6	5.32	5.54	0.23	0.23
11 - 22	17	2.30	2.35	0.34	0.34
22 - 44	33	1.60	1.57	3.61	3.61
44 - 66	55	1.30	1.36	0.31	0.31
66 - 99	83	0.84	1.10	0.32	0.32
99 - 149	124	0.36	0.38	0.57	0.57
149 - 97	123	0.06	0.08	18.43	18.45
97 - 44	71	0.13	0.16	2.07	2.07
44 - 88	66	0.12	0.12	2.81	2.81
88 - 176	132	0.23	0.26	1.42	1.42
176 - 352	264	0.28	0.36	0.81	0.79

* Calculated using e @ end of primary

Calculated using e @ end of stage

MOISTURE CONTENT (%)	67.7
WET DENSITY (t/m³)	1.60
DRY DENSITY (t/m³)	0.95
APPARENT PARTICLE DENSITY (t/m³)	2.52
DEGREE OF SATURATION (%)	100

Checked by

Signatory

Date reported

Report No. FG5658/GS06/865/Q183/AS1289.6.6.1

Variations to Procedure: Cumulative strain results and Voids Ratio, Mv and Cv results derived from the determination of consolidation at the end of primary are not required by this method. These results are provided as additional information. Deformation Vs Time plots are available on request.

Remarks: $C_{ae} = 0.5\%$ for 99kPa applied pressure.

Client Details: Department of Main Roads
Townsville District

Accreditation Number: 2302
Accredited for compliance
with ISO/IEC 17025

This document is issued in
accordance with NATA's
accreditation requirements.



F:GEOT 521/8

A-2.4: Piezocone Results

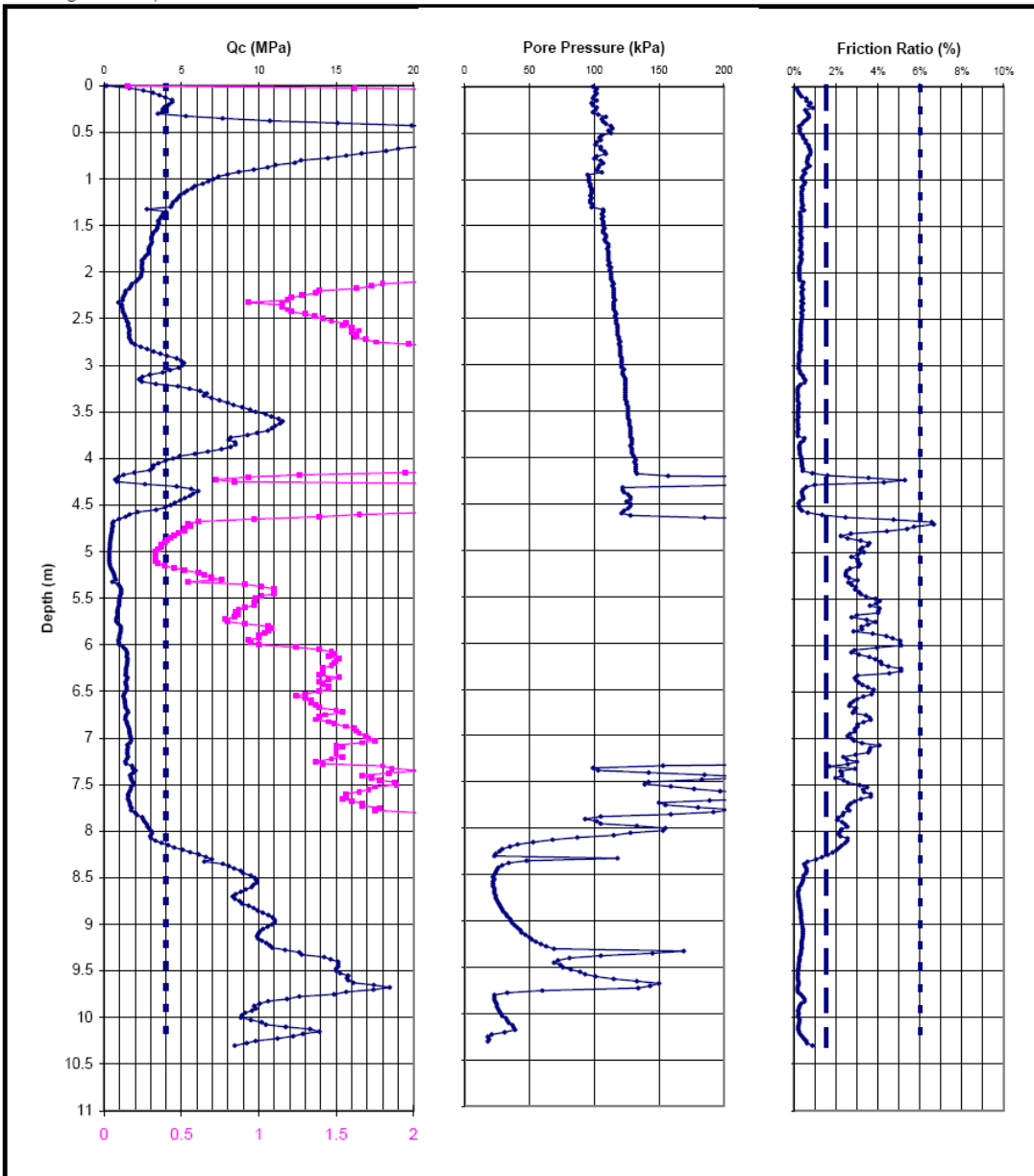
Maunsell | AECOM

PCP15.xls

28/03/2007

Project: Bruce Highway Upgrade - South of Tully
 Location: 385,237 E 8,004,757 N
 Chainage: 83,370

Surface RL: -
 Water Level: 1.5m
 Test Date: 16/10/2006



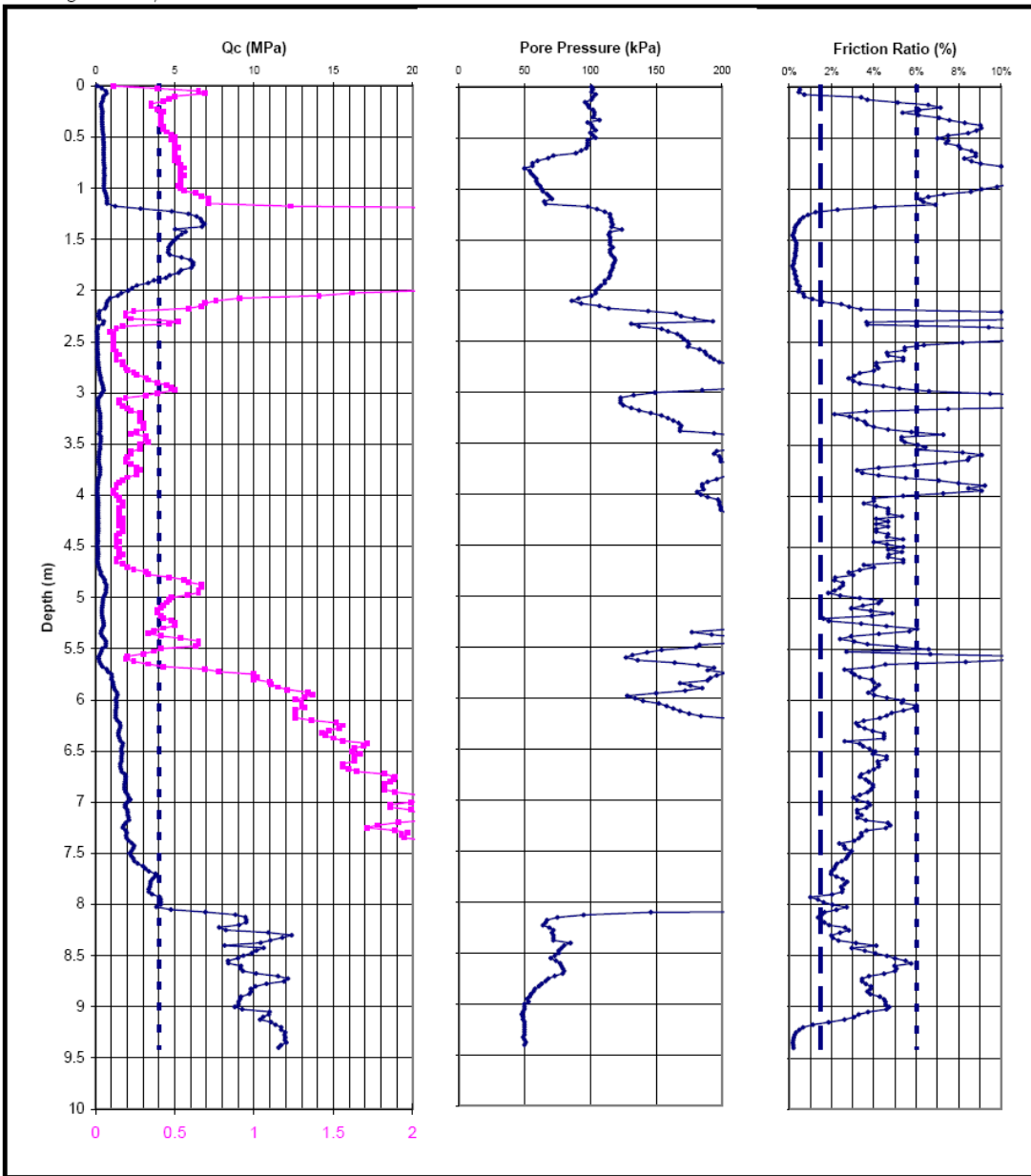
Maunsell | AECOM

PCP16.xls

28/03/2007

Project: Bruce Highway Upgrade - South of Tully
 Location: 385,322 E 8,004,869 N
 Chainage: 83,510

Surface RL: -
 Water Level: 1.5m
 Test Date: 24/10/2006



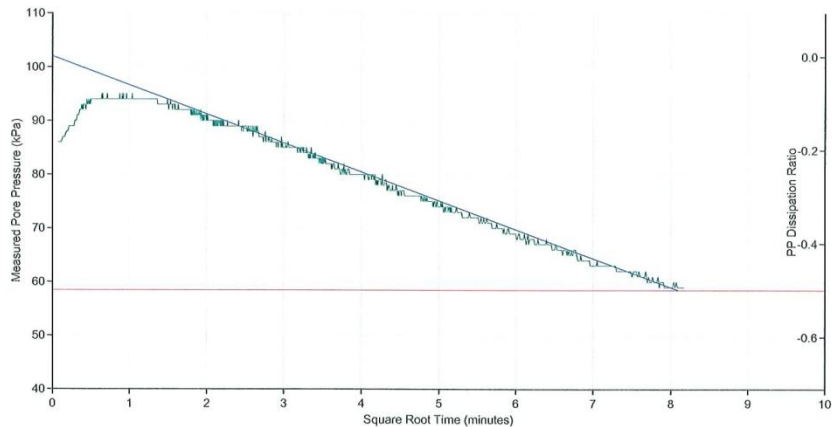
Dept of Main Roads
Pavements Materials & Geotechnical
Division Laboratory
35 Butterfield St, HERSTON QLD 4006



REPORT ON CPTu DISSIPATION TEST

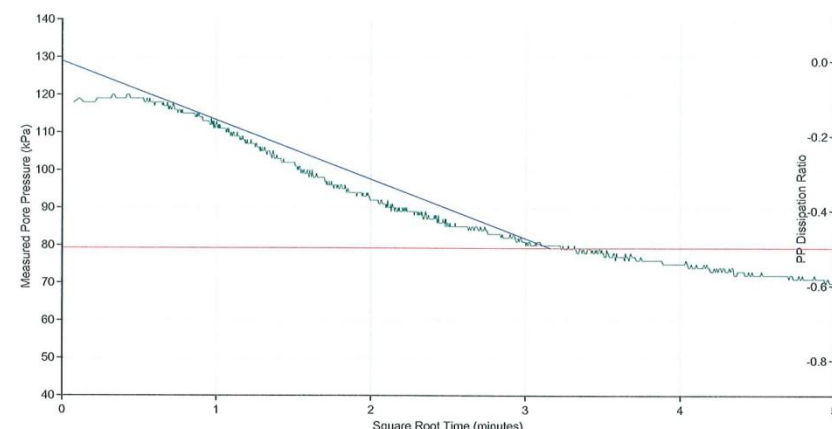
Client **MAIN ROADS**
 Project **BRUCE HIGHWAY UPGRADE - SOUTH OF TULLY**
 Job Ref.
 Location E 385322 N 8004870
 Chainage 83511
 Sounding PCP16D
 Test Date 17/10/2006
 Remarks Dissipation tests at 2.5m and 4.0m
 Water Table was not measured and is assumed.

Project No. **FG5658**
 Surface RL ~
 Water Table 1.000
 Start Depth 1.000



Client **MAIN ROADS**
 Project **BRUCE HIGHWAY UPGRADE - SOUTH OF TULLY**
 Job Ref.
 Location E 385322 N 8004870
 Chainage 83511
 Sounding PCP16D
 Test Date 17/10/2006
 Remarks Dissipation tests at 2.5m and 4.0m
 Water Table was not measured and is assumed.

Project No. **FG5658**
 Surface RL ~
 Water Table 1.000
 Start Depth 1.000



Date	14/11/2006	Cone Type	Piezocene
Checked	<i>B. Taylor</i>	Cone ID	3832
Signatory	<i>B. Taylor</i>	Factor "a"	0.580
		Factor "b"	0.014
	<th>Test Method</th> <td>Q151A-2002</td>	Test Method	Q151A-2002
	<th>Report No.</th> <td>FG5658/PCP16D/Q151A-2002</td>	Report No.	FG5658/PCP16D/Q151A-2002



Accreditation Number: 2302
 Accredited for compliance
 with ISO/IEC 17025
 This document is issued in
 accordance with NATA's
 accreditation requirements.
 full.

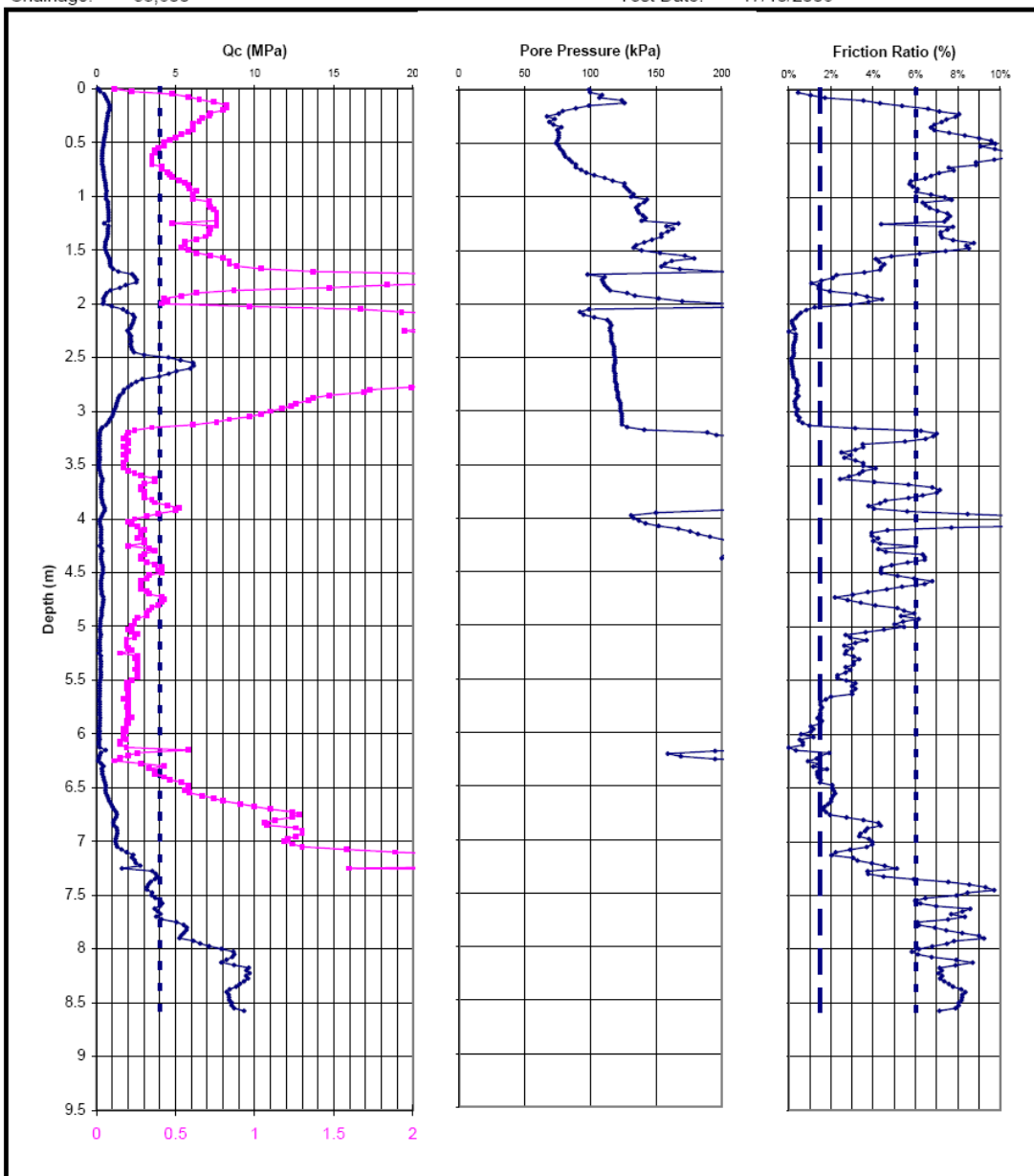
Maunsell | AECOM

PCP16A.xls

28/03/2007

Project: Bruce Highway Upgrade - South of Tully
Location: 385,386 E 8,004,932 N
Chainage: 83,600

Surface RL: -
Water Level: 1.5m
Test Date: 17/10/2006



Appendix B: Preliminary Modelling Data

B-1: Model FLAC Code

B-1.1: Original Two Layer Model

```

new
title
T5a - simple model
config gwflow extra 2
set gravity 10
set flow off
set plot jpg
set large
set fastflow on

define geometry
    no_grid_el_x=15
    no_grid_el_y=8
    imax=no_grid_el_x + 1
    jmax=no_grid_el_y + 1
    no_lay=6
    l1=-1.5          ;depth of bottom of layer 1
    l2=-5            ;depth of bottom of layer 2
    l7=-6            ;a value below lowest layer for window command later
    w=-3*l2
    w1=w+0.1
    w2=w+1          ;a value greater than width for window command
    lz1=6            ;vertical grid/zone coordinate at base of layer 1
    lz2=1            ;vertical zone coordinate at base of layer 2
    jsurf=9          ;j co-ord of GL
    jwat=9           ;j val of water table
    ;                jwat1=jwat+1
end

;-----
Define layprop
appstr=3.5e3
negappstr=-appstr
waterbulk=2e9

;layer 1
E1=19.3e6          ;Young's Mod
PR1=0.4             ;Poisson's ratio
d1=1.480e3          ;Density kg/m^3
p1=500e-15          ;permeability
G1=E1/(2*(1+PR1)) ;Shear mod
K1=E1/(3*(1-2*PR1)) ;bulk mod
n1=1-d1/2.65e3      ;Porosity
dsat1=d1+n1*1000    ;saturated density
c1=0
phi1=35
mv1=n1/waterbulk+1/(K1+0.75*G1)

```

```

thsett1=appstr*mv1*I1
cv1=p1/mv1

;layer 2
E2= 1e6 ;Young's Mod
PR2=0.4 ;Poisson's ratio
d2=6.50e2 ;Density kg/m^3
p2=30e-15 ;permeability
G2=E2/(2*(1+PR2)) ;Shear mod
K2=E2/(3*(1-2*PR2)) ;bulk mod
n2=1-d2/2.65e3 ;Porosity
dsat2=d2+n2*1000 ;saturated density
c2=0
phi2=25
mv2=n2/waterbulk+1/(K2+0.75*G2)
thsett2=appstr*mv2*(I2-I1)
cv2=p2/mv2

thsett=thsett1+thsett2

end
;-----
define inistress

isy1=10*(dsat1)*(I1)
isy2=isy1+10*(dsat2)*(I2-I1)
;isy1=10*dsat1*I2

vary1=0-isy1
vary2=isy1-isy2

isx1=0.913*isy1
isx2=0.913*isy2

varx1=0-isx1
varx2=isx1-isx2

basepp=5*10*1e3
negbasepp=-5*10*1e3

end
;-----
def ppgraph1

ytable(20,1)=y(1,9)
ytable(20,2)=y(1,8)
ytable(20,3)=y(1,7)
ytable(20,4)=y(1,6)
ytable(20,5)=y(1,5)
ytable(20,6)=y(1,4)
ytable(20,7)=y(1,3)
ytable(20,8)=y(1,2)
ytable(20,9)=y(1,1)

```

```

xtable(20,1)=gpp(1,9)
xtable(20,2)=gpp(1,8)
xtable(20,3)=gpp(1,7)
xtable(20,4)=gpp(1,6)
xtable(20,5)=gpp(1,5)
xtable(20,6)=gpp(1,4)
xtable(20,7)=gpp(1,3)
xtable(20,8)=gpp(1,2)
xtable(20,9)=gpp(1,1)

ytable(30,1)=y(1,8)
ytable(30,2)=y(1,7)
ytable(30,3)=y(1,6)
ytable(30,4)=y(1,5)
ytable(30,5)=y(1,4)
ytable(30,6)=y(1,3)
ytable(30,7)=y(1,2)
ytable(30,8)=y(1,1)

xtable(30,1)=syy(1,8)
xtable(30,2)=syy(1,7)
xtable(30,3)=syy(1,6)
xtable(30,4)=syy(1,5)
xtable(30,5)=syy(1,4)
xtable(30,6)=syy(1,3)
xtable(30,7)=syy(1,2)
xtable(30,8)=syy(1,1)
end

;-----

;----Definition of Grid----
geometry

grid no_grid_el_x, no_grid_el_y
mo mo
gen 0,l2 0,0 w,0 w,l2 rat 1.02,0.95 i=1,imax j=1,jmax

table 1 0,l1 w,l1
table 2 0,l2 w,l2
ini x=w y=l1 i=imax j=lz1

gen table 1
gen table 2

window
plot hold grid mark gnum

window

;----Layer Properties----
layprop

prop bulk=K1 shear=G1 dens=d1 reg 1,lz1
prop bulk=K2 shear=G2 dens=d2 reg 1,lz2

```

```

prop coh=c1 frict=phi1 reg 1,lz1
prop coh=c2 frict=phi2 reg 1,lz2

prop porosity=n1 perm=p1 reg 1,lz1
prop porosity=n2 perm=p2 reg 1,lz2

water bulk=waterbulk dens=1000 tens=1e10

print mv1
print thsett1
print cv1
print mv2
print thsett2
print cv2
print thsett

plot hold bulk fill grid mark fix
window

;----Initial stress state----
inistress

ini syy isy1 var 0 vary1 i=1,imax j=lz1,jsurf
ini syy isy2 var 0 vary2 i=1,imax j=lz2,lz1
;ini syy isy1 var 0 vary1 i=1,imax j=lz2,jsurf

ini sxx isx1 var 0 varx1 i=1,imax j=lz1,jsurf
ini sxx isx2 var 0 varx2 i=1,imax j=lz2,lz1
;ini sxx isx1 var 0 varx1 i=1,imax j=lz2,jsurf

ini szz isx1 var 0 varx1 i=1,imax j=lz1,jsurf
ini szz isx2 var 0 varx2 i=1,imax j=lz2,lz1
;ini szz isx1 var 0 varx1 i=1,imax j=lz2,jsurf

ini pp basepp var 0 negbasepp i=1,imax j=1,jwat
plot hold syy fill grid
plot hold pp fill grid

ppgraph1
plot hold table 20 30

;----Boundary Conditions---
fix x i=1
fix x i=imax
fix x y j=1

fix pp j=jwat
fix pp i=imax

fix sat j=jmax

;---Initilisation-----
set flow on
set step 300000
solve srat 1e-6

```

```

save ini5a.txt
plot hold pp fil grid
plot hold ydisp fil grid
plot hold state block
plot hold syy fill grid
plot hold sxx fill grid
set log on
print esxx i=1
print esyy i=1
set log off
ini ydisp=0 xdisp=0

;----Apply Stress----

apply nstress=negappstr i=1,4 j=jsurf
apply nstress=negappstr var appstr 0 i=4,5 j=jsurf
plot hold grid apply
copy mesh5a.jpg

;----Histories-----
his gwtime
his unbal
his ydisp i=1 j=jsurf
his ydisp i=1 j=lz1
his ydisp i=1 j=lz2
his syy i=1 j=no_grid_el_y
his sxx i=1 j=no_grid_el_y
his pp i=1 j=no_grid_el_y
his syy i=12 j=7
his sxx i=12 j=7
his pp i=12 j=7

;----Undrained response----
set flow off
solve sratio 1e-3
save t5aun.sav
plot hold apply grid
plot hold pp fill grid
copy udpp5a.jpg
plot hold ydisp fill grid
copy udydisp5a.jpg
plot hold state block grid
copy udstate5a.jpg

;----Drained reponse----
def agetime
agetime=gwtime+1e9
end
mo el
mo mo

prop bulk=K1 shear=G1 dens=d1 reg 1,lz1
prop bulk=K2 shear=G2 dens=d2 reg 1,lz2
prop coh=c1 frict=phi1 reg 1,lz1
prop coh=c2 frict=phi2 reg 1,lz2

```

```

set flow on
set nmech 100
solve auto on age agetime
save t5adr.sav
plot hold his 3,4,5 vs 1
copy ydisphis5a.jpg
plot hold pp fill grid
copy dpp5a.jpg
plot hold ydisp fill grid
copy dydisp5a.jpg
plot hold state block grid
copy dstate5a.jpg
print ydisp i=1 j=jsurf

```

B-1.2: Original Single Layer Model

```

new
title
T6e - simple model
config gwflow extra 2
set gravity 10
set flow off
set plot jpg
set large
set fastflow on

define geometry

    no_grid_el_x=15
    no_grid_el_y=8
    imax=no_grid_el_x + 1
    jmax=no_grid_el_y + 1
    no_lay=6
    l1=-1.5      ;depth of bottom of layer 1
    l2=-5        ;depth of bottom of layer 2
    l7=-6        ;a val below lowest layer for window command later
    w=-3*l2
    w1=w+0.1
    w2=w+1      ;a value greater than width for window command
    lz1=6        ;vertical grid/zone coordinate at base of layer 1
    lz2=1        ;vertical zone coordinate at base of layer 2
    jsurf=9      ;j co-ord of GL
    jwat=9       ;j val of water table
end

;-----
Define layprop

waterbulk=2e9

;Clay Layer

```

```

E2= 1e6           ;Young's Mod
PR2=0.4          ;Poisson's ratio
d2=6.50e2         ;Density kg/m^3
p2=30e-15        ;permeability
G2=E2/(2*(1+PR2)) ;Shear mod
K2=E2/(3*(1-2*PR2)) ;bulk mod
n2=1-d2/2.65e3    ;Porosity
dsat2=d2+n2*1000   ;saturated density
c2=0
phi2=25
mv2=n2/waterbulk+1/(K2+0.75*G2)
thsett2=3.5E3*mv2*l2

chigh=100000
phihigh=45

end
;-----
define inistress

isy1=10*dsat2*l2
vary1=0-isy1

isx1=0.666*isy1
varx1=0-isx1

basepp=5*10*1e3
negbasepp=-5*10*1e3

end
;-----
def ppgraph1

ytable(20,1)=y(1,9)
ytable(20,2)=y(1,8)
ytable(20,3)=y(1,7)
ytable(20,4)=y(1,6)
ytable(20,5)=y(1,5)
ytable(20,6)=y(1,4)
ytable(20,7)=y(1,3)
ytable(20,8)=y(1,2)
ytable(20,9)=y(1,1)

xtable(20,1)=gpp(1,9)
xtable(20,2)=gpp(1,8)
xtable(20,3)=gpp(1,7)
xtable(20,4)=gpp(1,6)
xtable(20,5)=gpp(1,5)
xtable(20,6)=gpp(1,4)
xtable(20,7)=gpp(1,3)
xtable(20,8)=gpp(1,2)
xtable(20,9)=gpp(1,1)

ytable(30,1)=y(1,8)
ytable(30,2)=y(1,7)

```

```

ytable(30,3)=y(1,6)
ytable(30,4)=y(1,5)
ytable(30,5)=y(1,4)
ytable(30,6)=y(1,3)
ytable(30,7)=y(1,2)
ytable(30,8)=y(1,1)

xtable(30,1)=syy(1,8)
xtable(30,2)=syy(1,7)
xtable(30,3)=syy(1,6)
xtable(30,4)=syy(1,5)
xtable(30,5)=syy(1,4)
xtable(30,6)=syy(1,3)
xtable(30,7)=syy(1,2)
xtable(30,8)=syy(1,1)
end
;-----

;----Definition of Grid----
geometry

grid no_grid_el_x, no_grid_el_y
mo mo
gen 0,l2 0,0 w,0 w,l2 rat 1.02,0.95 i=1,imax j=1,jmax

window
plot hold grid mark gnum
window

;----Layer Properties----
layprop

prop bulk=K2 shear=G2 dens=d2 reg 1,lz2
prop coh=c2 frict=phi2 reg 1,lz2
prop porosity=n2 perm=p2 reg 1,lz2

water bulk=waterbulk dens=1000 tens=1e10

print mv2
print thsett2
plot hold bulk fill grid mark fix
window

;----Initial stress state----
inistress

ini syy isy1 var 0 vary1 i=1,imax j=lz2,jsurf
ini sxx isx1 var 0 varx1 i=1,imax j=lz2,jsurf
ini szz isx1 var 0 varx1 i=1,imax j=lz2,jsurf
ini pp basepp var 0 negbasepp i=1,imax j=1,jwat

plot hold syy fill grid
plot hold pp fill grid
plot hold sxx fill grid

```

```

ppgraph1
plot hold table 20 30

;----Boundary Conditions----
fix x i=1
fix x i=imax
fix x y j=1

fix pp j=jwat
fix pp i=imax

fix sat j=jmax

;----Initialisation run----
set flow on
solve srat 1e-6
plot hold pp fil grid
plot hold ydisp fil grid
plot hold state block
plot hold syy fill grid
plot hold sxx fill grid
print sxx i=1
print syy i=1
ini ydisp=0 xdisp=0

;----Apply Stress-----
apply nstress=-3.5e3 i=1,4 j=9
apply nstress=-3.5e3 var 3.5e3 0 i=4,5 j=9
plot hold grid apply

;----Histories-----
his gwtime
his unbal
his ydisp i=1 j=jsurf
his ydisp i=1 j=lz1
his ydisp i=1 j=lz2
his syy i=1 j=no_grid_el_y
his sxx i=1 j=no_grid_el_y
his pp i=1 j=no_grid_el_y
his syy i=20 j=7
his sxx i=20 j=7
his pp i=20 j=7

;----Undrained response----
set flow off
solve sratio 1e-3
save t6eun.sav
plot hold apply grid
plot hold pp fill grid
copy udpp6e.jpg
plot hold ydisp fill grid
copy udydisp6e.jpg
plot hold state block grid
copy udstate6e.jpg

```

```

;----Drained reponse----
def agetime
  agetime=gwtime+1e9
end
mo el
mo mo
prop bulk=K2 shear=G2 dens=d2 reg 1,lz2
prop coh=c2 frict=phi2 reg 1,lz2

set flow on
set nmech 50
solve auto on age agetime
save t6edr.sav
plot hold his 3,4,5 vs 1
plot hold pp fill grid
copy dpp6e.jpg
plot hold ydisp fill grid
copy dydisp6e.jpg
plot hold state block grid
copy dstate6e.jpg

```

B-1.3: **Code for the Two Dimensional Consolidation Model Created by modifying the One Dimensional Consolidation Model**

```

new ;This tells FLAC that this is a new model unrelated to anything done previously,
;it is required if FLAC has been used to model another problem before this.
Title ;Sets the title which will appear on the output plots
d_2d
set plot jpg

```

```

;-----
;This section between the Def and the End is a FISH function in which all the soil and water
;properties required for the model are specified. It will not execute until it is called in
;the FLAC commands. The last three lines before the end calculate parameters not required
;for the simulation but which are required for theoretical calculations done separately

```

```

Def soil_properties
  bulk1 = 2e6          ; drained (dry) bulk modulus, Pa
  shear1 = 1e6         ; shear modulus, Pa
  perm1 = 1e-10        ; mobility coefficient, m2/(Pa.s)
  poros1 = 0.3          ; porosity
  waterbulk = 2e9       ; bulk modulus of water, Pa
  thickness = 10 ; layer thickness (drained only from top), m
  app_pressure = 1e5    ; vertical pressure applied at top, Pa

```

```

alpha1 = bulk1 + 1.333*shear1 ; Pa
Storativity = poros1/waterbulk + 1/alpha1      ; 1/Pa (this is equivalent to mv)
diffusivity = perm1/storativity      ; coefficient of consolidation cv in m2/s
End
;-----

soil_properties    ;this calls the FISH function soil_properties so that it runs
set log on
print diffusivity  ;prints value of diffusivity (cv) to the screen and records it in flac.log
print storativity   ;prints value of storativity (mv) to the screen and records it in flac.log
set log off

config gw extra 2      ;sets the model to include groundwater flow, and allows for two
                        ;extra 'vector timeseries' to be created
set flow on
set mech on
set fastflow on ;This changes the solution procedure to use fastflow logic. This is
                  ;done because the stiffness of the water is much greater than
                  ;the stiffness of the soil skeleton, and as such solution under the
                  ;standard scheme would be particularly slow, and potentially inaccurate.

set nmech 100 ;sets nmech so that when the model is solved there will be a maximum
               ;of 100 mechanical timesteps for each flow timestep

grid 20 10
generate 0,-10 0,0 20,0 20,-10
plot grid hold

;Above creates a grid 20m wide and 10 m deep consisting of 20 x 10 elements of size
;1mx1m
;Below assigns the required soil and fluid properties for the foundation

model elastic
prop dens=2000 bulk = bulk1 shear = shear1

prop perm = perm1 porosity = poros1
water bulk=waterbulk den=1000

set large      ;this causes the gridpoint coordinates to be recalculated after each
                ;time step taking account of the displacements

fix x  i=1    ;these specify that both vertical boundaries are fixed
fix x  i=21   ;in the horizontal direction and that the base of the model
fix x y j=1   ;is fixed in both vertical and horizontal directions

apply pressure=app_pressure j=11 i=1,5 ;applies the 100kPa load at the surface

```

;Note the line above is the only line of code which changes between the one
;dimensional model which works and the two dimensional model which doesn't.
;The 1D model is created by removing 'i=1,5' which is the command which restricts
;the loading to be only across one quarter of the surface elements

```
ini pp=0 j=11 ;these two lines fix the pore pressure at the surface to be zero
fix pp j=11
```

;

Define tot_vert_stress

```
tot_vert_stress=-syy(1,1)
porepress=pp(1,1)
eff_vert_stress=-syy(1,1)-porepress
time_days=gwtime/(60*60*24)
end
```

;

;----Histories-----

```
his gwtime ;1
his tot_vert_stress ;2
his porepress ;3
his eff_vert_stress ;4
his ydis i=1 j=11 ;5
```

```
his gpp i=1 j=1 ;6
his gpp i=1 j=6 ;7
his gpp i=1 j=11 ;8
```

```
his time_days ;9
his unbal ;10
```

;

```
set step 6000 ;sets the maximum number of timesteps evaluated to be 6000
solve auto on ;runs the model
```

;the commands below save the final state of the model, and prints and saves to file
;a number of graphs

save d_2d.sav

plot hold his 5 vs 9 ;To plot settlement with time

copy settim_2d.jpg

plot hold his 2 3 4 ;vs 9 ;To plot total, effective, and pore pressures with time

copy toteffpptim_2d.jpg

plot hold his 6 7 8 ;vs 9

copy pptime_2d.jpg ;plots pore pressures at varying depths with time

print ydisp i=1 j=11

Appendix C: Trial Embankment Code

File: te2a51a.txt

```
new
title
Trial embankment 2 - section with 1:2 batters te51a
config gwflow extra 2
set log on
call fish51a.txt

;----Definition of Grid----
geometry

grid no_grid_el_x, no_grid_el_y
mo mo
gen 0,l6 0,0 w,0 w,l6 rat 1.02,0.95 i=1,imax j=1,jsurf
gen 0,0 0,2.8 w,2.8 w,0 rat 1.02,0.98 i=1,imax j=jsurf,jmax
table 1 0,2.8 5.5,2.635 7.5,1.8 9.7,0.7 10.6,0.4 11.4,0.0 w,0
table 2 0,1.8 7.5,1.8
table 3 0,0.7 9.7,0.7
table 5 0,0.4 10.6,0.4
table 6 0,0 w1,0
table 7 0,11 w1,l1
table 8 0,l2 w1,l2
table 9 0,l3 w1,l3
table 10 0,l4 w1,l4
table 11 0,l5 w1,l5
table 12 0,l6 w1,l6
;ini x 0 y 2.57 i=1 j=33
;ini x=10.11 y=0.1 i=32 j=19
gen table 1
gen table 2
gen table 3
gen table 5
gen table 6
gen table 7
gen table 8
gen table 9
gen table 10
gen table 11
gen table 12
ini x=9.6 y=0.5 i=20 j=20

window
```

```

plot grid mark gnum

;----Layer Properties----
layprop

mo null j=jsurf,jmax

plot hold grid mark fix num

prop bulk=K1 shear=G1 dens=d1 reg 1,lz1
prop bulk=K2 shear=G2 dens=d2 reg 1,lz2
prop bulk=K3 shear=G3 dens=d3 reg 1,lz3
prop bulk=K4 shear=G4 dens=d4 reg 1,lz4
prop bulk=K5 shear=G5 dens=d5 reg 1,lz5
prop bulk=K6 shear=G6 dens=d6 reg 1,lz6

prop coh=c1 frict=phi1 tens=tens1 reg 1,lz1
prop coh=c2 frict=phi2 tens=tens2 reg 1,lz2
prop coh=c3 frict=phi3 tens=tens3 reg 1,lz3
prop coh=c4 frict=phi4 tens=tens4 reg 1,lz4
prop coh=c5 frict=phi5 tens=tens5 reg 1,lz5
prop coh=c6 frict=phi6 tens=tens6 reg 1,lz6

prop porosity=n1 perm=p1 reg 1,lz1
prop porosity=n2 perm=p2 reg 1,lz2
prop porosity=n3 perm=p3 reg 1,lz3
prop porosity=n4 perm=p4 reg 1,lz4
prop porosity=n5 perm=p5 reg 1,lz5
prop porosity=n6 perm=p6 reg 1,lz6

water bulk=waterbulk dens=1000 tens=1e10

set gravity 9.81
set plot jpg
set fastflow on

plot bulk fill grid mark fix
window

;----Initial stress state----
inistress

ini syy isy1 var 0 vary1 i=1,imax j=lz1,17
ini syy isy2 var 0 vary2 i=1,imax j=lz2,14
ini syy isy3 var 0 vary3 i=1,imax j=lz3,11
ini syy isy4 var 0 vary4 i=1,imax j=lz4,7
ini syy isy5 var 0 vary5 i=1,imax j=lz5,5
ini syy isy6 var 0 vary6 i=1,imax j=lz6,2

```

```

ini sxx isx1 var 0 varx1 i=1,imax j=lz1,17
ini sxx isx2 var 0 varx2 i=1,imax j=lz2,14
ini sxx isx3 var 0 varx3 i=1,imax j=lz3,11
ini sxx isx4 var 0 varx4 i=1,imax j=lz4,7
ini sxx isx5 var 0 varx5 i=1,imax j=lz5,5
ini sxx isx6 var 0 varx6 i=1,imax j=lz6,2

ini szz isx1 var 0 varx1 i=1,imax j=lz1,17
ini szz isx2 var 0 varx2 i=1,imax j=lz2,14
ini szz isx3 var 0 varx3 i=1,imax j=lz3,11
ini szz isx4 var 0 varx4 i=1,imax j=lz4,7
ini szz isx5 var 0 varx5 i=1,imax j=lz5,5
ini szz isx6 var 0 varx6 i=1,imax j=lz6,2

ini pp basepp var 0 negbasepp i=1,imax j=1,jwat
plot syy fill grid
plot pp fill grid

ppgraph1

;----Boundary Conditions----
fix x i=1
fix x i=imax
fix x y j=1

ini pp=0 j=jwat ;,jmax
fix pp j=jwat ;,jmax
fix pp i=imax

;fix sat j=jwat
;ini sat=0.25 j=jwat1,jmax

plot table 20 30

;----Initialise run-----
set flow on
set step 60000
set nmech=100 ngw=100
solve auto on
save ini51a.sav
plot pp fill fix grid
copy inippdist.jpg
plot ydisp fill grid
copy iniydisp.jpg
set large

;this is to reset the 'state' so I can see what is failing in the

```

;actual loading processes not in the initialisation as well
 mo el
 mo mo

 mo null reg 30,28
 mo null reg 1,29
 mo null reg 1,25
 mo null reg 1,20
 mo null reg 1,18

 prop bulk=K1 shear=G1 dens=d1 reg 1,lz1
 prop bulk=K2 shear=G2 dens=d2 reg 1,lz2
 prop bulk=K3 shear=G3 dens=d3 reg 1,lz3
 prop bulk=K4 shear=G4 dens=d4 reg 1,lz4
 prop bulk=K5 shear=G5 dens=d5 reg 1,lz5
 prop bulk=K6 shear=G6 dens=d6 reg 1,lz6

 prop coh=c1 frict=phi1 tens=tens1 reg 1,lz1
 prop coh=c2 frict=phi2 tens=tens2 reg 1,lz2
 prop coh=c3 frict=phi3 tens=tens3 reg 1,lz3
 prop coh=c4 frict=phi4 tens=tens4 reg 1,lz4
 prop coh=c5 frict=phi5 tens=tens5 reg 1,lz5
 prop coh=c6 frict=phi6 tens=tens6 reg 1,lz6

 window -1,51 -31,21

-----Histories-----

his gwtime	;1	time
his unbal	;2	unbalanced force
his sratio	;3	unbal force ratio
his ydisp i=1 j=jsurf	;4	sett plate
his ydisp i=1 j=lz1	;5	
his ydisp i=1 j=lz2	;6	
his ydisp i=1 j=lz3	;7	
his ydisp i=1 j=lz4	;8	
his ydisp i=1 j=lz5	;9	
his ydisp i=1 j=lz6	;10	
his pp i=1 j=10	;11	top piezo
his pp i=1 j=7	;12	lower piezo
his pp i=1 j=12	;13	curiosity
his pp i=1 j=3	;14	curiosity
his sratio	;15	
his xdisp i=27 j=18	;16	
his xdisp i=27 j=17	;17	
his xdisp i=27 j=16	;18	
his xdisp i=27 j=15	;19	inclinometer
his xdisp i=27 j=14	;20	

```

his xdisp i=27 j=13      ;21
his xdisp i=27 j=12      ;22
his xdisp i=27 j=11      ;23
his xdisp i=27 j=10      ;24
his xdisp i=27 j=9       ;25
his xdisp i=27 j=8       ;26
his xdisp i=27 j=7       ;27
his xdisp i=27 j=6       ;28
his xdisp i=27 j=5       ;29
his xdisp i=27 j=4       ;30
his xdisp i=27 j=3       ;31
his xdisp i=27 j=2       ;32
his xdisp i=27 j=1       ;33

;-----Add embankment-----
ini xdisp=0 ydisp=0
set nmech=200 step=10000
set gwt = 0

addrack
plot table 25
copy ppmechonly51a.jpg
plot table 21
copy @nameppgraph
plot state block

addlay1
plot table 22
copy @nameppgraph

addlay2
plot table 23
copy @nameppgraph

addsur
plot table 24
copy @nameppgraph

set log off

```

File: fish51a.txt

```

;-----
define geometry

no_grid_el_x=60
no_grid_el_y=30
imax=no_grid_el_x + 1

```

```

jmax=no_grid_el_y + 1
no_lay=6
l1=-1.2      ;depth of bottom of layer 1
l2=-2.2      ;depth of bottom of layer 2
l3=-4.7      ;depth of bottom of layer 3
l4=-5.7      ;depth of bottom of layer 4
l5=-8.1      ;depth of bottom of layer 5
l6=-9.3      ;depth of bottom of layer 6
l7=-10       ;a val below lowest layer for window command later
w=-5*l6
w1=w+0.1
w2=w+1       ;a value greater than width for window command
lz1=15       ;vertical grid/zone coordinate at base of layer 1
lz2=12       ;vertical zone coordinate at base of layer 2
lz3=8        ;vertical zone coordinate at base of layer 3
lz4=6        ;vertical zone coordinate at base of layer 4
lz5=3        ;vertical zone coordinate at base of layer 5
lz6=1        ;vertical zone coordinate at base of layer 6
jsurf=18     ;j co-ord of GL
jwat=18      ;j val of water table
jwat1=jwat+1
end
;-----
Define layprop

;embankment mat
Eem=30e6          ;Young's Mod
PRem=0.3           ;Poisson's ratio
dem=1.96e3         ;Density kg/m^3
pem=50e-12         ;permeability
Gem=Eem/(2*(1+PRem)) ;Shear mod
Kem=Eem/(3*(1-2*PRem)) ;bulk mod
nem=1-dem/2.65e3   ;Porosity
dsatem=dem+nem*1000 ;saturated density
c_em=5000
phi_em=28
tens_em=c_em/tan(phi_em*pi/360)

;rock mat
Ero=80e6          ;Young's Mod
PRro=0.3           ;Poisson's ratio
dro=1.85e3         ;Density kg/m^3
proc=50e-12         ;permeability
procreal=1e-6       ;permeability
Groc=Ero/(2*(1+PRro)) ;Shear mod
Kro=Ero/(3*(1-2*PRro)) ;bulk mod
nro=1-dro/2.65e3    ;Porosity
dsat_ro=dro+nro*1000 ;saturated density

```

```

c_ro=0
phi_ro=38
tens_ro=c_ro/tan(phi_ro*pi/360)

;layer 1
E1=2e6           ;Young's Mod
PR1=0.4          ;Poisson's ratio
d1=1.200e3       ;Density kg/m^3
p1=50e-14        ;permeability
G1=E1/(2*(1+PR1)) ;Shear mod
K1=E1/(3*(1-2*PR1)) ;bulk mod
n1=1-d1/2.5e3    ;Porosity
dsat1=d1+n1*1000 ;saturated density
c1=3000
phi1=25
tens1=c1/tan(phi1*pi/360)

;layer 2
E2=8.3e6         ;Young's Mod
PR2=0.4          ;Poisson's ratio
d2=1.480e3       ;Density kg/m^3
p2=500e-14       ;permeability
G2=E2/(2*(1+PR2)) ;Shear mod
K2=E2/(3*(1-2*PR2)) ;bulk mod
n2=1-d2/2.65e3   ;Porosity
dsat2=d2+n2*1000 ;saturated density
c2=0
phi2=35
tens2=c2/tan(phi2*pi/360)

;layer 3
E3= 0.8e6        ;Young's Mod
PR3=0.4          ;Poisson's ratio
d3=6.50e2         ;Density kg/m^3
p3=20e-14         ;permeability
G3=E3/(2*(1+PR3)) ;Shear mod
K3=E3/(3*(1-2*PR3)) ;bulk mod
n3=1-d3/2.65e3   ;Porosity
dsat3=d3+n3*1000 ;saturated density
c3=0
phi3=25
tens3=c3/tan(phi3*pi/360)

;layer 4
E4=2e6           ;Young's Mod
PR4=0.4          ;Poisson's ratio
d4=5e2            ;Density kg/m^3
p4=15e-14         ;permeability

```

```

G4=E4/(2*(1+PR4)) ;Shear mod
K4=E4/(3*(1-2*PR4)) ;bulk mod
n4=1-d4/2.65e3 ;Porosity
dsat4=d4+n4*1000 ;saturated density
c4=7000
phi4=25
tens4=c4/tan(phi4*pi/360)

;layer 5
E5=6e6 ;Young's Mod
PR5=0.4 ;Poisson's ratio
d5=1.38e3 ;Density kg/m^3
p5=20e-13 ;permeability
G5=E5/(2*(1+PR5)) ;Shear mod
K5=E5/(3*(1-2*PR5)) ;bulk mod
n5=1-d5/2.65e3 ;Porosity
dsat5=d5+n5*1000 ;saturated density
c5=21000
phi5=28
tens5=c5/tan(phi5*pi/360)

;layer 6
E6=15e6 ;Young's Mod
PR6=0.4 ;Poisson's ratio
d6=1.450e3 ;Density kg/m^3
p6=120e-14 ;permeability
G6=E6/(2*(1+PR6)) ;Shear mod
K6=E6/(3*(1-2*PR6)) ;bulk mod
n6=1-d6/2.65e3 ;Porosity
dsat6=d6+n6*1000 ;saturated density
c6=7000
phi6=38
tens6=c6/tan(phi6*pi/360)

;Water properties
waterbulk=2e9

end
;-----
define inistress

isy1=9.81*(dsat1)*(l1)
isy2=isy1+9.81*(dsat2)*(l2-l1)
isy3=isy2+9.81*(dsat3)*(l3-l2)
isy4=isy3+9.81*(dsat4)*(l4-l3)
isy5=isy4+9.81*(dsat5)*(l5-l4)
isy6=isy5+9.81*(dsat6)*(l6-l5)

```

```

vary1=0-isy1
vary2=isy1-isy2
vary3=isy2-isy3
vary4=isy3-isy4
vary5=isy4-isy5
vary6=isy5-isy6

isx1=0.666*isy1
isx2=0.666*isy2
isx3=0.666*isy3
isx4=0.666*isy4
isx5=0.666*isy5
isx6=0.666*isy6

varx1=0-isx1
varx2=isx1-isx2
varx3=isx2-isx3
varx4=isx3-isx4
varx5=isx4-isx5
varx6=isx5-isx6

basepp=9.3*9.81*1e3
negbasepp=-9.3*9.81*1e3

end
;-----
def ppgraph1
;this is just to produce a graph of pore pressure and
;vertical stress with depth

ytable(20,1)=y(1,18)
ytable(20,2)=y(1,17)
ytable(20,3)=y(1,16)
ytable(20,4)=y(1,15)
ytable(20,5)=y(1,14)
ytable(20,6)=y(1,13)
ytable(20,7)=y(1,12)
ytable(20,8)=y(1,11)
ytable(20,9)=y(1,10)
ytable(20,10)=y(1,9)
ytable(20,11)=y(1,8)
ytable(20,12)=y(1,7)
ytable(20,13)=y(1,6)
ytable(20,14)=y(1,5)
ytable(20,15)=y(1,4)
ytable(20,16)=y(1,3)
ytable(20,17)=y(1,2)
ytable(20,18)=y(1,1)

```

```
xtable(20,1)=pp(1,18)
xtable(20,2)=pp(1,17)
xtable(20,3)=pp(1,16)
xtable(20,4)=pp(1,15)
xtable(20,5)=pp(1,14)
xtable(20,6)=pp(1,13)
xtable(20,7)=pp(1,12)
xtable(20,8)=pp(1,11)
xtable(20,9)=pp(1,10)
xtable(20,10)=pp(1,9)
xtable(20,11)=pp(1,8)
xtable(20,12)=pp(1,7)
xtable(20,13)=pp(1,6)
xtable(20,14)=pp(1,5)
xtable(20,15)=pp(1,4)
xtable(20,16)=pp(1,3)
xtable(20,17)=pp(1,2)
xtable(20,18)=pp(1,1)
```

```
ytable(30,1)=y(1,18)
ytable(30,2)=y(1,17)
ytable(30,3)=y(1,16)
ytable(30,4)=y(1,15)
ytable(30,5)=y(1,14)
ytable(30,6)=y(1,13)
ytable(30,7)=y(1,12)
ytable(30,8)=y(1,11)
ytable(30,9)=y(1,10)
ytable(30,10)=y(1,9)
ytable(30,11)=y(1,8)
ytable(30,12)=y(1,7)
ytable(30,13)=y(1,6)
ytable(30,14)=y(1,5)
ytable(30,15)=y(1,4)
ytable(30,16)=y(1,3)
ytable(30,17)=y(1,2)
ytable(30,18)=y(1,1)
```

```
xtable(30,1)=syy(1,18)
xtable(30,2)=syy(1,17)
xtable(30,3)=syy(1,16)
xtable(30,4)=syy(1,15)
xtable(30,5)=syy(1,14)
xtable(30,6)=syy(1,13)
xtable(30,7)=syy(1,12)
xtable(30,8)=syy(1,11)
xtable(30,9)=syy(1,10)
```

```

xtable(30,10)=syy(1,9)
xtable(30,11)=syy(1,8)
xtable(30,12)=syy(1,7)
xtable(30,13)=syy(1,6)
xtable(30,14)=syy(1,5)
xtable(30,15)=syy(1,4)
xtable(30,16)=syy(1,3)
xtable(30,17)=syy(1,2)
xtable(30,18)=syy(1,1)
end

;-----

;-----  

def addrock
;this is the first layer in the construction process (which is a rock layer), this adds it gets the
; undrained response then allows it to consolidate until the next layer is due to be added.

initime=gwtime
agetime=initime + 2.592e5
command
mo mo i=1,22 j=18
mo mo i=1,21 j=19
prop bulk=kro shear=groc dens=dro i=1,22 j=18
prop co=c_ro frict=phi_ro i=1,22 j=18
prop bulk=kro shear=groc dens=dro i=1,21 j=19
prop co=c_ro frict=phi_ro i=1,21 j=19

ini pp=0 i=1,22 j=18
ini pp=0 i=1,21 j=19
ini sat=0 i=1,22 j=18
ini sat=0 i=1,21 j=19

;----Undrained-----
set flow off
solve sratio 1e-4
plot pp fill grid
copy mechpp.jpg
plot ydisp fill grid
copy mechydisp.jpg
plot state block grid
copy stateaddrackmech.jpg
plot esyy fill grid
copy mechesyy.jpg
plot esyy fill grid
copy mechsyy.jpg
set flow on

```

end_command

```
ytable(25,1)=y(1,18)
ytable(25,2)=y(1,17)
ytable(25,3)=y(1,16)
ytable(25,4)=y(1,15)
ytable(25,5)=y(1,14)
ytable(25,6)=y(1,13)
ytable(25,7)=y(1,12)
ytable(25,8)=y(1,11)
ytable(25,9)=y(1,10)
ytable(25,10)=y(1,9)
ytable(25,11)=y(1,8)
ytable(25,12)=y(1,7)
ytable(25,13)=y(1,6)
ytable(25,14)=y(1,5)
ytable(25,15)=y(1,4)
ytable(25,16)=y(1,3)
ytable(25,17)=y(1,2)
ytable(25,18)=y(1,1)
```

```
xtable(25,1)=pp(1,18)
xtable(25,2)=pp(1,17)
xtable(25,3)=pp(1,16)
xtable(25,4)=pp(1,15)
xtable(25,5)=pp(1,14)
xtable(25,6)=pp(1,13)
xtable(25,7)=pp(1,12)
xtable(25,8)=pp(1,11)
xtable(25,9)=pp(1,10)
xtable(25,10)=pp(1,9)
xtable(25,11)=pp(1,8)
xtable(25,12)=pp(1,7)
xtable(25,13)=pp(1,6)
xtable(25,14)=pp(1,5)
xtable(25,15)=pp(1,4)
xtable(25,16)=pp(1,3)
xtable(25,17)=pp(1,2)
xtable(25,18)=pp(1,1)
```

;----Drained-----

section

loop q (1,35)

command

solve age=agetime auto on

end_command

```

time1=gwtime-initime

nameydisp_gw= 'ydispro' + string(time1) + '.jpg'
namexdisp_gw= 'xdispro' + string(time1) + '.jpg'
namepp_gw= 'ppro' + string(time1) + '.jpg'
namesyy_gw= 'syryo' + string(time1) + '.jpg'
namesxx_gw= 'sxxro' + string(time1) + '.jpg'
nameppgraph= 'ppgraphro' + string(time1) + '.jpg'
namesave= 'te2a51aro_' + string(time1) +'.sav'
namedispvect_gw= 'dispvectro' + string(time1) + '.jpg'
namestate='stateaddrack' + string(time1) + '.jpg'

command
plot his 2 vs 1
copy unbalforce.jpg
plot his 4 5 6 7 8 9 vs 1
copy ydisptime_ro.jpg
plot ydisp fill grid
copy @nameydisp_gw
plot xdisp fill grid
copy @namexdisp_gw
plot pp fill grid
copy @namepp_gw
plot esyy fill grid
copy @namesyy_gw
plot sxx fill grid
copy @namesxx_gw
plot state block grid
copy @namestate

save @namesave
end_command

if gwtime >= agetime then
  exit section
endif

end_loop
end_section

ytable(21,1)=y(1,18)
ytable(21,2)=y(1,17)
ytable(21,3)=y(1,16)
ytable(21,4)=y(1,15)
ytable(21,5)=y(1,14)
ytable(21,6)=y(1,13)
ytable(21,7)=y(1,12)

```

```

ytable(21,8)=y(1,11)
ytable(21,9)=y(1,10)
ytable(21,10)=y(1,9)
ytable(21,11)=y(1,8)
ytable(21,12)=y(1,7)
ytable(21,13)=y(1,6)
ytable(21,14)=y(1,5)
ytable(21,15)=y(1,4)
ytable(21,16)=y(1,3)
ytable(21,17)=y(1,2)
ytable(21,18)=y(1,1)

xtable(21,1)=pp(1,18)
xtable(21,2)=pp(1,17)
xtable(21,3)=pp(1,16)
xtable(21,4)=pp(1,15)
xtable(21,5)=pp(1,14)
xtable(21,6)=pp(1,13)
xtable(21,7)=pp(1,12)
xtable(21,8)=pp(1,11)
xtable(21,9)=pp(1,10)
xtable(21,10)=pp(1,9)
xtable(21,11)=pp(1,8)
xtable(21,12)=pp(1,7)
xtable(21,13)=pp(1,6)
xtable(21,14)=pp(1,5)
xtable(21,15)=pp(1,4)
xtable(21,16)=pp(1,3)
xtable(21,17)=pp(1,2)
xtable(21,18)=pp(1,1)

command

plot disp bound
copy @namedispvect_gw
end_command
end
;-----
def addlay1
  command
  mo mo reg 1,20
  prop bulk=kem shear=gem dens=dem reg 1,20
  prop co=c_em frict=phi_em tens=tens_em reg 1,20

  ini pp=0 reg 1,20
  ini sat=0 reg 1,20

  set flow off

```

```

solve sratio 1e-4
set flow on
plot state block grid
copy statelay1mech.jpg
end_command

agetime=initime + 5.18e5

section
loop q (1,35)

command
solve age=agetime auto on
end_command

time1=gwtime-initime

nameydisp_gw= 'ydisp1_' + string(time1) + '.jpg'
namexdisp_gw= 'xdisp1_' + string(time1) + '.jpg'
namepp_gw= 'pp1_' + string(time1) + '.jpg'
namesyy_gw= 'syy1_' + string(time1) + '.jpg'
namesxx_gw= 'sxx1_' + string(time1) + '.jpg'
nameppgraph= 'ppgraph1_' + string(time1) + '.jpg'
namesave= 'te2a51a1_' + string(time1) + '.sav'
namedispvect_gw= 'dispvect1_' + string(time1) + '.jpg'
namestate='statelay1' + string(time1) + '.jpg'

command
plot his 2 vs 1
copy unbalforce.jpg
plot his 4 5 6 7 8 9 vs 1
copy ydisptime_11.jpg
plot ydisp fill grid
copy @nameydisp_gw
plot xdisp fill grid
copy @namexdisp_gw
plot pp fill grid
copy @namepp_gw
plot esyy fill grid
copy @namesyy_gw
plot esxx fill grid
copy @namesxx_gw
plot state block grid
copy @namestate

save @namesave
end_command

```

```

if gwtime >= agetime then
  exit section
endif
end_loop
end_section

```

```

ytable(22,1)=y(1,18)
ytable(22,2)=y(1,17)
ytable(22,3)=y(1,16)
ytable(22,4)=y(1,15)
ytable(22,5)=y(1,14)
ytable(22,6)=y(1,13)
ytable(22,7)=y(1,12)
ytable(22,8)=y(1,11)
ytable(22,9)=y(1,10)
ytable(22,10)=y(1,9)
ytable(22,11)=y(1,8)
ytable(22,12)=y(1,7)
ytable(22,13)=y(1,6)
ytable(22,14)=y(1,5)
ytable(22,15)=y(1,4)
ytable(22,16)=y(1,3)
ytable(22,17)=y(1,2)
ytable(22,18)=y(1,1)

```

```

xtable(22,1)=pp(1,18)
xtable(22,2)=pp(1,17)
xtable(22,3)=pp(1,16)
xtable(22,4)=pp(1,15)
xtable(22,5)=pp(1,14)
xtable(22,6)=pp(1,13)
xtable(22,7)=pp(1,12)
xtable(22,8)=pp(1,11)
xtable(22,9)=pp(1,10)
xtable(22,10)=pp(1,9)
xtable(22,11)=pp(1,8)
xtable(22,12)=pp(1,7)
xtable(22,13)=pp(1,6)
xtable(22,14)=pp(1,5)
xtable(22,15)=pp(1,4)
xtable(22,16)=pp(1,3)
xtable(22,17)=pp(1,2)
xtable(22,18)=pp(1,1)

```

command

```

plot disp bound
copy @namedispvect_gw

```

```

    end_command
end

;-----
def addlay2
    command
    mo mo reg 1,24
    prop bulk=kem shear=gem dens=dem reg 1,24
    prop co=c_em frict=phi_em tens=tens_em reg 1,24

    ini pp=0 reg 1,24
    ini sat=0 reg 1,24

    set flow off
    solve sratio 1e-4
    set flow on
    plot state block grid
    copy statelay2mech.jpg
end_command

agetime=initime + 5.18e6

section
loop q (1,60)

    command
    solve age=agetime auto on
end_command

time1=gwtime-initime

nameydisp_gw= 'ydisp2_' + string(time1) + '.jpg'
namexdisp_gw= 'xdisp2_' + string(time1) + '.jpg'
namepp_gw= 'pp2_' + string(time1) + '.jpg'
namesyy_gw= 'syy2_' + string(time1) + '.jpg'
namesxx_gw= 'sxx2_' + string(time1) + '.jpg'
nameppgraph= 'ppgraph2_' + string(time1) + '.jpg'
namesave= 'te2a51a2_' + string(time1) +'.sav'
namedispvect_gw= 'dispvect2_' + string(time1) + '.jpg'
namestate='statelay2' + string(time1) + '.jpg'

command
plot his 2 vs 1
copy unbalforce.jpg
plot his 4 5 6 7 8 9 vs 1
copy ydisptimel2.jpg
plot ydisp fill grid
copy @nameydisp_gw

```

```
plot xdisp fill grid
copy @namexdisp_gw
plot pp fill grid
copy @namepp_gw
plot esyy fill grid
copy @namesyy_gw
plot esxx fill grid
copy @namesxx_gw
plot state block grid
copy @namestate

save @namesave
end_command

if gwtime >= agetime then
  exit section
endif

end_loop
end_section

ytable(23,1)=y(1,18)
ytable(23,2)=y(1,17)
ytable(23,3)=y(1,16)
ytable(23,4)=y(1,15)
ytable(23,5)=y(1,14)
ytable(23,6)=y(1,13)
ytable(23,7)=y(1,12)
ytable(23,8)=y(1,11)
ytable(23,9)=y(1,10)
ytable(23,10)=y(1,9)
ytable(23,11)=y(1,8)
ytable(23,12)=y(1,7)
ytable(23,13)=y(1,6)
ytable(23,14)=y(1,5)
ytable(23,15)=y(1,4)
ytable(23,16)=y(1,3)
ytable(23,17)=y(1,2)
ytable(23,18)=y(1,1)

xtable(23,1)=pp(1,18)
xtable(23,2)=pp(1,17)
xtable(23,3)=pp(1,16)
xtable(23,4)=pp(1,15)
xtable(23,5)=pp(1,14)
xtable(23,6)=pp(1,13)
xtable(23,7)=pp(1,12)
xtable(23,8)=pp(1,11)
```

```

xtable(23,9)=pp(1,10)
xtable(23,10)=pp(1,9)
xtable(23,11)=pp(1,8)
xtable(23,12)=pp(1,7)
xtable(23,13)=pp(1,6)
xtable(23,14)=pp(1,5)
xtable(23,15)=pp(1,4)
xtable(23,16)=pp(1,3)
xtable(23,17)=pp(1,2)
xtable(23,18)=pp(1,1)

command
plot disp bound
copy @namedispvect_gw
end_command
end

;-----

def addsur
  command
  mo mo reg 1,29
  prop bulk=kem shear=gem dens=dem reg 1,29
  prop co=c_em frict=phi_em tens=tens_em reg 1,29

  ini pp=0 reg 1,29
  ini sat=0 reg 1,29

  set flow off
  solve sratio 1e-4
  set flow on
  plot state block grid
  copy statesurmech.jpg
  end_command

  agetime=initime + 1e7

  section
  loop q (1,200)

  command
  solve age=agetime auto on
  end_command

  time1=gwtime-initime

  nameydisp_gw= 'ydispsu' + string(time1) + '.jpg'
  namexdisp_gw= 'xdispsu' + string(time1) + '.jpg'

```

```

namepp_gw= 'ppsu' + string(time1) + '.jpg'
namesyy_gw= 'syysu' + string(time1) + '.jpg'
namesxx_gw= 'sxxsu' + string(time1) + '.jpg'
nameppgraph= 'ppgraphsu' + string(time1) + '.jpg'
namesave= 'te2a51asu_' + string(time1) + '.sav'
namedispvect_gw= 'dispvectsu' + string(time1) + '.jpg'
namestate='statesur' + string(time1) + '.jpg'

command
plot his 2 vs 1
copy unbalforce.jpg
plot his 4 5 6 7 8 9 vs 1
copy ydisptimesu.jpg
plot ydisp fill grid
copy @nameydisp_gw
plot xdisp fill grid
copy @namexdisp_gw
plot pp fill grid
copy @namepp_gw
plot esyy fill grid
copy @namesyy_gw
plot esxx fill grid
copy @namesxx_gw
plot state block grid
copy @namestate

save @namesave
end_command

if gwtime >= agetime then
  exit section
endif

end_loop
end_section

ytable(24,1)=y(1,18)
ytable(24,2)=y(1,17)
ytable(24,3)=y(1,16)
ytable(24,4)=y(1,15)
ytable(24,5)=y(1,14)
ytable(24,6)=y(1,13)
ytable(24,7)=y(1,12)
ytable(24,8)=y(1,11)
ytable(24,9)=y(1,10)
ytable(24,10)=y(1,9)
ytable(24,11)=y(1,8)
ytable(24,12)=y(1,7)

```

```
ytable(24,13)=y(1,6)
ytable(24,14)=y(1,5)
ytable(24,15)=y(1,4)
ytable(24,16)=y(1,3)
ytable(24,17)=y(1,2)
ytable(24,18)=y(1,1)

xtable(24,1)=pp(1,18)
xtable(24,2)=pp(1,17)
xtable(24,3)=pp(1,16)
xtable(24,4)=pp(1,15)
xtable(24,5)=pp(1,14)
xtable(24,6)=pp(1,13)
xtable(24,7)=pp(1,12)
xtable(24,8)=pp(1,11)
xtable(24,9)=pp(1,10)
xtable(24,10)=pp(1,9)
xtable(24,11)=pp(1,8)
xtable(24,12)=pp(1,7)
xtable(24,13)=pp(1,6)
xtable(24,14)=pp(1,5)
xtable(24,15)=pp(1,4)
xtable(24,16)=pp(1,3)
xtable(24,17)=pp(1,2)
xtable(24,18)=pp(1,1)

command
plot disp bound
copy @namedispvect_gw
end_command

end
```

Appendix D: Data and Code from Pavement Cracking Investigation

D-1: Code for Pavement Cracking models

D-1.1: Code for first model which determines the settlement profile

```

new
title
Parametric def_E8 -1:2 batters, Height=6m, Elastic, Single Layer Foundation
set plot jpg
set log on
;-----
define geometry

g_el_x=100
g_el_y=37
imax=g_el_x + 1
jmax=g_el_y + 1
l1=-10.0      ;depth of bottom of layer
l7=-12.0      ;a val below lowest layer for window command later
w=-5.0*l1
w0=1.0/1.27*w
w1=w+0.1
w2=w+1          ;a value greater than width for window command
lz1=1           ;vertical grid/zone coordinate at base of layer 1
jsurf=18         ;j co-ord of GL
jsurf1=jsurf-1
jwat=jsurf1
vv=85
vvv=1
vvvv=1
x_el_em=34
x_gp_em=x_el_em + 1
jbotpav=36
jbotpav4=jbotpav-1
end
;-----
Define layprop

;water prop
watbulk=2e9
watdens=1000.0

```

```

;embankment mat
Eem=20e6           ;Young's Mod
PRem=0.3            ;Poisson's ratio
dem=1.96e3          ;Density kg/m^3
; pem=50e-12         ;permeability
Gem=Eem/(2*(1+PRem)) ;Shear mod
Kem=Eem/(3*(1-2*PRem)) ;bulk mod
c_em=20e3
phi_em=32
tens_em=c_em/tan(phi_em*pi/360)

;Pavement mat
Epa=200e6           ;Young's Mod
PRpa=0.2             ;Poisson's ratio
dpa=2.17e3           ;Density kg/m^3
; ppa=50e-12          ;permeability (should be 3e-9)
Gpa=Epa/(2*(1+PRpa)) ;Shear mod
Kpa=Epa/(3*(1-2*PRpa)) ;bulk mod
c_pa=5e5
phi_pa=38
tens_pa=100000

;layer 1
E1= 8e6              ;Young's Mod
PR1=0.4               ;Poisson's ratio
d1=1.59e3             ;Density kg/m^3
; p1=30e-15            ;permeability
G1=E1/(2*(1+PR1))   ;Shear mod
K1=E1/(3*(1-2*PR1)) ;bulk mod
n1=1-d1/2.5e3          ;Porosity
dsat1=d1+n1*1000     ;saturated density
; c1=0
; phi1=25
; tens1=c1/tan(phi1*pi/360)

end
;-----
define inistress
isy1=9.81*(dsat1)*(11)
vary1=0-isy1

isx1=0.666*isy1
varx1=0-isx1
end
;-----
;Creates a table which records the horizontal displacement beneath the toe of the
;embankment

```

```

def xdispgraph
    ytable(vv,1)=y(x_gp_em,18)
    ytable(vv,2)=y(x_gp_em,17)
    ytable(vv,3)=y(x_gp_em,16)
    ytable(vv,4)=y(x_gp_em,15)
    ytable(vv,5)=y(x_gp_em,14)
    ytable(vv,6)=y(x_gp_em,13)
    ytable(vv,7)=y(x_gp_em,12)
    ytable(vv,8)=y(x_gp_em,11)
    ytable(vv,9)=y(x_gp_em,10)
    ytable(vv,10)=y(x_gp_em,9)
    ytable(vv,11)=y(x_gp_em,8)
    ytable(vv,12)=y(x_gp_em,7)
    ytable(vv,13)=y(x_gp_em,6)
    ytable(vv,14)=y(x_gp_em,5)
    ytable(vv,15)=y(x_gp_em,4)
    ytable(vv,16)=y(x_gp_em,3)
    ytable(vv,17)=y(x_gp_em,2)
    ytable(vv,18)=y(x_gp_em,1)

    xtable(vv,1)=xdisp(x_gp_em,18)
    xtable(vv,2)=xdisp(x_gp_em,17)
    xtable(vv,3)=xdisp(x_gp_em,16)
    xtable(vv,4)=xdisp(x_gp_em,15)
    xtable(vv,5)=xdisp(x_gp_em,14)
    xtable(vv,6)=xdisp(x_gp_em,13)
    xtable(vv,7)=xdisp(x_gp_em,12)
    xtable(vv,8)=xdisp(x_gp_em,11)
    xtable(vv,9)=xdisp(x_gp_em,10)
    xtable(vv,10)=xdisp(x_gp_em,9)
    xtable(vv,11)=xdisp(x_gp_em,8)
    xtable(vv,12)=xdisp(x_gp_em,7)
    xtable(vv,13)=xdisp(x_gp_em,6)
    xtable(vv,14)=xdisp(x_gp_em,5)
    xtable(vv,15)=xdisp(x_gp_em,4)
    xtable(vv,16)=xdisp(x_gp_em,3)
    xtable(vv,17)=xdisp(x_gp_em,2)
    xtable(vv,18)=xdisp(x_gp_em,1)
end
;-----
def settgraph
    vvv=vv+20
    ytable(vvv,1)=ydisp(1,jsurf)
    ytable(vvv,2)=ydisp(2,jsurf)
    ytable(vvv,3)=ydisp(3,jsurf)
    ytable(vvv,4)=ydisp(4,jsurf)
    ytable(vvv,5)=ydisp(5,jsurf)
    ytable(vvv,6)=ydisp(6,jsurf)

```

```
ytable(vvv,7)=ydisp(7,jsurf)
ytable(vvv,8)=ydisp(8,jsurf)
ytable(vvv,9)=ydisp(9,jsurf)
ytable(vvv,10)=ydisp(10,jsurf)
ytable(vvv,11)=ydisp(11,jsurf)
ytable(vvv,12)=ydisp(12,jsurf)
ytable(vvv,13)=ydisp(13,jsurf)
ytable(vvv,14)=ydisp(14,jsurf)
ytable(vvv,15)=ydisp(15,jsurf)
ytable(vvv,16)=ydisp(16,jsurf)
ytable(vvv,17)=ydisp(17,jsurf)
ytable(vvv,18)=ydisp(18,jsurf)
ytable(vvv,19)=ydisp(19,jsurf)
ytable(vvv,20)=ydisp(20,jsurf)
ytable(vvv,21)=ydisp(21,jsurf)
ytable(vvv,22)=ydisp(22,jsurf)
ytable(vvv,23)=ydisp(23,jsurf)
ytable(vvv,24)=ydisp(24,jsurf)
ytable(vvv,25)=ydisp(25,jsurf)
ytable(vvv,26)=ydisp(26,jsurf)
ytable(vvv,27)=ydisp(27,jsurf)
ytable(vvv,28)=ydisp(28,jsurf)
ytable(vvv,29)=ydisp(29,jsurf)
ytable(vvv,30)=ydisp(30,jsurf)
ytable(vvv,31)=ydisp(31,jsurf)
ytable(vvv,32)=ydisp(32,jsurf)
ytable(vvv,33)=ydisp(33,jsurf)
ytable(vvv,34)=ydisp(34,jsurf)
ytable(vvv,35)=ydisp(35,jsurf)
ytable(vvv,36)=ydisp(36,jsurf)
ytable(vvv,37)=ydisp(37,jsurf)
ytable(vvv,38)=ydisp(38,jsurf)
ytable(vvv,39)=ydisp(39,jsurf)
ytable(vvv,40)=ydisp(40,jsurf)
ytable(vvv,41)=ydisp(41,jsurf)
```

```
xtable(vvv,1)=x(1,jsurf)
xtable(vvv,2)=x(2,jsurf)
xtable(vvv,3)=x(3,jsurf)
xtable(vvv,4)=x(4,jsurf)
xtable(vvv,5)=x(5,jsurf)
xtable(vvv,6)=x(6,jsurf)
xtable(vvv,7)=x(7,jsurf)
xtable(vvv,8)=x(8,jsurf)
xtable(vvv,9)=x(9,jsurf)
xtable(vvv,10)=x(10,jsurf)
xtable(vvv,11)=x(11,jsurf)
xtable(vvv,12)=x(12,jsurf)
```

```

xtable(vvv,13)=x(13,jsurf)
xtable(vvv,14)=x(14,jsurf)
xtable(vvv,15)=x(15,jsurf)
xtable(vvv,16)=x(16,jsurf)
xtable(vvv,17)=x(17,jsurf)
xtable(vvv,18)=x(18,jsurf)
xtable(vvv,19)=x(19,jsurf)
xtable(vvv,20)=x(20,jsurf)
xtable(vvv,21)=x(21,jsurf)
xtable(vvv,22)=x(22,jsurf)
xtable(vvv,23)=x(23,jsurf)
xtable(vvv,24)=x(24,jsurf)
xtable(vvv,25)=x(25,jsurf)
xtable(vvv,26)=x(26,jsurf)
xtable(vvv,27)=x(27,jsurf)
xtable(vvv,28)=x(28,jsurf)
xtable(vvv,29)=x(29,jsurf)
xtable(vvv,30)=x(30,jsurf)
xtable(vvv,31)=x(31,jsurf)
xtable(vvv,32)=x(32,jsurf)
xtable(vvv,33)=x(33,jsurf)
xtable(vvv,34)=x(34,jsurf)
xtable(vvv,35)=x(35,jsurf)
xtable(vvv,36)=x(36,jsurf)
xtable(vvv,37)=x(37,jsurf)
xtable(vvv,38)=x(38,jsurf)
xtable(vvv,39)=x(39,jsurf)
xtable(vvv,40)=x(40,jsurf)
xtable(vvv,41)=x(41,jsurf)
end
;-----
def latbasemb
lvv=vvv+20
ytable(lvv,1)=xdisp(1,jsurf)
ytable(lvv,2)=xdisp(2,jsurf)
ytable(lvv,3)=xdisp(3,jsurf)
ytable(lvv,4)=xdisp(4,jsurf)
ytable(lvv,5)=xdisp(5,jsurf)
ytable(lvv,6)=xdisp(6,jsurf)
ytable(lvv,7)=xdisp(7,jsurf)
ytable(lvv,8)=xdisp(8,jsurf)
ytable(lvv,9)=xdisp(9,jsurf)
ytable(lvv,10)=xdisp(10,jsurf)
ytable(lvv,11)=xdisp(11,jsurf)
ytable(lvv,12)=xdisp(12,jsurf)
ytable(lvv,13)=xdisp(13,jsurf)
ytable(lvv,14)=xdisp(14,jsurf)
ytable(lvv,15)=xdisp(15,jsurf)

```

```
ytable(lvv,16)=xdisp(16,jsurf)
ytable(lvv,17)=xdisp(17,jsurf)
ytable(lvv,18)=xdisp(18,jsurf)
ytable(lvv,19)=xdisp(19,jsurf)
ytable(lvv,20)=xdisp(20,jsurf)
ytable(lvv,21)=xdisp(21,jsurf)
ytable(lvv,22)=xdisp(22,jsurf)
ytable(lvv,23)=xdisp(23,jsurf)
ytable(lvv,24)=xdisp(24,jsurf)
ytable(lvv,25)=xdisp(25,jsurf)
ytable(lvv,26)=xdisp(26,jsurf)
ytable(lvv,27)=xdisp(27,jsurf)
ytable(lvv,28)=xdisp(28,jsurf)
ytable(lvv,29)=xdisp(29,jsurf)
ytable(lvv,30)=xdisp(30,jsurf)
ytable(lvv,31)=xdisp(31,jsurf)
ytable(lvv,32)=xdisp(32,jsurf)
ytable(lvv,33)=xdisp(33,jsurf)
ytable(lvv,34)=xdisp(34,jsurf)
ytable(lvv,35)=xdisp(35,jsurf)
```

```
xtable(lvv,1)=x(1,jsurf)
xtable(lvv,2)=x(2,jsurf)
xtable(lvv,3)=x(3,jsurf)
xtable(lvv,4)=x(4,jsurf)
xtable(lvv,5)=x(5,jsurf)
xtable(lvv,6)=x(6,jsurf)
xtable(lvv,7)=x(7,jsurf)
xtable(lvv,8)=x(8,jsurf)
xtable(lvv,9)=x(9,jsurf)
xtable(lvv,10)=x(10,jsurf)
xtable(lvv,11)=x(11,jsurf)
xtable(lvv,12)=x(12,jsurf)
xtable(lvv,13)=x(13,jsurf)
xtable(lvv,14)=x(14,jsurf)
xtable(lvv,15)=x(15,jsurf)
xtable(lvv,16)=x(16,jsurf)
xtable(lvv,17)=x(17,jsurf)
xtable(lvv,18)=x(18,jsurf)
xtable(lvv,19)=x(19,jsurf)
xtable(lvv,20)=x(20,jsurf)
xtable(lvv,21)=x(21,jsurf)
xtable(lvv,22)=x(22,jsurf)
xtable(lvv,23)=x(23,jsurf)
xtable(lvv,24)=x(24,jsurf)
xtable(lvv,25)=x(25,jsurf)
xtable(lvv,26)=x(26,jsurf)
xtable(lvv,27)=x(27,jsurf)
```

```

xtable(lvv,28)=x(28,jsurf)
xtable(lvv,29)=x(29,jsurf)
xtable(lvv,30)=x(30,jsurf)
xtable(lvv,31)=x(31,jsurf)
xtable(lvv,32)=x(32,jsurf)
xtable(lvv,33)=x(33,jsurf)
xtable(lvv,34)=x(34,jsurf)
xtable(lvv,35)=x(35,jsurf)
end
;-----
def settgraphbp
bpv=lvv+20
ytable(bpv,1)=ydisp(1,jbotpav)
ytable(bpv,2)=ydisp(2,jbotpav)
ytable(bpv,3)=ydisp(3,jbotpav)
ytable(bpv,4)=ydisp(4,jbotpav)
ytable(bpv,5)=ydisp(5,jbotpav)
ytable(bpv,6)=ydisp(6,jbotpav)
ytable(bpv,7)=ydisp(7,jbotpav)
ytable(bpv,8)=ydisp(8,jbotpav)
ytable(bpv,9)=ydisp(9,jbotpav)
ytable(bpv,10)=ydisp(10,jbotpav)
ytable(bpv,11)=ydisp(11,jbotpav)
ytable(bpv,12)=ydisp(12,jbotpav)
ytable(bpv,13)=ydisp(13,jbotpav)
ytable(bpv,14)=ydisp(14,jbotpav)

xtable(bpv,1)=x(1,jbotpav)
xtable(bpv,2)=x(2,jbotpav)
xtable(bpv,3)=x(3,jbotpav)
xtable(bpv,4)=x(4,jbotpav)
xtable(bpv,5)=x(5,jbotpav)
xtable(bpv,6)=x(6,jbotpav)
xtable(bpv,7)=x(7,jbotpav)
xtable(bpv,8)=x(8,jbotpav)
xtable(bpv,9)=x(9,jbotpav)
xtable(bpv,10)=x(10,jbotpav)
xtable(bpv,11)=x(11,jbotpav)
xtable(bpv,12)=x(12,jbotpav)
xtable(bpv,13)=x(13,jbotpav)
xtable(bpv,14)=x(14,jbotpav)
end

;-----
def settgraphtp
tpv=bpv+20
ytable(tpv,1)=ydisp(1,jmax)
ytable(tpv,2)=ydisp(2,jmax)

```

```

ytable(tpv,3)=ydisp(3,jmax)
ytable(tpv,4)=ydisp(4,jmax)
ytable(tpv,5)=ydisp(5,jmax)
ytable(tpv,6)=ydisp(6,jmax)
ytable(tpv,7)=ydisp(7,jmax)
ytable(tpv,8)=ydisp(8,jmax)
ytable(tpv,9)=ydisp(9,jmax)
ytable(tpv,10)=ydisp(10,jmax)
ytable(tpv,11)=ydisp(11,jmax)
ytable(tpv,12)=ydisp(12,jmax)
ytable(tpv,13)=ydisp(13,jmax)

xtable(tpv,1)=x(1,jmax)
xtable(tpv,2)=x(2,jmax)
xtable(tpv,3)=x(3,jmax)
xtable(tpv,4)=x(4,jmax)
xtable(tpv,5)=x(5,jmax)
xtable(tpv,6)=x(6,jmax)
xtable(tpv,7)=x(7,jmax)
xtable(tpv,8)=x(8,jmax)
xtable(tpv,9)=x(9,jmax)
xtable(tpv,10)=x(10,jmax)
xtable(tpv,11)=x(11,jmax)
xtable(tpv,12)=x(12,jmax)
xtable(tpv,13)=x(13,jmax)
end

;-----

def syybp
  tps=tpv+20
  ytable(tps,1)=sxx(1,jbotpav)
  ytable(tps,2)=sxx(2,jbotpav)
  ytable(tps,3)=sxx(3,jbotpav)
  ytable(tps,4)=sxx(4,jbotpav)
  ytable(tps,5)=sxx(5,jbotpav)
  ytable(tps,6)=sxx(6,jbotpav)
  ytable(tps,7)=sxx(7,jbotpav)
  ytable(tps,8)=sxx(8,jbotpav)
  ytable(tps,9)=sxx(9,jbotpav)
  ytable(tps,10)=sxx(10,jbotpav)
  ytable(tps,11)=sxx(11,jbotpav)
  ytable(tps,12)=sxx(12,jbotpav)
  ytable(tps,13)=sxx(13,jbotpav)

  xtable(tps,1)=x(1,jbotpav)
  xtable(tps,2)=x(2,jbotpav)
  xtable(tps,3)=x(3,jbotpav)

```

```

xtable(tps,4)=x(4,jbotpav)
xtable(tps,5)=x(5,jbotpav)
xtable(tps,6)=x(6,jbotpav)
xtable(tps,7)=x(7,jbotpav)
xtable(tps,8)=x(8,jbotpav)
xtable(tps,9)=x(9,jbotpav)
xtable(tps,10)=x(10,jbotpav)
xtable(tps,11)=x(11,jbotpav)
xtable(tps,12)=x(12,jbotpav)
xtable(tps,13)=x(13,jbotpav)
end

;-----
;----Definition of Grid----
geometry

grid g_el_x, g_el_y
mo el
gen 0,11 0,0 w,0 w,11 rat 1.0,0.97 i=1,imax j=1,jsurf
gen 0,0 0,6.0 w0,6.0 w,0 rat 1.0,0.98 i=1,imax j=jsurf,jmax
table 1 (0,6) (5.5,6) (6.5,5.5) (17.5,0) (w,0)
table 2 (0,5.5) (6.5,5.5)
table 3 (0,0) (17.5,0) (w,0)
;ini x 11.0 y 0 i=x_gp_em j=jsurf
gen table 1
gen table 2
gen table 3

window
plot hold grid mark
window
;-----

FOR 4.5 m HIGH EMBANKMENT REPLACE ABOVE CODE WITH THIS
;----Definition of Grid----
geometry

grid g_el_x, g_el_y
mo el
gen 0,11 0,0 w,0 w,11 rat 1.0,0.97 i=1,imax j=1,jsurf
gen 0,0 0,4.5 w0,4.5 w,0 rat 1.0,0.98 i=1,imax j=jsurf,jmax
table 1 (0,4.5) (5.5,4.5) (6.5,4) (14.5,0) (w,0)
table 2 (0,4) (6.5,4)
table 3 (0,0) (14.5,0) (w,0)
;ini x 11.0 y 0 i=x_gp_em j=jsurf
gen table 1
gen table 2
gen table 3

```

```

window
plot hold grid mark
window
;-----
FOR 3 m HIGH EMBANKMENT REPLACE ABOVE CODE WITH THIS
;----Definition of Grid----
geometry

grid g_el_x, g_el_y
mo el
gen 0,11 0,0 w,0 w,11 rat 1.0,0.97 i=1,imax j=1,jsurf
gen 0,0 0,3 w,0,3 w,0 rat 1.0,0.98 i=1,imax j=jsurf,jmax
table 1 (0,3) (5.5,3) (6.5,2.5) (11.5,0) (w,0)
table 2 (0,2.5) (6.5,2.5)
table 3 (0,0) (11.5,0) (w,0)
;ini x 11.0 y 0 i=x_gp_em j=jsurf
gen table 1
gen table 2
gen table 3

window
plot hold grid mark
window
;-----
;----Layer Properties----
layprop

mo null ;reg g_el_x, g_el_y
mo el reg 1,1
mo el reg 1,jsurf
mo el reg 1,g_el_y

window
plot hold reg cols 3 grid iw ; mark
copy gridmeshdef_E8a.jpg
window

plot hold grid mark num
window
plot hold grid mark gnum
window

mo null reg 1,jsurf
mo null reg 1,g_el_y

plot hold grid mark fix num

prop bulk=K1 shear=G1 dens=dsat1 reg 1,lz1

```

```

;prop coh=C2 frict=phi1 tens=tens1 reg 1,lz1

water bulk=watbulk dens=watdens tens=1e10
set large
set gravity 9.81

;----Initial stress state----
inistress

ini syy isy1 var 0 vary1 i=1,imax j=lz1,jsurf
ini sxx isx1 var 0 varx1 i=1,imax j=lz1,jsurf
ini szz isx1 var 0 varx1 i=1,imax j=lz1,jsurf

plot hold syy fill grid

;----Boundary Conditions---
fix x i=1
fix x i=imax
fix x y j=1

;-----Histories-----
his unbal ;nstep=1           ;1 unbalanced force
his sratio                      ;2 unbal force ratio
his ydisp i=1 j=jsurf           ;3 sett plate
his ydisp i=1 j=8               ;4
his xdisp i=x_gp_em j=18         ;5
his xdisp i=x_gp_em j=17         ;6
his xdisp i=x_gp_em j=16         ;7
his xdisp i=x_gp_em j=15         ;8 inclinometer
his xdisp i=x_gp_em j=14         ;9
his xdisp i=x_gp_em j=13         ;10
his xdisp i=x_gp_em j=12         ;11
his xdisp i=x_gp_em j=11         ;12
his xdisp i=x_gp_em j=10         ;13
his xdisp i=x_gp_em j=9          ;14
his xdisp i=x_gp_em j=8          ;15
his xdisp i=x_gp_em j=7          ;16
his xdisp i=x_gp_em j=6          ;17
his xdisp i=x_gp_em j=5          ;18
his xdisp i=x_gp_em j=4          ;19
his xdisp i=x_gp_em j=3          ;20
his xdisp i=x_gp_em j=2          ;21
his xdisp i=x_gp_em j=1          ;22

his ydisp i=1 j=jbotpav        ;23
his ydisp i=2 j=jbotpav
his ydisp i=3 j=jbotpav

```

```

his ydisp i=4 j=jbotpav
his ydisp i=5 j=jbotpav
his ydisp i=6 j=jbotpav
his ydisp i=7 j=jbotpav
his ydisp i=8 j=jbotpav
his ydisp i=9 j=jbotpav
his ydisp i=10 j=jbotpav
his ydisp i=11 j=jbotpav;33
his ydisp i=12 j=jbotpav
his ydisp i=13 j=jbotpav
his ydisp i=14 j=jbotpav

his xdisp i=1 j=jbotpav      ;37
his xdisp i=2 j=jbotpav
his xdisp i=3 j=jbotpav
his xdisp i=4 j=jbotpav
his xdisp i=5 j=jbotpav
his xdisp i=6 j=jbotpav
his xdisp i=7 j=jbotpav
his xdisp i=8 j=jbotpav
his xdisp i=9 j=jbotpav
his xdisp i=10 j=jbotpav
his xdisp i=11 j=jbotpav;47
his xdisp i=12 j=jbotpav
his xdisp i=13 j=jbotpav
his xdisp i=14 j=jbotpav

;-----Initialise run-----
set step 100000
solve srat 1e-4
plot hold his 3
plot hold his 1
plot hold ydisp fill grid
plot hold syy fill grid
ini xdisp=0 ydisp=0
save inidef_E8.sav

his ydisp i=1 j=jsurf      ;51
;-----Add Embankment-----

def addem
vv=jsurf
loop vv (jsurf, jbotpav4)
  emiwidth=x_el_em+jsurf-vv
  command
    mo el i=1,emiwidth j=vv
    prop bulk=Kem shear=Gem dens=dem i=1,emiwidth j=vv
;   prop co=c_em frict=phi_em tens=tens_em i=1,emiwidth j=vv

```

```

set step 10000
solve srat 1e-3
; plot state block grid
; print y i=1

xdispgraph
settgraph
latbasemb

; movie off
plot ydis fi gri iw
plot table vv
plot table vvv
plot table lvv
plot his 51
; movie on
end_command
end_loop
end

def addpa
vv=jbotpav
loop vv (jbotpav, g_el_y)
emiwidth=x_el_em+jsurf-vv
command
mo el i=1,emiwidth j=vv
prop bulk=Kpa shear=Gpa dens=dpa i=1,emiwidth j=vv
; prop co=c_pa frict=phi_pa tens=tens_pa i=1,emiwidth j=vv

set step 50000
solve srat 1e-3
; plot state block grid

xdispgraph
settgraph
latbasemb
settgraphbp
settgraphhtp
set log on
print xdisp i=1,x_el_em j=jbotpav,jmax
print table vv      ;xdisplacement
print table vvv     ;settlement
print table lvv
; movie off
plot his 51
plot ydis fi gri iw

```

```
plot pp fil gri
plot table vv
plot table vvv line bpv line tpv line
; movie on
set log off
end_command
end_loop
end

;-----

window -2,19 -12,9
;movie file def_E8.dcx
;movie on

addem
print xdisp i=1,x_el_em j=jbotpav,jmax

addpa
;movie off

save built_def_E8.sav

plot hold his 51
copy ydisptime_def_E8.jpg
plot hold ydisp fill grid iw
copy ydisp_def_E8.jpg
plot hold syy fill grid iw
copy syy_def_E8.jpg
plot hold sxx fill grid iw
copy sxx_def_E8.jpg

plot hold table 18 line 20 line 22 line 24 line 26 line 28 line &
30 line 32 line 34 line 36 line 37 line
copy horizprofile_def_E8.jpg
plot hold table 38 line 40 line 42 line 44 line 46 line 48 line &
50 line 52 line 54 line 56 line 57 line
copy settprofile_def_E8.jpg

set log defprof.txt
set log on
;Settlement profile at base of Embankment
print table vvv
;Lateral Displacement Profile at base of Embankment
print table lvv
;Lateral displacement profile with depth beneath toe of embankment
print table g_el_y
set log off
```

```

set log flac.log

;-----
set hisfile settat2depths_his_def_E8.txt
his write 3 skip 100 4 skip 100
set hisfile xdisptoe_his_def_E8.txt
his write 5 skip 100 6 skip 100 7 skip 100 8 skip 100
his write 9 skip 100 10 skip 100 11 skip 100 12 skip 100
his write 13 skip 100 14 skip 100 15 skip 100 16 skip 100 17 skip 100
his write 18 skip 100 19 skip 100 20 skip 100 21 skip 100 22 skip 100

set hisfile ydisppav_his_def_E8.txt
his write 23 skip 100 24 skip 100 25 skip 100 26 skip 100 27 skip 100
his write 28 skip 100 29 skip 100 30 skip 100 31 skip 100 32 skip 100
his write 33 skip 100 34 skip 100 35 skip 100 36 skip 100

set hisfile xdisppav_his_def_E8.txt
his write 37 skip 100 38 skip 100 39 skip 100 40 skip 100 41 skip 100
his write 42 skip 100 43 skip 100 44 skip 100 45 skip 100 46 skip 100
his write 47 skip 100 48 skip 100 49 skip 100 50 skip 100

set hisfile flachis.txt

```

D-1.2: Second Model Where the Deformations from the First Model are Applied to the Embankment

```

new
title
Parametric emb_E8 -1:2 batters, Height=6m, Elastic, Single Layer Foundation
set plot jpg
set log on
;-----
define geometry

g_el_x=100
g_el_y=20
imax=g_el_x + 1
jmax=g_el_y + 1
l1=-10.0      ;depth of bottom of layer
l7=-12.0      ;a val below lowest layer for window command later
w=-5.0*l1
w0=1.0/1.27*w
w1=w+0.1
w2=w+1         ;a value greater than width for window command
lz1=1          ;vertical grid/zone coordinate at base of layer 1

```

```

        jsurf=1      ;j co-ord of GL
;    jsurf1=jsurf-1
;    jwat=jsurf1
        vv=10
        vvv=10
        vvvv=1
        x_el_em=34
        x_gp_em=x_el_em + 1
        jbotpav=19
        jbotpav4=jbotpav-1
end
;-----
Define layprop

;water prop
watbulk=2e9
watdens=1000.0

;embankment mat
Eem=20e6          ;Young's Mod
PRem=0.3          ;Poisson's ratio
dem=1.96e3         ;Density kg/m^3
; pem=50e-12        ;permeability
Gem=Eem/(2*(1+PRem)) ;Shear mod
Kem=Eem/(3*(1-2*PRem)) ;bulk mod
c_em=20e3
phi_em=32
tens_em=c_em/tan(phi_em*pi/360)

;Pavement mat
Epa=200e6          ;Young's Mod
PRpa=0.2            ;Poisson's ratio
dpa=2.17e3          ;Density kg/m^3
; ppa=50e-12        ;permeability (should be 3e-9)
Gpa=Epa/(2*(1+PRpa)) ;Shear mod
Kpa=Epa/(3*(1-2*PRpa)) ;bulk mod
c_pa=5e5
phi_pa=38
tens_pa=100000

end
;-----
def settgraph
    vvv=vv
    ytable(vvv,1)=ydisp(1,jsurf)
    ytable(vvv,2)=ydisp(2,jsurf)
    ytable(vvv,3)=ydisp(3,jsurf)
    ytable(vvv,4)=ydisp(4,jsurf)

```

```
ytable(vvv,5)=ydisp(5,jsurf)
ytable(vvv,6)=ydisp(6,jsurf)
ytable(vvv,7)=ydisp(7,jsurf)
ytable(vvv,8)=ydisp(8,jsurf)
ytable(vvv,9)=ydisp(9,jsurf)
ytable(vvv,10)=ydisp(10,jsurf)
ytable(vvv,11)=ydisp(11,jsurf)
ytable(vvv,12)=ydisp(12,jsurf)
ytable(vvv,13)=ydisp(13,jsurf)
ytable(vvv,14)=ydisp(14,jsurf)
ytable(vvv,15)=ydisp(15,jsurf)
ytable(vvv,16)=ydisp(16,jsurf)
ytable(vvv,17)=ydisp(17,jsurf)
ytable(vvv,18)=ydisp(18,jsurf)
ytable(vvv,19)=ydisp(19,jsurf)
ytable(vvv,20)=ydisp(20,jsurf)
ytable(vvv,21)=ydisp(21,jsurf)
ytable(vvv,22)=ydisp(22,jsurf)
ytable(vvv,23)=ydisp(23,jsurf)
ytable(vvv,24)=ydisp(24,jsurf)
ytable(vvv,25)=ydisp(25,jsurf)
ytable(vvv,26)=ydisp(26,jsurf)
ytable(vvv,27)=ydisp(27,jsurf)
ytable(vvv,28)=ydisp(28,jsurf)
ytable(vvv,29)=ydisp(29,jsurf)
ytable(vvv,30)=ydisp(30,jsurf)
ytable(vvv,31)=ydisp(31,jsurf)
ytable(vvv,32)=ydisp(32,jsurf)
ytable(vvv,33)=ydisp(33,jsurf)
ytable(vvv,34)=ydisp(34,jsurf)
```

```
xtable(vvv,1)=x(1,jsurf)
xtable(vvv,2)=x(2,jsurf)
xtable(vvv,3)=x(3,jsurf)
xtable(vvv,4)=x(4,jsurf)
xtable(vvv,5)=x(5,jsurf)
xtable(vvv,6)=x(6,jsurf)
xtable(vvv,7)=x(7,jsurf)
xtable(vvv,8)=x(8,jsurf)
xtable(vvv,9)=x(9,jsurf)
xtable(vvv,10)=x(10,jsurf)
xtable(vvv,11)=x(11,jsurf)
xtable(vvv,12)=x(12,jsurf)
xtable(vvv,13)=x(13,jsurf)
xtable(vvv,14)=x(14,jsurf)
xtable(vvv,15)=x(15,jsurf)
xtable(vvv,16)=x(16,jsurf)
xtable(vvv,17)=x(17,jsurf)
```

```

xtable(vvv,18)=x(18,jsurf)
xtable(vvv,19)=x(19,jsurf)
xtable(vvv,20)=x(20,jsurf)
xtable(vvv,21)=x(21,jsurf)
xtable(vvv,22)=x(22,jsurf)
xtable(vvv,23)=x(23,jsurf)
xtable(vvv,24)=x(24,jsurf)
xtable(vvv,25)=x(25,jsurf)
xtable(vvv,26)=x(26,jsurf)
xtable(vvv,27)=x(27,jsurf)
xtable(vvv,28)=x(28,jsurf)
xtable(vvv,29)=x(29,jsurf)
xtable(vvv,30)=x(30,jsurf)
xtable(vvv,31)=x(31,jsurf)
xtable(vvv,32)=x(32,jsurf)
xtable(vvv,33)=x(33,jsurf)
xtable(vvv,34)=x(34,jsurf)
end
;-----
def latbasemb
    lvv=vvv+20
    ytable(lvv,1)=xdisp(1,jsurf)
    ytable(lvv,2)=xdisp(2,jsurf)
    ytable(lvv,3)=xdisp(3,jsurf)
    ytable(lvv,4)=xdisp(4,jsurf)
    ytable(lvv,5)=xdisp(5,jsurf)
    ytable(lvv,6)=xdisp(6,jsurf)
    ytable(lvv,7)=xdisp(7,jsurf)
    ytable(lvv,8)=xdisp(8,jsurf)
    ytable(lvv,9)=xdisp(9,jsurf)
    ytable(lvv,10)=xdisp(10,jsurf)
    ytable(lvv,11)=xdisp(11,jsurf)
    ytable(lvv,12)=xdisp(12,jsurf)
    ytable(lvv,13)=xdisp(13,jsurf)
    ytable(lvv,14)=xdisp(14,jsurf)
    ytable(lvv,15)=xdisp(15,jsurf)
    ytable(lvv,16)=xdisp(16,jsurf)
    ytable(lvv,17)=xdisp(17,jsurf)
    ytable(lvv,18)=xdisp(18,jsurf)
    ytable(lvv,19)=xdisp(19,jsurf)
    ytable(lvv,20)=xdisp(20,jsurf)
    ytable(lvv,21)=xdisp(21,jsurf)
    ytable(lvv,22)=xdisp(22,jsurf)
    ytable(lvv,23)=xdisp(23,jsurf)
    ytable(lvv,24)=xdisp(24,jsurf)
    ytable(lvv,25)=xdisp(25,jsurf)
    ytable(lvv,26)=xdisp(26,jsurf)
    ytable(lvv,27)=xdisp(27,jsurf)

```

```

ytable(lvv,28)=xdisp(28,jsurf)
ytable(lvv,29)=xdisp(29,jsurf)
ytable(lvv,30)=xdisp(30,jsurf)
ytable(lvv,31)=xdisp(31,jsurf)
ytable(lvv,32)=xdisp(32,jsurf)
ytable(lvv,33)=xdisp(33,jsurf)
ytable(lvv,34)=xdisp(34,jsurf)

xtable(lvv,1)=x(1,jsurf)
xtable(lvv,2)=x(2,jsurf)
xtable(lvv,3)=x(3,jsurf)
xtable(lvv,4)=x(4,jsurf)
xtable(lvv,5)=x(5,jsurf)
xtable(lvv,6)=x(6,jsurf)
xtable(lvv,7)=x(7,jsurf)
xtable(lvv,8)=x(8,jsurf)
xtable(lvv,9)=x(9,jsurf)
xtable(lvv,10)=x(10,jsurf)
xtable(lvv,11)=x(11,jsurf)
xtable(lvv,12)=x(12,jsurf)
xtable(lvv,13)=x(13,jsurf)
xtable(lvv,14)=x(14,jsurf)
xtable(lvv,15)=x(15,jsurf)
xtable(lvv,16)=x(16,jsurf)
xtable(lvv,17)=x(17,jsurf)
xtable(lvv,18)=x(18,jsurf)
xtable(lvv,19)=x(19,jsurf)
xtable(lvv,20)=x(20,jsurf)
xtable(lvv,21)=x(21,jsurf)
xtable(lvv,22)=x(22,jsurf)
xtable(lvv,23)=x(23,jsurf)
xtable(lvv,24)=x(24,jsurf)
xtable(lvv,25)=x(25,jsurf)
xtable(lvv,26)=x(26,jsurf)
xtable(lvv,27)=x(27,jsurf)
xtable(lvv,28)=x(28,jsurf)
xtable(lvv,29)=x(29,jsurf)
xtable(lvv,30)=x(30,jsurf)
xtable(lvv,31)=x(31,jsurf)
xtable(lvv,32)=x(32,jsurf)
xtable(lvv,33)=x(33,jsurf)
xtable(lvv,34)=x(34,jsurf)

end
;-----
def settgraphbp
  bpv=lvv+20
  ytable(bpv,1)=ydisp(1,jbotpav)
  ytable(bpv,2)=ydisp(2,jbotpav)

```

```

ytable(bpv,3)=ydisp(3,jbotpav)
ytable(bpv,4)=ydisp(4,jbotpav)
ytable(bpv,5)=ydisp(5,jbotpav)
ytable(bpv,6)=ydisp(6,jbotpav)
ytable(bpv,7)=ydisp(7,jbotpav)
ytable(bpv,8)=ydisp(8,jbotpav)
ytable(bpv,9)=ydisp(9,jbotpav)
ytable(bpv,10)=ydisp(10,jbotpav)
ytable(bpv,11)=ydisp(11,jbotpav)
ytable(bpv,12)=ydisp(12,jbotpav)
ytable(bpv,13)=ydisp(13,jbotpav)
ytable(bpv,14)=ydisp(14,jbotpav)

xtable(bpv,1)=x(1,jbotpav)
xtable(bpv,2)=x(2,jbotpav)
xtable(bpv,3)=x(3,jbotpav)
xtable(bpv,4)=x(4,jbotpav)
xtable(bpv,5)=x(5,jbotpav)
xtable(bpv,6)=x(6,jbotpav)
xtable(bpv,7)=x(7,jbotpav)
xtable(bpv,8)=x(8,jbotpav)
xtable(bpv,9)=x(9,jbotpav)
xtable(bpv,10)=x(10,jbotpav)
xtable(bpv,11)=x(11,jbotpav)
xtable(bpv,12)=x(12,jbotpav)
xtable(bpv,13)=x(13,jbotpav)
xtable(bpv,14)=x(14,jbotpav)
end

;-----
def settgraphp
  tpv=bpv+20
  ytable(tpv,1)=ydisp(1,jmax)
  ytable(tpv,2)=ydisp(2,jmax)
  ytable(tpv,3)=ydisp(3,jmax)
  ytable(tpv,4)=ydisp(4,jmax)
  ytable(tpv,5)=ydisp(5,jmax)
  ytable(tpv,6)=ydisp(6,jmax)
  ytable(tpv,7)=ydisp(7,jmax)
  ytable(tpv,8)=ydisp(8,jmax)
  ytable(tpv,9)=ydisp(9,jmax)
  ytable(tpv,10)=ydisp(10,jmax)
  ytable(tpv,11)=ydisp(11,jmax)
  ytable(tpv,12)=ydisp(12,jmax)
  ytable(tpv,13)=ydisp(13,jmax)

  xtable(tpv,1)=x(1,jmax)
  xtable(tpv,2)=x(2,jmax)

```

```

xtable(tpv,3)=x(3,jmax)
xtable(tpv,4)=x(4,jmax)
xtable(tpv,5)=x(5,jmax)
xtable(tpv,6)=x(6,jmax)
xtable(tpv,7)=x(7,jmax)
xtable(tpv,8)=x(8,jmax)
xtable(tpv,9)=x(9,jmax)
xtable(tpv,10)=x(10,jmax)
xtable(tpv,11)=x(11,jmax)
xtable(tpv,12)=x(12,jmax)
xtable(tpv,13)=x(13,jmax)
end

;-----
def sxxbp
    bps=tpv+20
    ytable(bps,1)=sxx(1,jbotpav)
    ytable(bps,2)=sxx(2,jbotpav)
    ytable(bps,3)=sxx(3,jbotpav)
    ytable(bps,4)=sxx(4,jbotpav)
    ytable(bps,5)=sxx(5,jbotpav)
    ytable(bps,6)=sxx(6,jbotpav)
    ytable(bps,7)=sxx(7,jbotpav)
    ytable(bps,8)=sxx(8,jbotpav)
    ytable(bps,9)=sxx(9,jbotpav)
    ytable(bps,10)=sxx(10,jbotpav)
    ytable(bps,11)=sxx(11,jbotpav)
    ytable(bps,12)=sxx(12,jbotpav)
    ytable(bps,13)=sxx(13,jbotpav)
    ytable(bps,14)=sxx(14,jbotpav)
    ytable(bps,15)=sxx(15,jbotpav)

    xtable(bps,1)=x(1,jbotpav)
    xtable(bps,2)=x(2,jbotpav)
    xtable(bps,3)=x(3,jbotpav)
    xtable(bps,4)=x(4,jbotpav)
    xtable(bps,5)=x(5,jbotpav)
    xtable(bps,6)=x(6,jbotpav)
    xtable(bps,7)=x(7,jbotpav)
    xtable(bps,8)=x(8,jbotpav)
    xtable(bps,9)=x(9,jbotpav)
    xtable(bps,10)=x(10,jbotpav)
    xtable(bps,11)=x(11,jbotpav)
    xtable(bps,12)=x(12,jbotpav)
    xtable(bps,13)=x(13,jbotpav)
    xtable(bps,14)=x(14,jbotpav)
    xtable(bps,15)=x(15,jbotpav)
end

```

```

;-----
def sxxtcp
  tps=bps+20
  ytable(tps,1)=sxx(1,g_el_y)
  ytable(tps,2)=sxx(2,g_el_y)
  ytable(tps,3)=sxx(3,g_el_y)
  ytable(tps,4)=sxx(4,g_el_y)
  ytable(tps,5)=sxx(5,g_el_y)
  ytable(tps,6)=sxx(6,g_el_y)
  ytable(tps,7)=sxx(7,g_el_y)
  ytable(tps,8)=sxx(8,g_el_y)
  ytable(tps,9)=sxx(9,g_el_y)
  ytable(tps,10)=sxx(10,g_el_y)
  ytable(tps,11)=sxx(11,g_el_y)
  ytable(tps,12)=sxx(12,g_el_y)
  ytable(tps,13)=sxx(13,g_el_y)
  ytable(tps,14)=sxx(14,g_el_y)

  xtable(tps,1)=x(1,g_el_y)
  xtable(tps,2)=x(2,g_el_y)
  xtable(tps,3)=x(3,g_el_y)
  xtable(tps,4)=x(4,g_el_y)
  xtable(tps,5)=x(5,g_el_y)
  xtable(tps,6)=x(6,g_el_y)
  xtable(tps,7)=x(7,g_el_y)
  xtable(tps,8)=x(8,g_el_y)
  xtable(tps,9)=x(9,g_el_y)
  xtable(tps,10)=x(10,g_el_y)
  xtable(tps,11)=x(11,g_el_y)
  xtable(tps,12)=x(12,g_el_y)
  ytable(tps,13)=x(13,g_el_y)
  ytable(tps,14)=x(14,g_el_y)
end
;-----

def xdispbp
  bpx=tps+20
  ytable(bpx,1)=xdisp(1,jbotpav)
  ytable(bpx,2)=xdisp(2,jbotpav)
  ytable(bpx,3)=xdisp(3,jbotpav)
  ytable(bpx,4)=xdisp(4,jbotpav)
  ytable(bpx,5)=xdisp(5,jbotpav)
  ytable(bpx,6)=xdisp(6,jbotpav)
  ytable(bpx,7)=xdisp(7,jbotpav)
  ytable(bpx,8)=xdisp(8,jbotpav)
  ytable(bpx,9)=xdisp(9,jbotpav)
  ytable(bpx,10)=xdisp(10,jbotpav)
  ytable(bpx,11)=xdisp(11,jbotpav)
  ytable(bpx,12)=xdisp(12,jbotpav)

```

```
ytable(bpx,13)=xdisp(13,jbotpav)
ytable(bpx,14)=xdisp(14,jbotpav)
```

```
xtable(bpx,1)=x(1,jbotpav)
xtable(bpx,2)=x(2,jbotpav)
xtable(bpx,3)=x(3,jbotpav)
xtable(bpx,4)=x(4,jbotpav)
xtable(bpx,5)=x(5,jbotpav)
xtable(bpx,6)=x(6,jbotpav)
xtable(bpx,7)=x(7,jbotpav)
xtable(bpx,8)=x(8,jbotpav)
xtable(bpx,9)=x(9,jbotpav)
xtable(bpx,10)=x(10,jbotpav)
xtable(bpx,11)=x(11,jbotpav)
xtable(bpx,12)=x(12,jbotpav)
xtable(bpx,13)=x(13,jbotpav)
xtable(bpx,14)=x(14,jbotpav)
end
```

```
def xdisptp
tpx=bpx+20
ytable(tpx,1)=xdisp(1,jmax)
ytable(tpx,2)=xdisp(2,jmax)
ytable(tpx,3)=xdisp(3,jmax)
ytable(tpx,4)=xdisp(4,jmax)
ytable(tpx,5)=xdisp(5,jmax)
ytable(tpx,6)=xdisp(6,jmax)
ytable(tpx,7)=xdisp(7,jmax)
ytable(tpx,8)=xdisp(8,jmax)
ytable(tpx,9)=xdisp(9,jmax)
ytable(tpx,10)=xdisp(10,jmax)
ytable(tpx,11)=xdisp(11,jmax)
ytable(tpx,12)=xdisp(12,jmax)
ytable(tpx,13)=xdisp(13,jmax)
```

```
xtable(tpx,1)=x(1,jmax)
xtable(tpx,2)=x(2,jmax)
xtable(tpx,3)=x(3,jmax)
xtable(tpx,4)=x(4,jmax)
xtable(tpx,5)=x(5,jmax)
xtable(tpx,6)=x(6,jmax)
xtable(tpx,7)=x(7,jmax)
xtable(tpx,8)=x(8,jmax)
xtable(tpx,9)=x(9,jmax)
xtable(tpx,10)=x(10,jmax)
xtable(tpx,11)=x(11,jmax)
xtable(tpx,12)=x(12,jmax)
```

```

xtable(tpx,13)=x(13,jmax)
end

;-----
;----Definition of Grid----
geometry

grid g_el_x, g_el_y
mo el
gen 0,0 0,6.0 w0,6.0 w,0 rat 1.0,0.98 i=1,imax j=1,jmax
table 1 (0,6) (5.5,6) (6.5,5.5) (17.5,0) (w,0)
table 2 (0,5.5) (6.5,5.5)
table 3 (0,0) (17.5,0) (w,0)
;ini x 11.0 y 0 i=x_gp_em j=jsurf
gen table 1
gen table 2
gen table 3

window
plot hold grid mark
window
;-----

FOR 4.5M HIGH MODEL REPLACE ABOVE WITH THIS
;----Definition of Grid----
geometry

grid g_el_x, g_el_y
mo el
gen 0,0 0,4.5 w0,4.5 w,0 rat 1.0,0.98 i=1,imax j=1,jmax
table 1 (0,4.5) (5.5,4.5) (6.5,4) (14.5,0) (w,0)
table 2 (0,4) (6.5,4)
table 3 (0,0) (14.5,0) (w,0)
;ini x 11.0 y 0 i=x_gp_em j=jsurf
gen table 1
gen table 2
gen table 3

window
plot hold grid mark
window
;-----

FOR 3 M HIGH MODEL REPLACE ABOVE CODE WITH THIS
;----Definition of Grid----
geometry

grid g_el_x, g_el_y
mo el
gen 0,0 0,3 w0,3 w,0 rat 1.0,0.98 i=1,imax j=1,jmax

```

```

table 1 (0,3) (5.5,3) (6.5,2.5) (11.5,0) (w,0)
table 2 (0,2.5) (6.5,2.5)
table 3 (0,0) (11.5,0) (w,0)
;ini x 11.0 y 0 i=x_gp_em j=jsurf
gen table 1
gen table 2
gen table 3

window
plot hold grid mark
window
;-----
;----Layer Properties----
layprop

mo null ;reg g_el_x, g_el_y
mo el reg 1,jsurf
mo el reg 1,g_el_y

prop bulk=Kem shear=Gem dens=dem reg 1,jsurf
:prop co=c_em frict=phi_em tens=0 reg 1,jsurf
prop bulk=Kpa shear=Gpa dens=dpa reg 1,g_el_y
:prop co=c_pa frict=phi_pa tens=tens_pa reg 1,g_el_y

window
plot hold grid mark
copy gridmeshemb_E8.jpg
window

;mo null reg 1,jsurf
;mo null reg 1,g_el_y

water bulk=watbulk dens=watdens tens=1e10

set large
set gravity 9.81

;----Boundary Conditions---
fix x i=1
;fix x i=imax
fix x y j=1

;-----Histories-----
his unbal ;nstep=1          ;1 unbalanced force
his sratio                      ;2 unbal force ratio
his ydisp i=1 j=jsurf          ;3 sett plate

```

```

his ydisp i=1 j=jbotpav      ;4
his ydisp i=2 j=jbotpav
his ydisp i=3 j=jbotpav
his ydisp i=4 j=jbotpav
his ydisp i=5 j=jbotpav
his ydisp i=6 j=jbotpav
his ydisp i=7 j=jbotpav
his ydisp i=8 j=jbotpav
his ydisp i=9 j=jbotpav
his ydisp i=10 j=jbotpav
his ydisp i=11 j=jbotpav;14
his ydisp i=12 j=jbotpav
his ydisp i=13 j=jbotpav
his ydisp i=14 j=jbotpav

```

```

his xdisp i=1 j=jbotpav      ;18
his xdisp i=2 j=jbotpav
his xdisp i=3 j=jbotpav
his xdisp i=4 j=jbotpav
his xdisp i=5 j=jbotpav
his xdisp i=6 j=jbotpav
his xdisp i=7 j=jbotpav
his xdisp i=8 j=jbotpav
his xdisp i=9 j=jbotpav
his xdisp i=10 j=jbotpav
his xdisp i=11 j=jbotpav;28
his xdisp i=12 j=jbotpav
his xdisp i=13 j=jbotpav
his xdisp i=14 j=jbotpav

```

```

;-----Initialise run-----
set step 100000
solve srat 1e-4
plot hold his 3
plot hold his 1
plot hold ydisp fill grid
plot hold syy fill grid
ini xdisp=0 ydisp=0
save iniemb_E8.sav

```

```

his ydisp i=1 j=jsurf      ;32

```

```

;-----Settlement-----

```

THESE VALUES ARE THE DEFORMATIONS EXTRACTED FROM THE FIRST MODEL THEY ARE THEREFORE DIFFERENT FOR EACH MODEL

```

Apply yv= -8.11E-06    j=1    i=1
Apply yv= -8.11E-06    j=1    i=2
Apply yv= -8.09E-06    j=1    i=3

```

Apply	yv=	-8.06E-06	j=1	i=4
Apply	yv=	-8.01E-06	j=1	i=5
Apply	yv=	-7.95E-06	j=1	i=6
Apply	yv=	-7.88E-06	j=1	i=7
Apply	yv=	-7.79E-06	j=1	i=8
Apply	yv=	-7.68E-06	j=1	i=9
Apply	yv=	-7.56E-06	j=1	i=10
Apply	yv=	-7.42E-06	j=1	i=11
Apply	yv=	-7.27E-06	j=1	i=12
Apply	yv=	-7.10E-06	j=1	i=13
Apply	yv=	-6.91E-06	j=1	i=14
Apply	yv=	-6.70E-06	j=1	i=15
Apply	yv=	-6.47E-06	j=1	i=16
Apply	yv=	-6.22E-06	j=1	i=17
Apply	yv=	-5.96E-06	j=1	i=18
Apply	yv=	-5.68E-06	j=1	i=19
Apply	yv=	-5.38E-06	j=1	i=20
Apply	yv=	-5.07E-06	j=1	i=21
Apply	yv=	-4.74E-06	j=1	i=22
Apply	yv=	-4.40E-06	j=1	i=23
Apply	yv=	-4.04E-06	j=1	i=24
Apply	yv=	-3.68E-06	j=1	i=25
Apply	yv=	-3.30E-06	j=1	i=26
Apply	yv=	-2.92E-06	j=1	i=27
Apply	yv=	-2.54E-06	j=1	i=28
Apply	yv=	-2.16E-06	j=1	i=29
Apply	yv=	-1.77E-06	j=1	i=30
Apply	yv=	-1.40E-06	j=1	i=31
Apply	yv=	-1.04E-06	j=1	i=32
Apply	yv=	-6.94E-07	j=1	i=33
Apply	yv=	-3.72E-07	j=1	i=34
Apply	xv=	0.00E+00	j=1	i=1
Apply	xv=	1.32E-07	j=1	i=2
Apply	xv=	2.64E-07	j=1	i=3
Apply	xv=	3.95E-07	j=1	i=4
Apply	xv=	5.26E-07	j=1	i=5
Apply	xv=	6.57E-07	j=1	i=6
Apply	xv=	7.86E-07	j=1	i=7
Apply	xv=	9.15E-07	j=1	i=8
Apply	xv=	1.04E-06	j=1	i=9
Apply	xv=	1.17E-06	j=1	i=10
Apply	xv=	1.29E-06	j=1	i=11
Apply	xv=	1.41E-06	j=1	i=12
Apply	xv=	1.53E-06	j=1	i=13
Apply	xv=	1.64E-06	j=1	i=14
Apply	xv=	1.74E-06	j=1	i=15
Apply	xv=	1.84E-06	j=1	i=16

Apply xv=	1.94E-06	j=1	i=17
Apply xv=	2.03E-06	j=1	i=18
Apply xv=	2.10E-06	j=1	i=19
Apply xv=	2.18E-06	j=1	i=20
Apply xv=	2.24E-06	j=1	i=21
Apply xv=	2.29E-06	j=1	i=22
Apply xv=	2.34E-06	j=1	i=23
Apply xv=	2.37E-06	j=1	i=24
Apply xv=	2.40E-06	j=1	i=25
Apply xv=	2.42E-06	j=1	i=26
Apply xv=	2.43E-06	j=1	i=27
Apply xv=	2.43E-06	j=1	i=28
Apply xv=	2.42E-06	j=1	i=29
Apply xv=	2.41E-06	j=1	i=30
Apply xv=	2.39E-06	j=1	i=31
Apply xv=	2.36E-06	j=1	i=32
Apply xv=	2.34E-06	j=1	i=33
Apply xv=	2.31E-06	j=1	i=34

;-----Solve-----

```

step 10000
settgraph
latbasemb
settgraphbp
settgraphtp
sxxbp
sxxtp
xdispbp
xdisptp

```

```

label table vvv
Sett. Profile Below Embankment
label table lvv
Horiz. Disp. Below Embankment
label table bpv
Sett. Profile at base of Pavement
label table tpv
Sett. Profile at top of Pavement
label table bps
Horiz. Stress at base of Pavement
label table tps
Horiz. Stress at top of Pavement

```

```

plot hold table vvv line bpv line tpv line label
copy settprof_emb_E8.jpg
plot hold table lvv label
plot hold table bps line tps line label

```

```

copy horstresspav_emb_E8.jpg

set log disp_sxx_pav_emb_E8.txt
set log on
;Xdisp at bottom of pavement
print table bpx
;Xdisp at top of pavement
print table tpx
;horizontal Stress at bottom of pavement
print table bps
;horizontal stress at top of Pavement
print table tps
;ydisp at bottom of pavement
print table bpv
;ydisp at top of pavement
print table tpv
set log off
set log flac.log
set log off

save built_emb_E8.sav

plot hold his 32
copy ydisptime_emb_E8.jpg
plot hold ydisp fill grid iw
copy ydisp_emb_E8.jpg
plot hold syy fill grid iw
copy syy_emb_E8.jpg
plot hold sxx fill grid iw
copy sxx_emb_E8.jpg
plot hold vsi fill grid iw
copy volstrain_emb_E8.jpg

;-----
set hisfile settatbase_his_emb_E8.txt
his write 3 skip 10

set hisfile ydisppav_his_emb_E8.txt
his write 4 skip 10 5 skip 10 6 skip 10 7 skip 10 8 skip 10
his write 9 skip 10 10 skip 10 11 skip 10 12 skip 10
his write 13 skip 10 14 skip 10 15 skip 10 16 skip 10 17 skip 10

set hisfile xdisppav_his_emb_E8.txt
his write 18 skip 10 19 skip 10 20 skip 10 21 skip 10 22 skip 10
his write 23 skip 10 24 skip 10 25 skip 10 26 skip 10 27 skip 10
his write 28 skip 10 29 skip 10 30 skip 10 31 skip 10

set hisfile flachis.txt

```

D-2: Data from Pavement Cracking Models

Table D-1: Data Recorded from Pavement Cracking Investigation Models

E_{Emb}	E_{Pavt}	Height	E_{Found}	Max Sett	Max Lat Disp.	Depth of Max Lat Disp.	Ratio Lat Disp./Sett	Min Comp stress	Ratio
									E_{found}/E_{emb}
Mpa	Mpa	m	Mpa	mm	mm	m		kPa	
20	200	3	3	115	38.4	3.516	0.333913	109	0.15
20	200	3	4	86.3	29	3.513	0.336037	78.4	0.2
20	200	3	5	69.1	23.4	3.511	0.33864	60.5	0.25
20	200	3	6	57.6	19.6	3.509	0.340278	48.8	0.3
20	200	3	8	43.3	14.8	3.508	0.341801	34.8	0.4
20	200	3	10	34.62	11.85	3.507	0.342288	26.46	0.5
20	200	4.5	5	100	34.2	3.509	0.342	84.06	0.25
20	200	4.5	8	62.8	21.8	2.96	0.347134	51.54	0.4
20	200	4.5	10	50.33	17.6	2.959	0.349692	39.98	0.5
20	200	6	5	128.8	43.9	2.96	0.340839	106.7	0.25
20	200	6	8	81.14	28.24	2.958	0.34804	64.7	0.4
20	200	6	10	65.11	22.88	2.958	0.351405	51.06	0.5
40	200	3	5	68.57	22.85	3.511	0.333236	104.4	0.125
40	200	3	8	43.04	14.47	3.508	0.336199	62.91	0.2
40	200	3	10	34.34	11.64	3.507	0.338963	49.58	0.25
40	200	4.5	5	98.48	33.11	3.509	0.33621	129.1	0.125
40	200	4.5	8	62.13	21.13	3.507	0.340093	80.62	0.2
40	200	4.5	10	49.88	17.07	3.506	0.342221	64.47	0.25
40	200	6	5	126.1	41.87	3.507	0.332038	163.6	0.125
40	200	6	8	79.87	26.97	2.958	0.337674	102.1	0.2
40	200	6	10	64.23	21.9	2.958	0.340962	81.61	0.25

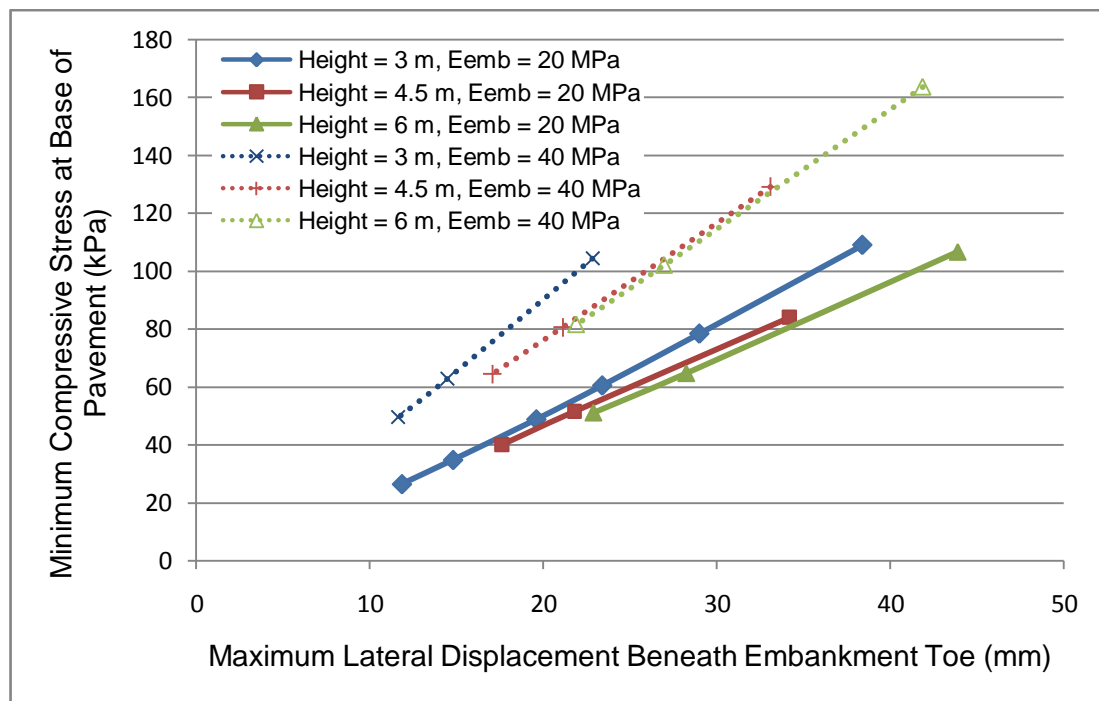


Figure 8.1: Variation of Pavement Stress with Lateral Displacement beneath the Embankment